SIMULATION OF FRACTURE FLUID CLEANUP AND ITS EFFECT ON LONG-TERM RECOVERY IN TIGHT GAS RESERVOIRS

A Dissertation

by

YILIN WANG

Submitted to the Office of Graduate Studies of
Texas A&M University
in partial fulfillment of the requirements for the degree of

DOCTOR OF PHILOSOPHY

December 2008

Major Subject: Petroleum Engineering

SIMULATION OF FRACTURE FLUID CLEANUP AND ITS EFFECT ON LONG-TERM RECOVERY IN TIGHT GAS RESERVOIRS

A Dissertation

by

YILIN WANG

Submitted to the Office of Graduate Studies of
Texas A&M University
in partial fulfillment of the requirements for the degree of

DOCTOR OF PHILOSOPHY

Approved by:

Co-Chairs of Committee,	Stephen A. Holditch
	Duane A. McVay
Committee Members,	Wayne Ahr
	Ding Zhu
Head of Department,	Stephen A. Holditch

December 2008

Major Subject: Petroleum Engineering

ABSTRACT

Simulation of Fracture Fluid Cleanup and Its Effect on Long-term Recovery in Tight Gas Reservoirs. (December 2008)

Yilin Wang, B.Sc., The University of Petroleum of China;

M.S., The University of Houston

Co-Chairs of Advisory Committee: Dr. Stephen A. Holditch
Dr. Duane A. McVay

In the coming decades, the world will require additional supplies of natural gas to meet the demand for energy. Tight gas reservoirs can be defined as reservoirs where the formation permeability is so low (< 0.1 md) that advanced stimulation technologies, such as large volume fracture treatments, are required before a reasonable profit can be made. Hydraulic fracturing is one of the best methods to stimulate a tight gas well. Most fracture treatments result in 3-6 fold increases in the productivity index. However, if one computes the effective fracture length of most wells, we usually find that the effective length is less than the designed propped fracture length. The "propped length" is the distance down the fracture from the wellbore where proppants have been placed at a high enough concentration to "prop open" the fracture. The "effective length" is the portion of the propped fracture that cleans up and allows gas flow from the reservoir into the fracture then down the fracture to the wellbore.

Whenever the effective length is much shorter than the designed propped length, several reasons must be evaluated to determine what might have occurred. For example, the difference could be caused by one or more of the following issues: insufficient fracture fluid cleanup, proppant settling, proppant embedment, proppant crushing, or poor reservoir continuity.

Although all these causes are possible, we believe that fracture fluid cleanup issues may be the most common reason the industry fails to achieve the designed propped fracture length in most cases. In this research, we have investigated fracture fluid cleanup

problems and developed a better understanding of the issues involved which hopefully will lead to ways to improve cleanup.

Fracture fluid cleanup is a complex problem, that can be influenced by many parameters such as the fluid system used, treatment design, flowback procedures, production strategy, and reservoir conditions. Residual polymer in the fracture can reduce the effective fracture permeability and porosity, reduce the effective fracture half-length, and limit the well productivity. Our ability to mathematically model the fundamental physical processes governing fluid recovery in hydraulic fractures in the past has been limited.

In this research, fracture fluid damage mechanisms have been investigated, and mathematical models and computer codes have been developed to better characterize the cleanup process. The codes have been linked to a 3D, 3-phase simulator to model and quantify the fracture fluid cleanup process and its effect on long-term gas production performances. Then, a comprehensive systematic simulation study has been carried out by varying formation permeability, reservoir pressure, fracture length, fracture conductivity, yield stress, and pressure drawdown. On the basis of simulation results and analyses, new ways to improve fracture fluid cleanup have been provided. This new progress help engineers better understand fracture fluid cleanup, improve fracture treatment design, and increase gas recovery from tight sand reservoirs, which can be extremely important as more tight gas reservoirs are developed around the world.

“THE FEAR OF GOD IS THE BEGINNING OF WISDOM.”

ACKNOWLEDGEMENTS

I would like to thank Dr Stephen Holditch for his advice, patience, and guidance with my study and research at Texas A&M University. This research would not have been possible without his guidance from the very beginning. Also I thank Drs Duane McVay, Ding Zhu, and Wayne Ahr for all the help and comments on my research. I would like to thank the faculty and staff in the department.

My appreciation goes to my friends, who made my study and life in College Station wonderful. Of course, I could not thank my family enough for their love and support in my study and life.

TABLE OF CONTENTS

Page

ABSTRACT iii

DEDICATION v

ACKNOWLEDGEMENTS vi

TABLE OF CONTENTS vii

LIST OF FIGURES ix

LIST OF TABLES xiv

CHAPTER

I INTRODUCTION TO TIGHT GAS FRACTURING 1

II LITERATURE REVIEW OF FRACTURE DAMAGE MECHANISM 5

2.1 Fracture damage mechanism and the cleanup process 5
2.2 Post-fracture evaluation 11
2.3 Research objectives 13
2.4 Procedures used for this research 13

III SIMULATION METHODOLOGY 15

3.1 Fractured well model 16
3.2 Reservoir, fracture and fluid properties 18
3.3 Initiation of simulation 25
3.4 Polymer properties 28
3.5 Relation between yield stress and flow initiation gradient 34
3.6 Simulation scenarios 35

IV STEPS IN MODELING FRACTURE FLUID CLEANUP 38

4.1 Simulation of single phase flow 38
4.2 Simulation of gas/water two-phase flow 39
4.3 Simulation of proppant crushing effect 44
4.4 Simulation of polymer filter cake 47
4.5 Simulation of yield stress effect 53
4.6 Other factors 71

V SIMULATION RESULTS AND ANALYSES 73

5.1 Simulation results for single-phase flow 73
5.2 Simulation results for gas/water two-phase flow 79
5.3 Simulation results for the effect of proppant crushing 85
5.4 Simulation results for the effect of polymer filter cake 94
5.5 Simulation results for the effect of yield stress 102

CHAPTER Page

VI FACTORS AFFECTING FRACTURE FLUID CLEANUP 113

6.1 Fracture conductivity..... 113
6.2 Yield stress for fracture fluid 118
6.3 Fracture length 123
6.4 Initial reservoir pressure 128

VII CONCLUSIONS AND RECOMMENDATIONS..... 132

NOMENCLATURE 134

REFERENCES 136

APPENDIX A 141

APPENDIX B 149

APPENDIX C 150

APPENDIX D 153

APPENDIX E 160

VITA 173

LIST OF FIGURES

Page

Figure 1.1 Microscopic section of conventional sandstone and tight gas sandstone (from DOE National Energy Technology Laboratory) 1

Figure 1.2 Gas flow mechanism before and after fracturing (from Holditch 2005) 2

Figure 2.1 Schematic of cleanup model by Tannich 1975 7

Figure 3.1 Hydraulically fractured well simulation model 17

Figure 3.2 Correlation of injected fracture fluid volume, propped half length, and zone thickness 18

Figure 3.3 Relative permeability curves..... 22

Figure 3.4 Capillary pressure curve in the reservoir formation (from Holditch 1979) 24

Figure 3.5 Gas saturation map after a fracture treatment with 80,000 gallons of fracture fluid 25

Figure 3.6 Water saturation map after a fracture treatment with 80,000 gallons of fracture fluid 27

Figure 3.7 Guar molecular structure (from Gidley et al., 1990) 29

Figure 3.8 HPG molecular structure (from Gidley et al., 1990) 30

Figure 3.9 CMHPG molecular structure (from Gidley et al., 1990) 31

Figure 3.10 HEC molecular structure (from Gidley et al., 1990) 32

Figure 4.2.1 Full capillary pressure curves: 1st drainage, 1st imbibition, and 2nd drainage. 40

Figure 4.3.1 Different proppant permeability vs. closure stress (from Carbo Creamics, 2007) 45

Figure 4.3.2 Proppant permeability reduction ratio under stress for Ottawa sand and Carbo HSP 20/40 46

Figure 4.4.1 Filter cake from 35ppt CMHPG Zr XL fluid, with breaker (StimLab Consortia, 1997-2006). 47

Figure 4.4.2 Polymer gel viscosity at zero shear vs. polymer concentration (From Barree) 48

Page

Figure 4.4.3 Polymer filter cake model inside the fracture proppant pack (from Ayoub et al., 2006)..... 50

Figure 4.5.1 Reproduction of the work by Voneiff et al. (1996) (Newtonian fracture fluid without yield stress) 53

Figure 4.5.2 Top view of a half fracture with proppant and polymer inside 55

Figure 4.5.3 Schematic plot of different fluid models (Schlumberger Oilfield Glosaary, 2008). 57

Figure 4.5.4 Schematic plot of different types of gel (Schlumberger Oilfield Glosaary, 2008) 59

Figure 4.5.5 Newtonian fractional flow curve at different yield stresses. 63

Figure 4.5.6 Simulation results for validation with 1D analytical solution. 64

Figure 4.5.7 BHP from a Cotton Valley tight gas well (May, 1997) 68

Figure 4.5.8 Cumulative gas production for two fracturing fluids. 68

Figure 4.5.9 Validation of simulation results with field data and May's simulation results..... 70

Figure 5.1.1 Gas production rate at different fracture conductivity for L_f = 528 ft, p_r = 3720 psi, k = 0.1 md , S_{wi} = 0.4 and h = 100 ft. 74

Figure 5.1.2 Cumulative gas production at different fracture conductivity for L_f = 528 ft, p_r = 3720 psi, k = 0.1 md, S_{wi} = 0.4 and h = 100 ft 75

Figure 5.1.3 Gas pressure map after 97.7 days of production for L_f = 528 ft, p_r = 3720 psi, k = 0.1 md, S_{wi} = 0.4 and h = 100 ft 76

Figure 5.1.4 Gas pressure map after 1026 days of production for L_f = 528 ft, p_r = 3720 psi, k = 0.1 md, S_{wi} = 0.4 and h = 100 ft. 77

Figure 5.2.1 Gas production rate at different fracture conductivity for L_f = 528 ft, p_r = 3720 psi, k = 0.1 md, S_{wi} = 0.4 and h = 100 ft 80

Figure 5.2.2 Cumulative gas production at different fracture conductivity for L_f = 528 ft, p_r = 3720 psi, k = 0.1 md, S_{wi} = 0.4 and h = 100 ft. 81

Figure 5.2.3 Gas production rate at different fracture conductivity for L_f = 528 ft, p_r = 1860 psi, k = 0.1 md, S_{wi} = 0.4 and h = 100 ft 82

Figure 5.2.4 Cumulative gas production at different fracture conductivity for L_f = 528 ft, p_r = 1860 psi, k = 0.1 md, S_{wi} = 0.4 and h = 100 ft 84

Figure 5.3.1 Gas production rate for different cases for L_f = 528 ft, p_r = 3720 psi, k = 0.1 md, C_r =1, S_{wi} = 0.4 and h = 100 ft. 86

Page

Figure 5.3.2 Cumulative gas production for different cases for L_f = 528 ft, p_r = 3720 psi, k = 0.1 md, C_r =1, S_{wi} = 0.4 and h = 100 ft 87

Figure 5.3.3 Water production rate for different cases for L_f = 528 ft, p_r = 3720 psi, k = 0.1 md, C_r =1, S_{wi} = 0.4 and h = 100 ft. 88

Figure 5.3.4 Gas production rate for different fracture conductivities for L_f = 528 ft, p_r = 3720 psi, k = 0.1 md, S_{wi} = 0.4 and h = 100 ft. 89

Figure 5.3.5 Cumulative gas production at different fracture conductivity for L_f = 528 ft, p_r = 3720 psi, k = 0.1 md, S_{wi} = 0.4 and h = 100 ft. 90

Figure 5.3.6 Gas production rate at different fracture conductivity for L_f = 528 ft, p_r = 1860 psi, k = 0.1 md, S_{wi} = 0.4 and h = 100 ft. 91

Figure 5.3.7 Cumulative gas production at different fracture conductivity for L_f = 528 ft, p_r = 1860 psi, k = 0.1 md, S_{wi} = 0.4 and h = 100 ft. 93

Figure 5.4.1 Gas production rate for different cases for L_f = 528 ft, p_r = 3720 psi, k = 0.1 md, C_r =1, S_{wi} = 0.4 and h = 100 ft. 95

Figure 5.4.2 Cumulative gas production for different cases for L_f = 528 ft, p_r = 3720 psi, k = 0.1 md, C_r =1, S_{wi} = 0.4 and h = 100 ft. 96

Figure 5.4.3 Water production rate for different cases for L_f = 528 ft, p_r = 3720 psi, k = 0.1 md, C_r =1, S_{wi} = 0.4 and h = 100 ft. 97

Figure 5.4.4 Gas production rate at different fracture conductivity for L_f = 528 ft, p_r = 3720 psi, k = 0.1 md, S_{wi} = 0.4 and h = 100 ft. 98

Figure 5.4.5 Cumulative gas production at different fracture conductivity for L_f = 528 ft, p_r = 3720 psi, k = 0.1 md, S_{wi} = 0.4 and h = 100 ft. 99

Figure 5.4.6 Gas production rate at different fracture conductivity for L_f = 528 ft, p_r = 1860 psi, k = 0.1 md, S_{wi} = 0.4 and h = 100 ft 100

Figure 5.4.7 Cumulative gas production at different fracture conductivity for L_f = 528 ft, p_r = 1860 psi, k = 0.1 md, S_{wi} = 0.4 and h = 100 ft 101

Figure 5.5.1 Gas saturation maps after a fracture treatment by modeling two phase flow with proppant crushing (case 3, run 18) where L_f = 528 ft, p_r = 3720 psi, k = 0.1 md, C_r =1, S_{wi} = 0.4 and h = 100 ft..... 103

Figure 5.5.2 Gas pressure maps after a fracture treatment by modeling two phase flow with proppant crushing (case 3, run 18) where L_f = 528 ft, p_r = 3720 psi, k = 0.1 md, C_r =1, S_{wi} = 0.4 and h = 100 ft..... 104

Figure 5.5.3 Gas saturation maps after a fracture treatment by modeling a non-Newtonian fracture fluid with yield stress of 3 pa (case 5a, run 18) where L_f = 528 ft, p_r = 3720 psi, k = 0.1 md, C_r =1, S_{wi} = 0.4 and h = 100 ft..... 106

Page

Figure 5.5.4 Gas saturation maps after a fracture treatment by modeling a non-Newtonian fracture fluid with yield stress of 20 pa (case 5c, run 18) where L_f = 528 ft, p_r = 3720 psi, k = 0.1 md, C_r =1, S_{wi} = 0.4 and h = 100 ft. 107

Figure 5.5.5 Saturation map for a non-Newtonian fluid with yield stress of 100pa (case 5d, run 18) 109

Figure 5.5.6 Gas production rate for different cases for L_f = 528 ft, p_r = 3720 psi, k = 0.1 md, C_r =1, S_{wi} = 0.4 and h = 100 ft. 110

Figure 5.5.7 Cumulative gas production for different cases for L_f = 528 ft, p_r = 3720 psi, k = 0.1 md, C_r =1, S_{wi} = 0.4 and h = 100 ft. 111

Figure 5.5.8 Water production rate for different cases for L_f = 528 ft, p_r = 3720 psi, k = 0.1 md, C_r =1, S_{wi} = 0.4 and h = 100 ft..... 112

Figure 6.1.1 Gas production rate at different conductivities for case 3 (L_f = 528 ft, p_r = 3720 psi, k = 0.1 md, S_{wi} = 0.4 and h = 100 ft). 113

Figure 6.1.2 Cumulative gas production at different conductivities for case 3 (L_f = 528 ft, p_r = 3720 psi, k = 0.1 md, S_{wi} = 0.4 and h = 100 ft) 114

Figure 6.1.3 Gas production rate at different conductivities for case 5a (L_f = 528 ft, p_r = 3720 psi, k = 0.1 md, S_{wi} = 0.4, h = 100 ft, and yield stress = 3 pa)……..... 115

Figure 6.1.4 Cumulative gas production at different conductivities for case 5a (L_f = 528 ft, p_r = 3720 psi, k = 0.1 md, S_{wi} = 0.4, h = 100 ft and yield stress = 3 pa) 116

Figure 6.2.1 Gas production rate for different cases for run 18 (L_f = 528 ft, p_r = 3720 psi, k = 0.1 md, C_r =1, S_{wi} = 0.4 and h = 100 ft) 118

Figure 6.2.2 Cumulative gas production rate for different cases for run 18 (L_f = 528 ft, p_r = 3720 psi, k = 0.1 md, C_r =1, S_{wi} = 0.4 and h = 100 ft) 119

Figure 6.2.3 Gas production rate for different cases for run 6 (L_f = 528 ft, p_r = 1860 psi, k = 0.1 md, C_r =1, S_{wi} = 0.4 and h = 100 ft) 120

Figure 6.2.4 Cumulative gas production rate for different cases for run 6 (L_f = 528 ft, p_r = 1860 psi, k = 0.1 md, C_r =1, S_{wi} = 0.4 and h = 100 ft)..... 121

Figure 6.3.1 Illustration of percentage of fracture that cleans up (the ratio of effective fracture length to propped fracture length) 123

Figure 6.3.2 Percentage of fracture that cleans up one year after a fracture treatment vs. yield strength for different fracture lengths for the scenario where p_r = 3720 psi, k = 0.1 md, C_r =0.1, S_{wi} = 0.4 and h = 100 ft 124

Page

Figure 6.3.3 Percentage of fracture that cleans up one year after a fracture treatment vs. yield strength for different fracture lengths for the scenario where p_r = 3720 psi, k = 0.1 md, C_r =0.1, S_{wi} = 0.4 and h = 100 ft 125

Figure 6.3.4 Percentage of fracture that cleans up one year after a fracture treatment vs. yield strength for different fracture lengths for the scenario where p_r = 3720 psi, k = 0.1 md, C_r =0.1, S_{wi} = 0.4 and h = 100 ft 126

Figure 6.3.5 Percentage of fracture that cleans up one year after a fracture treatment vs. yield strength for different fracture lengths for the scenario where p_r = 3720 psi, k = 0.1 md, C_r =0.1, S_{wi} = 0.4 and h = 100 ft 127

Figure 6.4.1 Percentage of fracture that cleans up one year after a fracture treatment vs. yield strength for different reservoir pressures for the scenario where L_f = 264 ft, k = 0.1 md, C_r =0.1, S_{wi} = 0.4 and h = 100 ft 128

Figure 6.4.2 Percentage of fracture that cleans up one year after a fracture treatment vs. yield strength for different reservoir pressures for the scenario where L_f = 264 ft, k = 0.1 md, C_r = 10, S_{wi} = 0.4 and h = 100 ft 129

Figure 6.4.3 Percentage of fracture that cleans up one year after a fracture treatment vs. yield strength for different reservoir pressures for the scenario where L_f = 528 ft, k = 0.1 md, C_r =0.1, S_{wi} = 0.4 and h = 100 ft 130

Figure 6.4.4 Percentage of fracture that cleans up one year after a fracture treatment vs. yield strength for different reservoir pressures for the scenario where L_f = 528 ft, k = 0.1 md, C_r = 10, S_{wi} = 0.4 and h = 100 ft 131

LIST OF TABLES

Page

Table 3.1 Data for simulation run of a fracture design software..... 16

Table 3.2 Basic reservoir and fracture parameters..... 21

Table 3.3 Relation between yield stress and flow initiation gradient 34

Table 3.4 Different simulation cases..... 35

Table 3.5 Simulation runs for each case..... 36

Table 4.4.1 Validation of the model..... 49

Table 4.5.1 Flow initiation gradient for high polymer concentration, proppant loading = 2 lbm/ft2, 20/40 sand (from Ayoub et al.)..... 55

Table 4.5.2 Flow initiation gradient for low polymer concentration, proppant loading = 2 lbm/ft2, 20/40 sand (by Ayoub et al)..... 56

Table 4.5.3 Data used for analytical solution 62

Table 4.5.4 Analytical solution by using Weldge's graphic method and front advance equation at different yield stress..... 62

Table 4.5.5 Data for validation of yield stress model with Friedel's work 65

Table 4.5.6 Relative permeability for validation with Friedel's work 66

Table 4.5.7 Validation results for the case dimensionless conductitivity, $C_r = 31$ 66

Table 4.5.8 Field Data (from May, 1997) 67

Table 4.5.9 Calculation of PI from simulation results for the case with yield of 3 pa from SABRE 69

CHAPTER I

INTRODUCTION TO TIGHT GAS FRACTURING

A tight gas reservoir is a low-porosity, low-permeability formation that must be fracture treated to flow at economic gas rates and to recover economic volumes of gas. Figure 1.1 shows that conventional sandstone (left) has well-connected pores (dark) and the tight gas sandstone (right) has irregular small pores that are poorly connected. Without a fracture treatment, gas from tight gas reservoirs will produce at low flow rates under radial flow conditions. After a successful fracture treatment, the gas flow mechanism in the reservoir will change from radial flow to linear flow as shown in Figure 1.2. As the propped fracture length increases, the well will produce more gas at higher flow rates provided that adequate fracture conductivity is also created.

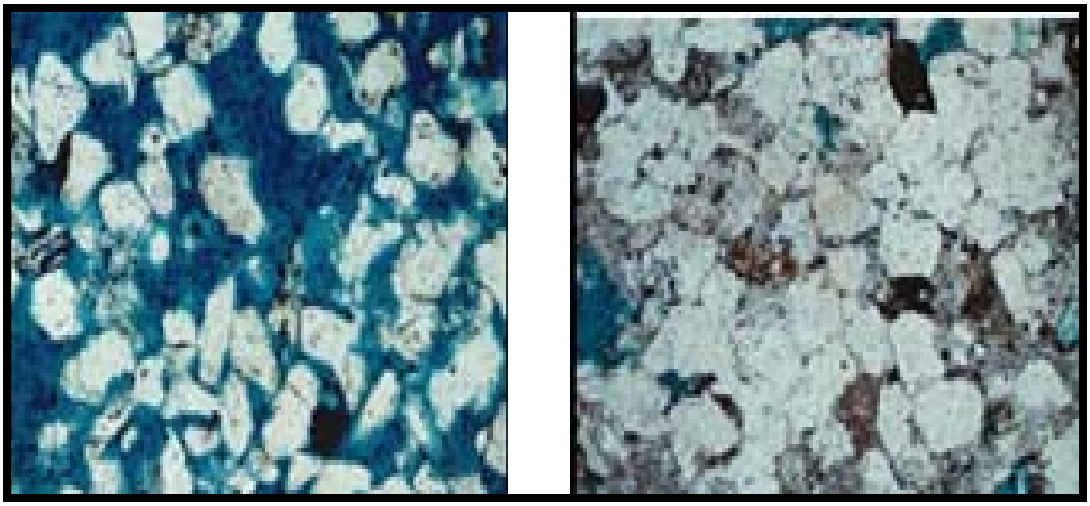

Figure 1.1—Microscopic section of conventional sandstone and tight gas sandstone (from DOE National Energy Technology Laboratory)

This dissertation follows the style of journal *SPE Production and Operations*.

Unconventional tight gas reservoirs have two distinct features that drive the optimal use of hydraulic fracturing: very low matrix permeability, which means that very long hydraulic fractures are desirable, and the presence of natural fractures, which may fundamentally alter the fracturing process.

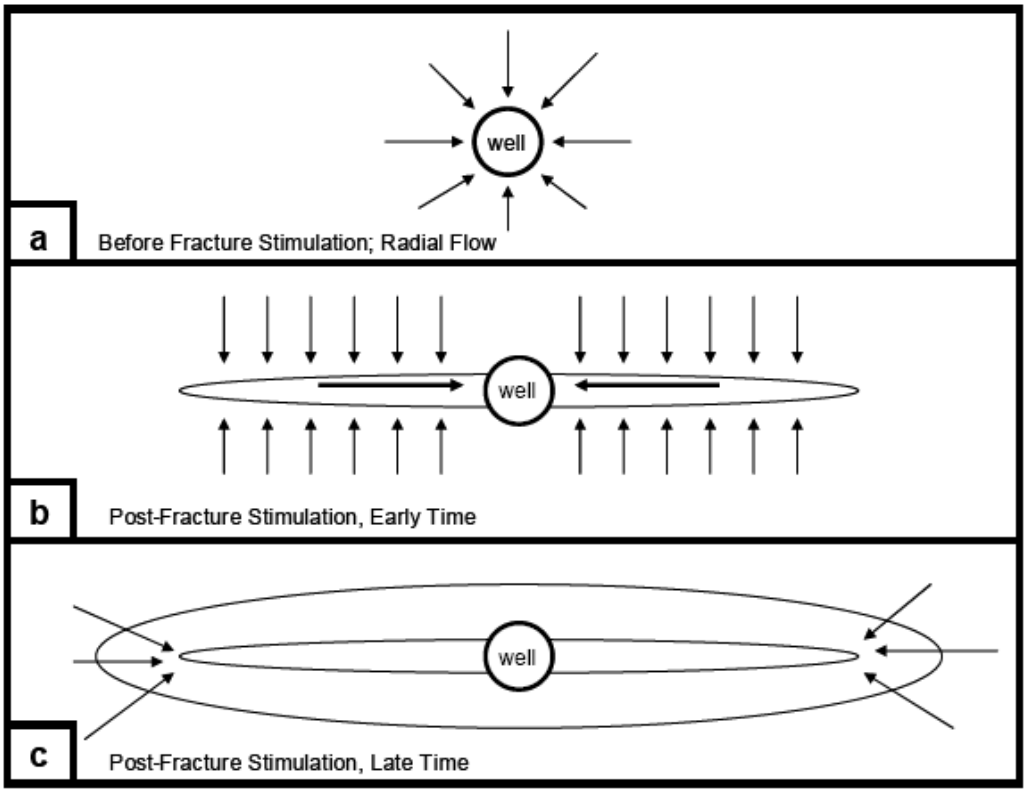

Figure 1.2—Gas flow mechanism before and after fracturing (from Holditch 2005)

Tight gas reservoirs are found at all depths in many geological basins around the world. The key to producing gas from a tight gas reservoir is to create a long, highly conductive flow path (a hydraulic fracture) to stimulate flow from the reservoir to the wellbore. To maintain conductivity in the fracture, sufficient quantifies of propping agent need to be pumped into the fracture. To carry high proppant concentrations deep into the fracture, we use viscous fluids. However, these same viscous fluids need to break back to thin fluids after the treatment is over so that the fracture fluid can clean up.

There are actually three values of fracture length that must be evaluated in any design. First, we must determine the **created fracture length**. This is the value of the crack length in the rock and can be estimated with fracture propagation models. Second, we need to estimate the **propped fracture length**. The propped length is the distance in the fracture from the wellbore that contains propping agents. In many cases, the propped length will be 70 to 80% or more of the created length. However, what really counts is the **effective fracture length**. The effective fracture length is that part of the propped length that has a high enough proppant concentration to allow the fracture fluid to clean up so natural gas can flow in the fracture. Unfortunately, the effective fracture length is often 10 to 50% of the propped fracture length.

In many situations, the created length was probably achieved, and maybe even the propped length was achieved. However, due to insufficient proppant concentration, or insufficient proppant transport, or the use of the wrong propping agent, or a fracture fluid that does not break to a low viscosity fluid, the effective fracture length does not provide optimal production results.

In deep, high-temperature (above 270^{o}F) reservoirs, the polymers normally used to create viscosity will break down and the fluid will clean up after the treatment. In deep reservoirs, we have to pump high concentrations of high-strength proppant to keep the fracture open. The use of gelled fracture fluid has proved to work well in deep, high-temperature reservoirs because the temperature causes the gel to break and allows the fluid to clean up. In fact, in many reservoirs we have to add gel stabilizer to keep the fluid from breaking too soon.

In shallower, lower-temperature (less than 250^{o}F) reservoirs, the choice of a fracture fluid is critical to the success of the treatment. We still need viscosity to carry proppant deeply into the fracture. However, unless the correct breakers are used, the viscous fracture fluids will not break, and the gel may cause significant damage in the fracture. We believe that better stimulation fluids can be developed for these low-temperature, tight gas reservoirs if we can better understand and model the physics of fracture fluid flow and polymer behavior inside the fracture and reservoir formation.

A water fracture treatment is a fracturing treatment using low concentrations of polymer in the fluid, less than 20 lb_m/1000 gallons, and low proppant concentrations, less than an average of 0.5 lb_m/gal (Griesser, 2003). Driven as much by economics (cost-savings) as by technical benefits, operators have increasingly used so-called "water fracture treatments" instead of more conventional gel fracture treatments over the last fifteen years in many unconventional reservoirs. The smaller amounts of proppant and polymer used in these treatments reduce the costs substantially; however, they also result in much less proppant being placed in the created fractures.

There is substantial evidence in the petroleum literature that the productivity of unconventional gas wells increases proportionately to the amount of proppant placed, even with water fracture treatments, such as are being applied in the Barnett shale (Coulter et al., 2004). In many tight gas provinces where conventional hydraulic fracture treatments are widely applied, the well productivity created increases proportionately to the amount of proppant placed (Coulter et al., 2004; Holditch and Ely, 1973). One explanation for the popularity of water fracture treatments is that they appear to clean up more easily than gelled fracture treatments in low temperature reservoirs. However, to judge the success of any fracture treatment, one also has to look at gas recovery over a 5-10 year period.

We believe that water fracture treatments are not optimal in many tight gas sand reservoirs, and a better stimulation method can be developed for the low-temperature tight gas reservoirs. To improve the fracture treatments, we first need to understand and model the physics of fracture fluid flow and polymer behavior inside the fracture and reservoir formation. After we better understand the problems, we can develop new methods for creating extensive, conductive hydraulic fractures and accelerate the cleanup process and gas production in unconventional tight gas reservoirs. The further understanding in this area will enable economic production from unconventional gas reservoirs and add substantial unconventional gas reserves to the world's future gas supply.

CHAPTER II

LITERATURE REVIEW OF FRACTURE DAMAGE MECHANISM

In this chapter, fracture damage mechanisms will be investigated through literature review of all factors affecting cleanup. All relevant research in this area—either from laboratory experiments and mathematical models or from field studies—has been investigated. The research objectives and the procedures to obtain the objectives are presented at the end of this chapter. The outline for this chapter is:

- Fracture damage mechanism and cleanup process
- Post-fracture evaluation
- Research objective
- Research procedure

2.1 Fracture damage mechanism and the cleanup process

The petroleum literature suggests that gel fracture treatments have such high residual damage from unbroken gel in the fracture that the residual conductivity is no better than that created with a water fracture treatment with considerably less proppant. The literature also suggests that gas flow rates and recoveries from many hydraulically fractured tight gas wells fall short of expectations. One of the possible reasons, especially when cross-linked polymer fluids are used in reservoirs with bottomhole temperatures of 250 ^{0}F or less, is that polymer concentrates in the fracture and does not clean up properly.

Holditch (1979) investigated various factors affecting water blocking in fractured gas wells and found that reservoir properties such as capillary pressure, change of capillary pressure and relative permeability are extremely important in determining the cleanup behavior. Also if the reservoir rock permeability is damaged by fracture fluid invasion, a large pressure drawdown will be needed to overcome the capillary end effect, or the water is trapped and a complete block of gas flow will occur. If reservoir permeability is not damaged, no serious water block will occur if the pressure drawdown is much greater than capillary pressure or capillary pressures are large enough to imbibe the fracture water further into the formation. Otherwise, the gas production can be severely curtailed. Figure 2.1 shows that flow is initiated close to the wellbore area and then the fracturing fluid cleans up gradually along the fracture as the production continues. Tannich (1975) concluded that permanent damage was not likely if fracture conductivity was high relative to the formation's. The fracture would clean up quickly if the fracture fluid would break to provide a low viscosity after treatment. Tannich stated that one-half of the fracturing fluid injected would be recovered within 2 to 6 days provided the gel broke and the fracture conductivity was sufficient. He suggested that gas would enter the fracture near the wellbore if the fracture conductivity were low, and the effective fracture length and well productivity would increase with time. However, his model did not consider capillary forces in the reservoir, closure stress effects, or damage in the fracture or the formation surrounding the fracture.

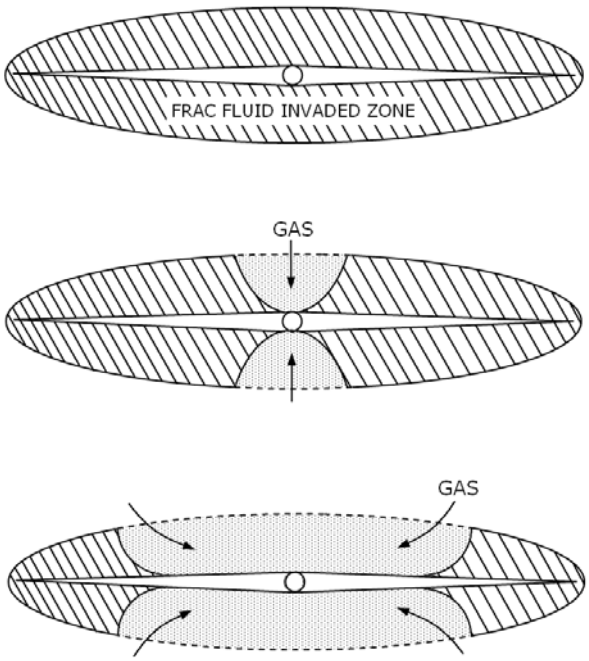

$t_1 > 0$

$t_2 > t_1$

$t_3 > t_2$

Fig. 2.1—Schematic of cleanup model by Tannich 1975

Recently Gdanski *et al* (2005) simulated fracture face damage and concluded that fracture face permeability damage of 90% or higher can cause a major increase in water production and reduction in gas production. Cinco-Ley and Samaniego (1981) provided a relationship for estimating the fracture face skin on well productivity. Lolon *et al* (2003, 2004) studied the effect of fracture conductivity using water-based fracturing fluids and drew conclusions that higher fracture conductivity would result in faster fracture fluid cleanup, longer effective fracture length, and greater cumulative gas production. The fracture cleans up faster with higher gas flow rates, and effective length is affected more by fracture conductivity than by formation permeability, fracture closure effects, and reservoir water mobility. Lolon looked only at Newtonian fluids.

Most fracture fluids are actually non-Newtonian and are affected by yield stress. The effect of yield stress on fracture fluid cleanup has recently been investigated by several groups. Balhoff and Miller (2002) derived an analytical model for yield stress to predict fracture fluid cleanup by incorporating fracture geometry (length and width) and fracture and reservoir properties (pressure, permeability, porosity and proppant diameter). Yi (2004) derived a model for non-Newtonian fracture fluid and used parametric analysis to study the effects of rheological parameters and injection rate. He concluded that if a pressure gradient is not high enough to overcome the yield stress, the polymer will not flow and high flow rate increases cleanup. May *et al* (1997) studied the effect of yield stress on fracture-fluid cleanup using a numerical simulation model. For the case they studied, May *et al* concluded that increasing drawdown did not affect the amount of cleanup, but increasing the fracture conductivity did increase the effective fracture length. However, their study did not consider the effect of capillary pressure, fracture face damage, or other factors.

A study by Cooke (1975) showed that the polymer residue can be trapped in the fracture. Other work suggests that polymer residue may leak off into the formation and be trapped in the invaded zone around the fracture. Siddiqui *et al* (2004) reported that some of the gel residue is present in the rock and cannot be displaced by production; it degrades and

is removed slowly. This residue occupies the pore spaces of the rock and reduces the rock permeability. They concluded that the structure and mineralogy of the formation rock play significant role in determining the amount of gel residue in the formation. A certain portion of the gel residue (as high as 25%) remains in the core plug and cannot be recovered by the cleanup process.

Generally, fracture damage falls into two categories: One is damage inside the fracture, and the other is damage inside the formation. Damage inside the fracture can be caused by proppant crushing, embedding, fracture face damage, or fracture plugging with chemicals and polymers. Damage inside the reservoir can be caused by excessive fluid leakoff, clay swelling, relative permeability hysteresis, and capillary effects. Of course, many other factors will affect the cleanup process such as pressure drawdown, fracture geometry, non-Darcy flow effect, fracture conductivity, heterogeneity, formation temperature, fracture fluid viscosity, viscous fingering, gel residue, breaker, and operational procedures.

The main causes of fracture face damage are polymer squeezing, clay swelling, proppant embedment, and proppant crushing. The damage caused by clay swelling can be minimized by properly choosing the base fluid during a fracture treatment. Polymer squeezing can be very critical though it can be reduced if suitable breakers are used in the fluid. So we believe that fracture fluid, especially the polymer, can be a big problem during the cleanup process and we will address this issue in more detail both experimentally and mathematically.

All of these referenced studies have led to a better understanding of fracture damage and the cleanup process. Fracturing fluids and proppants have been improved in recent years to enhance the cleanup process. However, many fracture treatments, particularly in shallow, tight gas reservoirs, seem to fall short of expectations and produce gas at a lower flow rate.

It is our opinion that insufficient fracture fluid cleanup is the primary cause of poor results when the optimal effective fracture length is not achieved. Fracture fluid cleanup

is affected by the static yield stress, the flowing yield stress, the amount of polymer residue in the fracture after the fracture closes, and the amount of polymer that forms a filter cake on the walls of the fracture. In addition, there are other issues such as proppant crushing, non-Darcy flow effects, multiphase flow effects, and operational conditions that also affect fracture fluid cleanup.

Some conclusions from literature review are summarized as follows:

1. Fracture damage with 90% or higher reservoir formation permeability loss will decrease the gas production rate (Gdanski et al., 2005).
2. High fracture conductivity will help the fracture fluids to clean up after the fracture treatment (Lolon et al., 2003; May et al., 1996; Tannich, 1975).
3. Capillary pressure will affect fracture fluid cleanup. The higher the capillary pressure, the less fluids will be recovered (Holditch, 1976). To recover more of the fracture fluids, we need to use surfactants and increase the pressure gradient in the fracture.
4. A large pressure drawdown helps to clean up the fracture fluid more quickly and produce more gas as long as the fracture propping agent is not crushed. However, not all of the fracture fluid can be recovered during the cleanup process. (Lolon, 2004)
5. It is necessary to take relative permeability hysteresis into account in the mathematical analysis of the cleanup process and well productivity performances (Holditch, 1979).

2.2 Post-fracture evaluation

To evaluate the cleanup process and optimize the performance of a hydraulically fractured tight gas well, reliable estimates of effective fracture length and effective fracture conductivity are essential. We have to use post-fracture production and pressure data to evaluate the effective fracture length and fracture conductivity. A brief summary of the methods and current techniques are given here on how to determine the fracture and reservoir properties during the post-fracture treatment evaluation.

Carr and Yang (1998) proposed an improved flowback analysis for the evaluation of polymer damage and treatment load recovery. The cumulative polymer recovered can be measured by using their method. Samuelson and Constien (1996) presented laboratory fracture conductivity and residual polymer analysis for degraded fracture fluid at temperatures above 180^0F and provided correlations of fracture permeability with volume of polymer recovered. Their results are verified by field data.

Lee and Holditch (1981) presented the results of pressure transient analysis of thirteen hydraulic-fractured, low-permeability gas wells and discussed the major strengths and weaknesses of analysis methods including Horner analysis, linear flow analysis, type curves and finite difference reservoir simulation. They showed that using some of these analysis methods, the calculated fracture half-lengths were only 5% to 11% of the designed lengths. However, fracture lengths determined from reservoir simulation history matching were about 68% of the designed lengths. Later Holditch also found out that non-Darcy flow in the fracture is one reason that the calculated fracture length is significantly less than the designed length even after a long period of shut-in time. If substantial non-Darcy flow occurs in the fracture, the calculated fracture lengths using conventional techniques are less than designed lengths when the data are analyzed using methods that do not include non-Darcy effects.

Hresko (1985) suggested that if the fracture conductivity is high (C_r is greater than 1,000), non-Darcy flow has no effect on pressure drawdown and buildup type curve shapes. However, if the C_r value is less than 1,000, the non-Darcy flow effect can make a big difference.

The integration of available data such as well tests, production data, fracturing data, well logs, and core analysis data is helpful in evaluating hydraulically fractured wells. Elbel and Ayoub (1992) gave a variety of reasons for apparent shorter fracture lengths: insufficient shut-in time, cleanup effects, use of homogeneous models and non-Darcy flow effects.

Barree *et al* (2003) proposed an empirical method for predicting the effective fracture lengths from proppant conductivity data for a low-pressure tight gas reservoir in the Rocky Mountain Region. Their calculated fracture lengths under flowing conditions are only 3% of the designed values accounting for all of the conductivity losses.

2.3 Research objectives

Fracture fluid cleanup is a complicated process. Even though a lot of research has been done in this area, we still need better tools to model the cleanup process by understanding the physics of fracture fluid flow and polymer behavior inside fracture.

The overall objectives of this research have been to:

- Identify mechanisms that affect the fracture fluid cleanup process;
- Develop mathematical expressions and computer code to model the cleanup process;
- Link the new code to a 3D, 3-phase reservoir simulator to investigate the fracture fluid cleanup process and long-term gas recovery in tight gas reservoirs;
- Run parametric studies to understand the factors affecting cleanup; and
- Develop new ideas to improve fracture fluid cleanup.

2.4 Procedures used for this research

1. Perform a detailed literature search to review all papers with information concerning laboratory measurements, field case histories, and mathematical analyses of the fracture fluid damage and the cleanup process, especially the behavior of polymer fluids.
2. Derive and validate the mathematical expressions to describe fracture fluid and fracture fluid slurry behavior as it flows down a fracture, leaks off into formation, breaks down in the fracture, and flows back to the well through the fracture or imbibes into the reservoir.
3. Couple the mathematical models derived in Step 3 to the 3D, 3-phase version of SABRE. SABRE is a model developed by Texas A&M University and S.A. Holditch & Associates, Inc. and was donated to Texas A&M University by Schlumberger. We have converted the oil/gas/water model into a gas/water/fracture fluid model. The resulting code is for a single well containing a

vertical fracture in a gas reservoir. The model will be the "ultimate fracture fluid cleanup model" by incorporating all the features necessary to simulate the problem correctly.

4. Validate the model using analytical solutions, experimental data, and field data.
5. Run parametric studies to understand the factors affecting the fracture fluid cleanup process, and how the integration of all the processes modeled can be used to explain the observed cleanup in the field.
6. Use the integrated model to develop new ideas on how to better clean up a well after a fracture treatment.

CHAPTER III

SIMULATION METHODOLOGY

The reservoir and hydraulic fracture properties used in this study have been chosen after reviewing typical fracture treatment data and also based on previous research conducted by previous teams at Texas A&M University. A data set from over 150 wells in the Moxa Arch Frontier formation in southwest Wyoming was provided by Norton Proppants Inc. and consisted of injected fluid and estimated leakoff volume, average fluid viscosity, fracture gradient, reservoir permeability, pore pressure, and proppant concentration. In addition, we have used published data on tight gas wells and laboratory experimental data on fracture fluids and fracture conductivities. We have improved a reservoir simulator to be able to study factors such as yield stress, polymer residue, filter cake, gravity, and proppant crushing during the cleanup process. This chapter is divided into five sections:

- Fractured well model;
- Reservoir, fracture, and fluid properties;
- Initiation of simulation;
- Polymer gel properties; and
- Simulation runs.

3.1 Fractured well model

We used a 3D, 3-phase black oil simulator to model the fracture fluid cleanup and long-term gas production in a tight gas well. Figure 3.1a shows a schematic of the fractured well model used in this study and Figure 3.1b show the gridding, created fracture length, propped fracture length, and effective fracture length. Because of the symmetry of the well configuration, we simulate just ¼ of the drainage area from a fractured well. The gridding details are shown in Appendix A. We assume that the fracture extends an equal distance on two sides of the wellbore and fully penetrates the formation. The fracture length, width, and fracture fluid volumes were obtained by running a fracture design model. The relationship between fracture fluid volume, created half length, and zone thickness are shown in Figure 3.2. The width of the fracture is assumed to be constant from the wellbore to the tip, while the porosity of the fracture is 30%. The reservoir is assumed to be homogeneous and isotropic.

Table 3.1—Data for simulation run of a fracture design software

Reservoir fluid type	Gas
Gas gravity	0.6
Bottom hole temperature	275^{o}F at 12,300 ft
Reservoir pressure gradient	0.55 psi/ft
Overburden pressure gradient	1.05 psi/ft
Casing	5.5”, 23 lb/ft, N-80
Fracture fluid	HPG 40lbm/1,000gallons
Well spacing	160 acre

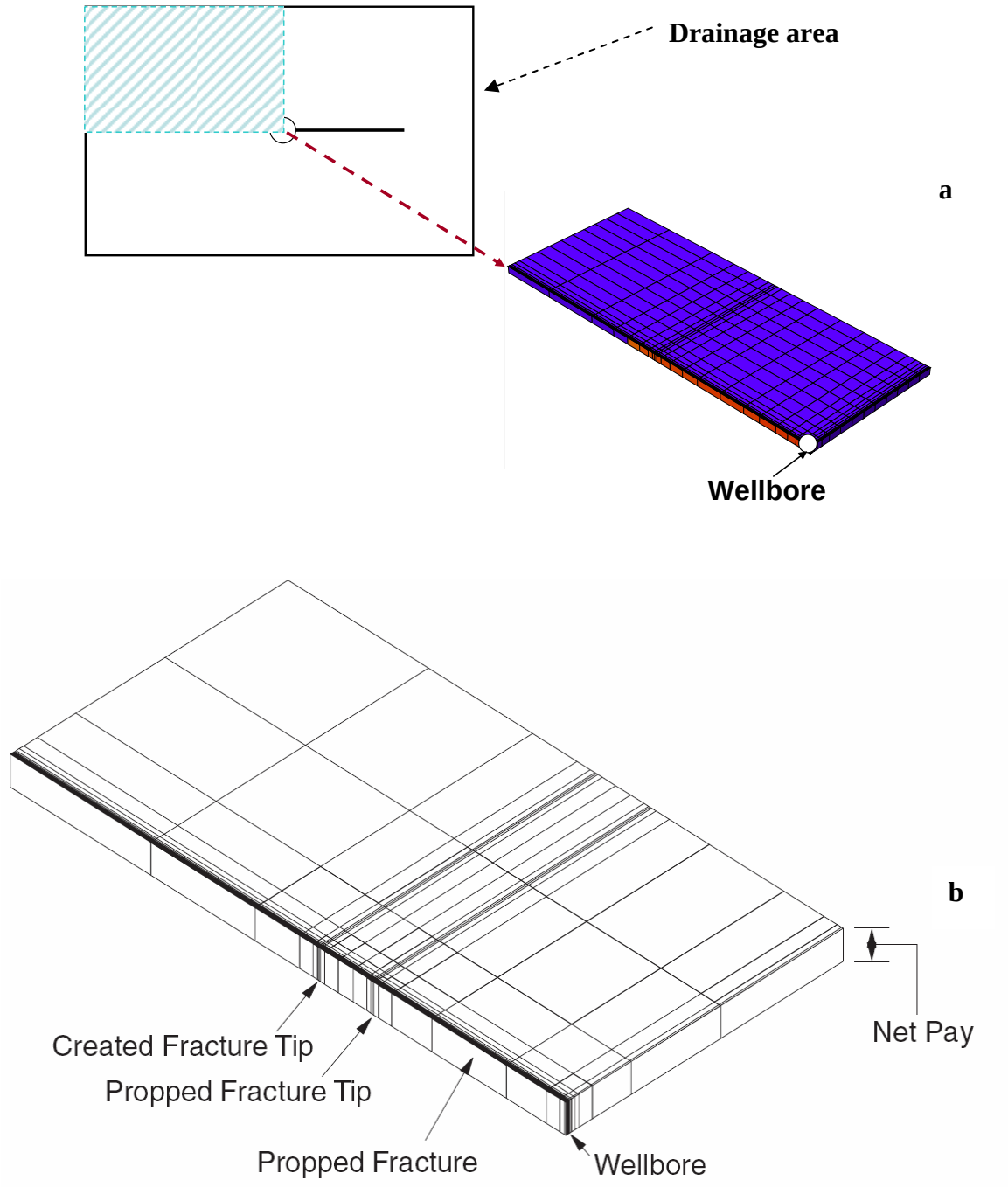

Figure 3.1—Hydraulically fractured well simulation model

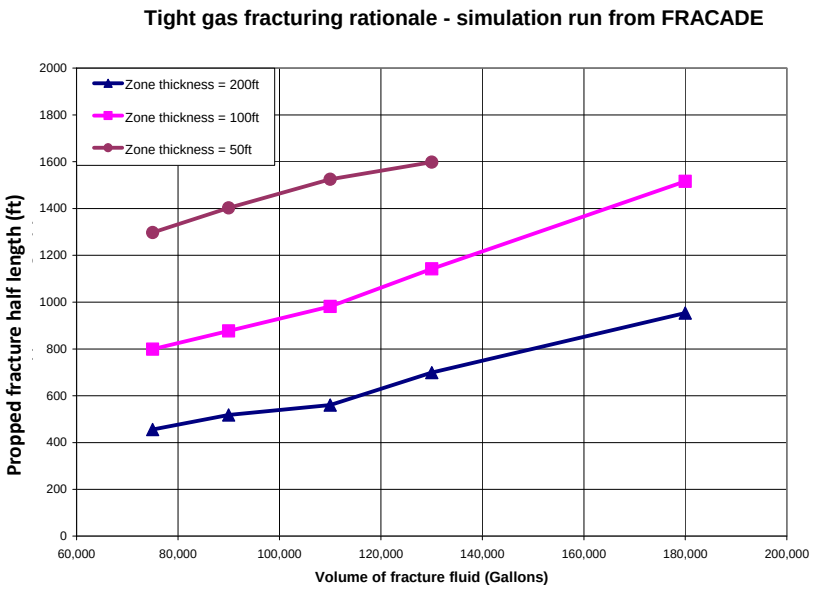

Figure 3.2—Correlation of injected fracture fluid volume, propped half length, and zone thickness

Table 3.1 shows the data used in running the fracture design software. Figure 3.2 shows the fracture fluid volume required to create fracture lengths as a function of created fracture height. If one tries to run a simulation for fractured tight gas wells, based on the formation thickness, reservoir permeability and fracture fluid volume, it is easy to pick a reasonable fracture length as input data into the simulator. However, to perform a simulation study for a specific well, where the injected fracture fluid volume, formation thickness, and other reservoir formation and fluid properties are already known, a fracture design simulation is recommended to get a more realistic propped fracture length.

Grid dimensions in the fracture direction are varied as that the grids are very small in the fracture plane near the wellbore, increase towards the middle of the propped fracture half-length, decrease until the tip of the propped fracture, and increase again to the drainage boundary. In this study, the fracture length that is propped open during the fracture treatment is referred to as the "created" fracture length. The length supported by proppant after the fracture treatment is defined as the "propped" fracture length. This gridding technique was used by others (Lolon, 2004; and Voneiff et al., 1996) for

research work and field studies. Lolon verified the model by back-calculating the input parameters using pressure transient analysis and found that proper selection of time steps and grid-cell sizes would be the key to a correct simulation study of fractured tight gas well.

The wellbore is in cell (1x1x1) as shown in Figure 3.1, and is operated at constant bottomhole pressure (BHP). All simulation results—which include gas production rate, cumulative gas production, saturation maps, and pressure maps—are presented just ¼ of drainage area because our simulation configuration and strategy. The real gas production from the well should be four times of that in our figures. However, the gas recovery and percentage of fracture cleanup should not be affected.

3.2 Reservior, fracture, and fluid properties

The reservoir and fracture properties used in this study are presented in Table 3.2. For this work, we kept the drainage area, net reservoir thickness, and water saturation constant. The initial reservoir pressures are 5,580 psi ("high" pressure cases), 3,720 psi (“intermediate” pressure cases) and 1,860 psi ("low" pressure cases), which correspond to formation depths of 12,000 ft, 8,000 ft, and 4,000 ft with a normal pressure gradient of 0.465 psi/ft. The reservoir permeability investigated varies from 0.001 to 0.1 md (tight gas reservoirs). The fracture half length of 264 ft, 528 ft and 924 ft represent fracture penetrations (L_f/x_e) of 0.2, 0.4, and 0.7 respectively of the drainage length (x_e), which was 1320 ft for a 160 acre well spacing. The values of dimensionless fracture conductivity ($C_r = k_f \cdot w/\pi k \cdot L_f$) range from 0.1, 1, 10, to 100.

The pressure gradient is the change in pressure per unit of depth, typically in units of psi/ft or kPa/m. Pressure increases predictably with depth in areas of normal pressure. The normal hydrostatic pressure gradient for freshwater is 0.433 psi/ft (9.792 kPa/m) and 0.465 psi/ft (10.516 kPa/m) for water with 100,000 ppm total dissolved solids (a typical gulf coast water). Formation pressure tends to increase with depth according to the

pressure gradient. Some basin type tight gas reservoirs tend to be over pressured (Sulliven *et al* 2005).

The geothermal gradient is the rate of increase in temperature per unit depth in the earth. Temperatures at the surface of the earth are controlled by the sun and the atmosphere, except for areas such as hot springs and lava flows. From earth's surface to a shallow depth (400 ft), the gradient is variable because it is affected by atmospheric changes and circulating ground water. Below that zone, temperature almost always increases with depth. However, the rate of increase with depth (geothermal gradient) varies considerably with both tectonic setting and the thermal properties of the rock. High gradients (up to 11°F/100 ft, or 200°C/km) are observed along the oceanic spreading centers (for example, the Mid-Atlantic Rift) and along island arcs (for example, the Aleutian chain) (www.enotes.com/earth 2008). The high rates are caused by molten volcanic rock (magma) rising to the surface. Low gradients are observed in tectonic subduction zones because of thrusting of cold, water-filled sediments beneath an existing crust. The tectonically stable shield areas and sedimentary basins have average gradients that typically vary from 0.82 to 1.65°F/100 ft (15–30°C/km). For this study, we choose a geothermal gradient of 1.5 °F/100 ft.

Table 3.2—Basic Reservoir and Fracture Parameters

Base Data Set for Parametric Simulation Study	
Parameter	**Base value**
Drainage Area (acre)	160
Reservoir Thickness (ft)	100
Formation Permeability (md)	0.001, 0.01, 0.1
Formation Porosity (%)	10
Formation Depth (ft)	4000, 8000, 12000
Reservoir Pressure (psi)	1860, 3720, 5580
Reservoir Temperature (^{0}F)	130, 190, 250
Formation Water Saturation	0.4
Water Compressibility (psi^{-1})	3.00E-06
Gas Specific Gravity	0.6
Fracture Half Length (ft)	264, 528, 924
Dimensionless Fracture Conductivity	0.1, 1, 10, 100
Fracture Fluid (mgallon)	105, 235, 420
Bottomhole pressure	10% of reservoir pressure
Fracture Fluid (gallon)	80000

To model the multiphase flow, we used two-phase or three-phase relative permeability curves depending on the situation being modeled. A set of curves measured from tight gas cores in east Texas were used, as shown in Figures 3.3a and 3.4 (Holditch 2005). The Stone II method was applied to compute the relative permeability for the third phase – gel. These figures show the relative permeability curves, the first one Figure 3.3a for flow in the reservoir formation and Figure 3.3b and 3.3c for flow inside the fracture. The fracture relative permeability is represented by two 45° lines, with the water relative permeability becoming zero at zero water saturation. However, we want to point out that this is hypothetical based on fluid flow in highly conductive, smooth, parallel fracture planes, and the real curve should be non-linear. We will address this issue in the section of relative permeability and capillary pressure in Chapter IV. The irreducible water saturation is assumed to be 40% in the reservoir.

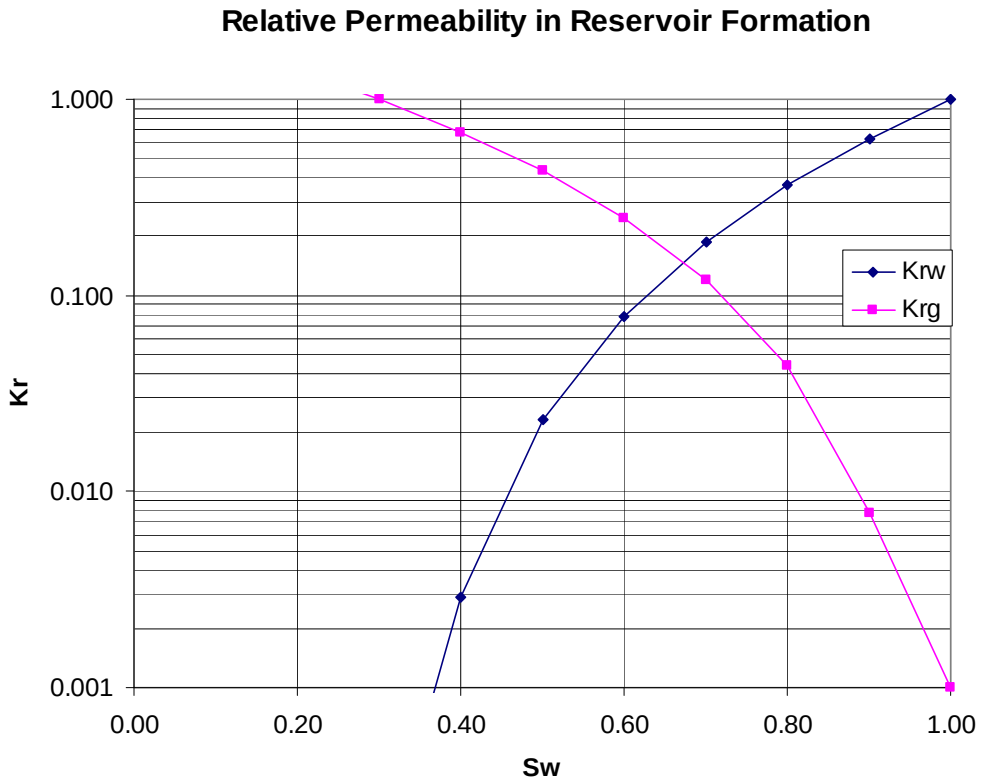

a

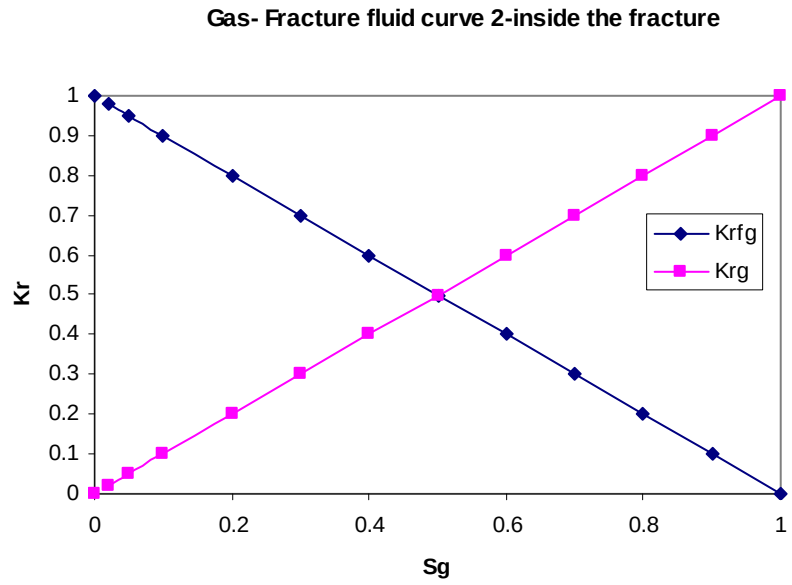

b

Figure 3.3—Relative permeability curves

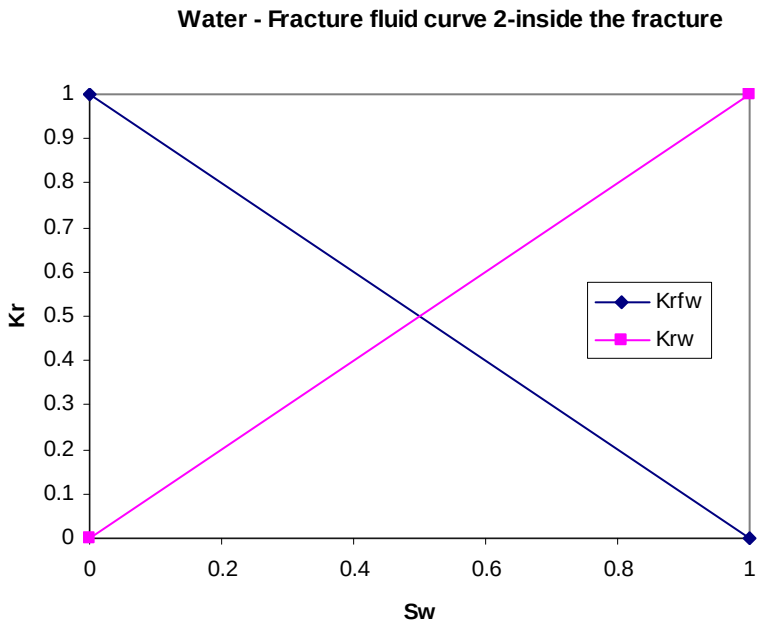

c

Figure 3.3—Continued

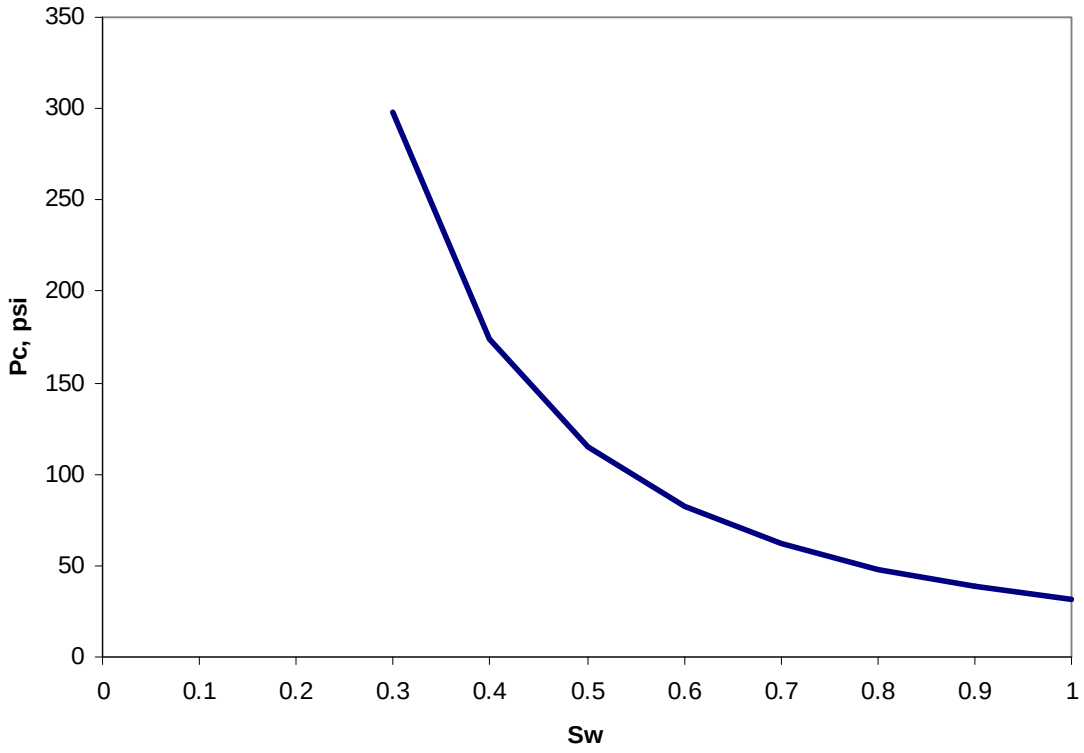

Figure 3.4—Capillary pressure curve in the reservoir formation (from Holditch 1979)

For detailed reservoir, fracture and fluid properties, please refer to the data file in the Appendix A.

3.3 Initiation of simulation

The fracture fluid was injected into the reservoir to create a filtrate zone, first water injection and then gel. The fracture fluid leaked off into the reservoir formation, created a water zone around the fracture, and built a polymer face inside the fracture. Because of the tight formation, we assumed the polymer gel phase stayed inside the fracture and displaced all the gas and water out of the propped fracture by the end of the treatment. Then we took the three saturation tables as initial conditions for all simulation runs for the convenience of comparison. The initial gas and water saturation maps are shown in Figure 3.5 and Figure 3.6.

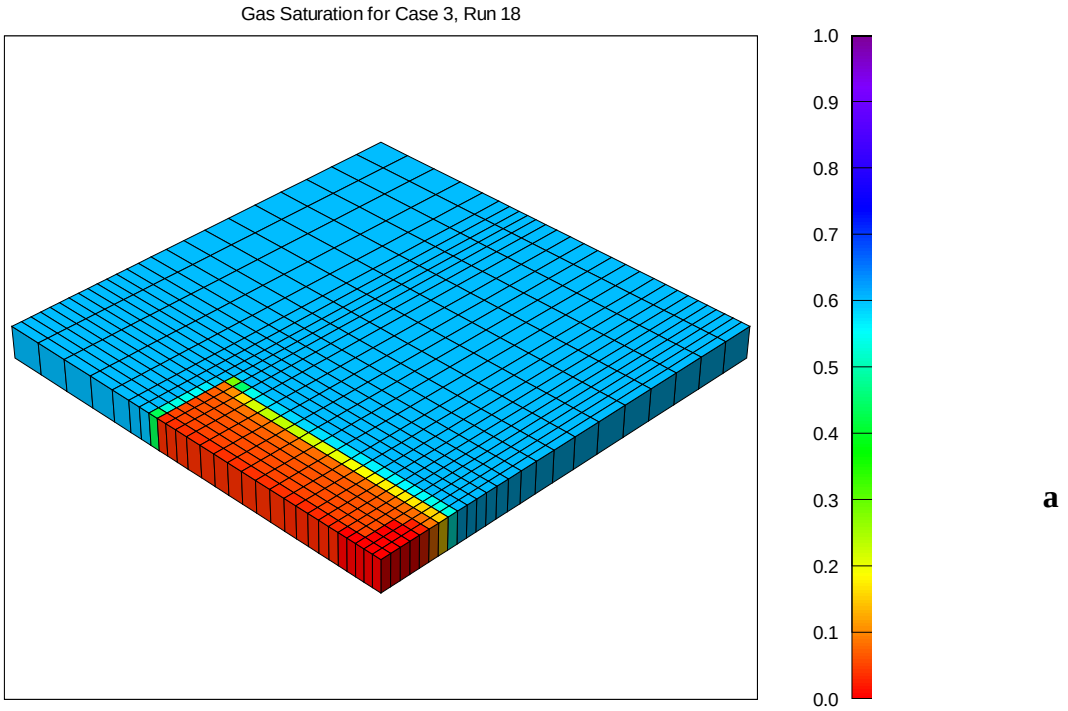

Figure 3.5—Gas saturation map after a fracture treatment with 80,000 gallons of fracture fluid

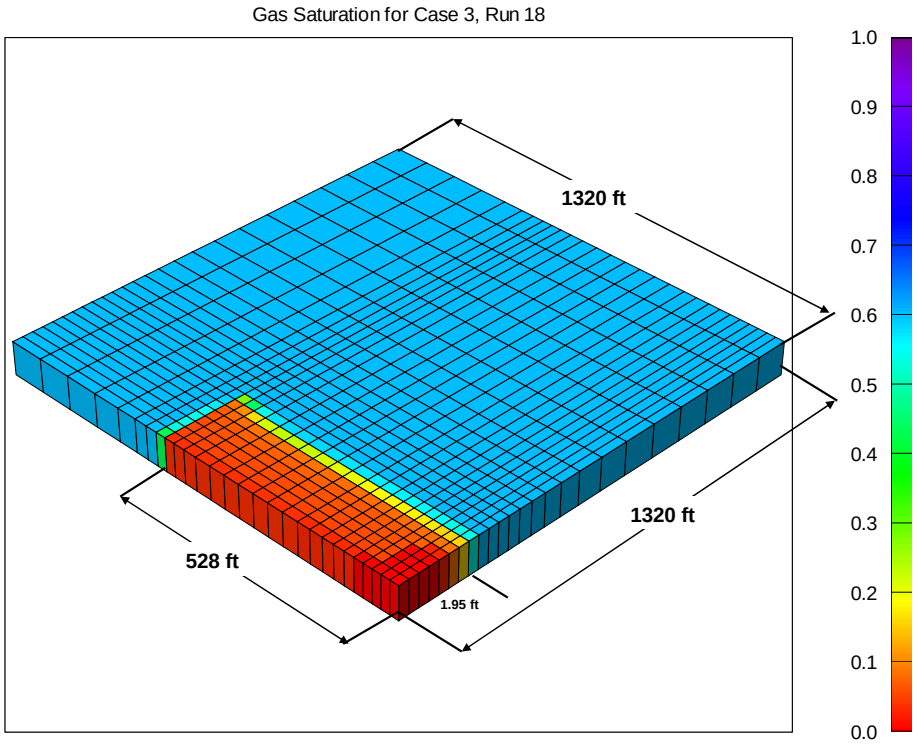

b

Figure 3.5—Continued

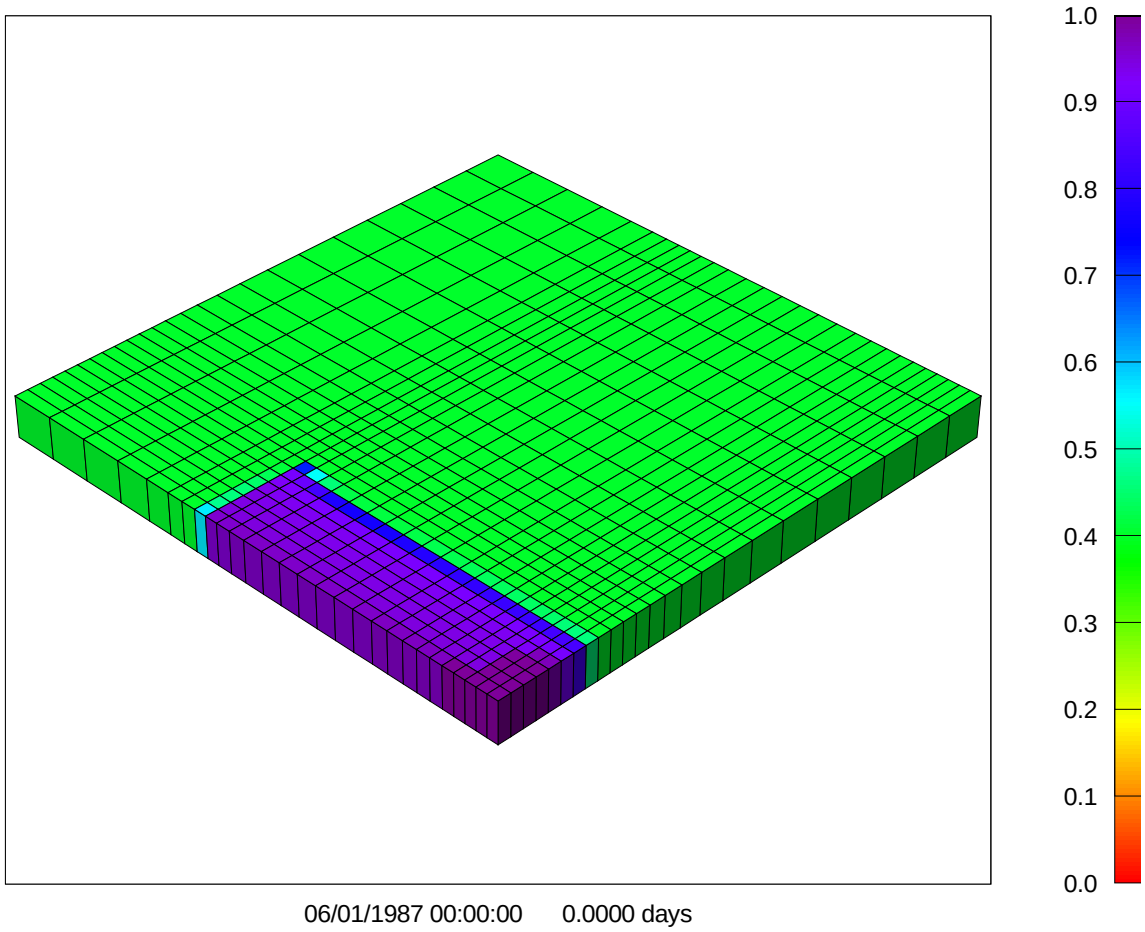

Figure 3.6—Water saturation map after a fracture treatment with 80,000 gallons of fracture fluid

Figure 3.5 and Figure 3.6 show the gas and water saturation distribution after a fracture treatment. Figure 3.5a and Figure 3.5b are the same saturation map, but Figure 3.5a shows the real scale, while the grids in Figure 3.5b has been expanded to be able to see the leakoff zone around the fracture. The fracture fluid has displaced the gas further into the reservoir formation and created a water zone abound the fracture. For this case, the water saturation is 0.4, and gas saturation is 0.6. After treatment, the saturations are shown in Figure 3.6, with 100% gel inside the fracture.

3.4 Polymer properties

The objective of a hydraulic fracturing treatment is to create a conductive fracture in gas producing zones, which allows reservoir fluid to flow from the reservoir through the fracture to the wellbore. Viscous fracturing fluid is pumped to suspend and transport proppant into the fracture. The viscous fluid should break into a low-viscosity fluid after the treatment is completed. Selection of the fracturing fluid, job design, and flowback procedures all help to determine the productivity of a well after the hydraulic fracture treatment. Guar based polymers are used in most treatments. The recent trend has been to design fracture treatments using the minimum amount of polymer required to pump the treatment successfully. To correctly model the cleanup process and long-term production in tight gas reservoirs, we need a clear understanding of the effect of polymer on fracture conductivity and cleanup behavior.

Water-based fracturing fluids are currently used on the majority of hydraulic fracturing treatments. Water-based fluids are used because they are inexpensive, available, easy to viscosify, and safe to handle. Water-based fluids use viscosity-enhancing polymers that are common throughout the oil industry, as shown in Appendix B. Though many books and articles have been published on polymers, a brief review of the four most common polymers in the industry is given below to provide background information, advantages, and disadvantages of these polymers.

Guar Gum belongs to the family of galactomannans and is considered to be a natural polymer. Guar is a hydrocolloid that swells upon contact with water to provide viscosity and fluid loss control. Guar gum is derived from the seed of the guar plant that is commonly grown in such areas as India, Pakistan, and occasionally the United States. The guar bean consists of three main components, the seed coat or hull, the endosperm, and the cotyledon. The endosperm portion of the guar seed is the desired portion that is used to viscosify water. The endosperm is ground into a powder and when combined with water, it produces a highly viscous fluid. The refined guar will contain approximately 5 to 15% impurities in the form of the hull and embryo (mostly protein). The impurities

though, have an advantage of giving guar increased fluid loss control. The impurities create a filter cake at the facture interface providing the fluid loss control.

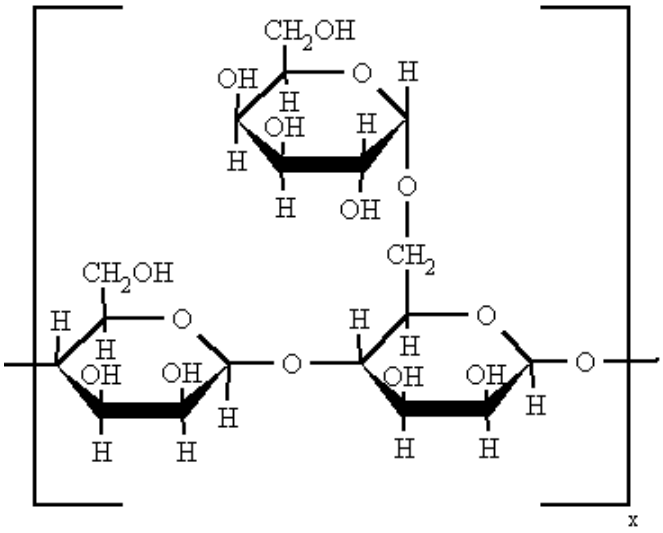

Figure 3.7—Guar molecular structure (from Gidley et al., 1990)

Unfortunately, the impurities can also cause formation damage or a loss of permeability in the proppant pack. Guar is a long-chain copolymer consisting of a mannose sugar backbone and galactose sugar side chains. The average molecular weight of guar ranges upwards from 1,500,000 g/gmol, which is 83,333 times of the weight of water. The typical structure of a nonionic guar molecular is illustrated in Figure 3.7. Guar is capable of hydrating in many different types of water and is capable of tolerating sodium chloride (NaCl) and potassium chloride (KCl) up to 5% by weight. It is also compatible with polyvalent metal ions Ca2+, Mg2+, and Al2+.

The optimal pH range for hydration of guar is 6.5 to 7.5, but guar will still hydrate at a higher or lower pH. Once the guar is hydrated, it is stable at a high pH but not at very low pH. Guar as a linear gel is stable up to 176°F (80°C). The temperature stability can be increased up to 302°F (150°C) for short time periods by cross-linking the gel with a metal ion. Further advances in guar technology have been achieved through reactions to produced guars.

Hydroxypropyl guar (HPG) was developed in the early 1970s as an alternative to natural guar. HPG is manufactured by reacting a highly purified guar stock with propylene oxide. The highly purified guar is achieved by exposing the guar endosperm splits to a series of acid and water soaks to remove the majority of the hull and embryo prior to grinding. The purification reduces the impurities in the guar to approximately 2% insoluble material. The resulting HPG molecule is nonionic. The molecular structure of HPG is shown in Figure 3.8.

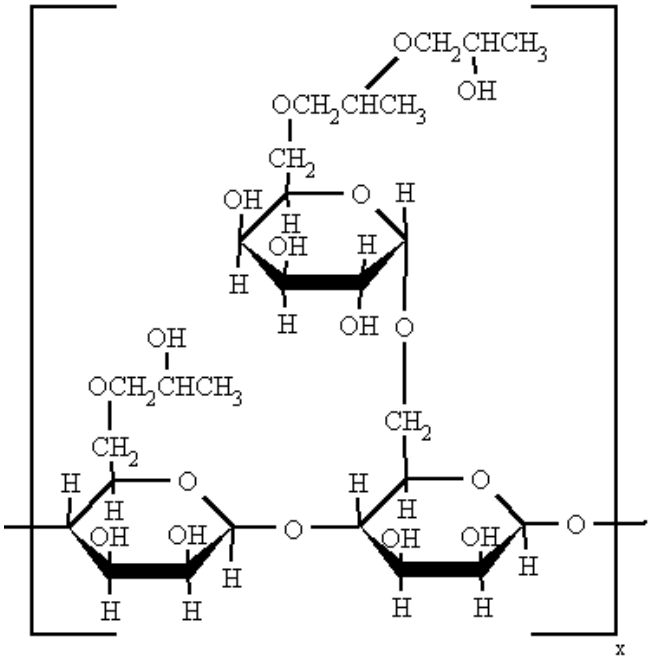

Figure 3.8—HPG molecular structure (from Gidley et al., 1990)

HPG has many advantages over guar making it a versatile viscosifier. HPG hydrates faster than guar and has somewhat higher viscosity at similar concentrations. HPG also has better temperature stability, which is achieved by the addition of the propylene oxide group, which stabilizes the polymer against thermal degradation. Unlike guar, HPG is soluble in water-miscible solvents such as methanol. The reduction of residue limits the filter-cake buildup on the fracture face, which could be a disadvantage in fracturing a high-permeability zone. Therefore, HPG is less damaging, more temperature stable, and methanol compatible, but it has higher fluid loss.

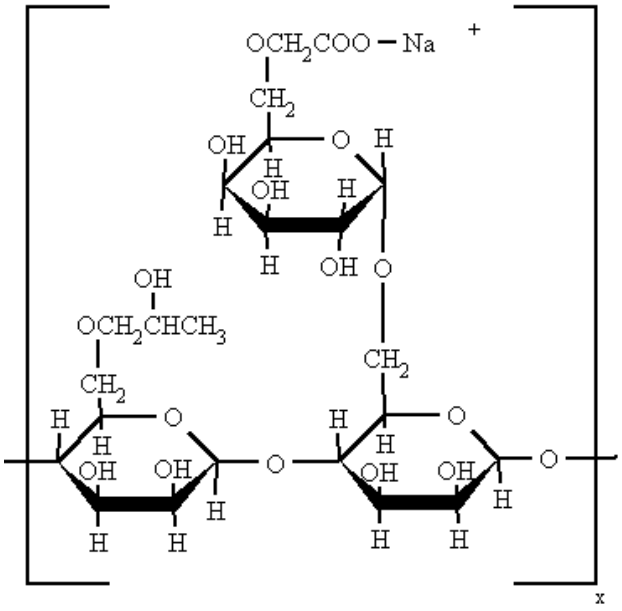

Figure 3.9—CMHPG molecular structure (from Gidley et al., 1990)

Carboxymethylhydroxypropyl guar (CMHPG) is a double-derived polymer by reacting HPG with sodium monochloroacetate. CMHPG has even lower residue than HPG, having only 1 to 2% impurities. CMHPG has better temperature stability than either HPG or guar. In addition, CMHPG hydrates faster than either HPG or guar. The molecular structure of CMHPG is shown in Figure 3.9. Similar to HPG, CMHPG is highly tolerant of water-miscible solvents such as methanol. Methanol concentrations up to 40 to 50% are sometimes used in the industry; therefore, the CMHPG provides a super "clean" gel system. CMHPG is also compatible with carbon dioxide (CO_2) which provides extra potential energy to assist in the cleanup and recovery of the load fluid. Another advantage of CMHPG is its capability to be cross-linked at both high and low PH. Similar to HPG, CMHPG has a common disadvantage in the reduction in fluid-loss control. The disadvantage is the increased cost of CMHPG over HPG and guar.

Hydroxyethylcellulose (HEC) is considered a synthetic polymer. It is formed by modifying natural cellulose from cotton or wood to form the derivative. This product is generated by treating cellulose with sodium hydroxide and reacting it with ethylene oxide. The molecular structure of HEC is shown in Figure 3.10.

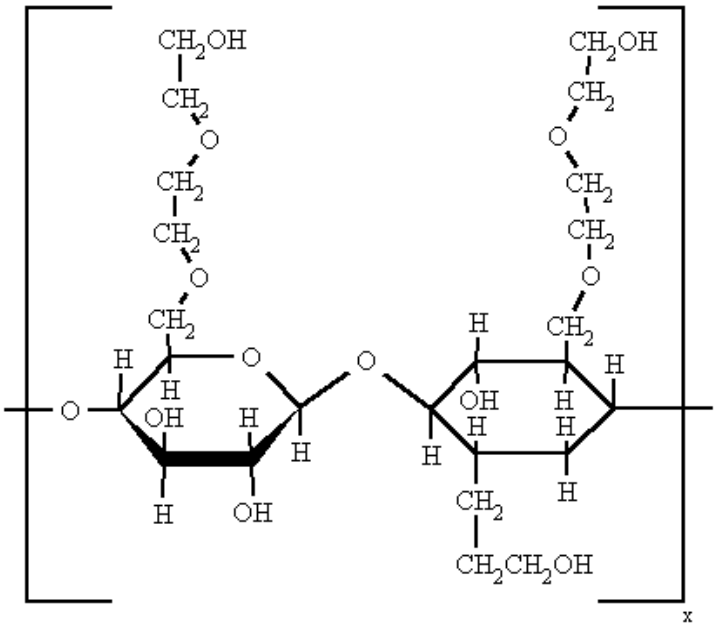

Figure 3.10—HEC molecular structure (from Gidley et al., 1990)

HEC, when hydrated in water, yields a high-viscosity fluid that has essentially no residue upon degradation. However, HEC is difficult to cross-link and is costly; therefore, its use is limited.

Polymer hydration

Ground purified natural polymer particles can undergo intramolecular hydrogen bonding. Because of the disorganized nature of the molecules, the hydrogen bond is not always completed. Therefore, when water contacts the natural polymers, the water molecules penetrate the polymer molecule and hydrogen bond to the available sites. This causes the polymer chain to uncoil, swell, and expose new charged sites for bonding. This process hydrates the polymer. The process continues until each polymer molecule is surrounded by partially immobilized hydrogen-bonded water molecules. This in turn creates viscosity through the interaction of the polymer coils with each other in the water. The rate of hydration is also controlled by the water PH. Guar's optimal pH range is 6.5 to 7.5, while HPG's and CMHPG's is 4 to 5.

Discussion of polymers

One major advance in fracturing fluid technology was the development of cross-linked gels, which are shown in the tables in Appendix C. The first cross-linked gels were developed in 1968 (Ely, 1985). When cross-linking agents are added to linear gels, the result is a complex, high-viscosity fracturing fluid that provides higher proppant transport performance than do linear gels (Ely, 1985). Cross-linking reduces the need for adding fluid thickener and extends the viscous life of the fluid. Cross-linked gels are typically metal ion-cross-linked guar (Ely, 1985). Service companies have used metal ions such as chromium, aluminum, and titanium to achieve cross-linking (Ely, 1985). In 1973, low-residue crosslinked gels, such as cross-linked HPG, were developed (Ely, 1985). According to Table 2 in Appendix C, cross-linked gels may contain boric acid, sodium tetraborate decahydrate, ethylene glycol, and monoethylamine. The fracturing fluid remains viscous until a breaking agent is introduced to break the cross-linker and, eventually, the polymer. Although adding cross-linkers makes the fluid more expensive, it can considerably improve hydraulic fracturing performance for high- and low-permeability formations.

The existing of polymer residue is an important issue in the design of a fracture treatment, in the cleanup process, and in long-term gas production. The residue is the material that remains as an insoluble product upon degradation of the polymer. This is important because it could plug the proppant pack or the formation pore spaces. On the other hand, the polymer provides fluid-loss control on the fracture face by building a filter cake. The filter cake reduces the amount of fluid loss to the formation as the fracture extends, therefore reducing the risk of a tip screenout. The derived polymers, HPG and CMHPG, were developed to have better temperature stability and lower residue. The proper selection of the viscosifying agent for a particular application depends on the formation properties and fracture fluid requirements.

Analysis of the fluid returned to the surface after a hydraulic fracture treatment indicates that usually less than 50% of the guar-based polymer pumped during the treatment returns from the well during the flowback period. Polymer residues that remain in the

fracture may significantly contribute to lower proppant-pack permeability and a less effective fracture treatment.

The field success of a viscoelastic surfactant-based (VES) polymer-free fluid in frac-pack applications has led to the development of a similar fluid for hydraulic fracturing. The VES fluid can be used for the fracturing treatment of potentially all gas and oil wells below 240 ^{0}F (Samuel, 1997). The principal advantage of this fluid system is operational simplicity, and it is easy to break by hydrocarbons or dilute by formation fluids. Other new polymer-free fluids developed by oil and chemical companies in recent years have advantages and limitation during field application. However, we will not discuss all in detail here because they are not in the scope of this study.

3.5 Relation between yield stress and flow initiation gradient (FIG)

Table 3.3—Correlation of gel yield stress with FIG inside proppant pack.

Yield (Pa)	FIG (psi/ft)		
	k_f = 100 Darcy	k_f = 20 Darcy	k_f = 10 Darcy
0	0	0	0
3	4	8	11
10	12	26	38
20	24	53	76
100	119	267	378

$$FIG = 21.8\ \tau_0 \sqrt{\frac{\phi}{k}} \quad \text{..... 3.1}$$

where FIG (psi/ft) is flow initiation gradient, τ_0 (pa) is yield stress, and k (darcy) is permeability. This correlation is derived by Ayoub et al. (2006).

Yield stress is property of fracture fluid – gel. After a fractured well is put on production, the BHP drops and creates a pressure gradient inside the fracture, which acts as the external forces to move the fracture fluid to wellbore. FIG is the minimum amount of pressure gradient to yield the gel. Otherwise, the gel will not move.

3.6 Simulation scenarios

Previously, we discussed how a simulation model for a hydraulically fractured well can be built, the data needed for the model, and initiation of simulation. We now show the simulation cases for each run in Table 3.3 and 3.4. The formation permeability k, reservoir pressure p_r, fracture half length L_f, and dimensionless fracture conductivity C_r have been varied in a systematical way. Table 3.4 shows the simulation run designs we used.

Table 3.4—Different simulation cases

Case	
1	Single phase
2	Gas-water two phase
3	Proppant crushing
4	Filter cake
5	Yield stress
5a	3 pa
5b	10 pa
5c	20 pa
5d	100 pa

Table 3.5—Simulation runs for each case

Run	Permeability k (md)	Reservoir Pressure p_r (psi)	Fracture Half Length L_f (ft)	Dimensionless Fracture Cond C_r
1	0.1	1860	264	0.1
2				1
3				10
4				100
5			528	0.1
6				1
7				10
8				100
9			924	0.1
10				1
11				10
12				100
13		3720	264	0.1
14				1
15				10
16				100
17			528	0.1
18				1
19				10
20				100
21			924	0.1
22				1
23				10
24				100
25		5580	264	0.1
26				1
27				10
28				100
29			528	0.1
30				1
31				10
32				100
33			924	0.1
34				1
35				10
36				100
37	0.001	1860	264	0.1
38				1
39				10
40				100
41			528	0.1
42				1
43				10

Table 3.5 continued

Run	Permeability k (md)	Reservoir Pressure p_r (psi)	Fracture Half Length L_f (ft)	Dimensionless Fracture Cond C_r
44				100
45			924	0.1
46				1
47				10
48				100
49		3720	264	0.1
50				1
51				10
52				100
53			528	0.1
54				1
55				10
56				100
57			924	0.1
58				1
59				10
60				100
61		5580	264	0.1
62				1
63				10
64				100
65			528	0.1
66				1
67				10
68				100
69			924	0.1
70				1
71				10
72				100

CHAPTER IV

STEPS IN MODELING FRACTURE FLUID CLEANUP

Steps for our systematic study of fracture fluid cleanup are discussed in this chapter. For each of the 72 runs in table 3.5, we make simulations for 8 cases, for a total of 576 simulations. The 8 cases are single phase, gas/water two phase, proppant crushing, polymer filter cake, and 4 values of yield stress. We begin with a single-phase run to get a base case for each run. As the cases are simulated, all simulations are additive.

4.1 Simulation of single phase flow

To begin the numerical study of fracture fluid cleanup, the first step is simulation of the ideal, single-phase flow case. We assume that a 100% gas-saturated reservoir has been hydraulically fractured but without any damage, which means that no fracture fluid has been left to recover after the fracture treatment. The cumulative gas production from this case will be considered the maximum amount of producible gas from a given reservoir with the given operating conditions. The effective gas permeability for the multiphase cases in the following sections will be the same as the single phase permeability, so a fair comparison can be obtained. All the simulation runs for this case can be found in Table 3.4 in previous chapter. The advantages of single-phase model are: easy to build, less data required, and fast to run. The disadvantages are that important basic physics controlling the reservoir fluid flow and gas recovery are neglected, and gas production can be overestimated in most cases.

4.2 Simulation of gas/water two-phase flow

After we simulated how hydraulic fractures behave under the ideal, single-phase case, we can start adding complexity to investigate various factors affecting fracture fluid cleanup.

We begin by switching from a single phase to a two-phase model while keeping the gas permeability the same in the two cases. For two-phase flow problems, relative permeability and capillary pressure inside the fracture and reservoir will play important roles in the fracture fluid cleanup behavior and long-term gas production in a tight gas reservoir. The gas relative permeability will be decreased by the fracture fluid saturation increase in the reservoir and by the hysteresis effect (Holditch 1979). Holditch found that both the relative permeability and capillary pressure were important in the analysis of the cleanup process. We have also investigated the shape of relative permeability curve inside the fracture upon the cleanup behavior.

We have run a fracture design model to determine the volume of water required to create various hydraulic fractures of specified lengths. For the two-phase runs, we have allowed the volume of water required for a specified fracture length to surround the fracture in a uniform manner. Such uniform saturation profiles will be created in low-permeability gas reservoirs, especially if a fluid loss additive is used during the treatment. The reservoir, fracture, and fluid data are shown in details in Section 3.2.

Wettability describes the relative preference of a rock to be covered by a certain phase. A water-wet rock means that most pores will be covered with a water layer. Wettability will be affected by the minerals present in the pores. Clean sandstone or quartz is extremely water-wet, but sandstone reservoir rocks are usually intermediate-wet, which means that some are water wet, and others are oil wet. Carbonates are believed to be more oil-wet than sandstone: a major part of the rock surface in the pores is covered with oil. In practice extreme water-wetness or extreme oil-wetness is rare. Only for gas/liquid systems, can we safely assume that gas is always the non-wetting phase. Basic reservoir properties like relative permeability, capillary pressure, and resistivity depend strongly on wettability.

Capillary pressure p_c is defined as the pressure difference between the non-wetting phase and the wetting phase as a function of the wetting-phase saturation. For gas/water systems in porous rock, gas is in general considered to be the least wetting phase. Therefore, we will define the capillary pressure as:

$$p_c(sw) = p_g - p_w . \quad \text{..... 4.1}$$

In reservoir engineering, p_c is an important parameter for simulation studies and analysis, especially for heterogeneous reservoirs. In many cases the inflow of water needs to be modeled, so particularly the imbibition capillary pressure is of importance. Note that an Hg-air measurement will result in the primary drainage curve and that this data is only used in the initialization of a simulation model.

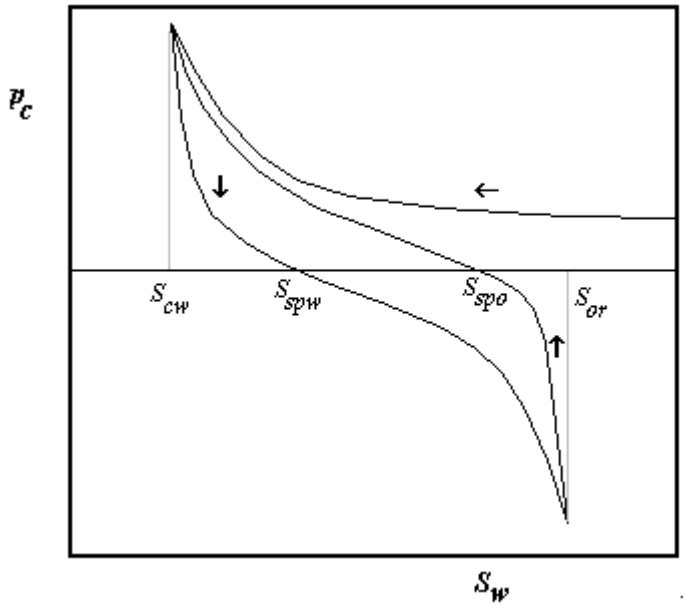

Figure 4.2.1—Full capillary pressure curves: 1st drainage, 1st imbibition, and 2nd drainage

Figure 4.2.1 shows a typical capillary pressure curve for a water/gas system in a porous rock. The capillary pressure curve consists of three curves: a primary drainage, a primary imbibition, and a second drainage branch. For the first drainage curve, at water saturation $S_w = 1$, an "entrance" pressure needs to be exceeded before gas can enter the core sample and then reach a plateau. With decreasing water saturations, the capillary pressure rises to a higher value. The capillary pressure goes to infinity at the connate water saturation S_{cw} (Dake, 1997). For the first imbibition curve, when the gas pressure is slowly decreased, water will spontaneously imbibe and the saturation will increase. The capillary pressure decreases, and is smaller than the drainage capillary pressure at the same water saturation, an effect called capillary hysteresis. When the gas pressure is equal to the water pressure ($p_c = 0$), the saturation reaches the spontaneous water imbibition saturation. Increasing the water saturation from this point can be accomplished only by forcing the water in, hence by increasing the water pressure above the gas pressure. An ever higher water pressure is required to force more gas out to reach the residual gas saturation. Capillary pressure p_c goes to minus infinity at water saturations near $1 - S_{gr}$. In summary, a negative capillary pressure means that a larger water injection pressure than the gas-phase pressure has to be applied to displace gas, the non-wetting phase out (Dake 1997). For the second drainage curve, the non-wettting phase, gas, will spontaneously imbibe and the water saturation will decrease when the water pressure is slowly decreased. The capillary pressure will be larger than the imbibition capillary pressure at the same water saturation because of the capillary hysteresis. At $p_c = 0$, the capillary pressure curve crosses the spontaneous gas-imbibition saturation. More water can only be removed by increasing the gas pressure (also p_c)—a forced drainage process. The capillary pressure goes to infinite around connate water saturation (Dake, 1997).

As already discussed, wettability determines the distribution of fluids in the porous rock and affects parameters like connate water and residual saturation. The capillary pressure also depends strongly on the wettability. In the extreme water-wet situation, the drainage and the imbibition capillary pressure are positive over the whole saturation range. Water will spontaneously imbibe from S_{cw} to 1 - S_{or}. A kind of inverse situation holds for an extremely oil-wet system; the drainage as well as the imbibition capillary pressure are negative. As mentioned before, most tight gas reservoirs are intermediate wet, so the capillary pressure for our simulation study will have the first drainage curve and the first imbibition curve.

For modeling and correlation purposes, the capillary pressure can be described by a dimensionless Leverett-J function:

$$J(S_w) = \frac{P_c(S_w)}{\sigma}\sqrt{\frac{k}{\phi}} \quad \text{.....4.2}$$

with σ the interfacial tension between the two phases and ϕ the porosity of the rock.

Multi-phase flow through porous media is governed by the interplay between capillary, viscous, and gravitational forces. The flow regime can be characterized by the capillary number and the bond number. Capillary forces usually dominate in reservoir flow. Therefore, although the actual flow is driven by viscous or gravitational forces, the flow paths at the pore scale are determined by the capillary forces.

Relative permeability

In the case where two or more fluids are flowing simultaneously through a porous medium, we can define a relative permeability for each of the fluids that describes the extent to which one fluid is hindered by the other. The relative permeability is defined by setting up the Darcy equation individually for each phase i that flows in the pore space:

$$q_i = (\frac{kk_{ri}}{\mu_i})A\frac{\Delta p_i}{\Delta x} \quad \text{.....4.3}$$

with q_i being the flow rate of phase *i*, k_{ri} the relative permeability of phase *i*, μ_i the viscosity of phase *i* and Δp_i the pressure drop within phase *i*. The term in brackets is denoted the "mobility" of phase *i*. kk_{ri} represents the total permeability of phase *i*. Usually, the wetting and the non-wetting phase relative permeability are normalised to $k_{ro,cw}$. The usual assumption is that k_{ri} is a function of the saturation of phase i and constitutes a rock property (i.e. k_{ri} is independent of the fluids used).

The wettability affects the relative permeability of each phase. For that reason, the relative permeability of the wetting phase at residual non-wetting phase saturation is much smaller than the relative permeability of the non-wetting phase at the irreducible wetting-phase saturation. A well-known model of the water and oil relative permeability functions is the Corey-exponent representation (Sherman):

$$S_{n1} = \frac{S_1 - S_{1r}}{1 - S_{1r}} \quad \text{.....4.4}$$

$$k_{r1} = k_{r1}{}^0 (S_{n1})^{n1} \quad \text{.....4.5}$$

$$k_{r2} = k_{r2}{}^0 (1 - S_{n1})^{n2} \quad \text{.....4.6}$$

where, S_{1r} is the residual water saturation, S_{nl} is normalized saturation, $k_{r1}{}^0$ and $k_{r2}{}^0$ are relative permeability end points for phase 1 and phase 2 respectively.

4.3 Simulation of proppant crushing effect

The stress acting on the proppant during fracture closure can cause proppant crushing which reduces the particle size. The closure stress can also cause the proppant to embed in soft formations. In addition, the compaction of the proppant pack further reduces its porosity and permeability. Cycling of stress, caused by shutting in the well and then re-openning it to flow, may also reduce the fracture conductivity.

Proppant crushing is inevitable after a fracture treatment especially in deep formations. During early flowback, the effective stress on the proppant should be minimized to avoid severe crushing. The effective stress on the proppant is equal to the in-situ stress minus the flowing bottomhole pressure. In-situ stress is very important for a fracture treatment design and evaluation. It depends on overburden pressure, pore pressure, rock properties, and tectonic forces. In-situ stress may vary in different local geological settings, and may change in response to reservoir depletion. One equation used to calculate in-situ stress is as follows:

$$\sigma_{\min} = \frac{\nu}{1-\nu}(\sigma_z - p) + p + \sigma_{ext} \quad \text{.....4.7}$$

Where, ν is poison's ratio, σ_z is overburden pressure, p is pore pressure, and σ_{ext} represents any externally applied stress.

The in-situ stress, closure pressure, and σ_{min} are different terminologies with the same meaning. Net pressure $p_{net} = p_{frac} - \sigma_{min}$. p_{net} will affect fracture width and fracture propagation. If p_{net} is less than zero, the fracture is closed.

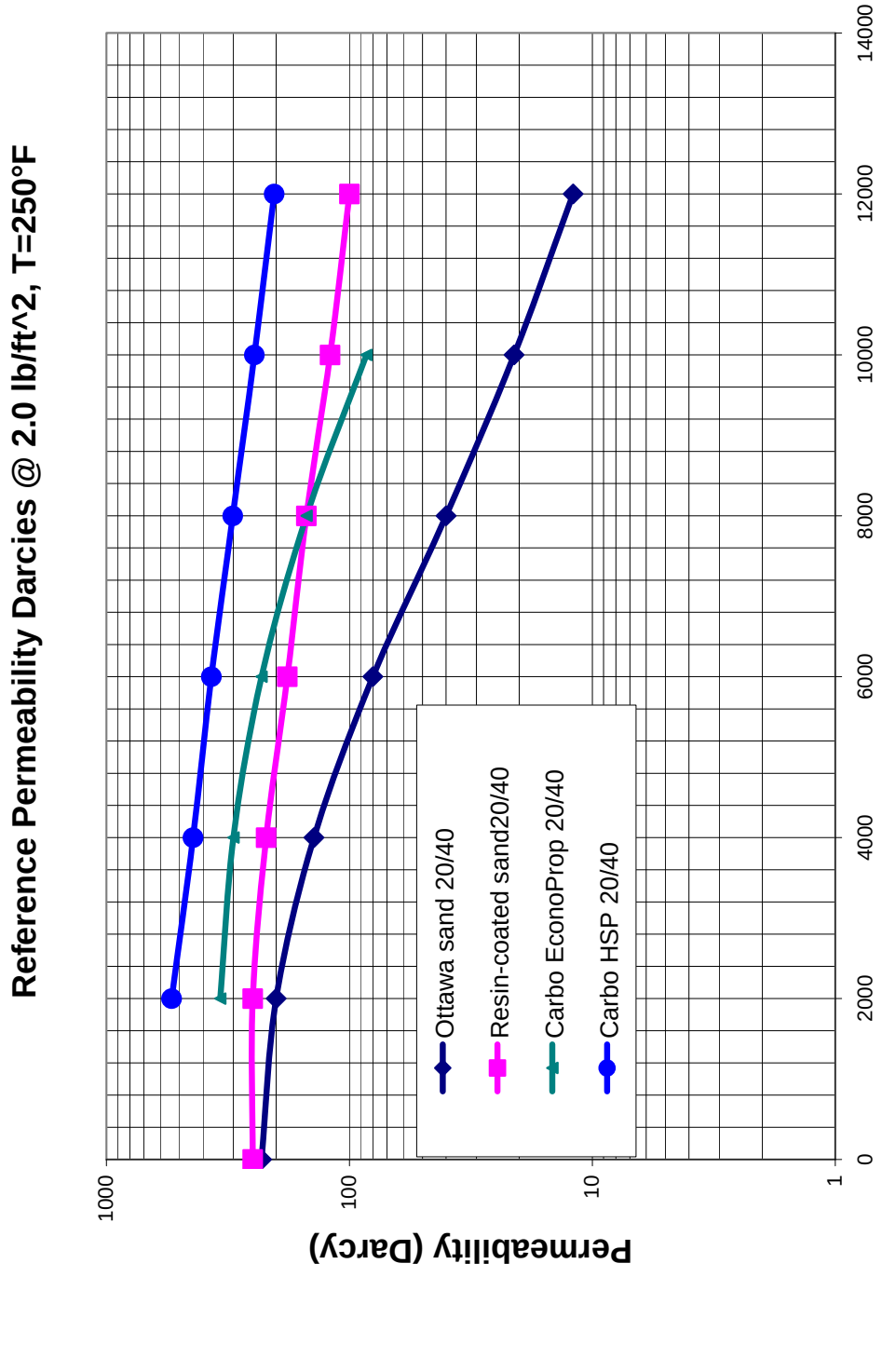

Figure 4.3.1—Different proppant permeability vs. closure stress (from Carbo Ceramics, 2007)

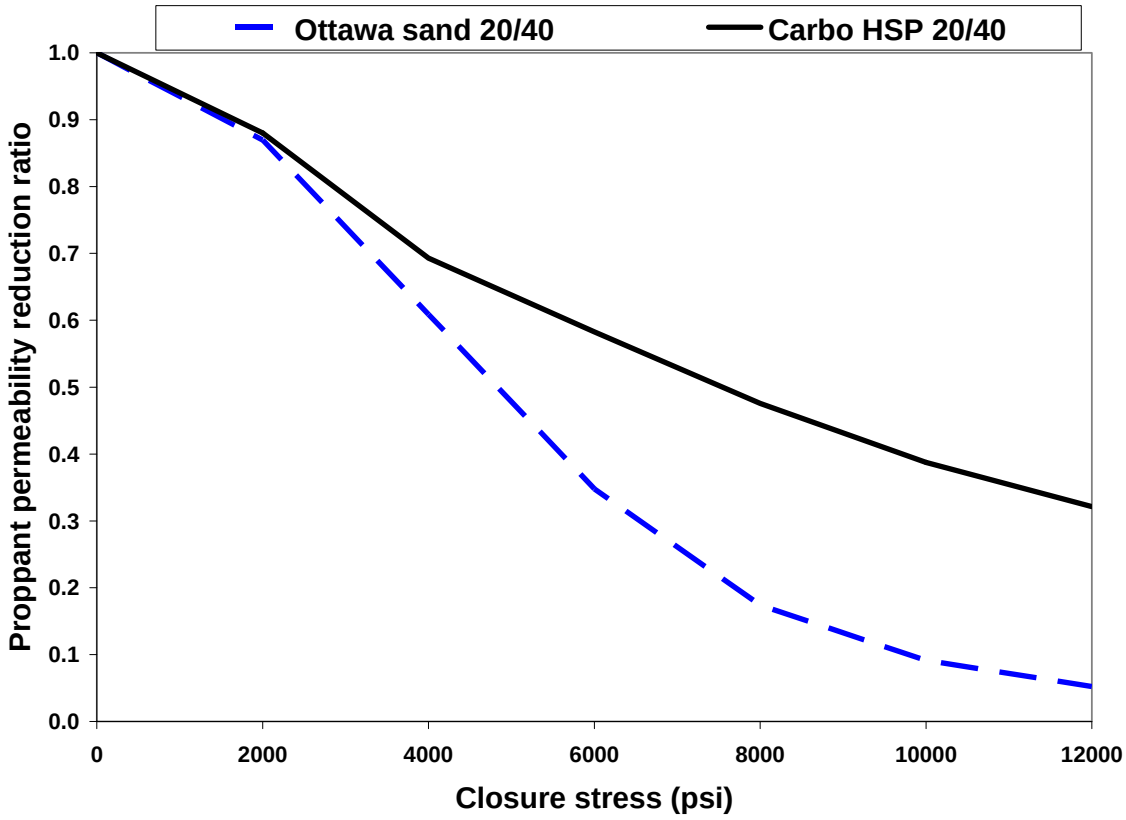

Figure 4.3.2—Proppant permeability reduction ratio under stress for Ottawa sand and Carbo HSP 20/40

To investigate the effect of proppant crushing on the short-term cleanup and long-term gas production, we used the two-phase, two-dimensional reservoir simulation model. The reservoir is assumed to be homogeneous, and isotropic. The base reservoir and fracture data are shown in Section 3.2 of Chapter III. Base relative permeability and capillary pressure are shown in Figure 3.3.

We conducted a study on the effects of proppant crushing combined with the two-phase flow case. The simulation study was done for three cases: no proppant crushing, slight crushing (Carbo HSP), and high crushing (Ottawa sand), as shown in Figure 4.3.1 and 4.3.2. The simulation results are more realistic by adding the proppant crushing effect.

4.4 Simulation of polymer filter cake

During fracturing, the fracture fluid leaks off into the reservoir formation, while most polymers stay inside the proppant pack creating a filter cake. A polymer filter cake is beneficial during fracturing because it helps decrease the fracture fluid leakoff into the reservoir formation, maintain the hydraulic pressure inside the fracture, and increase the fracture propagation. However, after a fracture treatment, the filter cake needs to be removed to achieve high conductivity and to create a flow path for gas. After closure, the polymer concentration in the gel could go up from 20 to 40 up to 300 to 1,000 lbm/1,000 gallon (Ayoub et al., 2006). At times, the polymer concentration becomes so high that the breaker additives are no longer able to fully degrade it. It is a common phenomenon in both low- and high- permeability reservoirs. Then, the goal becomes to reduce or remove the filter cake to increase fracture width and to obtain optimal fracture conductivity in the most cost-effective manner. The general physical processes for filter-cake buildup are agreed upon, but the basic property and removal mechanism of filter cake have not been fully understood. Here, we show the basic physics and property of the filter cake, mathematical equation, simulation methodology, and simulation results of the filter-cake effect on the cleanup process and long-term recovery in tight gas wells.

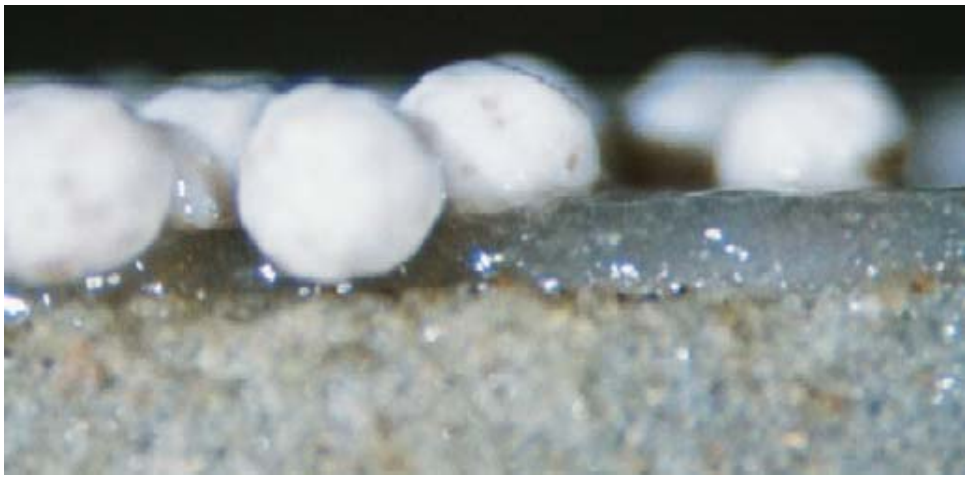

Figure 4.4.1—Filter cake from 35ppt CMHPG Zr XL fluid, with breaker (StimLab Consortia, 1997-2006)

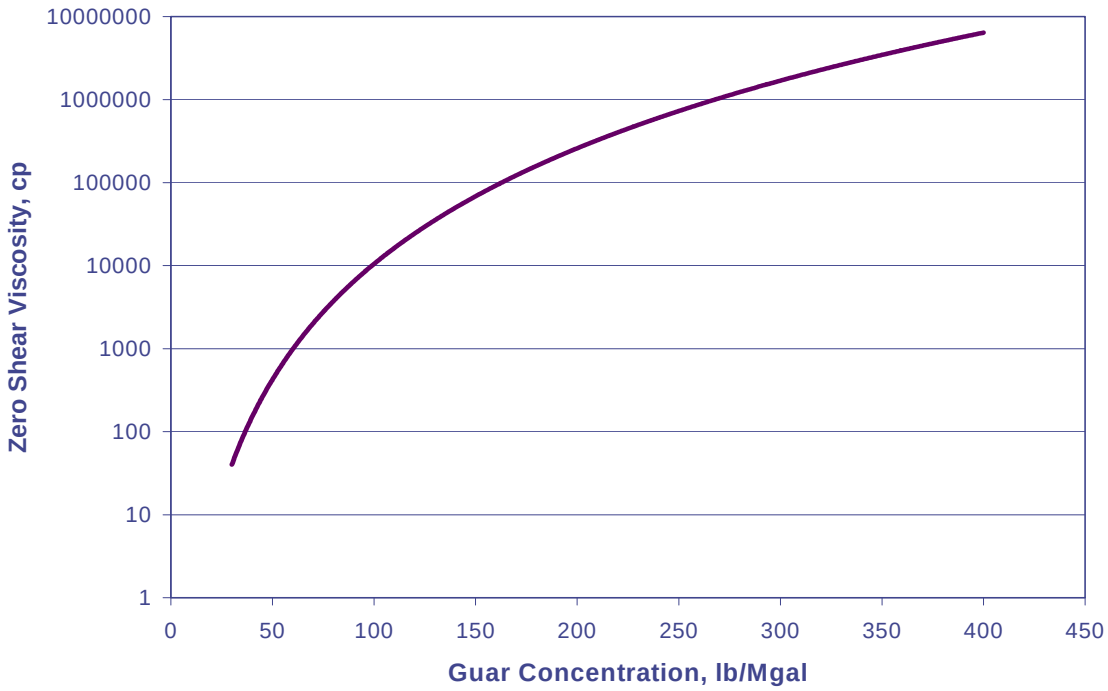

Figure 4.4.2—Polymer gel viscosity at zero shear vs. polymer concentration (From Barree)

Figure 4.4.1 illustrates the existence of a filter cake between the proppant and the formation rock after a laboratory experiment. The filter cake is a thin layer of highly concentrated polymer gel that will increase the pressure drop between the formation and the fracture. The permeability of the filter cake can range from 0.01 to 0.0001 md, and porosity may be 0.2 to 0.3. The viscosity of the gel is shown in Figure 4.4.2. As we can see the gel viscosity at zero shear rate will increase with increasing polymer concentration. In our simulation study, the filter cake viscosity is assumed to be 1,000,000 cp, which corresponds to a polymer concentration of 275 lb/1,000gallon. This is in the lower range as measured from laboratory experiments, so the real filter cake concentration and viscosity could be higher.

To calculate the average thickness of the filter cake, we used the following equation.

$$2L_f \cdot h \cdot h_{cake} \cdot \phi = \frac{m_{polymer} \times 1000 \times 5.615}{42c} \quad \text{.....4.8}$$

Rearranging the above equation, the thickness of the polymer filter cake should be

$$h_{cake} = 66.8452 \frac{m_{polymer}}{L_f \cdot h \cdot \phi \cdot c} \quad \text{.....4.9}$$

where h_{cake} is the thickness of filter cake (ft), L_f is the fracture half length (ft), h is zone thickness (ft), ϕ is the fracture proppant porosity (fractional), $m_{polymer}$ is the mass of polymer in the fracture fluid (lbm), and c is polymer concentration in the filter cake (lb/1,000gallon). The polymer concentration can range from 300 to 1,000 lb/1,000gallon depending on the amount of polymer used during fracturing. If unknown, a typical value may be 400.

For example, if we use the data from Table 7 in a paper by McDaniel and Parker (1988), then we can calculate the filter cake width as follows:

$$h_{\text{cake}} = 66.8452 \frac{m_{\text{polymer}}}{L_f \cdot h \cdot \phi \cdot c} = 66.8452 \frac{357.5}{900 \cdot 40 \cdot 4 \cdot 450} = 0.04 \ in$$

Assuming the fracture width equals 0.2 in., then the filter cake will occupy 22.13% of the fracture proppant pack. This agrees with the percentage of conductivity loss calculated from data from the same paper, which is shown below. This probably means that the filter cake will reduce the fracture width, which results in lower fracture conductivity, as observed by Ayoub et al. (2006).

Table 4.4.1—Validation of the model

Data from Table 4 in SPE 17541 by McDanial and Parker.			
Closure stress (psi)	Long-term conductivity with filter cake (md-ft)	Long-term conductivity without filter cake (md-ft)	Percentage of conductivity loss (%)
2000	1400	3500	40.00
4000	520	2200	23.64
6000	230	950	24.21

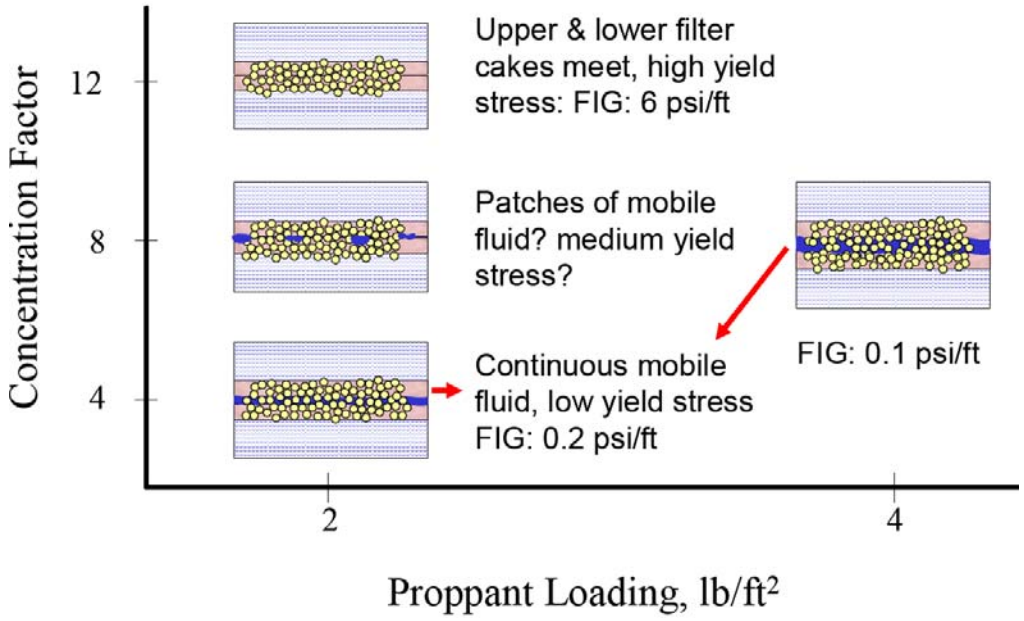

Figure 4.4.3—Polymer filter cake model inside the fracture proppant pack (from Ayoub et al., 2006)

The filter cake inside the fracture may be more complicated than many engineers thought. It can have different geometries and different properties depending on the type and amount of polymer, formation rock permeability, proppant concentration, and flowback procedure. Thus, it will require different strategies to remove the filter cake and to clean up the fracture. In general, the filter cake can be described by three models in Figure 4.4.3. One model is the proppant pack filled with filter cake, which will need a high pressure gradient and energy to remove. This scenario has been simulated and the results are shown in Section 5.4. The second model assumes that in the proppant pack the filter cake does not fill up, but there is a not continuous flow zone. The third model assumes that in the proppant pack there are two thin filter cakes plugging the fracture face, but a continuous flow zone exists between the two cakes. So the flow initiation gradient (FIG) from the second model will be higher than that from the third model.

One thing that needs to be pointed out is that the FIG does not equal to the yield stress of the filter cake. Obviously, the FIG in the third model is low because of the continuous flow zone, which reduces the energy to have the same flow rate as that in the first model. The mechanism to remove the cake may be different for each model. The yield stress of filter cake depends on particle size of long-chain polymer and solids, and over-balance pressure on the cake during fracturing. The mechanism of cake removal can be cake liftoff or breakage, flow back after yield, or dispersion. Yield stress may be the dominant factor in the removal of the filter cake. Filter cake liftoff is not correlated with yield stress. A larger yield stress for bentonite cake can tolerate a higher pressure gradient imposed across it, making cake removal possible (Zain and Sharma, 2001). The formation of pinholes and cracks in the cake is related to tensile and shear strength of the cake. So a strong, low-permeability cake is critical for complete filter-cake liftoff and breakage.

To study the effect of unbroken filter cake on the cleanup process and long-term gas recovery, a simulation model has been developed. The cells that represent the fracture proppant have been re-gridded by a local fine grid. Some grids represent the filter cake, while others represent the continuous flow zone. The fracture conductivity, porosity, polymer gel amount, and fracture fluid amount are maintained the same. It is assumed that in the model the filter cake is not cracked or lifted off, but remains there. However, there is a continuous flow zone between the two filter cakes, and the fluid inside will vary from Newtonian to non-Newtonian fluid with a yield stress. The following results show the effect of polymer filter cake on the cumulative gas production and fracture fluid recovery.

In general, a comprehensive study has carried out on the basic physics and properties of the filter cake effect and its effect on the cleanup process and long-term production in tight gas reservoirs. Even though the polymer filter cake is beneficial during fracturing to reduce fluid leakoff and help propagate the fracture further into the reservoir formation, it needs to be removed or reduced effectively to create a highly conductive fracture.

After this study, we can draw the following conclusions:

1. Filter cake is inevitable if long-chain polymers or other solids are used during fracturing. It is beneficial during fracturing.
2. A thin filter cake will lower the fracture conductivity, the gas productivity, and fracture fluid recovery if the fracture conductivity is low.
3. Yield stress will affect the cleanup of filter cake but may not be the only dominant factor. The tensile and shear strength and dispersion of filter cake will also be important. The removal mechanism for the filter cake needs to be studied further in laboratory.
4. A simple correlation has been recommended to calculate the filter-cake thickness for analyzing fractured well performance.
5. The filer cake does not make much difference on the gas production and fracture fluid recovery if the fracture conductivity $C_r > 100$. For a specific reservoir and fracture fluid, an optimal conductivity could be determined to overcome the polymer filter cake effect, so a better fracture treatment can be designed.

4.5 Simulation of yield stress effect

Voneiff et al. (1996) used a three-phase, 2D simulator to investigate the effects of unbroken fracture fluid on gas well performance. Their model had three phases: gas, formation water, and unbroken fracture fluid. The fracture fluid that leaked off was treated as the same phase as the formation water. The gel remaining in the proppant pack was assigned as the third phase. The reservoir was assumed to have gas and water two phases initially and the third phase—fracture fluid in the proppant pack—was injected during the fracture treatment. The viscosity of the unbroken gel was assumed to be constant at values of 1 cp, 1,000 cp, 10,000 cp, and 15,000cp. Before we work on the yield stress model, we have reproduced Voneiff et al.'s work and the results are shown in Figure 4.5.1.

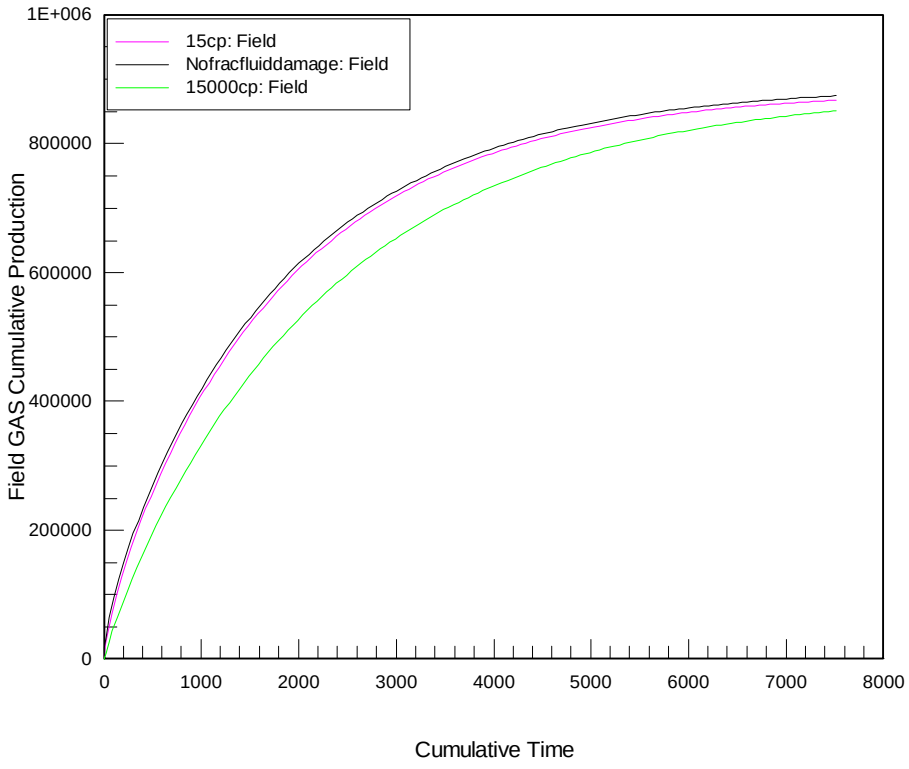

Figure 4.5.1—Reproduction of the work by Voneiff et al. (1996) (Newtonian fracture fluid without yield stress)

Figure 4.5.1 shows cumulative gas production for different fracture fluids that we have generated to check our results with those published by Voneiff et al. It is clear that the unbroken fracture fluid will reduce the cumulative gas production. The conclusion by the paper is that the fracture fluids need to be degraded to 50 cp or less to be considered broken, and the effective fracture length increases as the fracture cleans up. However, after 20 years, the cumulative gas production for the case with 15,000 cp is similar to the ideal case with 1 cp, which means that the fracture cleans up with time even when the fluid does not break and behaves like a Newtonian fluid. It is possible to have this kind fractured well performance, if the fracture fluid can behave like a Newtonian fluid. But for the widely used polymer fracture treatment fluids, there is evidence the fluids do not act as Newtonian fluids and the fracture may not clean up even after 20 years. It is important to incorporate the yield stress model into our study so we can better understand the cleanup process and predict the long-term gas recovery.

4.5.1 Introduction to yield stress model

The viscous properties of fracture fluid are very important. In some cases, if the fracture fluid viscosity is low, proppant may settle down to the bottom of the fracture below the pay zone and reduce the effective fracture length. To transport the proppant down the fracture, place the proppant uniformly inside the fracture and create a long highly conductive fracture in the tight gas formation, the fracture fluid has to be viscous. Once the treatment is over, we want the fluid to break to a low viscosity fluid so it will clean up.

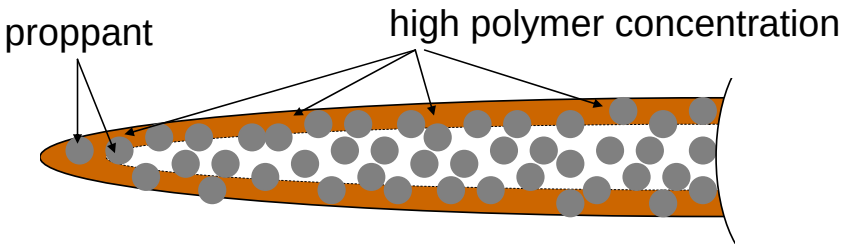

Figure 4.5.2—Top view of a half fracture with proppant and polymer inside

Successful fracture treatments require that fracturing fluids should degrade rapidly after the treatment to prevent plugging the proppant pack with highly viscous fluids. However, due to leakoff and fracture closure, virtually all of the polymers pumped in the treatments end up in the fracture, which can be a big problem during cleanup if the polymers do not break down into smaller molecules. The polymer inside the fracture pack will create a filter cake as shown in Figure 4.1.2. If not broken, the concentrated gel will have a yield stress as shown in the following Tables 4.5.1 and 4.5.2.

Table 4.5.1—Flow initiation gradient for high polymer concentration, proppant loading = 2 lbm/ft2, 20/40 sand (from Ayoub et al. 2006)

Test	Breaker, lbm/1,000 gal	Flow Initiation Gradient, psi/ft	Average Concentration, lbm/1000 gal	Conc Factor
H	--	7.9	580	14.5
I	--	14	1090	27.3
J	--	9.5	750	18.8
K	--	11	610	15.3
L	4	1.5	490	12.3
M	4	4.5	570	14.3
N	4	7.6	410	10.3
O	4	6.0	600	15.0

Table 4.5.2—Flow initiation gradient for low polymer concentration, proppant loading = 2 lbm/ft2, 20/40 sand (by Ayoub et al. 2006)

Test	Breaker, lbm/1,000 gal	Flow Initiation Gradient, psi/ft	Average Concentration, lbm/1000 gal	Conc Factor
A	--	0.69	150	3.75
B	--	1.6	150	3.75
C	--	2.5	150	3.75
D	--	3.0	160	4.00
E	4	0.17	160	4.00
F	4	0.34	200	5.00
G	4	0.26	140	3.50

Table 4.5.1 and Table 4.5.2 show the existence of yield stress of the fracture fluid as measured in the laboratory. The yield stress increases as the polymer concentration increases in the fracture fluid. If the pressure gradient is smaller than the yield point of the gel, the fracture fluid will not flow but will stay inside the fracture, reducing the conductivity. The yield stress of typical fracture fluid ranges from 0.04 to 17 pa (Ayoub *et al* 2006), and it can be compared to the yield stress of more common fluids, such as ketchup (38 pa typically), mustard (50 pa), and mayonnaise (130 pa) (Poloski et al. 2004). To study the yield stress effect on the fracture fluid cleanup and gas production, we need to look at the basic rheological models for the fracture fluids.

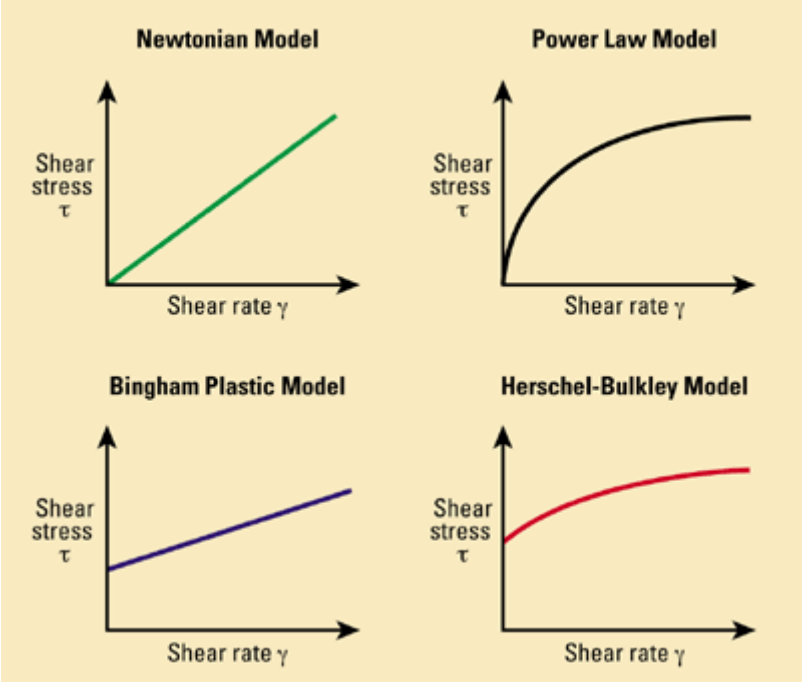

Figure 4.5.3—Schematic plot of different fluid models (Schlumberger Oilfield Glossary, 2008)

Figure 4.5.3 shows basic characteristics of different fluid flow models. The Newtonian model shows a constant viscosity at any shear rate. The Bingham plastic model describes a fluid that needs a finite force (yield point) to initiate flow. The power law model tries to solve the shortcomings of the Bingham plastic model at low shear rates, so it is used for a non-Newtonian fluid that does not have a yield stress. So a modified power law model, the Herschel-Bulkley model, can be used to better describe the fluid flow behavior of most fracture fluid that do have finite values for yield stress.

Non-Newtonian flow behavior can be divided into time-independent and time-dependent flow. Time-independent flow behavior may depend only on shear rate and not on the duration of shear, whereas time-dependent flow behavior depends also on the duration of shear (Rao, 1999). Time-dependent flow behavior can be divided into thixotropic and antithixotropic (rheopectic). A Herschel-Bulkley fluid is time-independent fluid (Khouryieh, 2006).

Rheology is the science of deformation and flow of matter. Certain measurements on a fluid indicate how that fluid will flow under different conditions, including temperature, pressure and shear rate. The following are some useful definitions used in this chapter.

Viscosity (μ) is defined as the ratio of the shear stress (τ) to the shear rate (γ).

$$\mu = \frac{\tau}{\gamma} \quad \text{.....4.11}$$

The concept of shear rate and shear stress apply to all kinds of fluid flow. When a fluid is flowing, the force acting opposite to the flow direction is known as shear stress. It can be thought of as a friction force, and is equal to the amount of force required to sustain the flow. The rate at which one layer of fluid moves past the next layer is called shear rate. The shear rate is a velocity gradient, which is defined as the following,

$$\textit{Shear rate}\ \gamma\ (\sec^{-1}) = \frac{V_a - V_b}{d} \quad \text{.....4.12}$$

where *Va* is the velocity at layer A (ft/sec), *Vb* is the velocity at layer B (ft/sec), and *d* is the distance between layer A and B (ft).

The viscosity of a non-Newtonian fluid changes with shear rate. The effective viscosity, sometimes called apparent viscosity, is the non-Newtonian fluid viscosity under specific conditions, including shear rate, temperature, and pressure.

The yield point (in units of Pascal) is a measurement of the electro-chemical or attractive forces in a fluid. It depends upon the surface property of the fluid solids, concentration of the solids, and types of ions in the fluid phase. The yield point will decrease if the attraction forces are reduced by chemical treatment to break the bond valences, to precipitate the cations, or to lower the concentration with water. The yield point can be increased by adding a commercial viscosifier to produce flocculation.

Gel strength and yield point are both measures of the attractive forces in a fluid system. However, gel strength is the static attractive force, while yield point is the dynamic

attractive force. Based on gel strength, gel can be divided into three categories: flat gel, progressive gel, and high-flat gel.

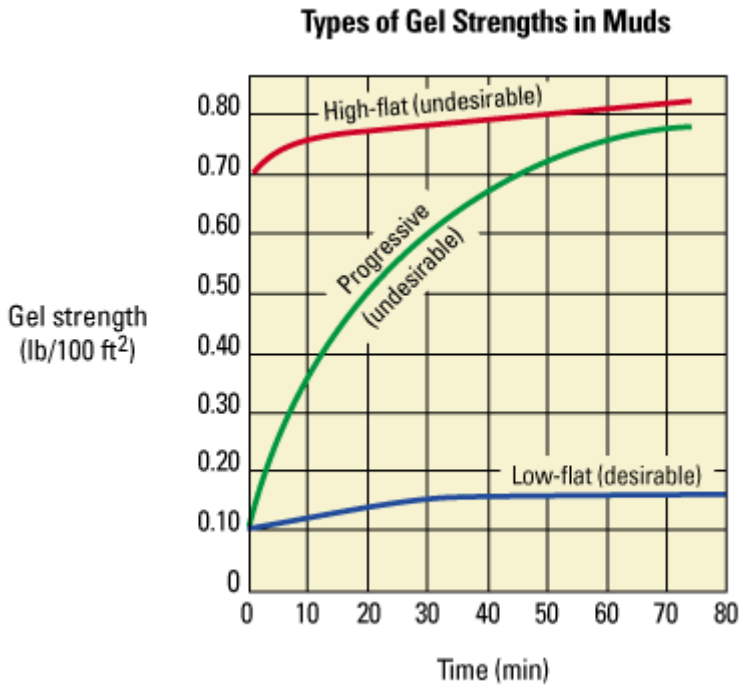

Figure 4.5.4—Schematic plot of different types of gel (Schlumberger Oilfield Glossary, 2008)

In this research, we use static yield stress and flowing yield stress, which correspond to gel strength and yield point in some other literature.

To characterize the fracture fluid flow and polymer behavior, we choose yield-power model, which is Herschel-Bulkley model in the Figure 4.5.3. It can be shown mathematically as:

$$\tau = \tau_0 + K\gamma^n \quad \text{.....4.13}$$

Where:

τ: the shear stress,

τ_0: static yield stress,

K: consistency index

γ: shear rate,

n: power law index

K is the viscosity at a shear rate of one reciprocal second. If power law index $n < 1$, the fluid is shear-thinning; if $n = 1$, the fluid is Newtonian; and if $n > 1$, the fluid is dilatant, shear-thickening.

The fracturing polymer may exhibit yield stress after leakoff and the rheology can be described by the Herschel-Bulkley model. The yield stress can be the reason for low fracture fluid cleanup efficiency. To investigate this effect, the next step is to incorporate the yield-power law model by Yi (2004) shown below into the simulator and compare the result to the Newtonian fracture fluid.

$$\tau = \tau_0 + K'\left(\frac{dv}{dr}\right)^{n'} \quad \text{.....4.14}$$

$$\mu_{nn} = \begin{cases} \dfrac{\mathrm{kk_r}\left(-\dfrac{\partial\Phi}{\partial L}\right)}{\left[\dfrac{\mathrm{kk_r}}{\mu_{\mathrm{eff,nn}}}\left(\left(-\dfrac{\partial\Phi}{\partial L}\right)-\beta\tau_0\right)\right]^{\frac{1}{n'}}} & \left(-\dfrac{\partial\Phi}{\partial L}\right) > \beta\tau_0 \\ +\infty & \left(-\dfrac{\partial\Phi}{\partial L}\right) \le \beta\tau_0 \end{cases} \quad \text{.....4.15}$$

$$\mu_{\mathrm{eff,nn}} = \frac{K'}{12}\left(9+\frac{3}{n'}\right)^{n'}\left(72C\phi(S_{nn}-S_{ir,nn})\mathrm{kk_{r,nn}}\right)^{\frac{1-n'}{2}} \quad \text{.....4.16}$$

$$\beta = N_n \sqrt{\frac{\phi(S_{nn} - S_{ir,nn})C}{2kk_{r,nn}}} \quad \text{...}\ldots\ldots\ldots\ldots\ldots\ldots\ldots\ldots\ldots\ldots\ldots\ldots\ldots\ldots\ldots\ldots 4.17$$

The capillary pressure is $p_c = p_{ne} - p_{nn}$ ……4.18

$S_w + S_g + S_{gel} = 1.0$. ……..4.19

For the simulation purpose, the viscosity of the fracture fluid is assumed to be 1,000,000 cp if the pressure gradient inside the fracture is less than the yield point.

4.5.2 Validation of yield stress model

Before we started the simulation study of the effect of static yield stress on the cleanup process and long-term gas production, we generated an analytical solution of the model (above), programming the mathematical model into our reservoir simulator, and validated the model by comparing simulation results to analytical solutions, pressure transient analysis and field data. The validations are accomplished in four steps.

We first need to produce an analytical solution for the yield stress model. The data used are shown in Table 4.5.3. We assume the porous medium is initially saturated with fracture fluid, which is not degraded after the treatment. We are interested in the displacement efficiency when a Newtonian fluid is injected. The relative permeability curve and other parameters are not shown here. The residue saturation of fracture fluid is about 0.2. The injection duration is 0.1 day, and the results are shown in Table 4.5.4 and Figure 4.5.5.

Table 4.5.3—Data used for analytical solution

Data for analytical solution from paper by Yi (2004)			
Table 1 Data used in parametric analysis		Table 1 Data used in parametric analysis	
Length, L(m)	250	Length, L(ft)	820
Area(m^2)	0.25	Area(ft^2)	2.69
Inclination angle(degree)	0	Inclination angle(degree)	0
k(darcy)	100	k(md)	1.00E+05
Porosity(fraction)	0.3	Porosity(fraction)	0.3
Visc of Newtonian Fluid(cp)	4	Visc of Newtonian Fluid(cp)	4
Density of Newtonian fluid(g/cm^3)	8	Density of Newtonian fluid(psi/ft)	3.467778
Fluid index, n'	0.5	Fluid index, n'	0.5
Consistency index, K'	0.05	Consistency index, K'	0.05
Yield stress(pa)	5	Yield stress(pa)	5
Non-Newtonian fluid density(g/cm3)	1200	Non-Newtonian fluid density(psi/ft)	520.1667
Injection rate(m^3/s)	7.23E-4	Injection rate(stb/d)	3.93E+02
Irreducible Non-newtonian Sat,Snnir	0.2	Irreducible Non-newtonian Sat,Snnir	0.2

Table 4.5.4—Front saturation for Newtonian fluid by using Weldge's graphic method and front advance equation at different yield stress

Yield stress (pa)	Dimensionless position	Front Saturation	df/ds
0	0.416	0.68	1
1	0.516	0.63	1.24
5	0.745	0.5	1.79
10	0.812	0.38	1.95

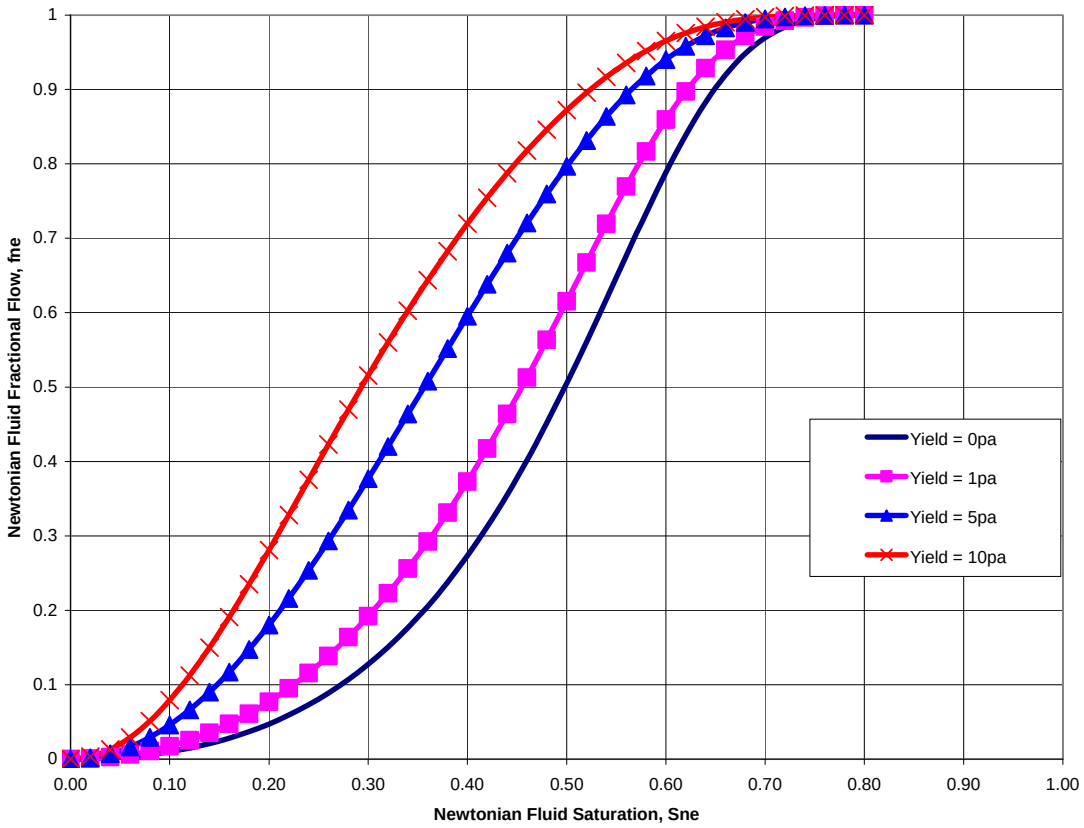

Figure 4.5.5—Newtonian fractional flow curve at different yield stresses

Table 4.5.4 and Figure 4.5.5 show the analytical solution from the yield-power law model. By using Weldge's graphic method and front advance equation, I have calculated the shock front saturation and saturation distribution along the flow path at different yield stress. We can see that the shock front saturation will decrease with increasing yield stress, and the displacement efficiency will be less. That means that more energy will be needed to move the non-Newtonian fluid out of the porous media if the yield stress is higher. The plot of Newtonian fluid saturation profile will be shown in next figure with simulation results.

We next ran numerical simulations to validate our model with the analytical solution. We built the yield-stress model into our reservoir simulator as a separate module. The non-Newtonian fluid viscosity is updated at every time step at each grid cell. 1D reservoir model has been constructed with one injector and one producer using the parameters used for the analytical solution, as shown in Table 4.3. Simulations were run for different yield stresses.

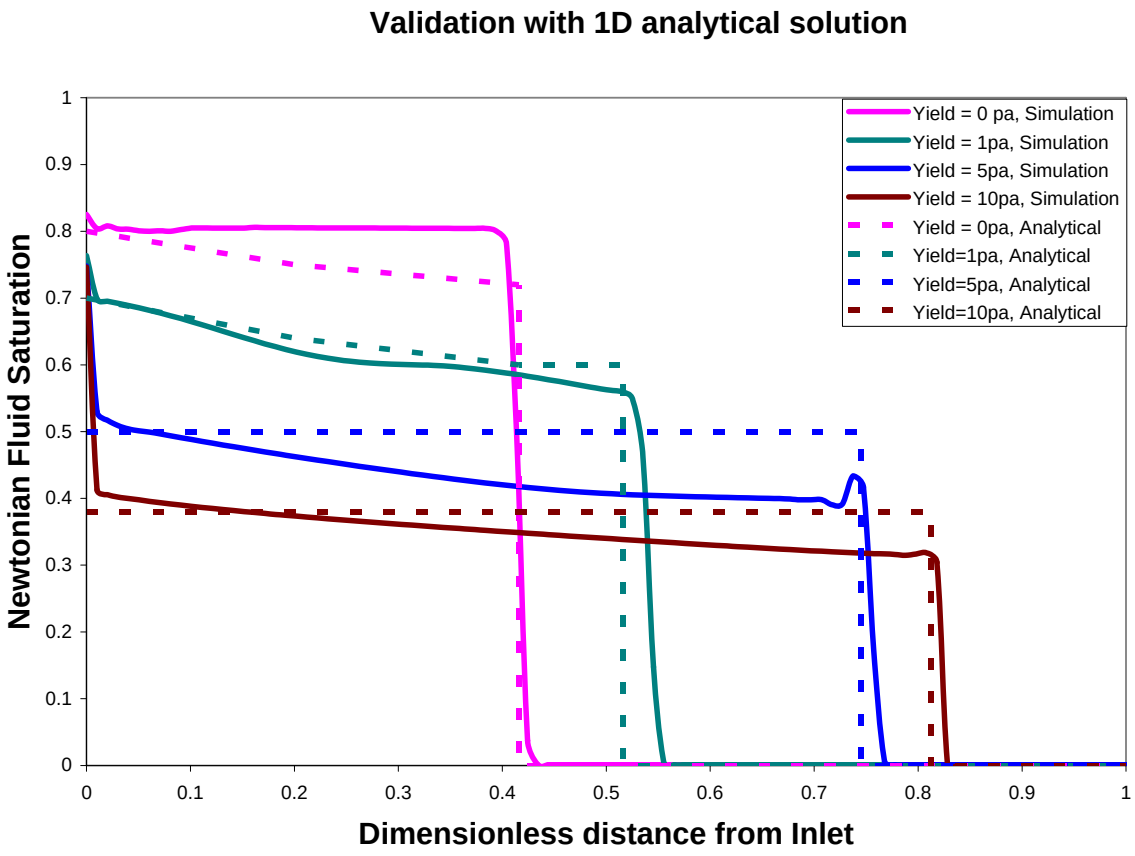

Figure 4.5.6—Simulation results for validation with 1D analytical solution

Figure 4.5.6 shows the simulation run vs 1D analytical solution. The solid lines show the simulation results, and dotted lines are analytical solutions. The comparisons include for yield stress of 0 pa, 1 pa, 5 pa, and 10 pa. Even though there are some small disagreements, it is a reasonable match with reasonable error. So we can conclude that the yield stress model has been built into the simulator correctly, and the simulation results are representative of what happens in field.

Next step was to validate our simulations with simulation results from the literature. The simulation results from our work have been compared to the results in Table 2 from a SPE paper by Friedel (2006). Friedel's model included a gas/water system in the reservoir, and a gas/water/gel system in the fracture proppant. His assumption was that long-molecular polymers stay inside the fracture, while fracture fluid filtrates into the reservoir formation. Assuming that all the polymers remain in the fracture is a reasonable assumption for tight gas sands. Another assumption is that inside the fracture proppant, the relative permeability of each phase is equal to the saturation. In our work, we have used exactly the same reservoir, fracture, and fluid data as Friedel so we could reproduce his work to validate our model. Tables 4.5.5 and 4.5.6 show the data used for the simulation runs.

Table 4.5.5— Data for validation of yield stress model with Friedel's work

Reservoir Parameters		Fracturing process	
Permeability (md)	0.05	Leakoff Volume (m^3)	60
Porosity	0.1	Well shut-in (hour)	0
Residual water saturation	0.5		
Corey exponent	1	Cleanup process	
Initial pressure (bar)	600	Bottomhole pressure(bar)	600-150
		Duration (day)	2
Fracture Parameters		Production period	
Fracture half length (m)	75	Bottomhole pressure (bar)	150
Dimensionless Conductivity	20	Duration (day)	365
Porosity	0.25		

Table 4.5.6— Relative permeability for validation with Friedel's work

Water saturation	Water relative permeability	Gas relative permeability
0.5000	0.0000	1.0000
0.5500	0.0000	0.8092
0.6000	0.0001	0.6349
0.6500	0.0005	0.4768
0.7000	0.0020	0.3370
0.7500	0.0063	0.2188
0.8000	0.0156	0.1254
0.8500	0.0336	0.0591
0.9000	0.0655	0.0195
0.9500	0.1181	0.0027
1.0000	0.2000	0.0000

Table 4.5.7— Validation results for the case dimensionless conductitivity, F_{cd} = 10

Yield Stress (pa)	0.5		1		2.5		10	
	Sabre	Friedel's	Sabre	Friedel's	Sabre	Friedel's	Sabre	Friedel's
Gas Recovery	0.99	0.99	0.97	0.98	0.90	0.94	0.56	0.61
Fracture Fluid Recovery	1.00	0.95	1.00	0.94	0.94	0.93	0.63	0.6
Gel Recovery	0.76	0.71	0.51	0.57	0.25	0.38	0.02	0.06

Recovery is referred to the case with yield stress of 0 pa.

Table 4.5.7 shows the simulation results from SABRE compared to the results in Table 2 of Friedel's paper. The recovery is measured with respect to the case with yield stress of 0 pa. More gas, fracture fluid, and gel will be recovered with lower yield stress. From this validation, we can conclude that the yield stress model has been incorporated successfully into the reservoir simulator SABRE, and it appears to be an acceptable method to evaluate the effects of yield stress on the cleanup behavior.

The last step is to validate with field data. The data are from a Cotton Valley tight gas well, which are taken from a paper by May et al. (1997). We try to reproduce the simulation work in the paper. Table 4.5.8 shows the main data for our simulation runs.

Figure 4.5.7 shows the bottomhole pressure (BHP). The BHP will be lowered step by step during the production after the fracture treatment. After about 120 days, BHP will be constant at 1,200 psi for another 5 years. Then reservoir model is constructed by using the data available and average reservoir pressure is calculated from the simulation model. The pressure difference, average reservoir pressure minus BHP, has been used to calculate the well productivity index as shown in the Figure 4.5.9. Before comparing the simulation results to that in the paper, we show a comparison between two cases, a Newtonian fluid and a non-Newtonian fluid with small yield stress (0.01 pa) in Figure 4.5.8.

Table 4.5.8—Field Data (from May, 1997)

Field data from Cotton Valley for validation simulation	
Porosity (%)	7.2
Permeability (md)	0.01
Formation thickness (ft)	40
Drainage area (acres)	160
Pressure(psi)	5830
Fracture half length (ft)	2500
Fracture conductivity (md-ft)	188
Gel viscosity (cp)	9.56

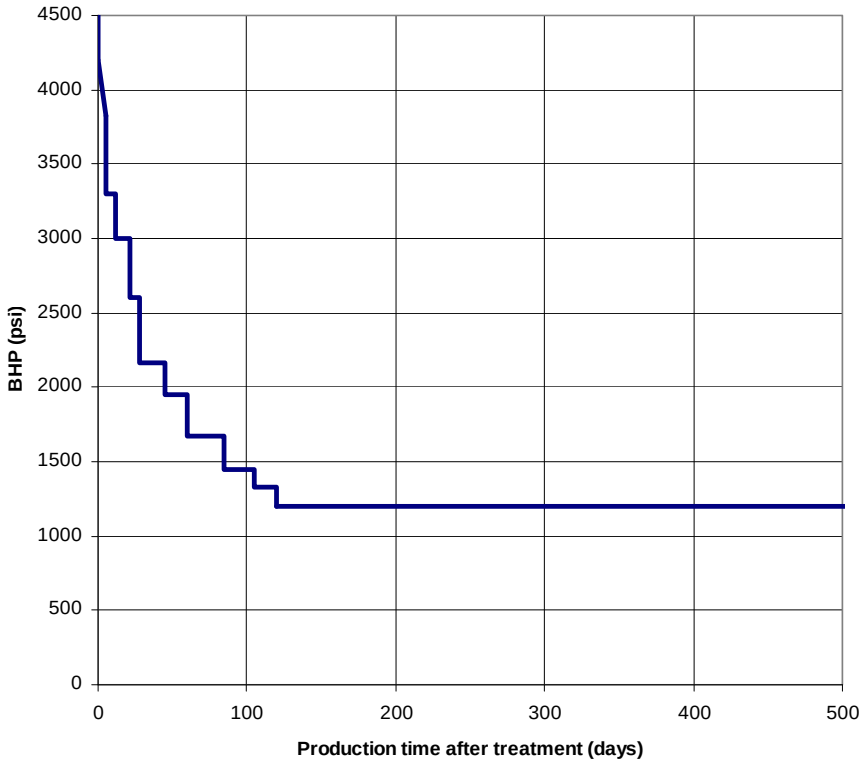

Figure 4.5.7—BHP from a Cotton Valley tight gas well (May, 1997)

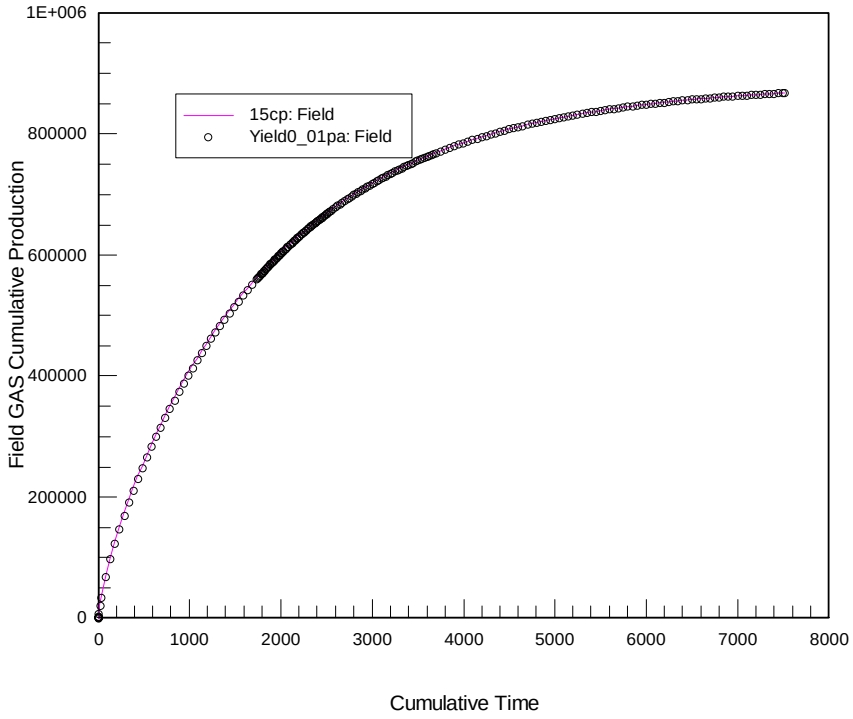

Figure 4.5.8—Cumulative gas production for two fracturing fluids

Figure 4.5.8 shows the cumulative gas production for a fractured tight gas well. The pink solid-line curve shows the case of a Newtonian fracture fluid with viscosity of 15 cp. The black dotted curve shows the case of a non-Newtonian fracture fluid with a small yield stress (0.01 pa). The two curves match well, so it is indicated the yield-power law model in the simulator has been built correctly.

Table 4.5.9—Calculation of PI from simulation results for the case with yield of 3 pa from SABRE

PI	BHP	GRID	Time -DAYS- ----	Reservoir P -PSI- ------	Gel Rate -STB/D- -----	Gas Rate -MCF/D- -------	Water Rate -STB/D- -------	Cum Gel -STB- -------	Cum Gas -MCF- -------	Cum Gel -STB- -------
8.86E-03	4200	69	5.41E-01	5.85E+03	1.27957	3.66022	17.5425	1.0983	1.0105	8.2296
9.11E-03	4200	70	5.51E-01	5.85E+03	1.26595	3.76654	17.5846	1.11095	1.04816	8.40545
9.39E-03	4200	71	5.61E-01	5.85E+03	1.25306	3.87861	17.6293	1.12349	1.08695	8.58174
9.67E-03	4200	72	5.71E-01	5.85E+03	1.24046	3.99542	17.671	1.13589	1.1269	8.75845
9.96E-03	4200	73	5.81E-01	5.85E+03	1.22824	4.11749	17.7111	1.14817	1.16808	8.93556
1.03E-02	4200	74	5.91E-01	5.85E+03	1.21641	4.24558	17.75	1.16034	1.21053	9.11306
1.06E-02	4200	75	6.01E-01	5.85E+03	1.20474	4.383	17.7848	1.17238	1.25436	9.29091
1.10E-02	4200	76	6.11E-01	5.85E+03	1.19354	4.53056	17.8199	1.18432	1.29967	9.46911
1.13E-02	4200	77	6.21E-01	5.85E+03	1.18267	4.68746	17.8539	1.19615	1.34654	9.64765
1.17E-02	4200	78	6.31E-01	5.85E+03	1.17161	4.85246	17.8793	1.20786	1.39507	9.82644
1.22E-02	4200	79	6.41E-01	5.85E+03	1.16055	5.02658	17.8989	1.21947	1.44533	10.0054
1.26E-02	4200	80	6.51E-01	5.85E+03	1.14928	5.20965	17.9092	1.23096	1.49743	10.1845
1.31E-02	4200	81	6.61E-01	5.85E+03	1.13832	5.40753	17.9181	1.24234	1.5515	10.3637
1.36E-02	4200	82	6.71E-01	5.85E+03	1.12755	5.62654	17.9233	1.25362	1.60777	10.5429
1.42E-02	4200	83	6.81E-01	5.85E+03	1.11628	5.86423	17.9142	1.26478	1.66641	10.7221
1.48E-02	4200	84	6.91E-01	5.85E+03	1.10456	6.11667	17.8915	1.27583	1.72758	10.901
1.54E-02	4200	85	0.7005	5.85E+03	1.09272	6.38389	17.8605	1.28675	1.79142	11.0796
1.62E-02	4200	86	0.7105	5.85E+03	1.08009	6.67932	17.8093	1.29756	1.85821	11.2577
1.71E-02	4200	87	0.7205	5.85E+03	1.06589	7.05546	17.7208	1.30821	1.92877	11.4349
1.81E-02	4200	88	0.7305	5.85E+03	1.05103	7.45995	17.6131	1.31872	2.00337	11.611
4.85E-02	4200	122	1.0705	5853	0.6981	20.0603	13.982	1.60802	6.80085	16.9622
4.94E-02	4200	123	1.0805	5853	0.689529	20.428	13.8544	1.61491	7.00513	17.1008
5.03E-02	4200	124	1.0905	5853	0.681149	20.7823	13.729	1.62173	7.21296	17.2381
5.11E-02	4200	125	1.1005	5853	0.672964	21.1234	13.6062	1.62845	7.42419	17.3741
5.19E-02	4200	126	1.1105	5853	0.664963	21.4522	13.4856	1.6351	7.63871	17.509
5.27E-02	4200	127	1.1205	5853	0.657196	21.7725	13.3683	1.64168	7.85644	17.6427
5.35E-02	4200	128	1.1305	5853	0.649837	22.0932	13.2578	1.64817	8.07737	17.7753
8.15E-02	4200	490	4.7505	5852	0.119719	33.6563	2.31128	2.53009	133.552	36.555
8.14E-02	4200	491	4.7605	5852	0.119469	33.6386	2.30533	2.53128	133.888	36.578
6.16E-02	1950	573	60.15	5839	0.040295	59.8792	0.637819	5.949	2715.73	99.928
6.36E-02	1950	574	60.31	5838	0.041502	61.8342	0.652024	5.95564	2725.62	100.032
5.96E-02	1950	575	60.63	5838	0.038571	57.914	0.595488	5.96798	2744.16	100.223
5.69E-02	1950	576	61.27	5838	0.036413	55.3434	0.547187	5.99129	2779.58	100.573
5.50E-02	1950	577	62.55	5838	0.034457	53.4302	0.498879	6.03539	2847.97	101.212
5.72E-02	1450	597	105.31	5827	0.036576	62.5624	0.638331	7.22076	4979.21	119.437
5.35E-02	1450	598	105.63	5827	0.034011	58.5215	0.584666	7.23165	4997.94	119.625
5.13E-02	1450	599	106.27	5827	0.032305	56.1158	0.542683	7.25232	5033.85	119.972
4.98E-02	1450	600	107.55	5826	0.030929	54.5062	0.510792	7.29191	5103.62	120.626
4.88E-02	1450	601	110.11	5826	0.029641	53.3711	0.498673	7.36779	5240.25	121.902
4.79E-02	1450	602	115.23	5824	0.028046	52.3661	0.507699	7.51139	5508.36	124.502
4.75E-02	1450	603	120	5823	0.026922	51.8777	0.5174	7.63981	5755.82	126.97
2.03E-01	1200	604	92987	5823	0.156006	234.956	2.6847	7.64137	5758.17	126.997
9.45E-02	1200	605	92987	5823	0.067195	109.23	1.22931	7.64271	5760.36	127.021
7.42E-02	1200	606	92987	5823	0.052532	85.7439	0.966307	7.64481	5763.79	127.06
6.40E-02	1200	607	92987	5823	0.045218	74.0066	0.832031	7.64843	5769.71	127.126
5.74E-02	1200	608	92987	5823	0.040351	66.3544	0.73236	7.65488	5780.32	127.244
5.32E-02	1200	609	92987	5823	0.037116	61.4873	0.655628	7.66676	5800	127.453
5.06E-02	1200	610	93087	5823	0.034886	58.4316	0.595016	7.68909	5837.39	127.834
4.90E-02	1200	611	100187	5822	0.03327	56.5928	0.55504	7.73168	5909.83	128.545
4.81E-02	1200	612	100487	5822	0.031878	55.5396	0.537805	7.81328	6052.01	129.921

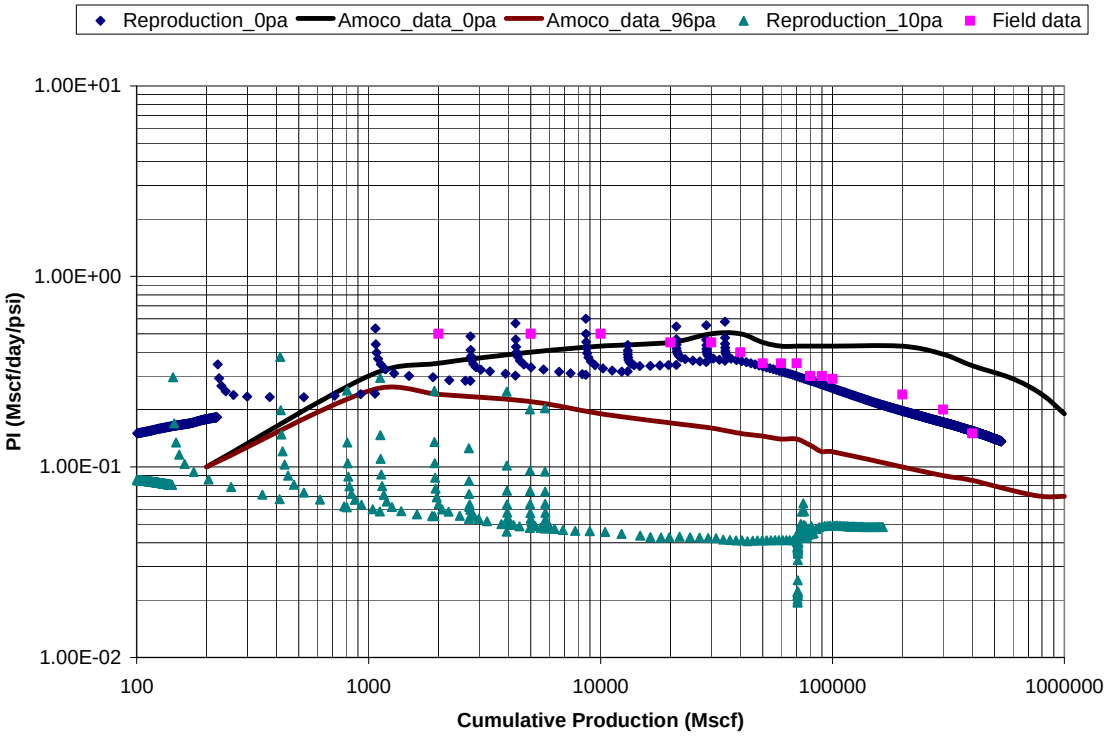

Figure 4.5.9—Validation of simulation results with field data and May's simulation results

Figure 4.5.9 shows the productivity index for five cases, one set of field data in pink color square dots, two cases from May's paper with solid lines(fracturing fluid with yield stress of 0 pa and 96 pa) and two cases from our simulation (fracturing fluid with yield stress of 0 and 10pa). It is not a perfect match because our simulated PIs are lower. However, the late-time PI from yield stress of 0 pa matches the field data. One reason for the difference could be that the paper assumed the fracture fluid behaves like a power law fluid after it yields, which is not true, and there may be errors in the mathematical model in the paper. Another reason could be that some parameters like the fracture fluid and the relative permeability are not known from this field. Though I can not conclude much from this plot, a useful technology for validation and gel damage recognition has been identified.

In the future, more case histories need to be analyzed to learn more about fracture fluid cleanup. Below are bullet points on the data needed and the steps required to analyze a field case.

Data needed from a tight gas reservoir:

- Real fracture treatment data (reservoir data, fracture fluid, proppant, polymer, etc)
- Production data (gas production, water production, pressure vs. time)
- A commercial fracture treatment design software like FracCADE, StimPlan, and FracproPT

The procedures are shown as the following:

1. Use fracture design software to determine the fracture half length, width, leakoff, and other data from the actual treatment.
2. Use mSABRE* to create a filtration zone around the fracture as initiation for simulation runs.
3. Use mSABRE to match production data and to determine the yield stress value.
4. Use the correlation we derived from the experimental data from Ayoub et al., to determine another yield stress value for the given fracture fluid, amount of polymer, filter cake, and fracture geometry in Step 1.
5. Compare the two yield stress values in Step 3 and Step 4.
6. Analyze simulation runs to identify the reason why the fracture does not clean up.

* mSABRE is the modified version of SABRE that is a product of this research. So if the real fracture treatment and production data are available from a fractured tight gas well, it is not difficult to analyze and identify the problems associated with the cleanup process, and a remedial technology may be recommended for future field operations.

4.6 Other factors

Other factors like non-Darcy flow and gravity should also be considered in the modeling of fracture fluid cleanup. Even though it is not in the scope of this study, we have a brief

discussion of these two factors. At high fluid velocities, the pressure drop in the proppant pack increases more than the proportional increase in velocity. Forchheimer proposed that the pressure gradient is the sum of the viscous forces ($\mu v/k$) and the inertial forces ($\beta\rho v^2$),

$$\Delta p/\Delta L = \mu v/k + \beta \rho v^2 \quad \text{.....4.20}$$

where β is referred to as beta factor or non-Darcy coefficient which is essentially a measure of the tortuosity of the flow path. For single-phase flow in the presence of irreducible water saturation, Geertsma (1974) proposed the following equation for β:

$$\beta = 48511.34\ (k_g)^{-0.5}\ [\phi\,(1 - S_w)]^{-5.5} \quad \text{.....4.21}$$

where β is in 1/ft and k_g is effective gas permeability in md.

For multiphase flow, Frederick and Graves (1994) proposed the following correlation for β:

$$\beta = 7.89 \text{ x } 10^{10}\ (k_g)^{-1.60}\ [\phi\,(1 - S_w)]^{-0.404} \quad \text{.....4.22}$$

This correlation was derived from laboratory measurements on core samples with permeabilities ranging from 0.00197 to 1,230 md. Eq. 18 is used in modeling the non-Darcy flow in the fracture. Again, β is in 1/ft and k_g is effective gas permeability in md.

Gravity can play an important role in the fracture fluid cleanup. The density difference causes the water to move downward while gas tends to move upward inside the fracture and reservoir formation. This effect will make the upper fracture more conductive to gas than the lower fracture. The perforation and flow back rate could be optimized by using this phenomenon to improve fracture fluid cleanup and increase gas recovery. Dickens and McVay (2008) have done some research in this area and concluded that the perforations and flow rates can be optimized to improve the fracture cleanup.

CHAPTER V

SIMULATION RESULTS AND ANALYSES

In this research, we have indentified five major factors that affect fracture fluid cleanup. We have also developed an approach to evaluate the cumulative effect of these five factors upon gas flow rates during cleanup and the 10-year gas recovery. The five factors are multi-phase flow, proppant crushing, effect of polymer filter cake on the fracture width, and the gel strength. In Chapter V, we systematically evaluate the cumulative effect of these factors upon cleanup and gas recovery. Some results are analyzed in this chapter. All others are included in the Appendix E.

5.1 Simulation results for single-phase flow

The single phase flow solution for a vertical well containing a vertical fracture has been well known for 50 years. For every computer run, as shown in Table 3.4, we have made a single phase run as the "base case" for each run. As we develop the scenarios associated with fracture fluid cleanup, we can compare each case to the base case (single phase flow) to evaluate its effect on both cleanup and gas recovery. We present our results in graphs of log (gas flow rate) vs. log (time) to evaluate fracture fluid cleanup and cumulative gas produced, which show the early time transient flow and late pseudo-steady state flow.

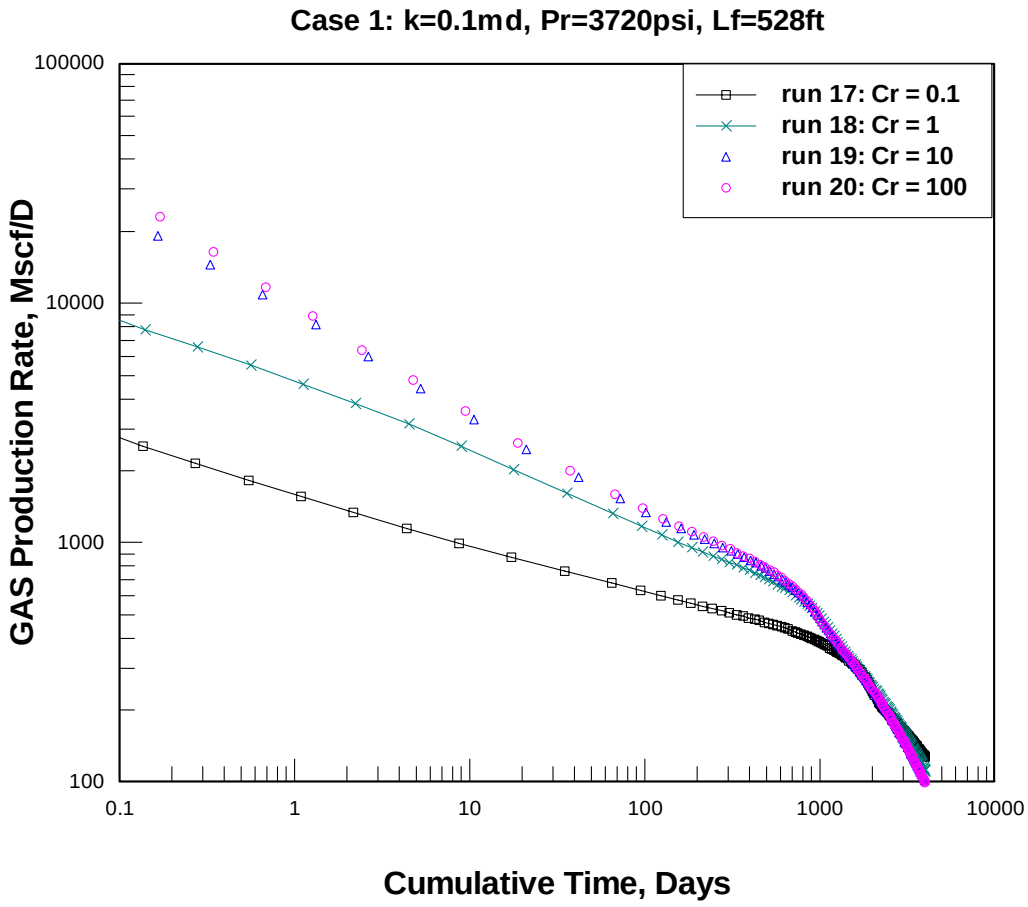

Figure 5.1.1—Gas production rate at different fracture conductivity for L_f = 528 ft, p_r = 3720 psi, k = 0.1 md , S_{wi} = 0.4 and h = 100 ft

Figure 5.1.1 shows the gas production rate vs time after a fracture treatment for a reservoir where L_f = 528 ft, p_r = 3720 psi, k = 0.1 md, S_{wi} = 0.4 and h = 100 ft. The assumption for single phase flow is that a hydraulic fracture has been created, but without any fracture fluid damage, so the gas production rate reaches a maximum value once the well is put on production. This is the ideal case where the fractured well does not need time to clean up at all. As expected, with higher fracture conductivity, the gas production rate is higher. If the dimensionless fracture conductivity (C_r) is above 10, a higher conductivity does not make substantially affect the gas flow rate in the idealized case. We are using $C_r = k_f w/\pi k \bullet L_f$ as proposed by Cinco-Ley (1980). If C_r = 100, the fracture conductivity is essentially infinite. From production point of view, a proppant that can provide dimensionless fracture conductivity of 10 or more is sufficient for optimizing gas production when one only considers the single-phase flow case.

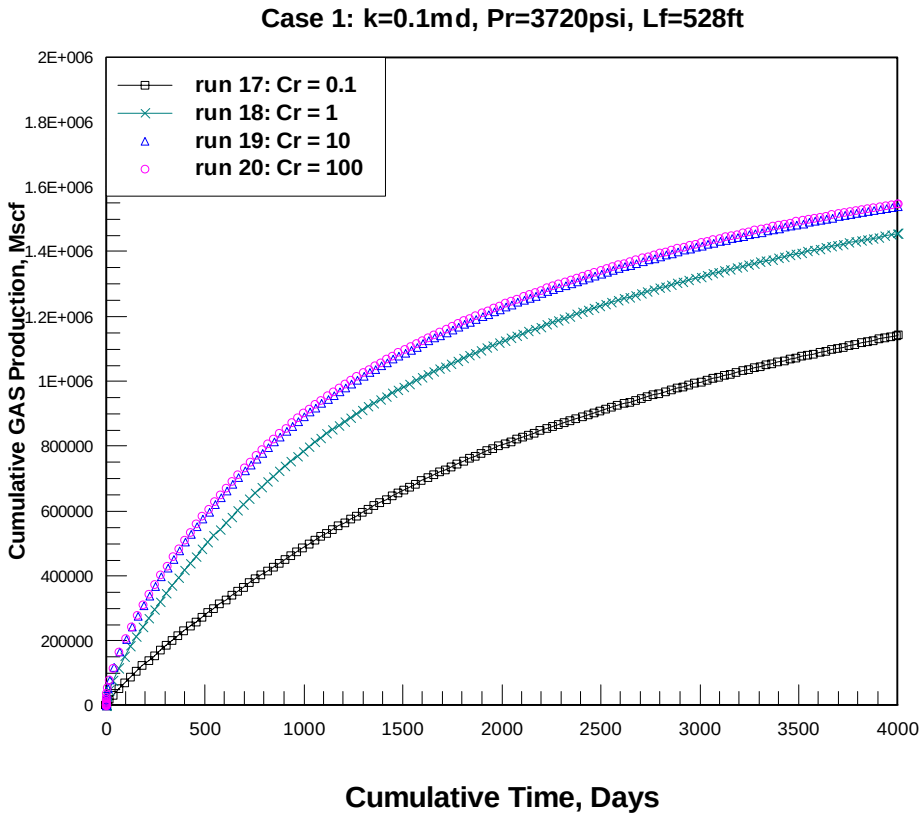

Figure 5.1.2—Cumulative gas production at different fracture conductivity for L_f = 528 ft, p_r = 3720 psi, k = 0.1 md, S_{wi} = 0.4 and h = 100 ft

Figure 5.1.2 shows cumulative gas production after a fracture treatment for case of L_f = 528 ft, p_r = 3720 psi, k = 0.1 md, S_{wi} = 0.4 and h = 100 ft, which are the same data as presented in Figure 5.1.1. The assumption for single phase flow is that a hydraulic fracture has been created, but without any fracture fluid damage. We can see for these examples that gas production will be higher if fracture conductivity is higher. However, the cumulative gas production does not differ much once the fracture conductivity is above 10. If the fracture conductivity can be increased from 0.1 to 10, the cumulative gas production will be increased by 36% in ten years, which is about 1.3 bcf per well. Thus, from a production point of view, a proppant that can provide dimensionless fracture conductivity of 10 is good enough for gas production when only single-phase flow is considered.

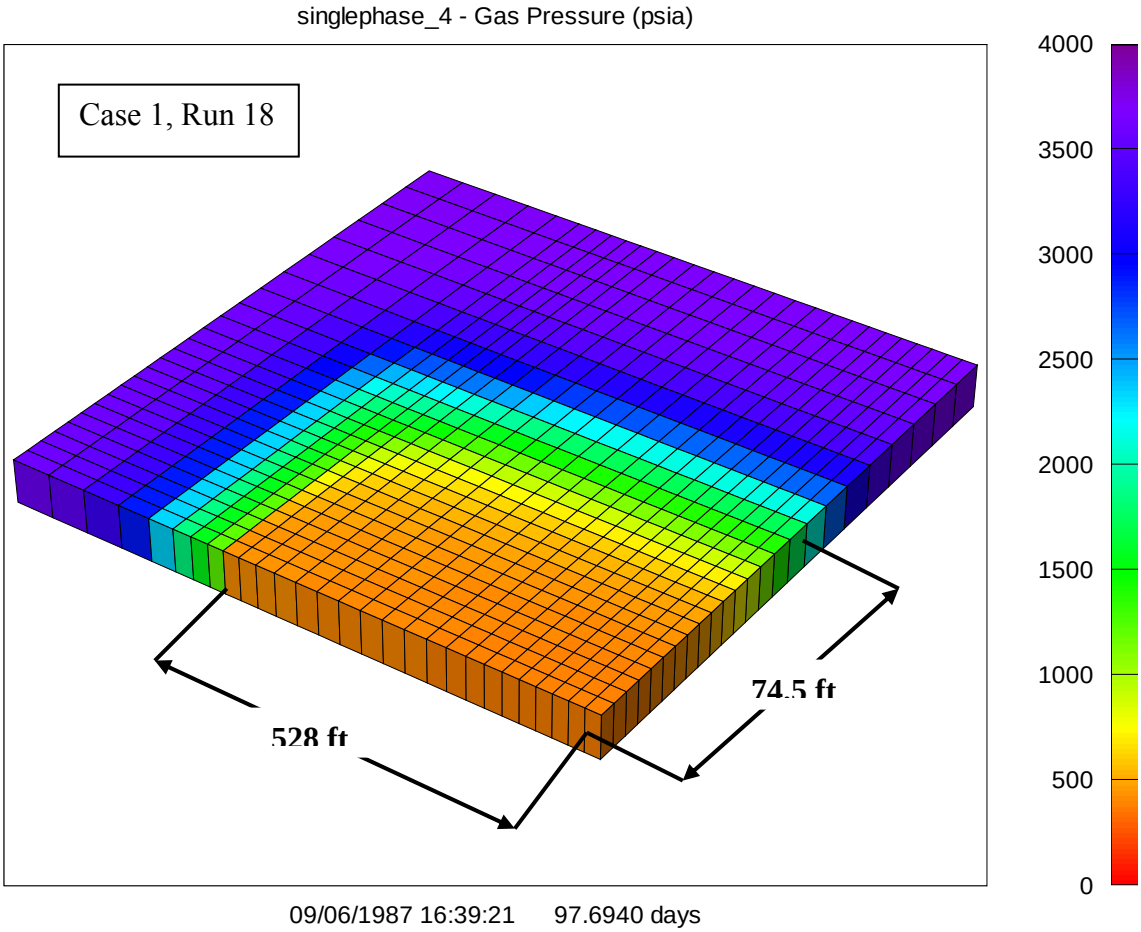

Figure 5.1.3—Gas pressure map after 97.7 days of production for L_f = 528 ft, p_r = 3720 psi, C_r = 1, k = 0.1 md, S_{wi} = 0.4 and h = 100 ft

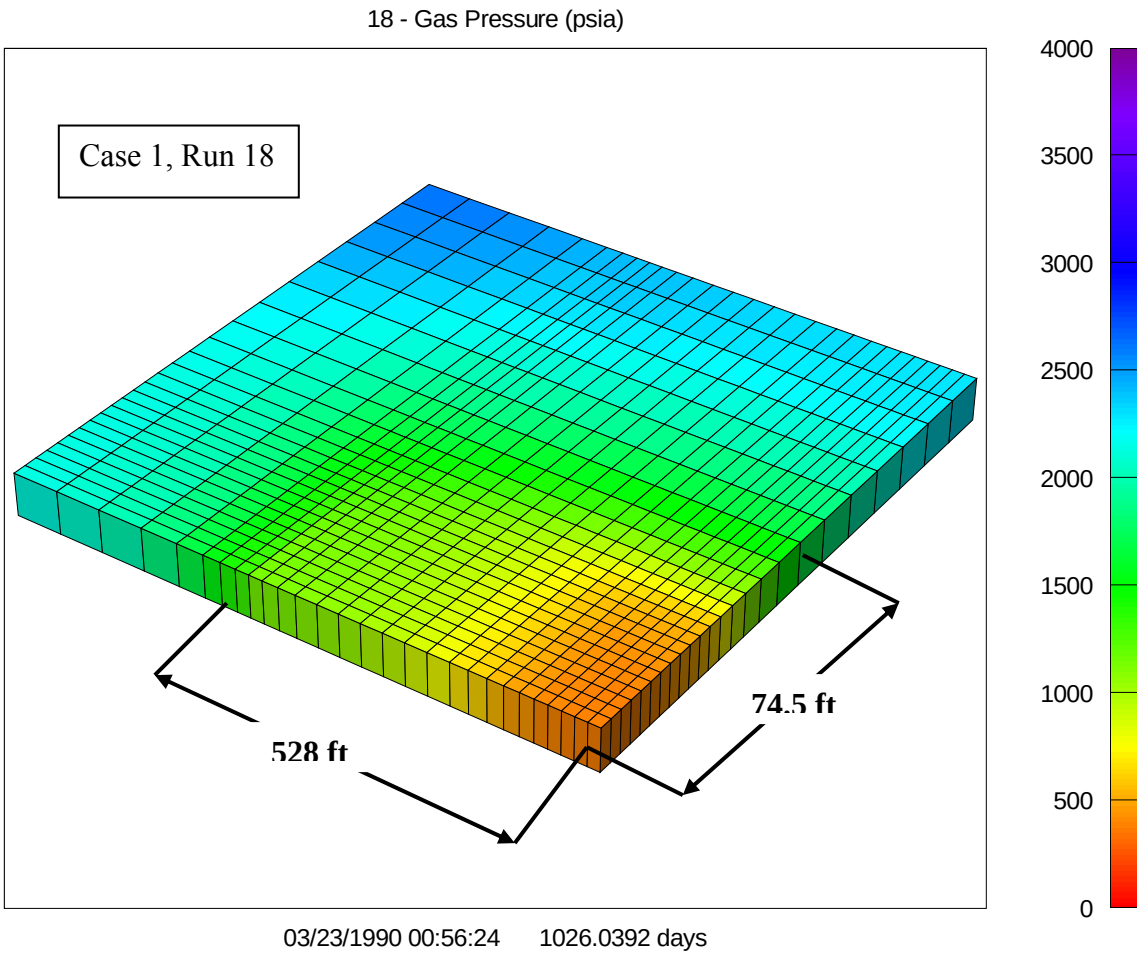

Figure 5.1.4—Gas pressure map after 1026 days of production for L_f = 528 ft, p_r = 3720 psi, C_r = 1, k = 0.1 md, S_{wi} = 0.4 and h = 100 ft

Figure 5.1.3 shows the gas pressure map 97 days after a fracture treatment for case of L_f = 528 ft, p_r = 3720 psi, C_r = 1, k = 0.1 md, S_{wi} = 0.4 and h = 100 ft, which is case 1, run 18. The gridding has been designed to show the vicinity around fracture and the wellbore. For high conductivity fractures, the gas flows linearly from the reservoir formation into the fracture, and then into the wellbore. This can also been observed in Figure 5.1.1, and at about 700 days, the flow becomes psudo radial flow.

Figure 5.1.4 shows the gas pressure map 1,026 days after a fracture treatment for case of L_f = 528 ft, p_r = 3720 psi, C_r = 1, k = 0.1 md, S_{wi} = 0.4 and h = 100 ft. The gridding has been designed to show the vicinity around fracture and wellbore. We can see that the gas flow reaches drainage area boundary, and flow becomes psudo-radial which can also been observed in Figure 5.1.1. It is an effective technology to identify the gas flow mechanism and drainage area by plotting field production data in log (gas rate) vs log (time). At least, one can decide if the well has reached a boundary or is still draining a larger area.

5.2 Simulation results for gas/water two-phase flow

This section shows the numerical simulation results and analyses for gas/water two-phase flow. Just like single phase flow in a hydraulically fractured well, there have been many papers published showing the effects of two-phase flow upon gas recovery in a hydraulically fractured well. As such, the work in this research is not new, but needs to be presented to expand the base case scenario. Later, when we evaluate the effect gel strength and filter cake upon gas flow rate, we need to be able to compare those results to the single phase and two-phase runs. We choose to show just two scenarios of the research work on two-phase flow, which illustrates the effect of fracture conductivity on the early time transient flow and long-term cumulative gas production in the figures below. The results from all the runs are in Appendix E. The assumption for two-phase flow is that a hydraulic fracture has been created, and the fracture fluid filtrate that leaks off into the reservoir formation has the same properties as the formation water. So after a fracture treatment the vicinity around fracture is saturated by the water phase. The water phase temporally reduces the gas from flowing into the fracture and into wellbore. The well takes time to clean up the fracture fluid before gas can flow at a maximum rate.

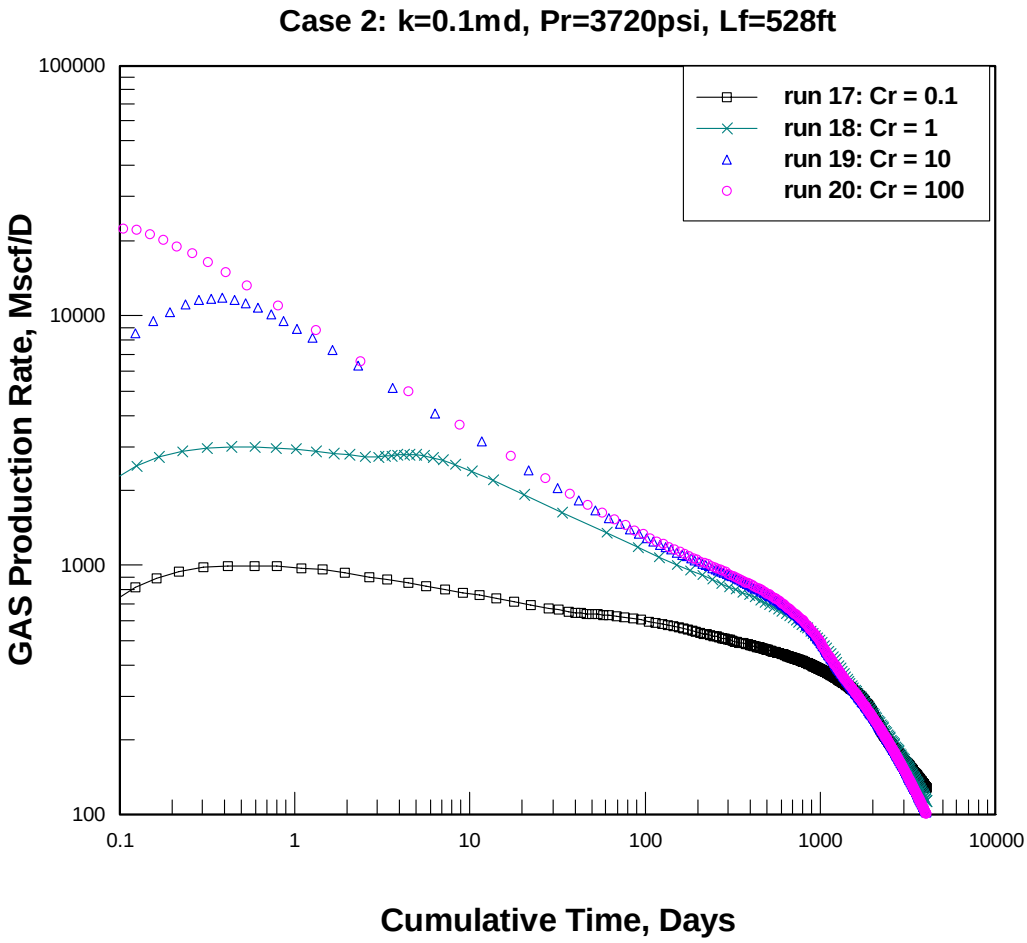

Figure 5.2.1—Gas production rate at different fracture conductivity for L_f = 528 ft, p_r = 3720 psi, k = 0.1 md, S_{wi} = 0.4 and h = 100 ft

Figure 5.2.1 shows the gas production rate vs time after a fracture treatment for runs 17-20 for case 2 where L_f = 528 ft, p_r = 3720 psi, k = 0.1 md, S_{wi} = 0.4 and h = 100 ft. We can see that the gas production rate increases for a period of time before it reaches a maximum value, which is the cleanup time. The fracture cleans up faster if the fracture conductivity is higher. For a dimensionless fracture conductivity of 0.1, which is a very low conductivity fracture, the gas production rate is much lower during the first three years' of production. But if the fracture conductivity is above 10, a higher conductivity does not make much difference on the gas flow rate any more. Thus, from a production point of view, a proppant that can provide dimensionless fracture conductivity of 10 or

more is good enough for gas production when only two-phase flow is considered and the fracture fluid filtrate viscosity is the same as the formation water.

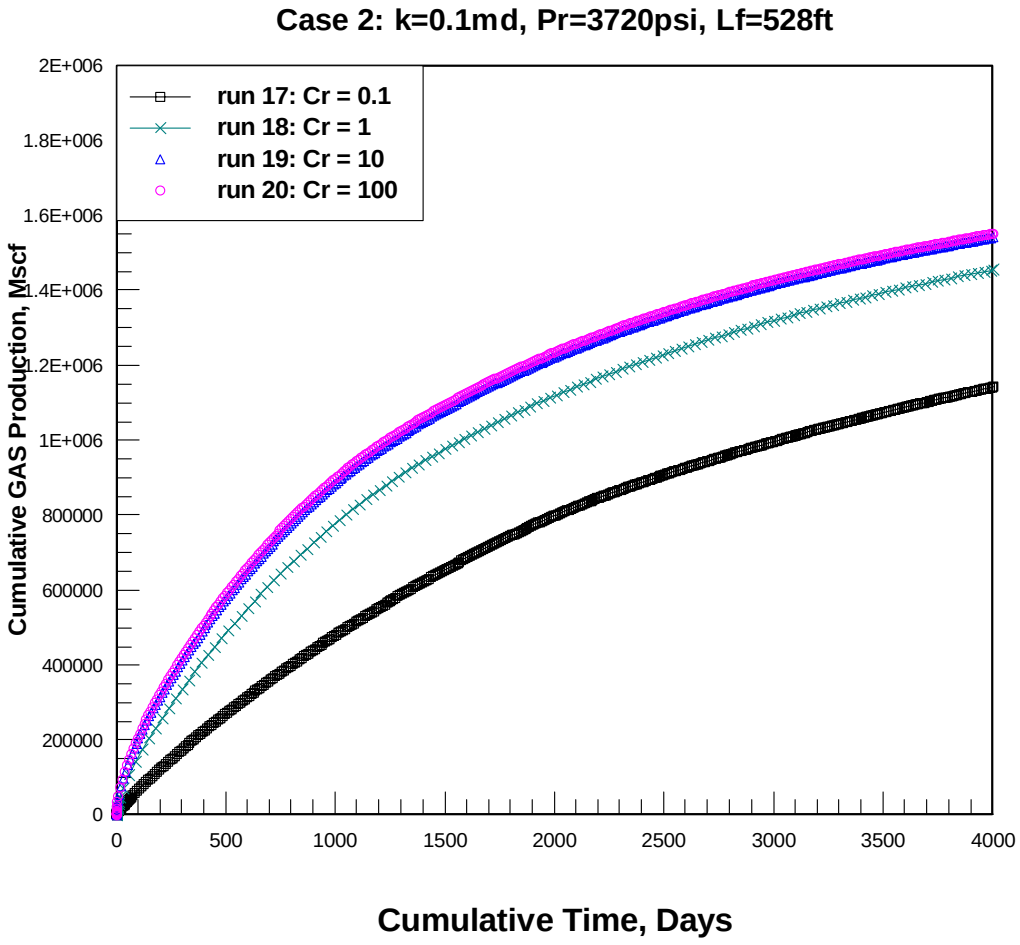

Figure 5.2.2—Cumulative gas production at different fracture conductivity for L_f = 528 ft, p_r = 3720 psi, k = 0.1 md, S_{wi} = 0.4 and h = 100 ft

Figure 5.2.2 shows cumulative gas production at different values of dimensionless fracture conductivity after a fracture treatment for L_f = 528 ft, p_r = 3720 psi, k = 0.1 md, S_{wi} = 0.4 and h = 100 ft. We can see that cumulative gas production will be higher if the fracture conductivity is higher. However, the cumulative gas production does not differ much once the fracture conductivity is above 10. If the fracture conductivity can be increased from 0.1 to 10, the cumulative gas production will increase by 36% in ten years, which is about 1.3 bcf for one well in 160 acre spacing. Thus, strong proppants and

high fracture conductivity are critical to the success of fracture treatment and long-term gas production. However, from a production point of view, a proppant that can provide dimensionless fracture conductivity of 10 is good enough for gas production.

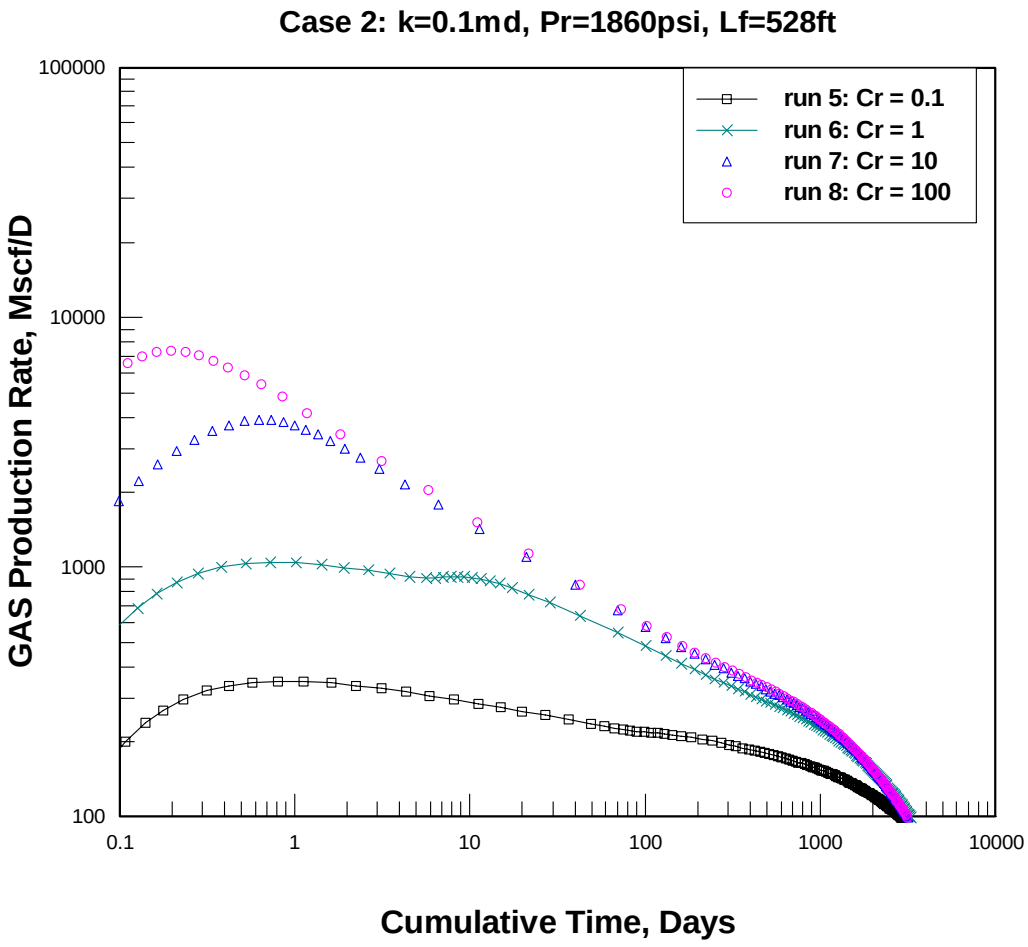

Figure 5.2.3—Gas production rate at different fracture conductivity for L_f = 528 ft, p_r = 1860 psi, k = 0.1 md, S_{wi} = 0.4 and h = 100 ft

Figure 5.2.3 shows the gas production rate vs time at different values of fracture conductivity after a fracture treatment when L_f = 528 ft, p_r = 1860 psi, k = 0.1 md, S_{wi} = 0.4 and h = 100 ft. The difference here from the prior example is that the reservoir pressure is only 1860 psi. We can see that the gas production rate increases for a period of time before it reaches a maximum value, which is the cleanup time. The fracture cleans up faster if the fracture conductivity is higher. For this low pressure case, one can

clearly see the effect of fracture conductivity upon fracture fluid cleanup. We normally try to design for a C_r of 10 or better. Notice in Figure 5.2.3, the early gas flow rate for a C_r of 10 is around 2,000 Mscf/day and peaks out at around 4,000 Mscf/day after one day. For the infinite fracture conductivity case (C_r = 100), the gas flow rate starts out at 8,000 Mscf/day, and declines to around 5,000 Mscf/day after one day. Thus, after a few days, C_r = 10 and C_r = 100 behave very similarly.

The cleanup for this scenario in Figure 5.2.3 is similar to the higher pressure scenario in Figure 5.2.1, but at the same fracture conductivity, the cleanup time is longer, and the gas flow rate is lower. This implies that the reservoir energy is a very important factor in analysis of fracture fluid cleanup, which is not expected.

Figure 5.2.4 shows cumulative gas production for different values of fracture conductivity after a fracture treatment for L_f = 528 ft, p_r = 1860 psi, k = 0.1 md, S_{wi} = 0.4 and h = 100 ft for the low pressure scenario. We can see that cumulative gas production will be higher if the fracture conductivity is higher. However the cumulative gas production does not differ much once the fracture conductivity is above 10.

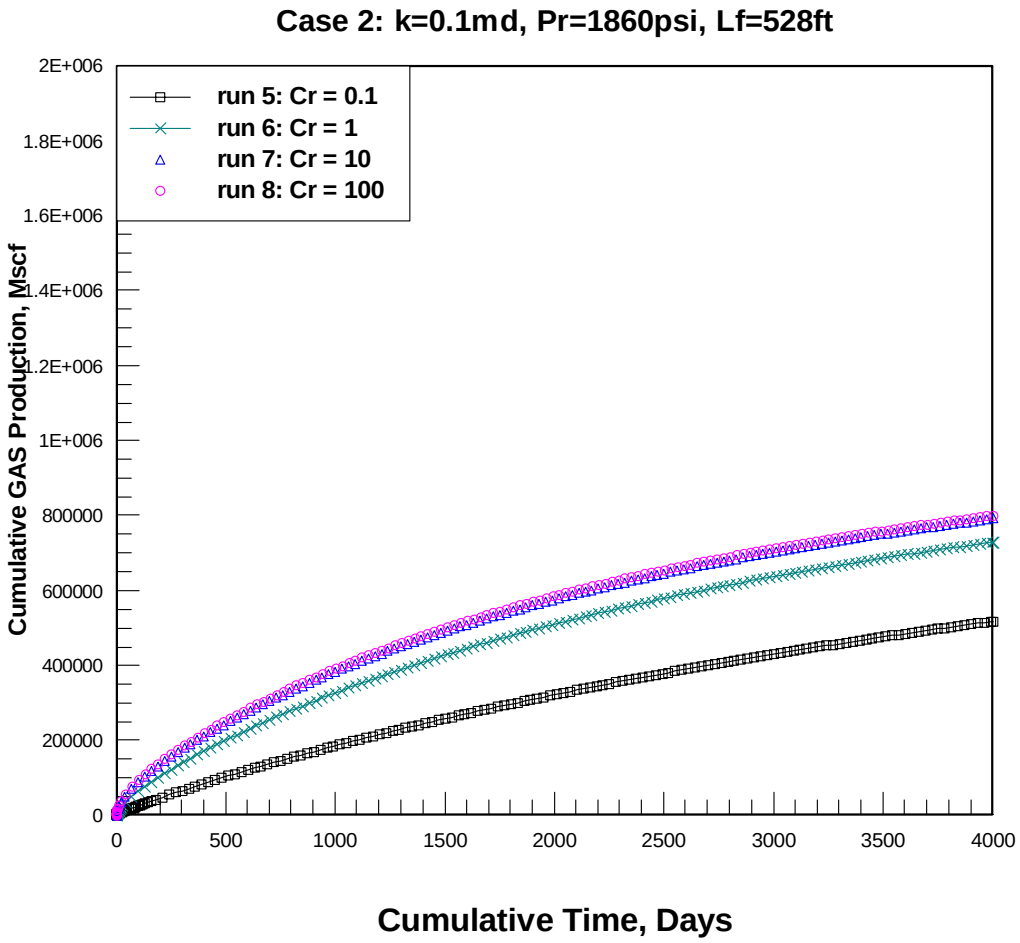

Figure 5.2.4—Cumulative gas production at different fracture conductivity for L_f = 528 ft, p_r = 1860 psi, k = 0.1 md, S_{wi} = 0.4 and h = 100 ft

If the dimensionless fracture conductivity can be increased from 0.1 to 10, the cumulative gas production will be increase by 32% in ten years, which is about 1.04 bcf for one well in 160 acre spacing. Thus, strong proppants and high fracture conductivity are critical to the success of a fracture treatment and long-term gas production. However, from a production point of view, a proppant that can provide dimensionless fracture conductivity of 10 or more is good enough for gas production. The trend of cumulative gas production values as a function of dimensionless conductivity for the two scenarios shown in Figure 5.2.2 and 5.2.4 are similar. However, the flow pressure scenario recovers less gas because of lower value of gas-in-place and lower energy.

5.3 Simulation results for the effect of proppant crushing

In this section, we build upon the results from the previous computer runs for both single-phase flow and gas/water two-phase flow by adding the effect of proppant crushing. It is well known that the value of fracture conductivity will decrease as the value of closure pressure on the proppant increases. We can model these effects and we generally call this "proppant crushing". The proppant crushing data we have used are from tests run using Ottawa sands as shown in Figure 4.3.1 and 4.3.2. The assumption we used to include the effects of proppant crushing is that a hydraulic fracture has been created and the fracture fluid that leaks off into the reservoir formation has the same properties as the formation water. Thus, after a fracture treatment, the vicinity around fracture is saturated with water phase, which is a combination of fracture fluid filtrate and formation water. The water phase can temporally reduce the gas from flowing into the fracture and into wellbore. The well takes time to clean up the fracture fluid filtrate before gas can flow at a maximum rate. When we include proppant crushing, the effect is additive, and our analysis of cleanup becomes more complex and more realistic.

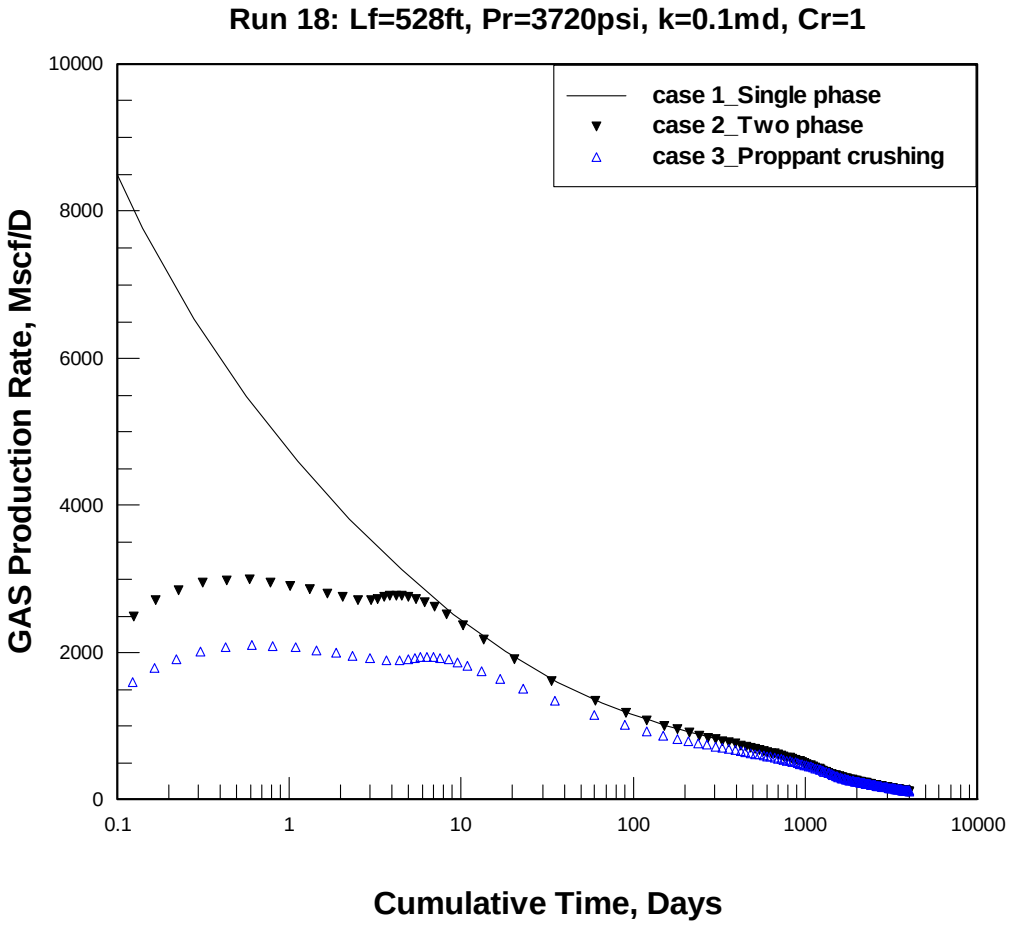

Figure 5.3.1—Gas production rate for different cases for L_f = 528 ft, p_r = 3720 psi, k = 0.1 md, C_r =1, S_{wi} = 0.4 and h = 100 ft

Figure 5.3.1 shows the gas production rate vs time for different cases after a fracture treatment for Run 18, where L_f = 528 ft, p_r = 3720 psi, k = 0.1 md, C_r =1, S_{wi} = 0.4 and h = 100 ft. We can see that the gas production rate increases for a certain period of time before it reaches a maximum value, which is the cleanup time. For Case 2 (two-phase flow), it takes about 10 days to clean up, and for case 3 of proppant crushing, it takes over 100 days to clean up. Thus, when more factors are considered, the cleanup process takes longer and results should be more realistic. This should help everyone including researchers and engineers, to understand how the cleanup process has been affected by the values of fracture conductivity.

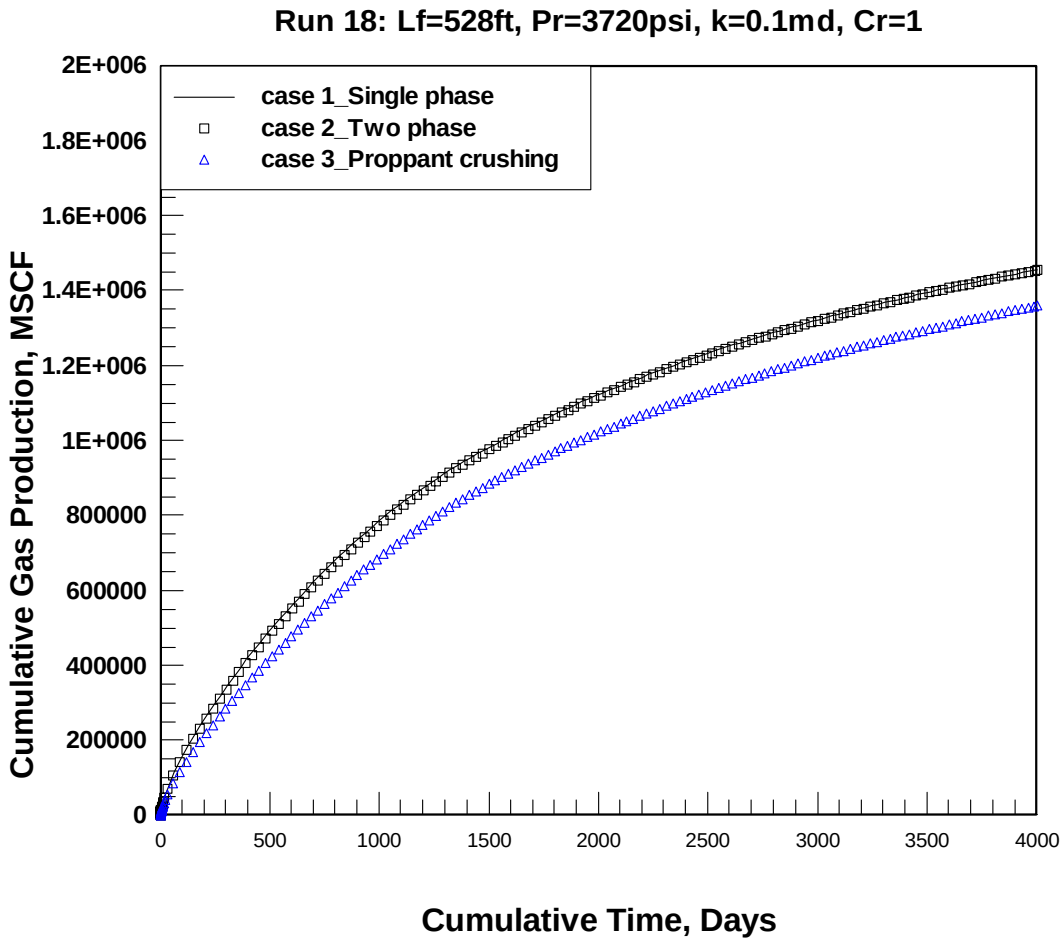

Figure 5.3.2—Cumulative gas production for different cases for L_f = 528 ft, p_r = 3720 psi, k = 0.1 md, C_r =1, S_{wi} = 0.4 and h = 100 ft

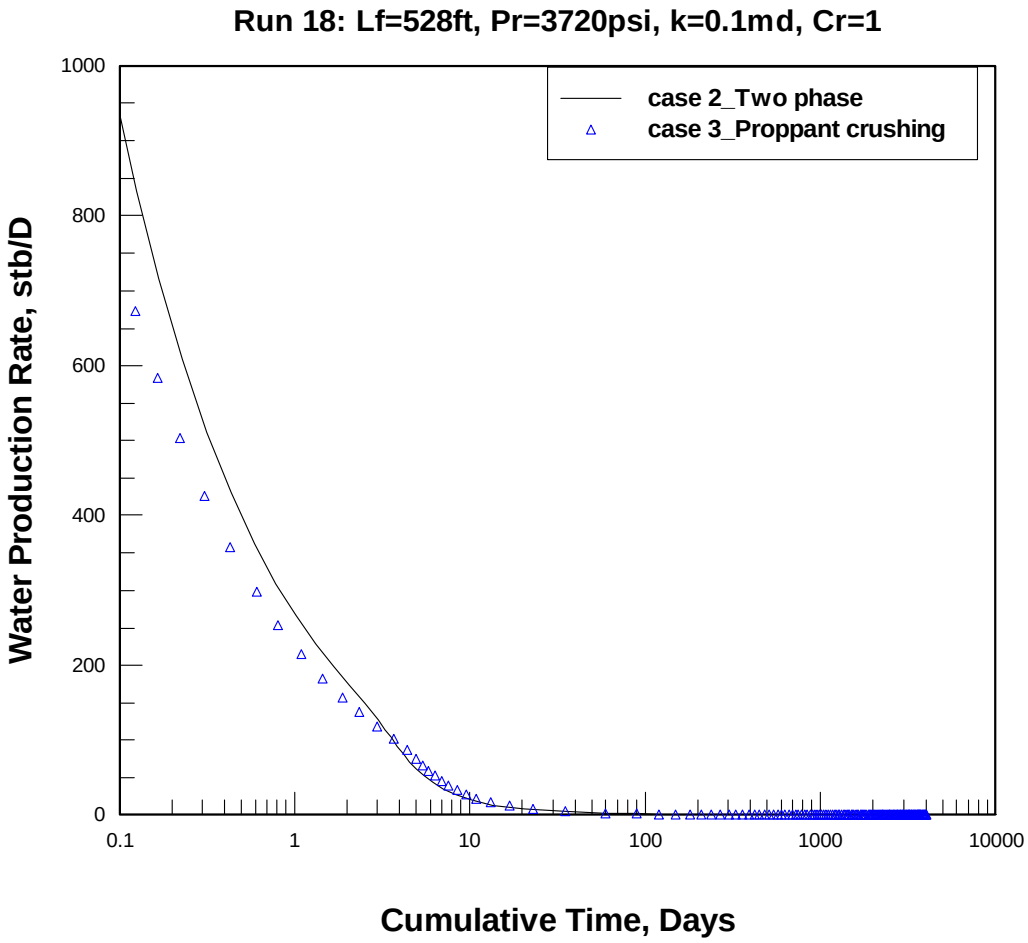

Figure 5.3.3—Water production rate for different cases for L_f = 528 ft, p_r = 3720 psi, k = 0.1 md, C_r =1, S_{wi} = 0.4 and h = 100 ft

Figure 5.3.2 shows the cumulative gas production vs time for three different cases after a fracture treatment for L_f = 528 ft, p_r = 3720 psi, k = 0.1 md, C_r =1, S_{wi} = 0.4 and h = 100 ft. We can see that more gas will be produced if proppant crushing does not happen. Figure 5.3.3 shows the water production rate. For case 1 (single-phase flow), there is no formation water and no fracture fluid, so water production is zero. For case 2 and case 3, the produced water is similar. Remember that the water can be a combination of both fracture fluid filtrate and formation water. We can see that most water is produced during early time. After about 10 days, the water production levels off at a very low rate.

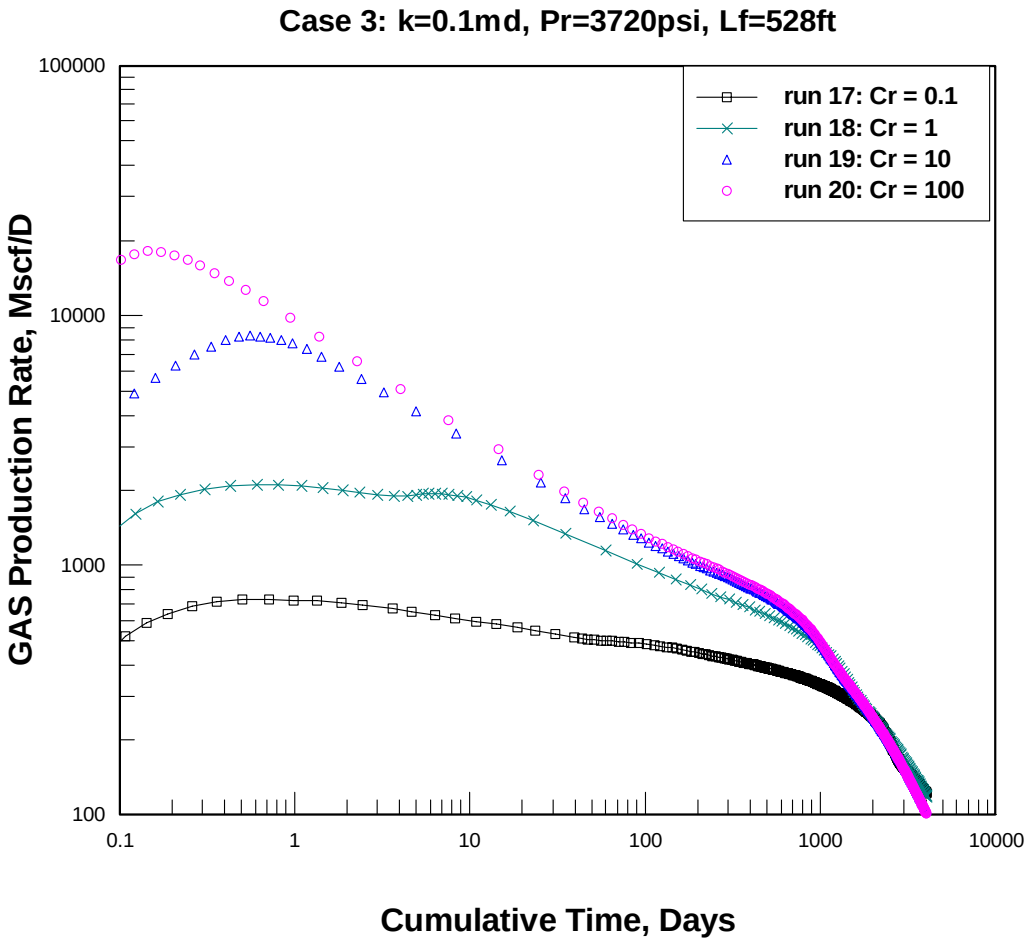

Figure 5.3.4—Gas production rate for different fracture conductivities for L_f = 528 ft, p_r = 3720 psi, k = 0.1 md, S_{wi} = 0.4 and h = 100 ft

Figure 5.3.4 shows the gas production rate vs time for different values of fracture conductivity after a fracture treatment where L_f = 528 ft, p_r = 3720 psi, k = 0.1 md, S_{wi} = 0.4 and h = 100 ft. We can see that the gas production rate increases for a certain period of time before it reaches a maximum value, which is the cleanup time. The fracture fluid cleans up faster if the fracture conductivity is higher. For a fracture conductivity of 0.1, the gas production rate is much lower during the first three years of production.

For this medium pressure example, one can clearly see the effect of fracture conductivity upon fracture fluid cleanup. We normally try to design for a C_r of 10 or larger. Notice in

Figure 5.3.4, the early gas flow rate for a C_r of 10 is around 4,000 Mscf/day and peaks out at around 8,000 Mscf/day after one day. For the infinite fracture conductivity (C_r = 100), the gas flow rate starts out at 20,000 Mscf/day, and declines to around 10,000 Mscf/day after a few days. Thus, after a few days, C_r = 10 and C_r = 100 behave very similarly.

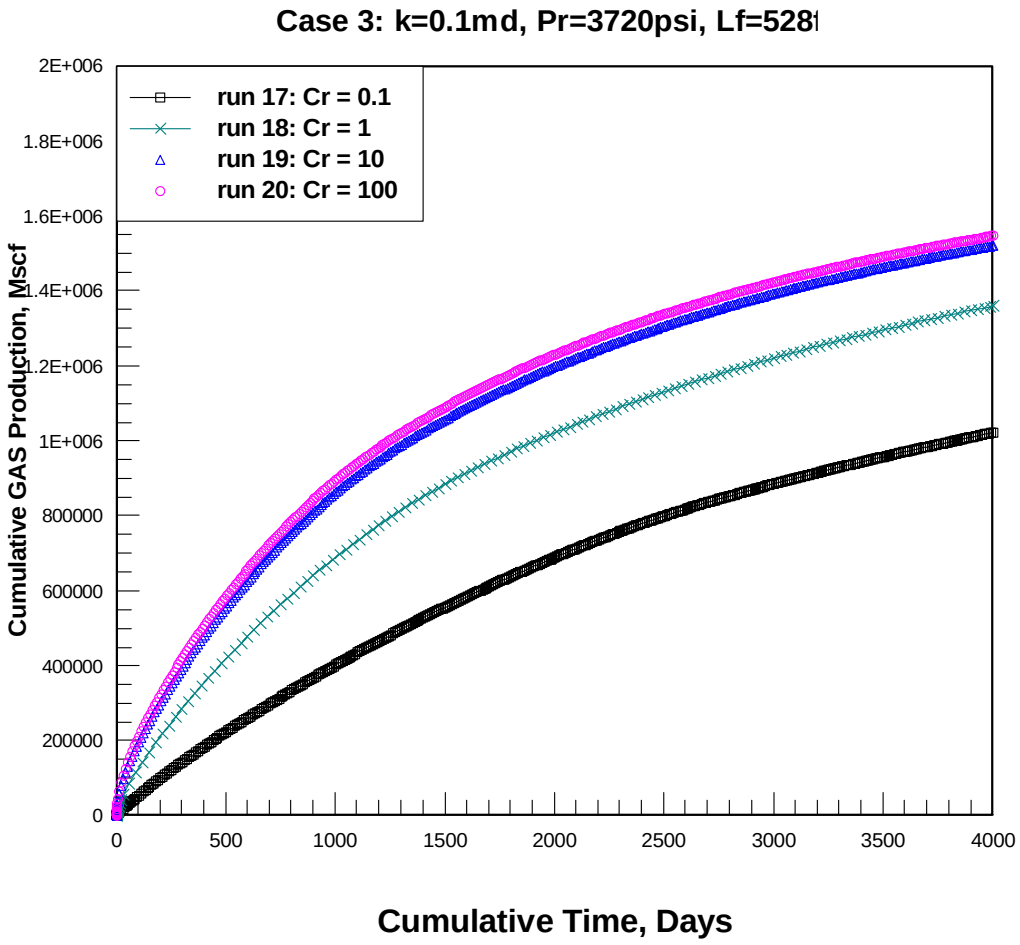

Figure 5.3.5—Cumulative gas production at different fracture conductivity for L_f = 528 ft, p_r = 3720 psi, k = 0.1 md, S_{wi} = 0.4 and h = 100 ft

Figure 5.3.5 shows cumulative gas production at different values of dimensionless fracture conductivity after a fracture treatment for Case 3 and Runs 17-20 where L_f = 528 ft, p_r = 3720 psi, k = 0.1 md, S_{wi} = 0.4 and h = 100 ft. We can see that cumulative gas production will be higher if the fracture conductivity is higher. However, the cumulative

gas production does not differ much once the fracture conductivity is above 10. If the fracture conductivity can be increased from 0.1 to 10, the cumulative gas production will be increased by 50% in ten years, which is about 2.0 bcf for one well on a 160 acre spacing. So, strong proppants and high fracture conductivity are critical to the success of fracture treatment and long-term gas production.

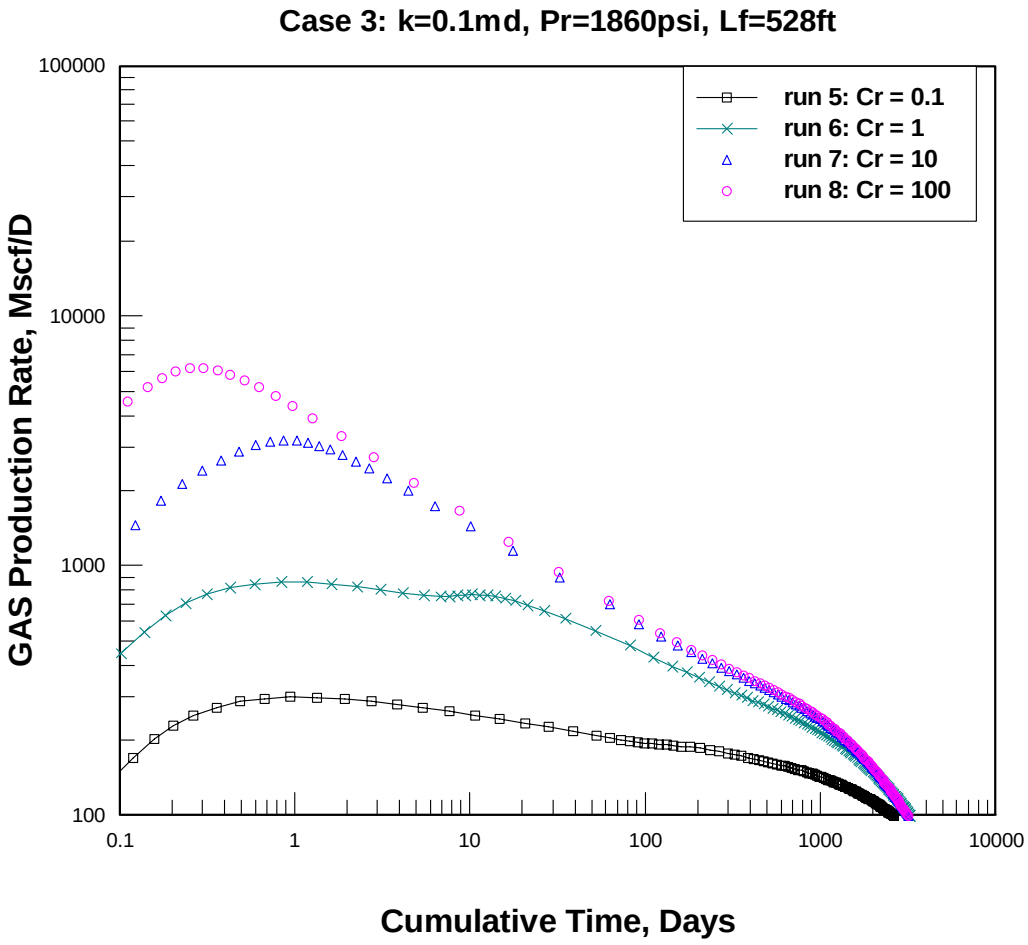

Figure 5.3.6—Gas production rate at different fracture conductivity for L_f = 528 ft, p_r = 1860 psi, k = 0.1 md, S_{wi} = 0.4 and h = 100 ft

Figure 5.3.6 shows the gas production rate vs time at different fracture conductivity after a fracture treatment for Case 3 and Run 5-8, where L_f = 528 ft, p_r = 1860 psi, k = 0.1 md, S_{wi} = 0.4 and h = 100 ft for the low reservoir pressure scenario. We can see that the gas production rate increases for a period of time before it reaches a maximum value, which is the cleanup time. The fracture cleans up faster if the fracture conductivity is higher. For values of dimensionless fracture conductivity of 0.1 and 1.0, the gas production rate is much lower during the first three years of production comparing to C_r = 10.

For this low pressure example, one can clearly see the effect of fracture conductivity upon fracture fluid cleanup. We normally try to design for a C_r of 10 or higher. Notice in Figure 5.3.6, the early gas flow rate for a C_r of 10 is around 1,400 Mscf/day and peaks out at around 3,000 Mscf/day after one day. For the infinite fracture conductivity (C_r = 100), the gas flow rate starts out at 4,500 Mscf/day, increases to 7,000 Mscf/day, and then declines to around 4,000 Mscf/day after one day. Thus, after a few days, C_r = 10 and C_r = 100 behave very similarly.

The cleanup for this case is similar to the medium pressure case in Figure 5.3.4, but at the same fracture conductivity, the cleanup time is longer, and the gas rate is lower. This means that the reservoir energy is a very important factor in analysis of fracture fluid cleanup as one would expect.

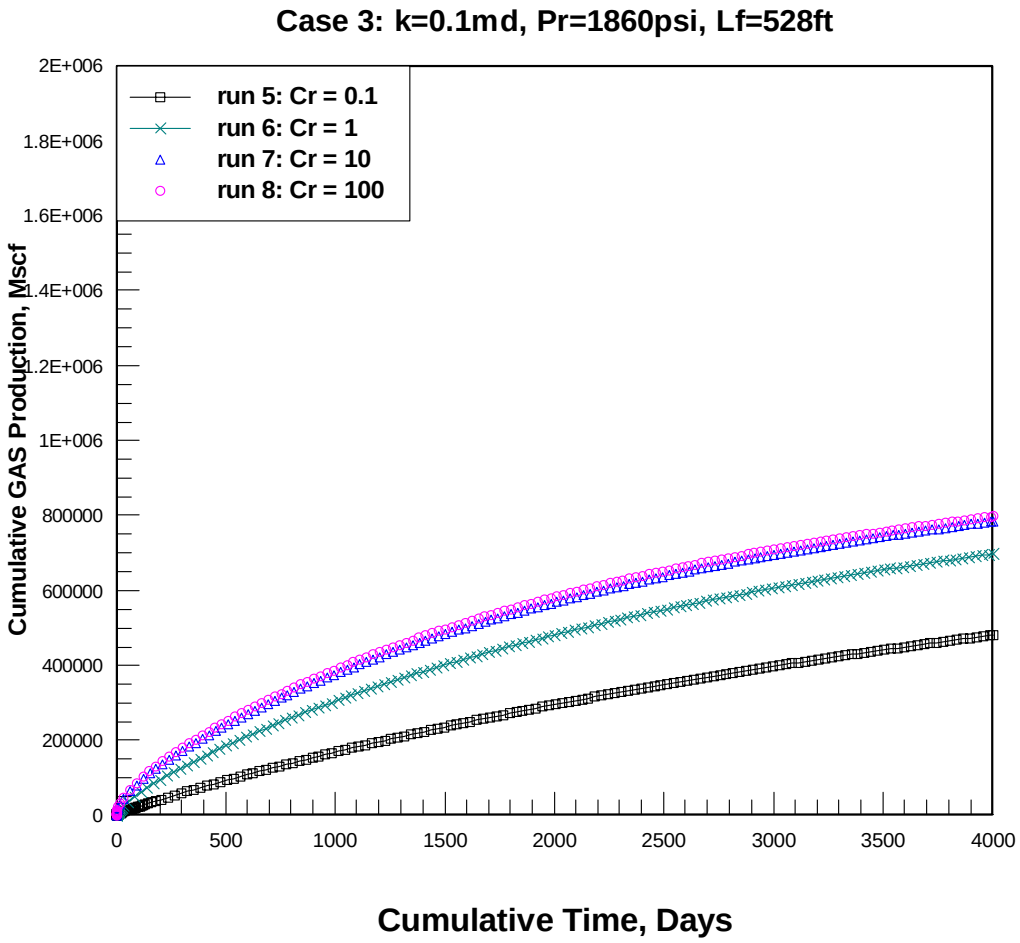

Figure 5.3.7—Cumulative gas production at different fracture conductivity for L_f = 528 ft, p_r = 1860 psi, k = 0.1 md, S_{wi} = 0.4 and h = 100 ft

Figure 5.3.7 shows cumulative gas production at different fracture conductivity after a fracture treatment for Case 3 and Runs 5-8, where L_f = 528 ft, p_r = 1860 psi, k = 0.1 md, S_{wi} = 0.4 and h = 100 ft. We can see that cumulative gas production will be higher if fracture conductivity is higher. However, the cumulative gas production does not differ much once the dimensionless fracture conductivity is above 10. If the dimensionless fracture conductivity can be increased from 0.1 to 10, the cumulative gas production will be increase by 68% in ten years, which is about 1.24 bcf for one well on a 160 acre well spacing. Thus, strong proppants and high fracture conductivity are critical to the success of fracture treatment and long-term gas production for cases at high and low reservoir pressures.

However, from a production point of view, a proppant which can provide dimensionless fracture conductivity of 10 is good enough for gas production. The cumulative gas productions for these runs are similar to the higher pressure runs in Figure 5.3.5, but at the same fracture conductivity, the cumulative gas production is lower due to the lower reservoir pressure.

5.4 Simulation results for the effect of polymer filter cake

In this section, we continue by using the previous simulation of gas-water, two-phase flow with proppant crushing by adding the effect of a polymer filter cake inside the fracture pack. Simulation results, analyses, and new findings are reported here. The filter cake is represented as separate cells that have properties to simulate a filter cake as shown in Figure 4.4.1. For this study, the filter cake properties, such as porosity and permeability, are assumed to be constant. The main effect of the filter cake in our simulation will be reduction of fracture width, which, in turn, reduces fracture conductivity.

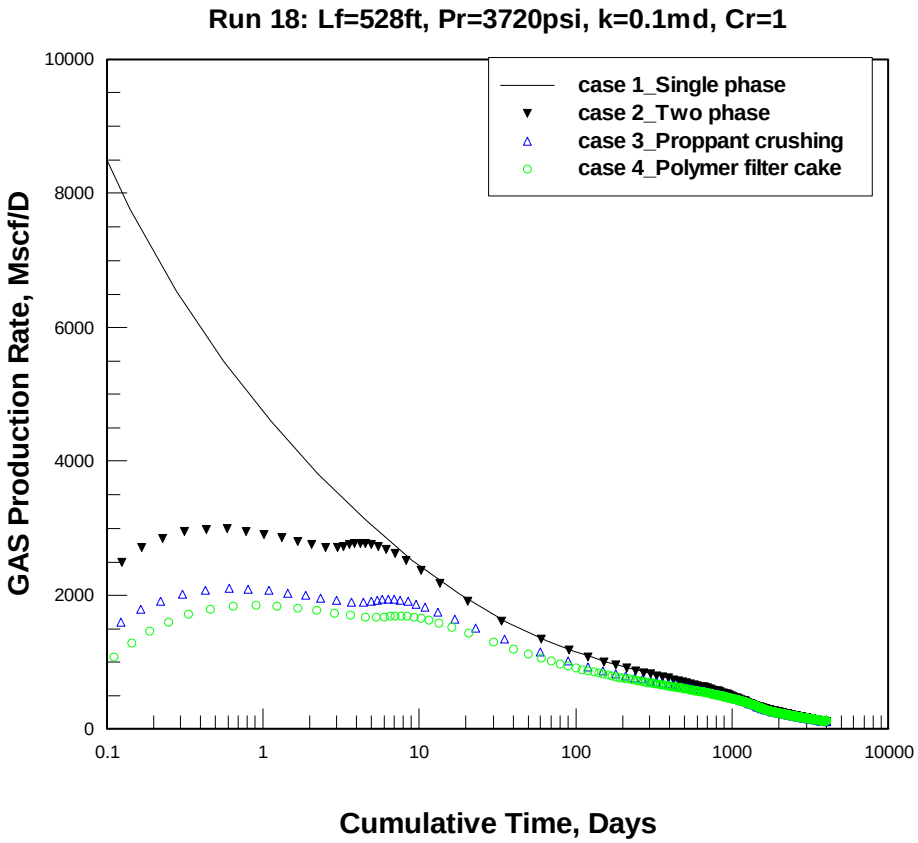

Figure 5.4.1—Gas production rate for different cases for L_f = 528 ft, p_r = 3720 psi, k = 0.1 md, C_r =1, S_{wi} = 0.4 and h = 100 ft

Figure 5.4.1 shows the gas production rate vs time for different cases after a fracture treatment for Run 18 and Case 1-4, where L_f = 528 ft, p_r = 3720 psi, k = 0.1 md, C_r =1, S_{wi} = 0.4 and h = 100 ft. We can see that the effect of filter cake does reduce the gas production rate during early time. After 30 days, there is not much difference between the curves with and without filter cake. If the filter cake thickness is minimal, the effect on gas production will minimal. So when more factors are considered, the cleanup process takes longer and results should be more realistic. This should help both researchers and engineers to understand how the cleanup process has been affected by fracture width reduction due to filter cake deposition.

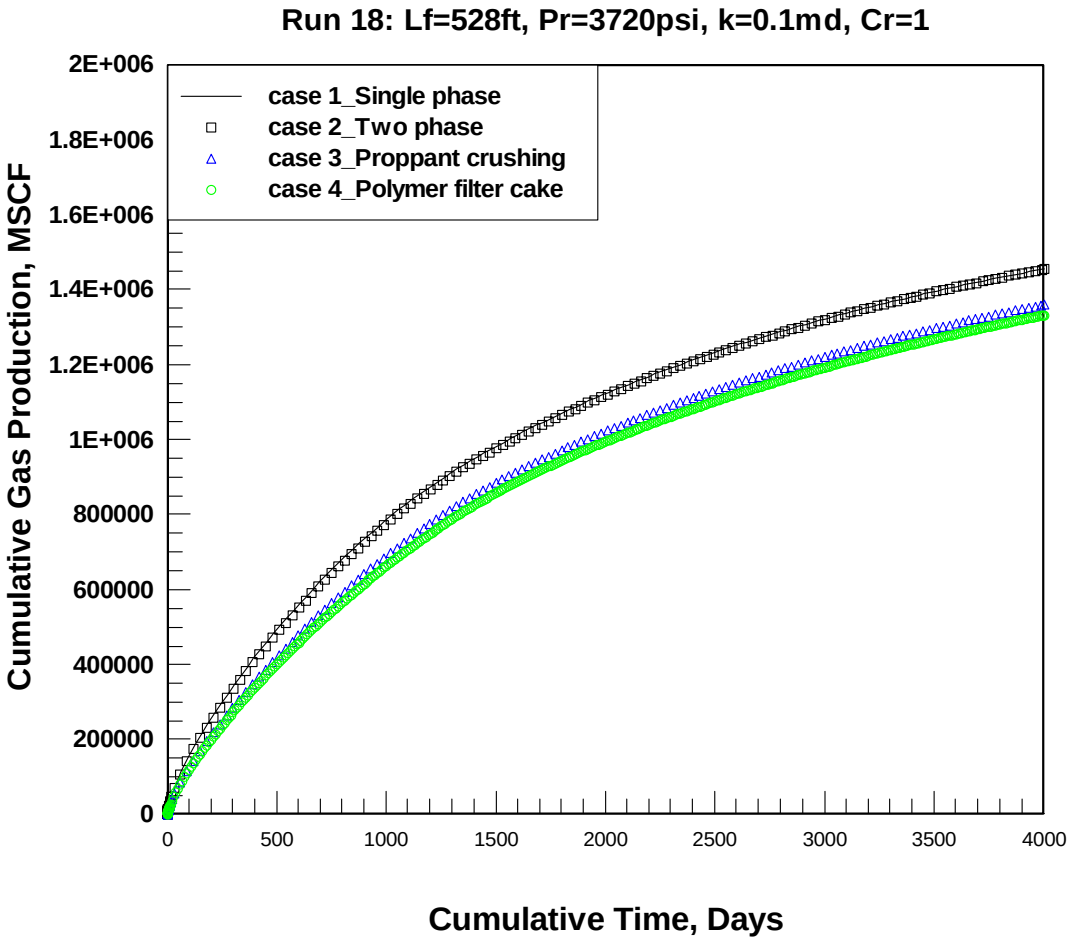

Figure 5.4.2—Cumulative gas production for different cases for L_f = 528 ft, p_r = 3720 psi, k = 0.1 md, C_r =1, S_{wi} = 0.4 and h = 100 ft

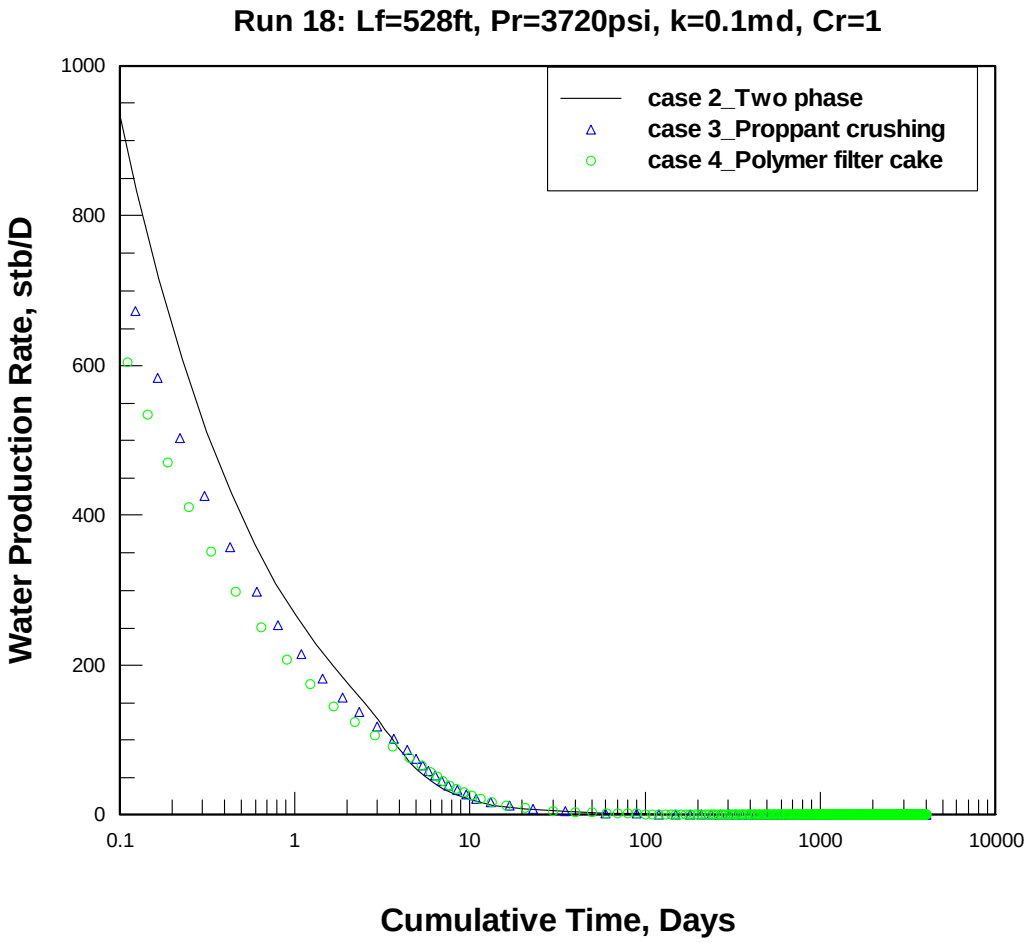

Figure 5.4.3—Water production rate for different cases for L_f = 528 ft, p_r = 3720 psi, k = 0.1 md, C_r =1, S_{wi} = 0.4 and h = 100 ft

Figure 5.4.2 shows the cumulative gas production vs time for Run 18 and Case 2-4, where L_f = 528 ft, p_r = 3720 psi, k = 0.1 md, C_r =1, S_{wi} = 0.4 and h = 100 ft. The filter cake does not make much difference on the cumulative gas production comparing to the case 3 without filter cake for the scenario we are describing in this example. Figure 5.4.3 shows the water production rate. For cases 2, 3 and 4, the produced water can come from formation water or fracture fluid, which is considered to be the same as formation water. We can see that most water is produced during early time; after about 10 days, the water production levels off at a very low rate. The filter cake does reduce the water production rate.

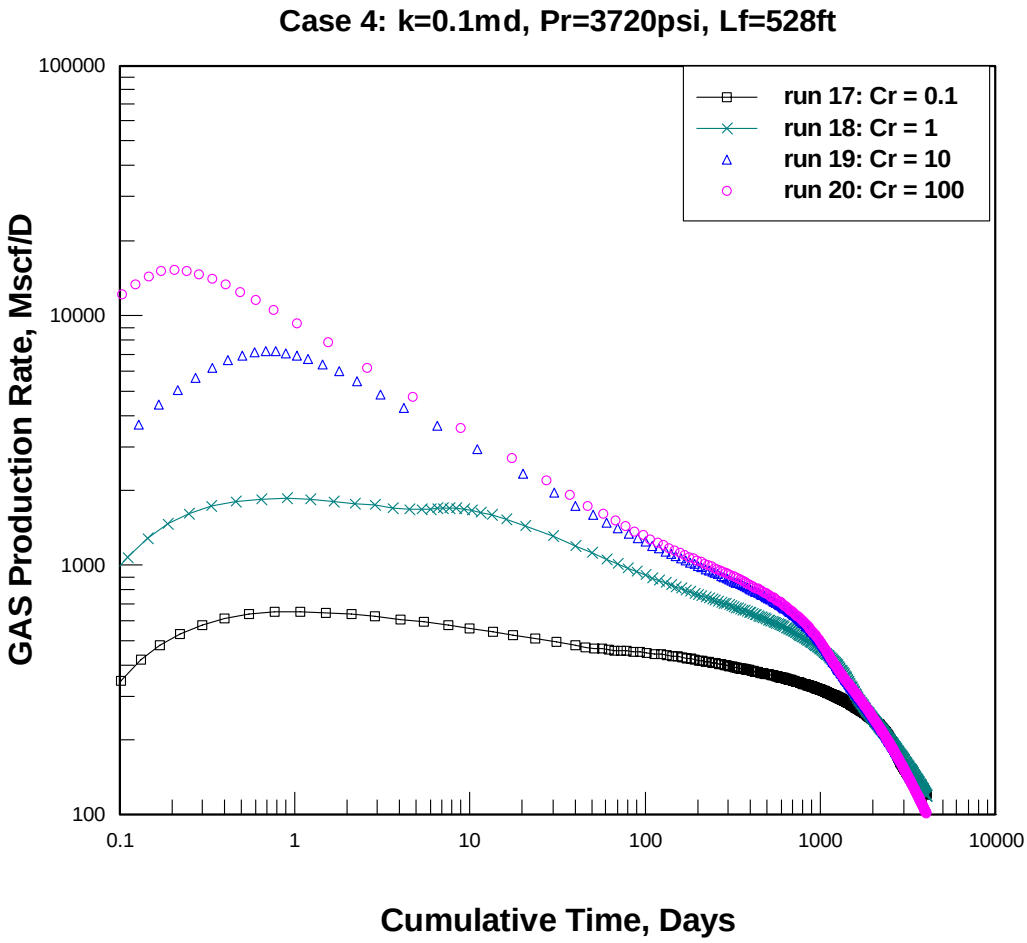

Figure 5.4.4—Gas production rate at different fracture conductivity for L_f = 528 ft, p_r = 3720 psi, k = 0.1 md, S_{wi} = 0.4 and h = 100 ft

Figure 5.4.4 shows the gas production rate vs time at different fracture conductivity after a fracture treatment for Case 4 and Run 17-20, where L_f = 528 ft, p_r = 3720 psi, k = 0.1 md, S_{wi} = 0.4 and h = 100 ft. We can see that the gas production rate increases for a certain period of time before it reaches a maximum value as before, which is the cleanup time. The fracture cleans up faster if the fracture conductivity is higher, but after about 3 years, there is not much difference between the cases except for C_r = 0.1. For a dimensionless fracture conductivity of 0.1, the gas production rate is much lower during the first three years of production.

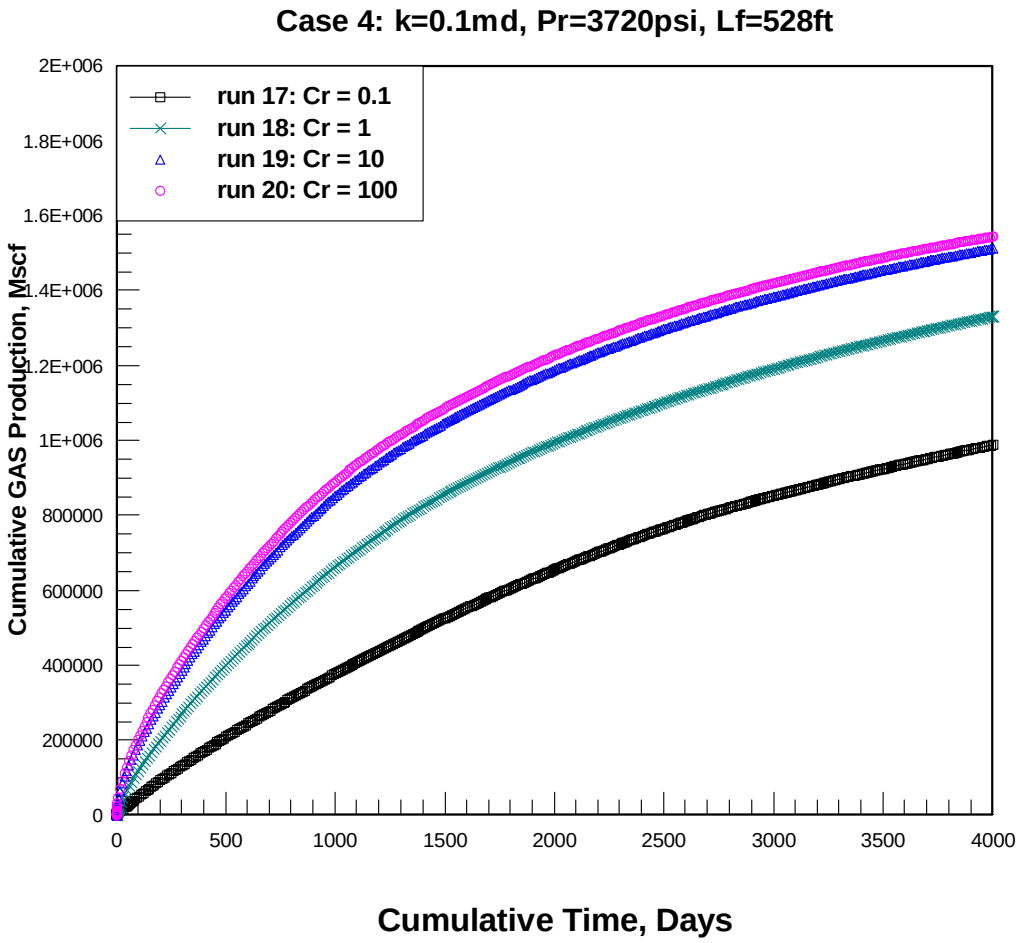

Figure 5.4.5—Cumulative gas production at different fracture conductivity for L_f = 528 ft, p_r = 3720 psi, k = 0.1 md, S_{wi} = 0.4 and h = 100 ft

Figure 5.4.5 shows cumulative gas production at different values of dimensionless fracture conductivity after a fracture treatment considering the effect of filter cake for Case 4, where L_f = 528 ft, p_r = 3720 psi, k = 0.1 md, S_{wi} = 0.4 and h = 100 ft. We can see that cumulative gas production will be higher if fracture conductivity is higher. However, the cumulative gas production does not differ much once the dimensionless fracture conductivity is above 10. If the dimensionless fracture conductivity can be increased from 0.1 to 10, the cumulative gas production will increase by 50% in ten years, which is about 2.0 bcf for one well of 160-acre drainage area. This is almost the same as the case without considering filter cake. The conclusion is same as previous Section 5.3 that

strong proppants and high fracture conductivity are critical to the success of fracture treatment and long-term gas production. Only if the filter cake approaches the fracture width, does it make a big difference on the gas production.

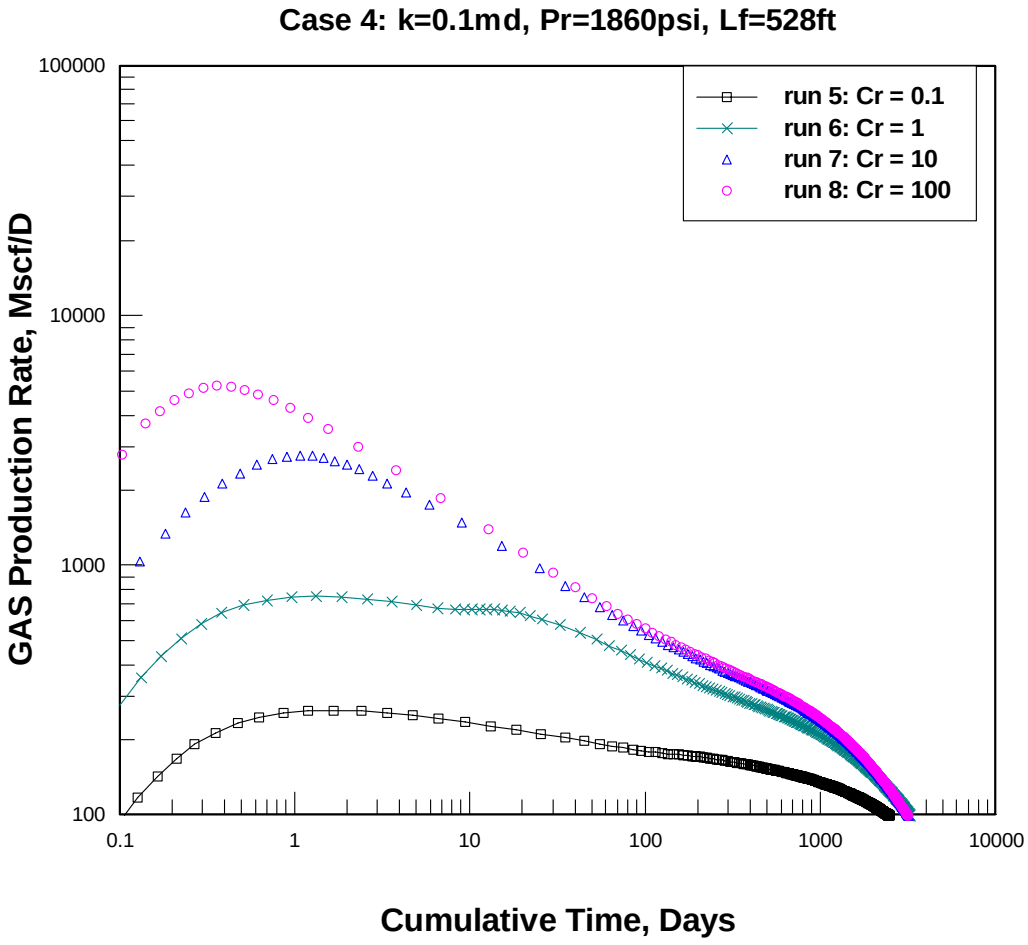

Figure 5.4.6—Gas production rate at different fracture conductivity for L_f = 528 ft, p_r = 1860 psi, k = 0.1 md, S_{wi} = 0.4 and h = 100 ft

Figure 5.4.6 shows the gas production rate vs time at different fracture conductivity considering filter cake inside the fracture after a treatment for L_f = 528 ft, p_r = 1860 psi, k = 0.1 md, S_{wi} = 0.4 and h = 100 ft. This is a low reservoir pressure scenario. We can see that the gas production rate increases for a period of time before it reaches a maximum value, which is the cleanup time. The fracture cleans up faster if the fracture conductivity is higher. For a dimensionless fracture conductivity of 0.1 and 1.0, the gas production rate

is much lower during the first three years of production comparing to C_r = 10. The cleanup for these runs is similar to the higher pressure runs in Figure 5.4.4, but at the same fracture conductivity, the cleanup time is longer, and the gas flow rate is lower. This means that the reservoir energy is a very important factor in analysis of fracture fluid cleanup.

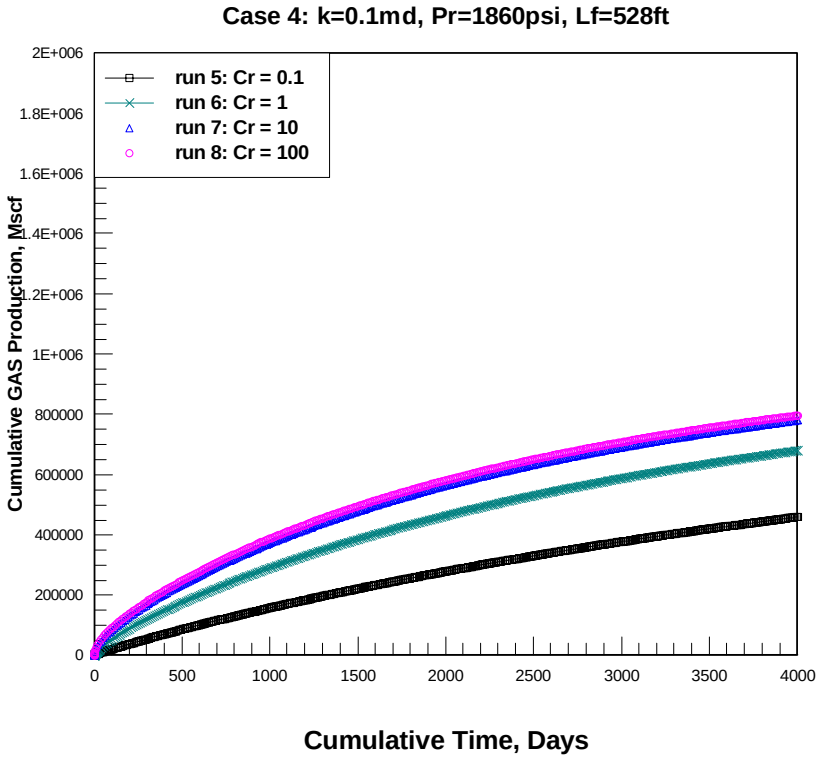

Figure 5.4.7—Cumulative gas production at different fracture conductivity for L_f = 528 ft, p_r = 1860 psi, k = 0.1 md, S_{wi} = 0.4 and h = 100 ft

Figure 5.4.7 shows the cumulative gas production at different fracture conductivity considering filter cake inside a fracture after a fracture treatment for L_f = 528 ft, p_r = 1860 psi, k = 0.1 md, S_{wi} = 0.4 and h = 100 ft. We can see that cumulative gas production will be higher if fracture conductivity is higher. However, the cumulative gas production does not differ much once the dimensionless fracture conductivity is above 10. If the fracture conductivity can be increased from 0.1 to 10, the cumulative gas production will increase by 63% in ten years, which is almost the same as the case without the effect of filter cake.

5.5 Simulation results for the effect of yield stress

After we validated that our yield-power law model was programmed correctly, we made a series of simulation runs to study and quantify the effect of gel yield stress upon the cleanup behavior of a well. The model is different from previous two-phase flow cases. We now model three phases: gas, fracture fluid filtrate, and gel. Fracture fluid filtrate is the part that leaks off into reservoir formation, and the properties of the fracture fluid filtrate are assumed to be the same as the properties of the formation water. Gel is the part of fracture fluid that stays inside the fracture pack after the fracture fluid leaks off. The gel in the fracture will be a concentrated polymer with concentrations up to 300 to 1,000 lbm/1,000 gallon. The detailed properties of the gel in the fracture have been discussed in Section 4.5 of Chapter IV.

Some of the simulation results and analyses are presented in pressure and saturation maps at different times during the cleanup process for a variety of conditions. The maps are shown at different times from 0 day to 1,000 days, after a fracture treatment. We can use these maps to see how the fracture cleans up with time.

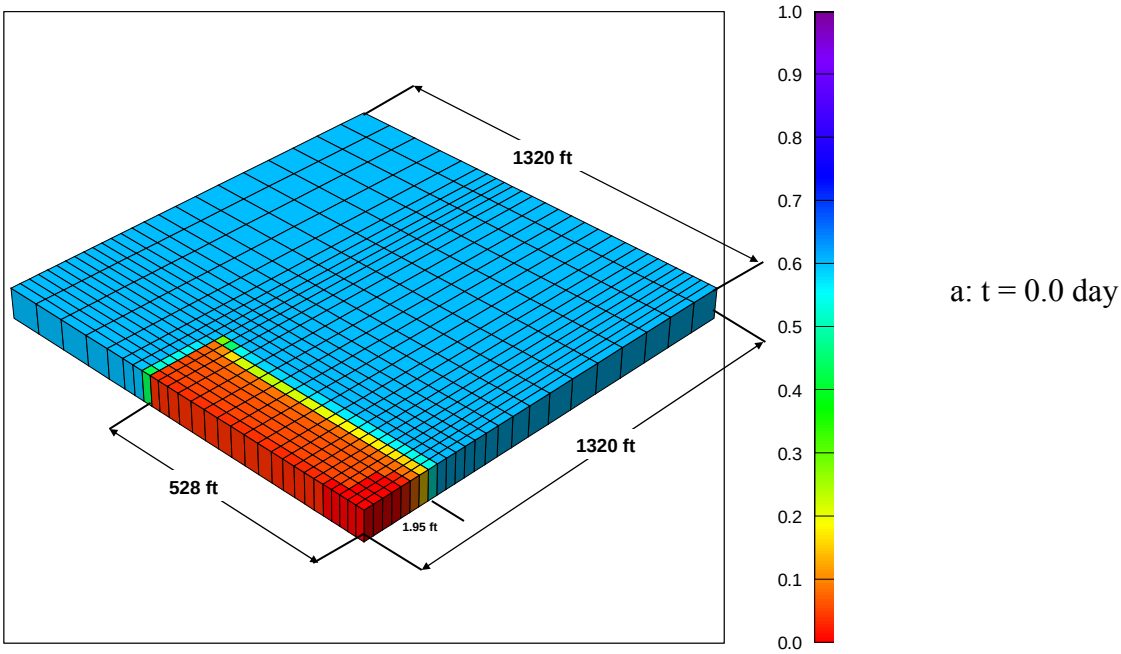

a: t = 0.0 day

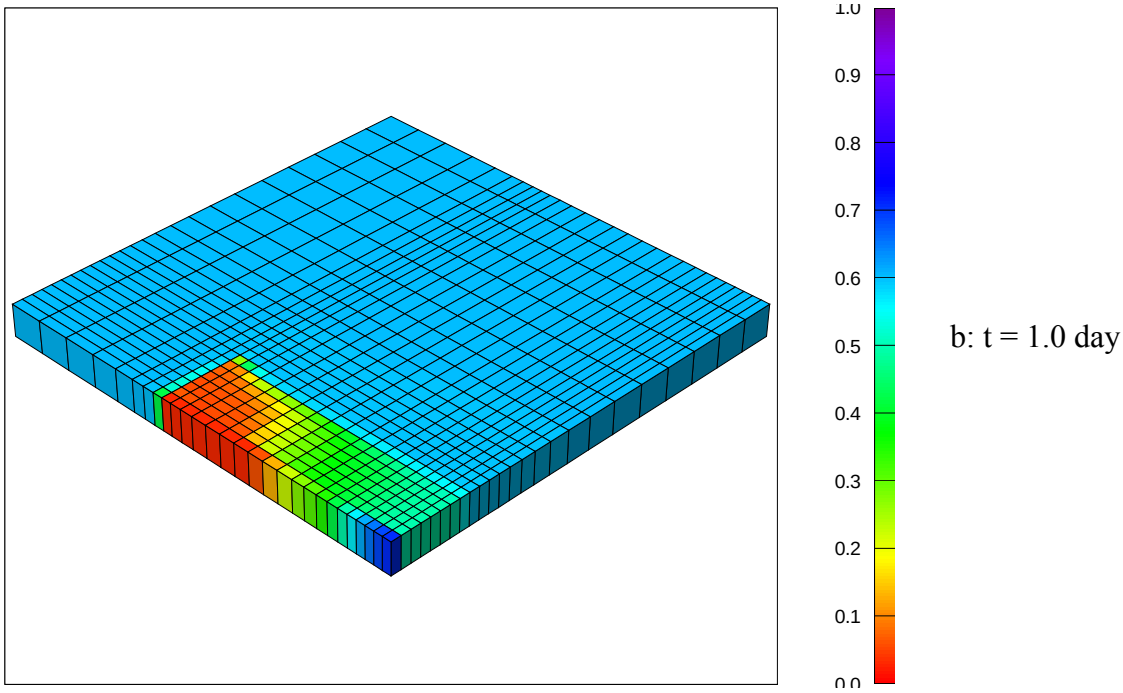

b: t = 1.0 day

Figure 5.5.1—Gas saturation maps after a fracture treatment by modeling two phase flow with proppant crushing (case 3, run 18) where L_f = 528 ft, p_r = 3720 psi, k = 0.1 md, C_r =1, S_{wi} = 0.4 and h = 100 ft

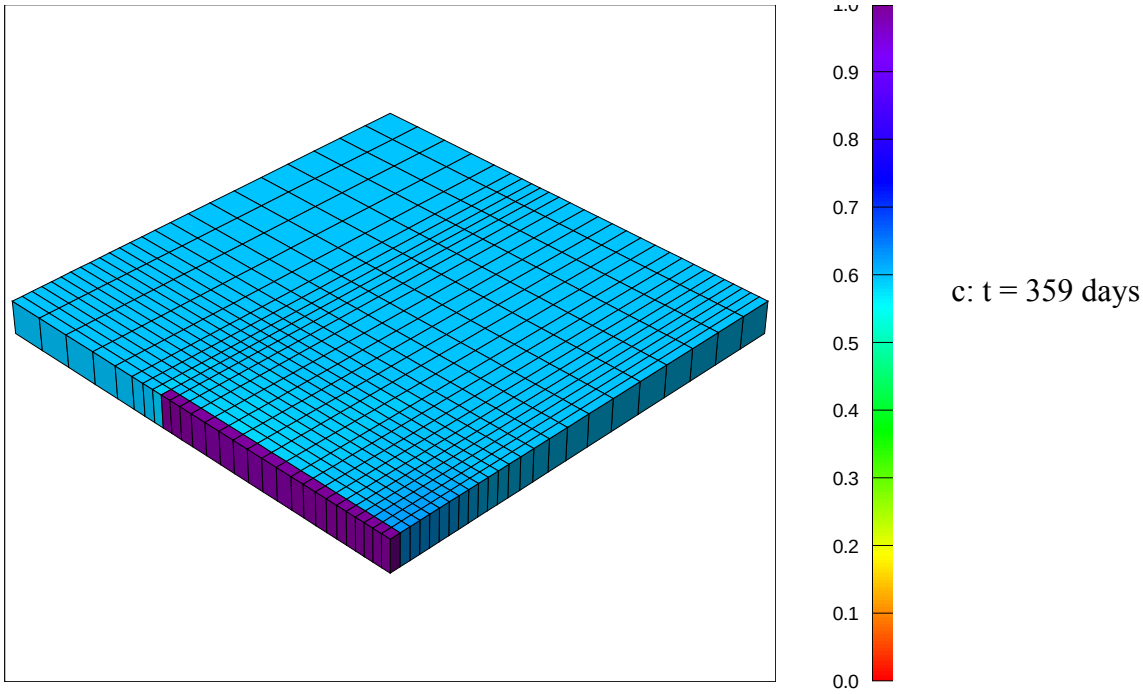

Figure 5.5.1—Continued

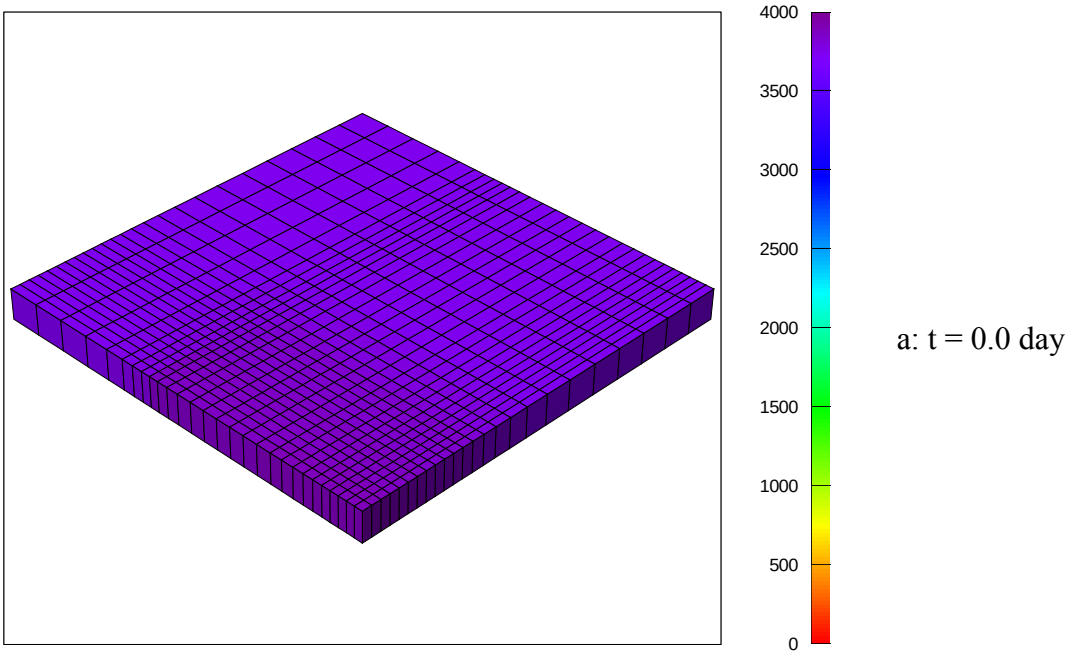

Figure 5.5.2—Gas pressure maps after a fracture treatment by modeling two phase flow with proppant crushing (case 3, run 18) where L_f = 528 ft, p_r = 3720 psi, k = 0.1 md, C_r =1, S_{wi} = 0.4 and h = 100 ft

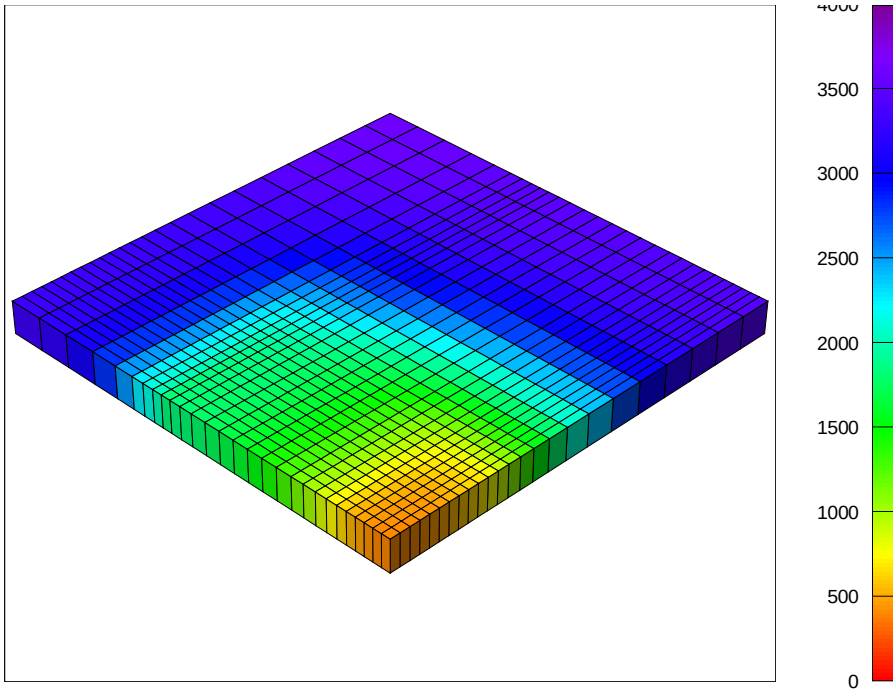

b: t = 359 days

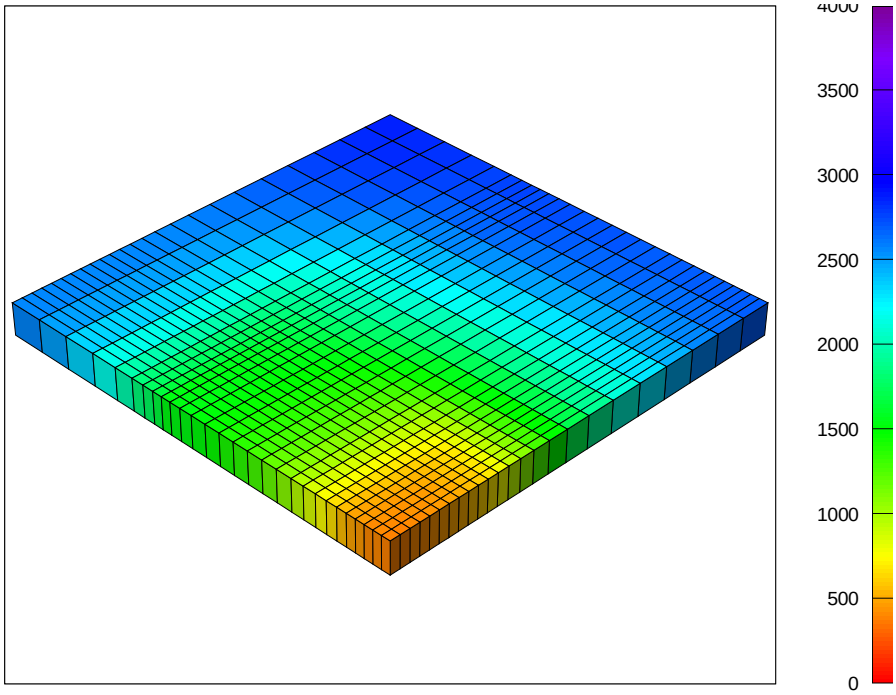

c: t = 1019 days

Figure 5.5.2—Continued

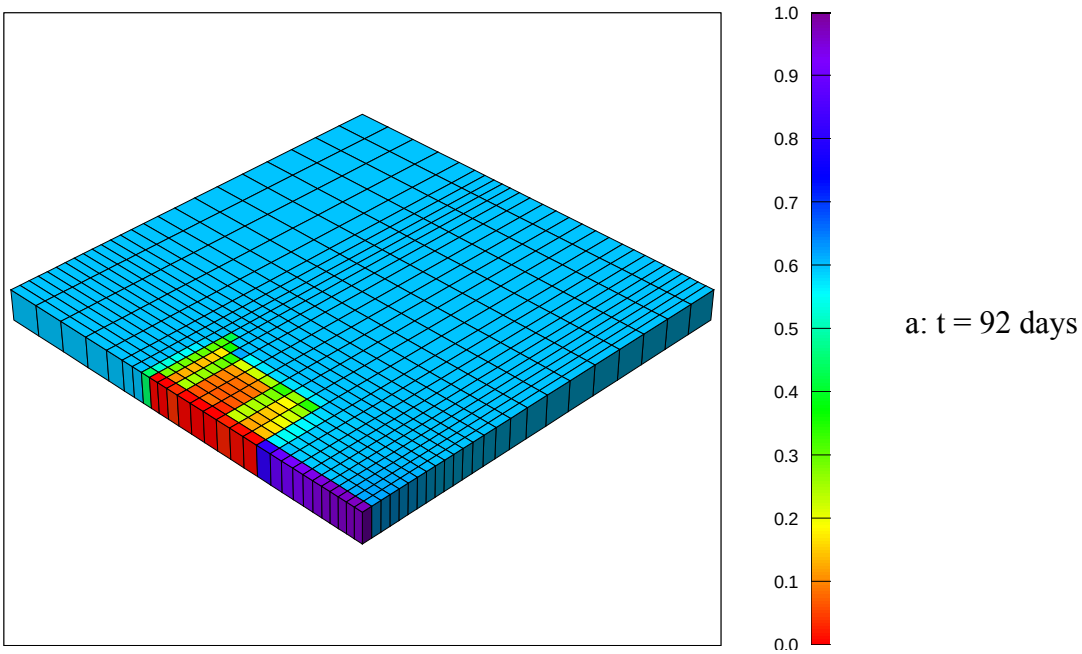

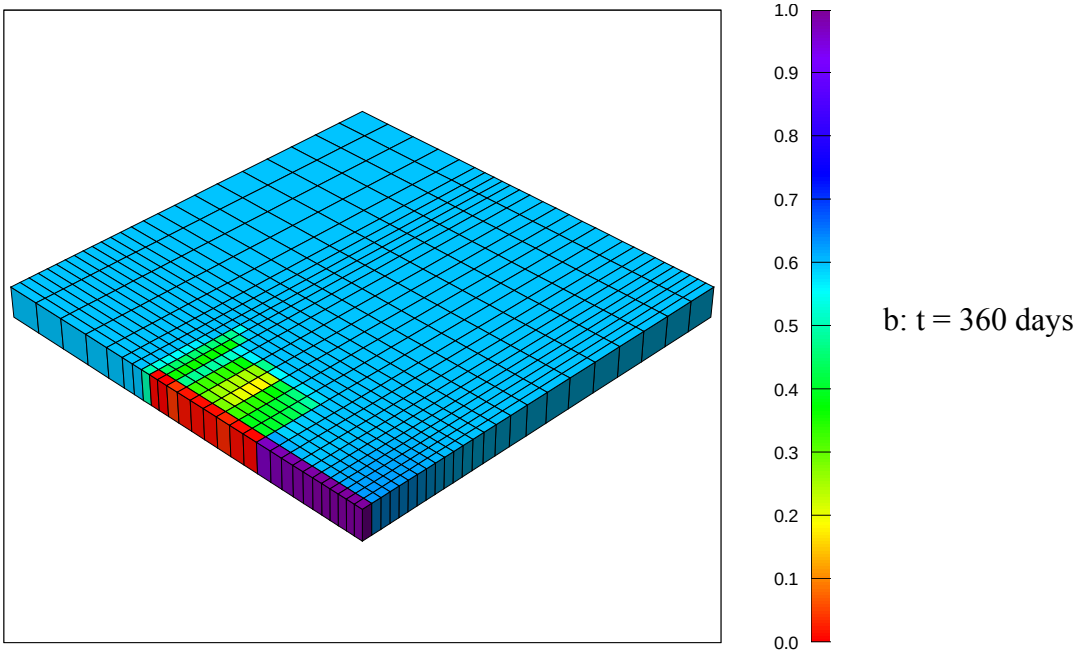

Figure 5.5.3—Gas saturation maps after a fracture treatment by modeling a non-Newtonian fracture fluid with yield stress of 3 pa (case 5a, run 18) where L_f = 528 ft, p_r = 3720 psi, k = 0.1 md, C_r =1, S_{wi} = 0.4 and h = 100 ft

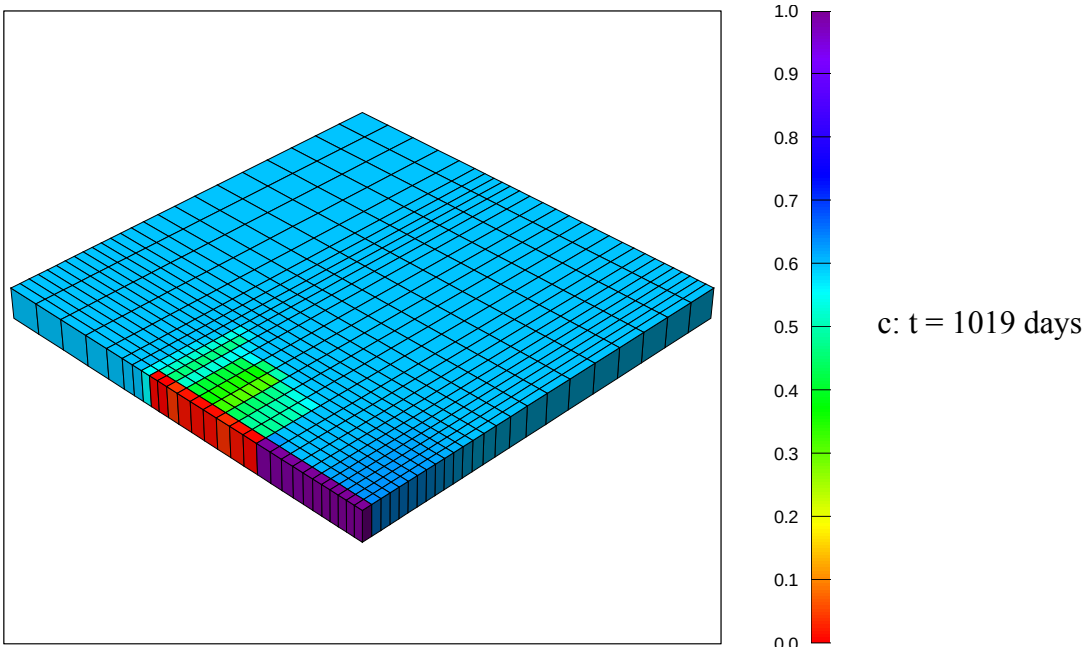

Figure 5.5.3—Continued

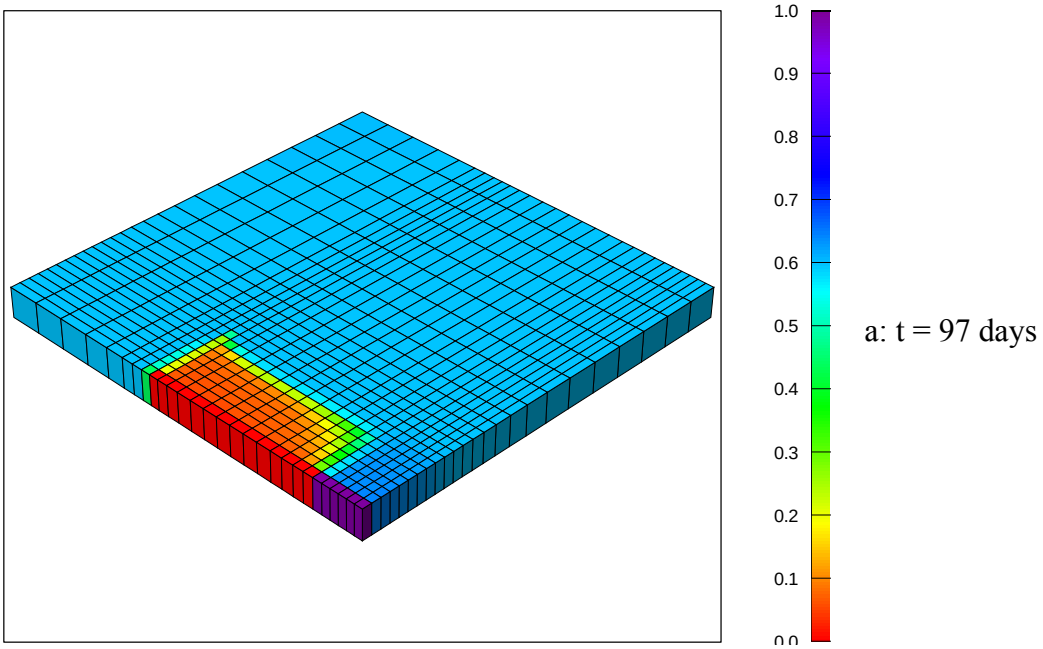

Figure 5.5.4—Gas saturation maps after a fracture treatment by modeling a non-Newtonian fracture fluid with yield stress of 20 pa (case 5c, run 18) where L_f = 528 ft, p_r = 3720 psi, k = 0.1 md, C_r =1, S_{wi} = 0.4 and h = 100 ft

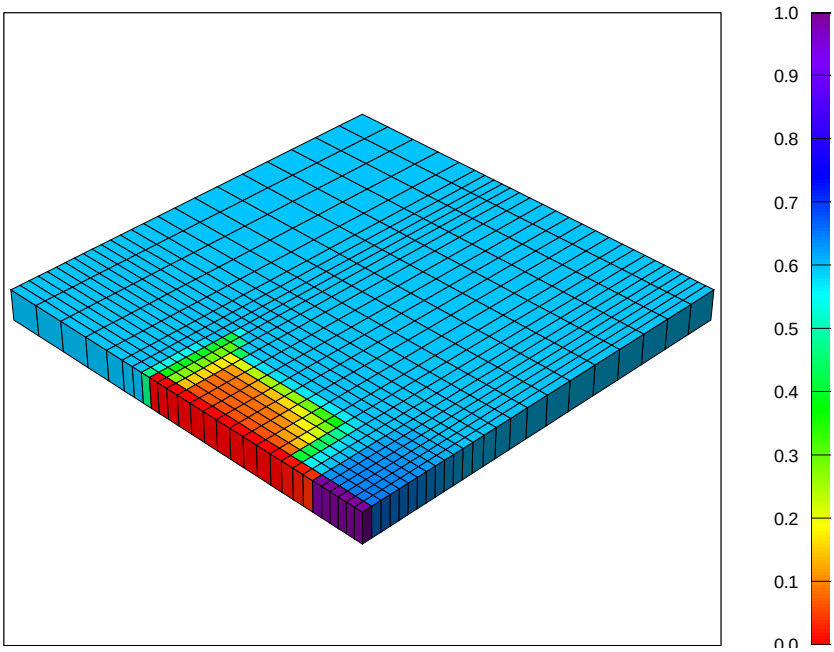

b: t = 347 days

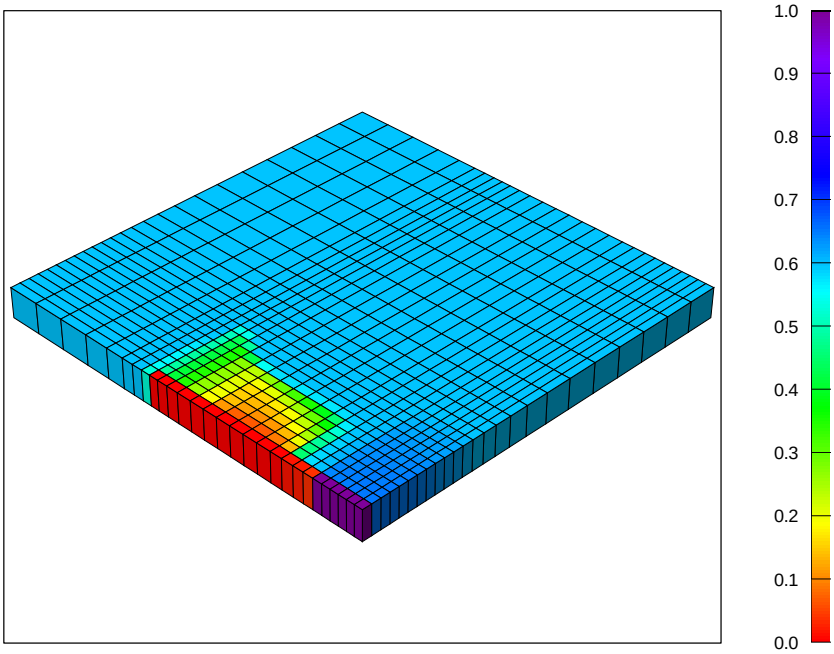

c: t = 1097 days

Figure 5.5.4—Continued

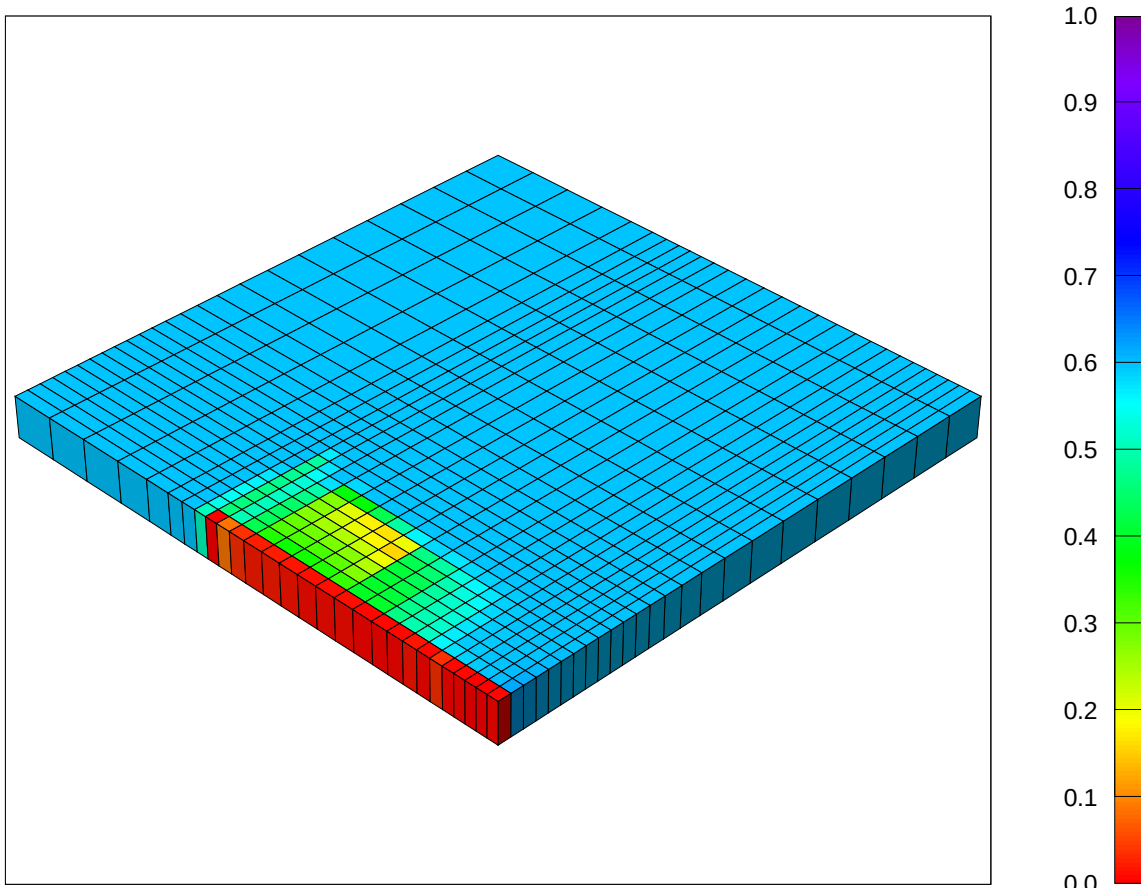

Figure 5.5.5—Gas saturation map at 1090 days after a fracture treatment by modeling a non-Newtonian fracture fluid with yield stress of 100 pa (case 5d, run 18) where L_f = 528 ft, p_r = 3720 psi, k = 0.1 md, C_r =1, S_{wi} = 0.4 and h = 100 ft)

Figure 5.5.1 to Figure 5.5.5 show the saturation and pressure maps during fracture fluid cleanup for different scenarios. It is obvious the Newtonian fracture fluid with a viscosity of 10 cp will clean up 100% after 351 days. The non-Newtonian fracture fluid with a yield stress of 10 pa cleans up to 23 ft after 3 years, which is around 3% of the propped fracture length. The case with 100 pa does not clean up at all. In the following sections, we will quantify the cleanup process by analyzing early gas production rate and long-term gas recovery.

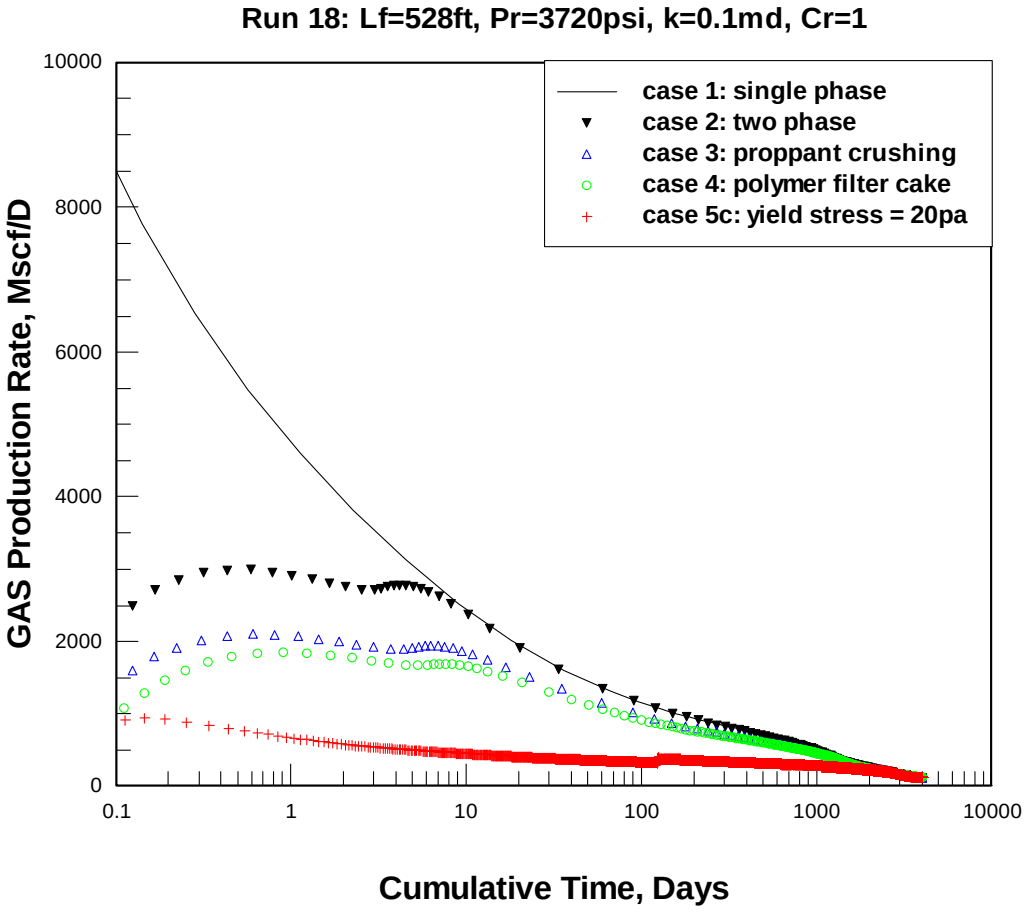

Figure 5.5.6—Gas production rate for different cases for L_f = 528 ft, p_r = 3720 psi, k = 0.1 md, C_r =1, S_{wi} = 0.4 and h = 100 ft

Figure 5.5.6 shows the gas production rate vs time for different cases after a fracture treatment for L_f = 528 ft, p_r = 3720 psi, k = 0.1 md, C_r =1, S_{wi} = 0.4 and h = 100 ft. The gas production rate becomes lower and cleanup time is longer as additional factors have been considered from case 1 to case 5. If the gel has a yield stress of 20 pa or more, the gas flow rate never peaks and remains much lower compared to cases 1-4. If the flowing yield stress is considered for this case or yield stress gets higher, there will be no gas production for a short time, like several days. For case 1 through case 4, we can see that the gas production rate increases for a certain period of time before it reaches a maximum value, which is the cleanup time. For case 2 (two-phase flow), it takes about 10 days to clean up, and for case 3 (proppant crushing), it takes about 1,000 days to clean up. So

when more factors are considered, the cleanup process takes longer and results should be more realistic. These concepts should help both researchers and engineers to understand how the cleanup process occurs in real wells.

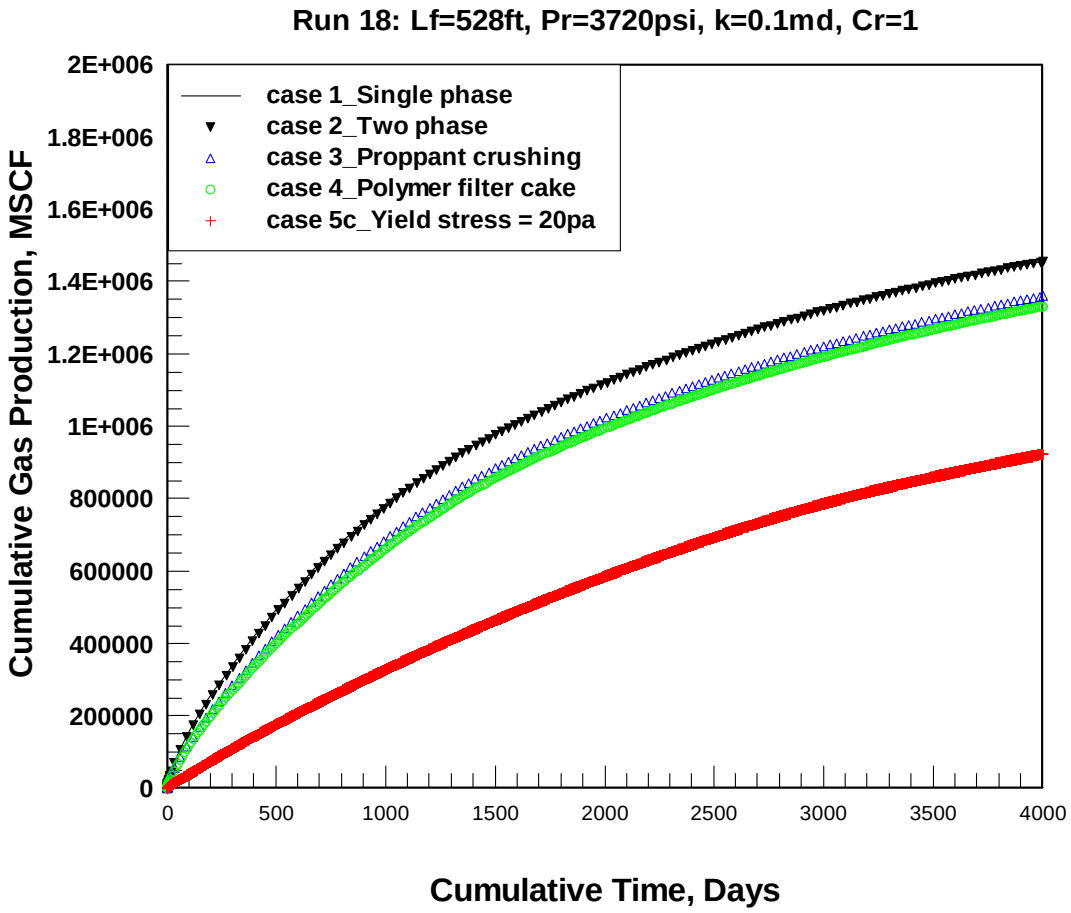

Figure 5.5.7—Cumulative gas production for different cases for L_f = 528 ft, p_r = 3720 psi, k = 0.1 md, C_r =1, S_{wi} = 0.4 and h = 100 ft

Figure 5.5.7 shows the cumulative gas production vs time for different cases after a fracture treatment for L_f = 528 ft, p_r = 3720 psi, k = 0.1 md, C_r =1, S_{wi} = 0.4 and h = 100 ft. We can see that in ten years proppant crushing reduces the cumulative gas production to 93% of the ideal case. The addition of filter cake does not make much difference, but the inclusion of gel yield stress of 20 pa in the fracture will reduce cumulative gas production to 63% comparing to ideal single phase case.

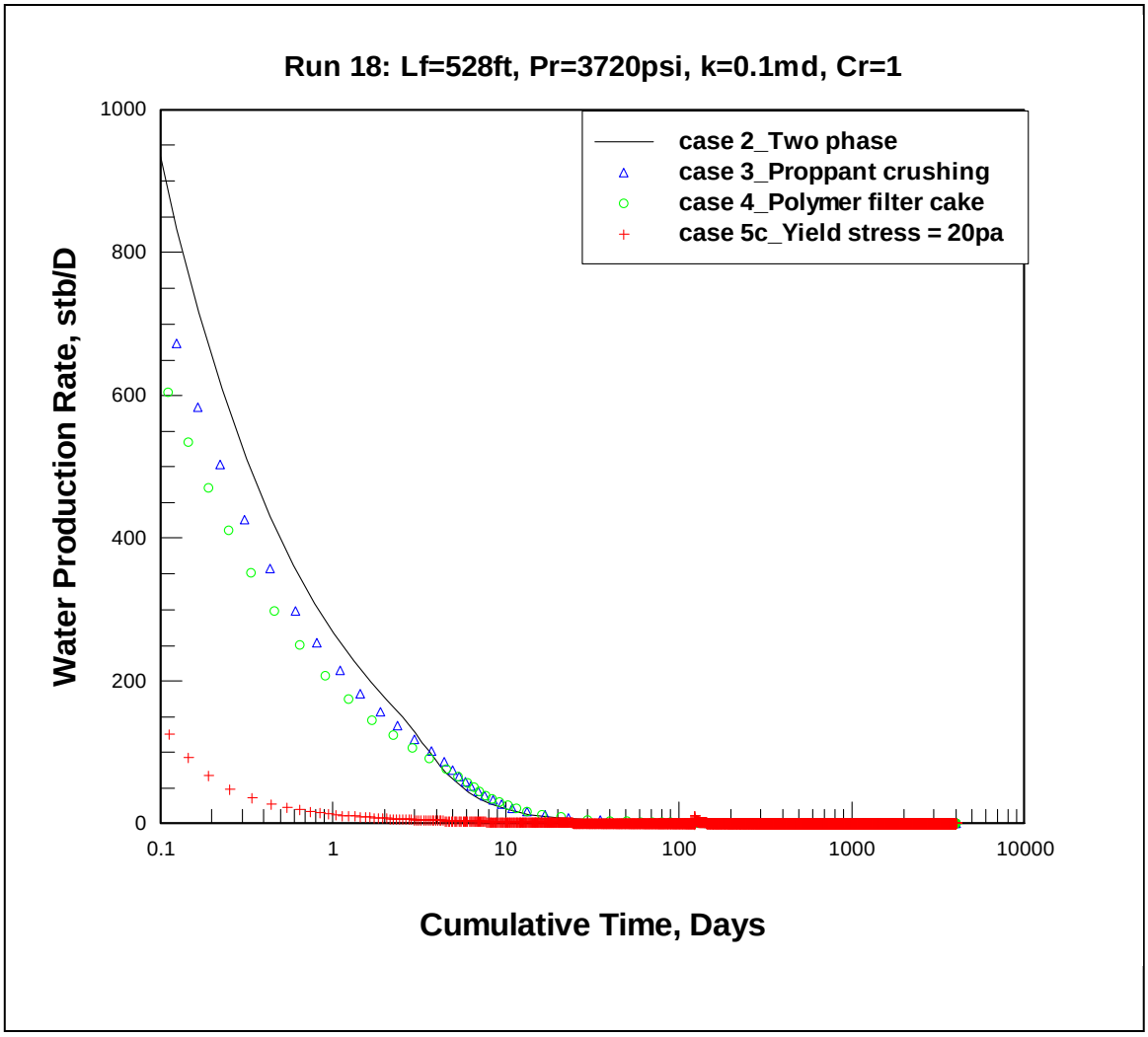

Figure 5.5.8—Water production rate for different cases for L_f = 528 ft, p_r = 3720 psi, k = 0.1 md, C_r =1, S_{wi} = 0.4 and h = 100 ft

Figure 5.5.8 shows the water production rate for different cases after a fracture treatment for L_f = 528 ft, p_r = 3720 psi, k = 0.1 md, C_r =1, S_{wi} = 0.4 and h = 100 ft. For case 1 which is a single-phase flow, there is no formation water and no fracture fluid, so water production is zero. For cases 2 - 5, the produced water can come from either formation water or fracture fluid filtrate, which is considered to have the same properties as formation water. We can see that most water is produced during early time; after about 10 days, the water production levels off at a very low rate. For the case with yield stress of 20 pa, the water production rate is even lower.

CHAPTER VI

FACTORS AFFECTING FRACTURE FLUID CLEANUP

In this chapter, concepts to improve fracture fluid cleanup will be discussed. Some simulation results and analyses are shown here, and other results are shown in Appendix E.

6.1 Fracture conductivity

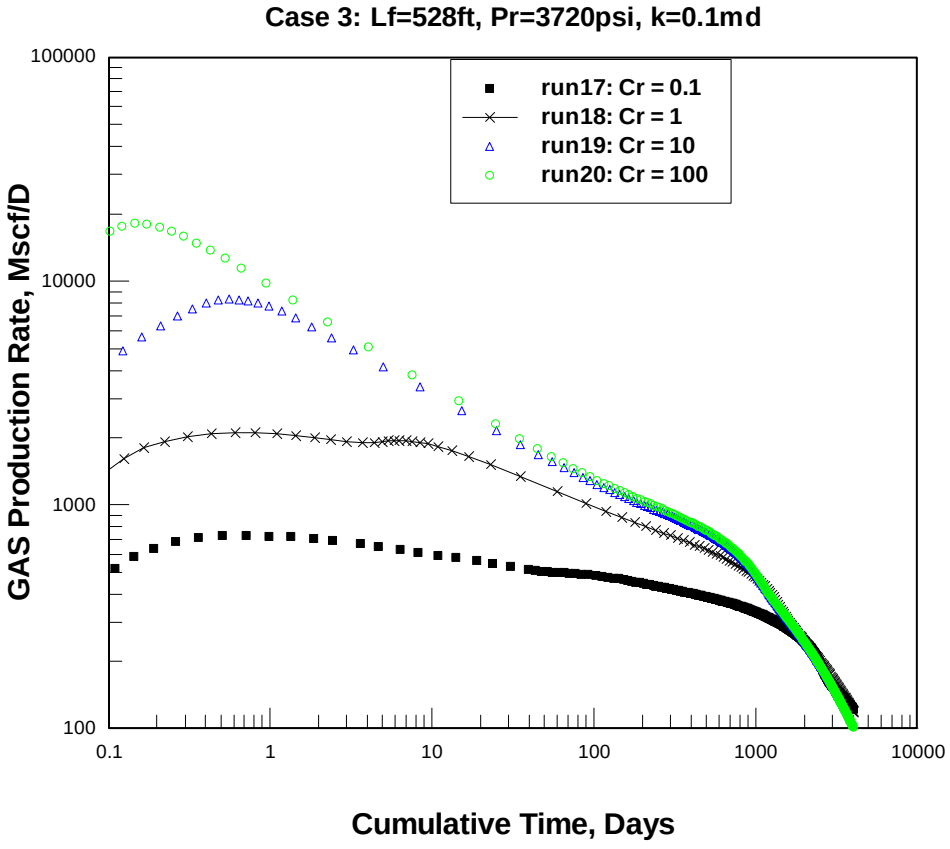

Figure 6.1.1—Gas production rate at different conductivities for case 3 (L_f = 528 ft, p_r = 3720 psi, k = 0.1 md, S_{wi} = 0.4 and h = 100 ft)

Figure 6.1.1 shows the gas production rate at different fracture conducitivities for case 3, a gas/water two-phase system with the effects of proppant crushing. We can see that the

fracture cleans up faster and gas flow rate is higher with a higher fracture concductivity. However, when the dimensionless fracture conductivity increases to 10, a higher conductivity does not substantially improve the gas flow rates.

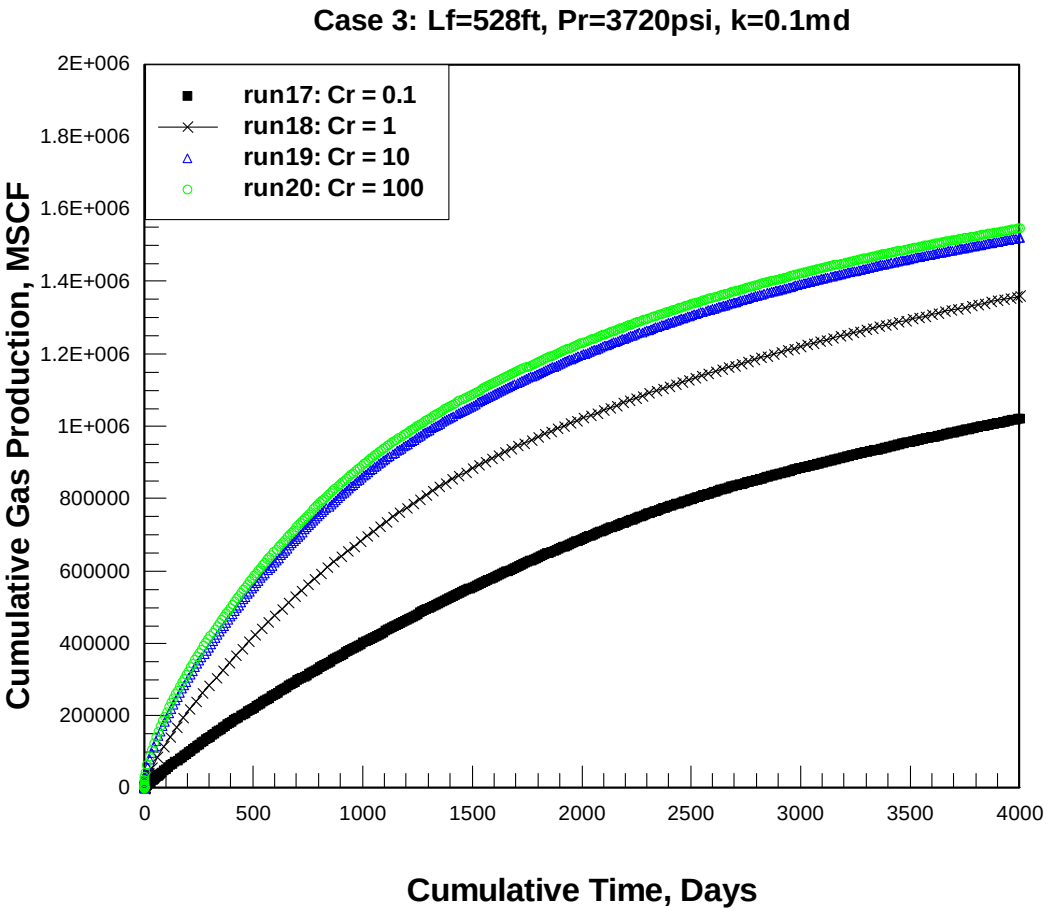

Figure 6.1.2—Cumulative gas production at different conductivities for case 3 (L_f = 528 ft, p_r = 3720 psi, k = 0.1 md, S_{wi} = 0.4 and h = 100 ft)

Figure 6.1.2 shows the cumulative gas production at different fracture conducitivities for case 3, a gas/water two-phase system with the effects of proppant crushing. We can see that more gas will be produced with a higher fracture concductivity. The difference is very small when fracture conductivity goes above 10. However, if the fracture conductivity can be increased from 0.1 to 10, the cumulative gas production will increase by 50% in ten years, which is about 2.0 bcf for one well in 160 acre spacing.

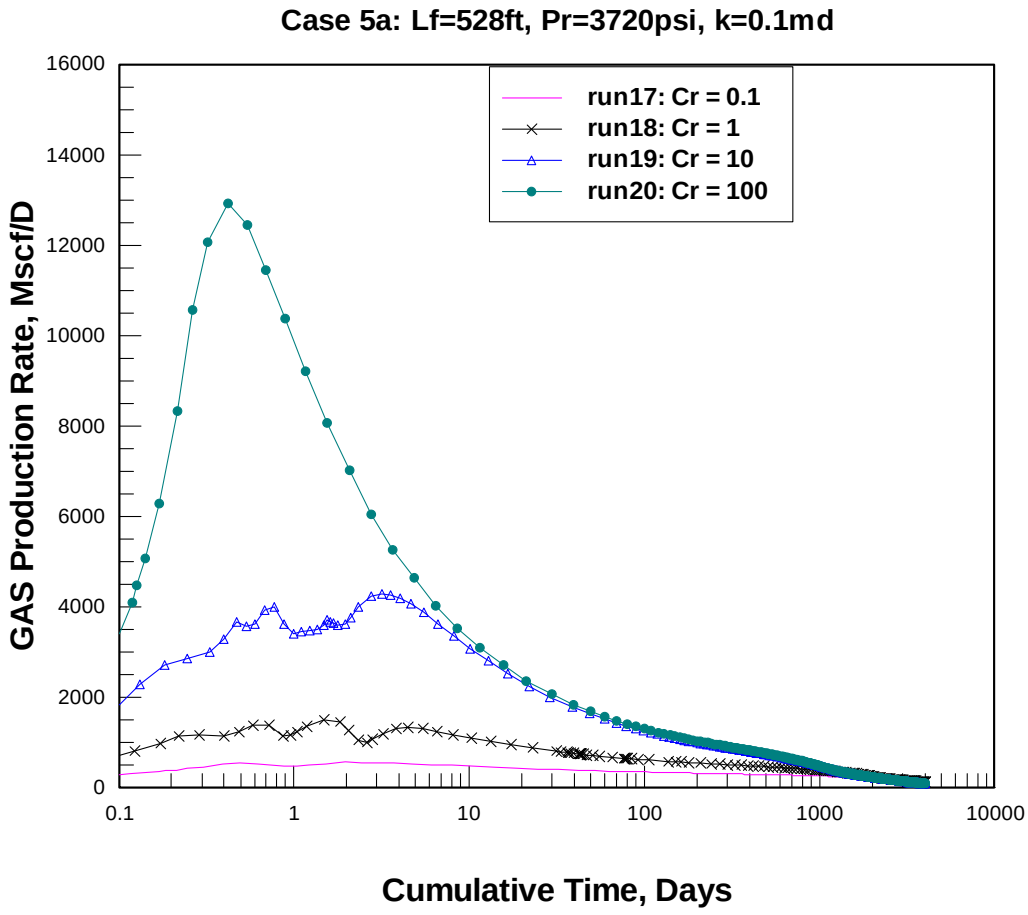

Figure 6.1.3—Gas production rate at different conductivities for case 5a (L_f = 528 ft, p_r = 3720 psi, k = 0.1 md, S_{wi} = 0.4, h = 100 ft, and yield stress = 3 pa)

Figure 6.1.3 shows the gas production rate at different values of dimensionless fracture conductivity for case 5a, modeling a gas/water-fracture fluid three-phase system. We can see that the fracture cleans up faster and gas flow rate is higher with a higher fracture concductivity, which is similar to Figure 6.1.1 because of the gel strength of the fluid left in the fracture. However, the difference is more pronounced between different curves than in Figure 6.1.1. The fracture takes a longer time to clean up, even for fracture conductivity of 10. For values of C_r = 1 and C_r = 0.1, the fracture never cleans up.

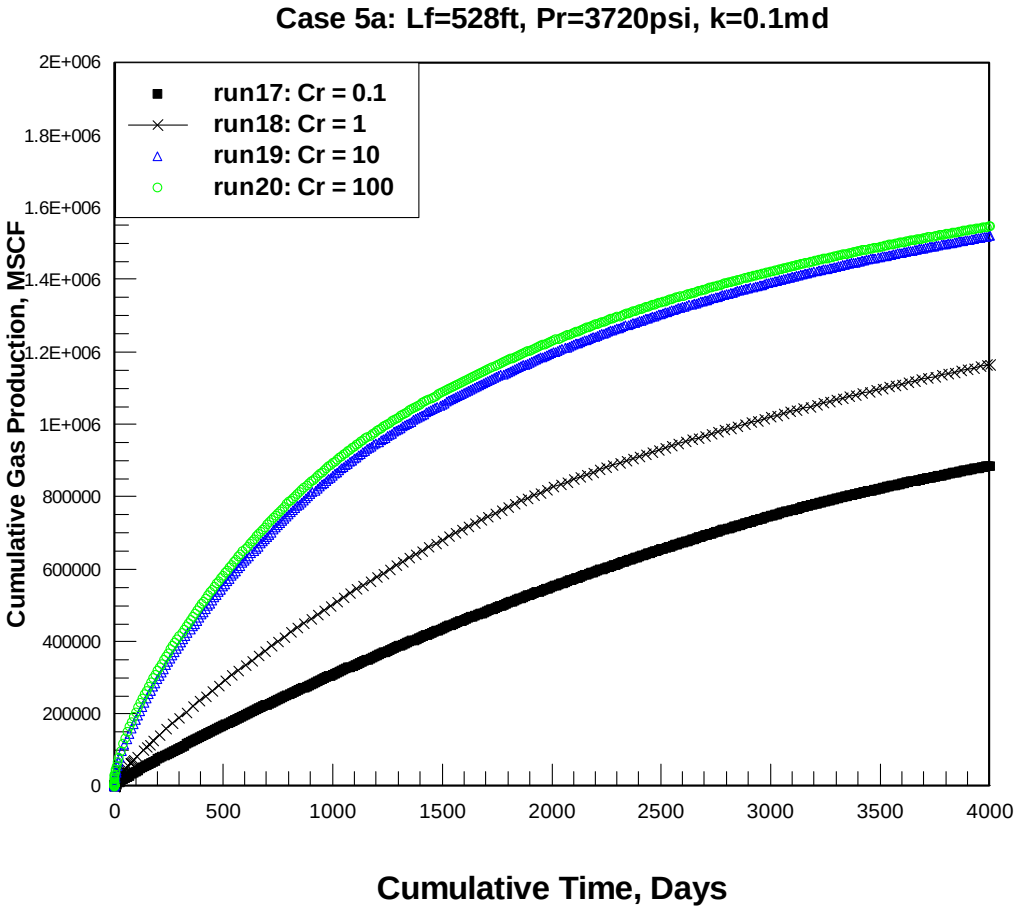

Figure 6.1.4—Cumulative gas production at different conductivities for case 5a (L_f = 528 ft, p_r = 3720 psi, k = 0.1 md, S_{wi} = 0.4, h = 100 ft and yield stress = 3 pa)

Figure 6.1.4 shows the cumulative gas production for different values of dimensionless fracture conductivity for case 5a, modeling a gas/water-fracture fluid three-phase system with a yield stress of 3 pa. We can see that more gas will be produced with higher fracture conductivity. The increase in gas recovery is very small when fracture conductivity goes above 10. However, if the dimensionless fracture conductivity can be increased from 0.1 to 10, the cumulative gas production will increase by 76% in ten years, which is about 2.6 bcf per well with 160 acre spacing.

Simulation results show that higher fracture conductivity will result in a higher gas production rates, faster fracture fluid cleanup, and more cumulative gas. We can see that the gas production rate increases for a certain period of time before it reaches a maximum value from the plot of gas flow rate vs. time, which is the cleanup time. Without considering the yield stress effect, fracture conductivity higher than 10 does not make much difference on gas production rate and cumulative gas produced. This means that from a production point of view, a proppant which can provide dimensionless fracture conductivity of 10 is good enough for gas production. However, Figure 5.5.6 to 5.5.8 with effect of yield stress, show that very high fracture conductivity is required for a fracture to clean up if highly concentrated gel is left inside the fracture. Proppant crushing lowers the cumulative gas production to 93%, the filter cake does not make much difference for this case 5, and gel with a yield stress of 20 pa will reduce cumulative gas production to 63% compared to the ideal single-phase case in ten years. Since the fracture tends to be damaged by proppant crushing, embedment, plugging by formation fines, it may be very difficult to achieve high enough fracture conductivity to clean up the gel.

6.2 Yield stress for fracture fluid

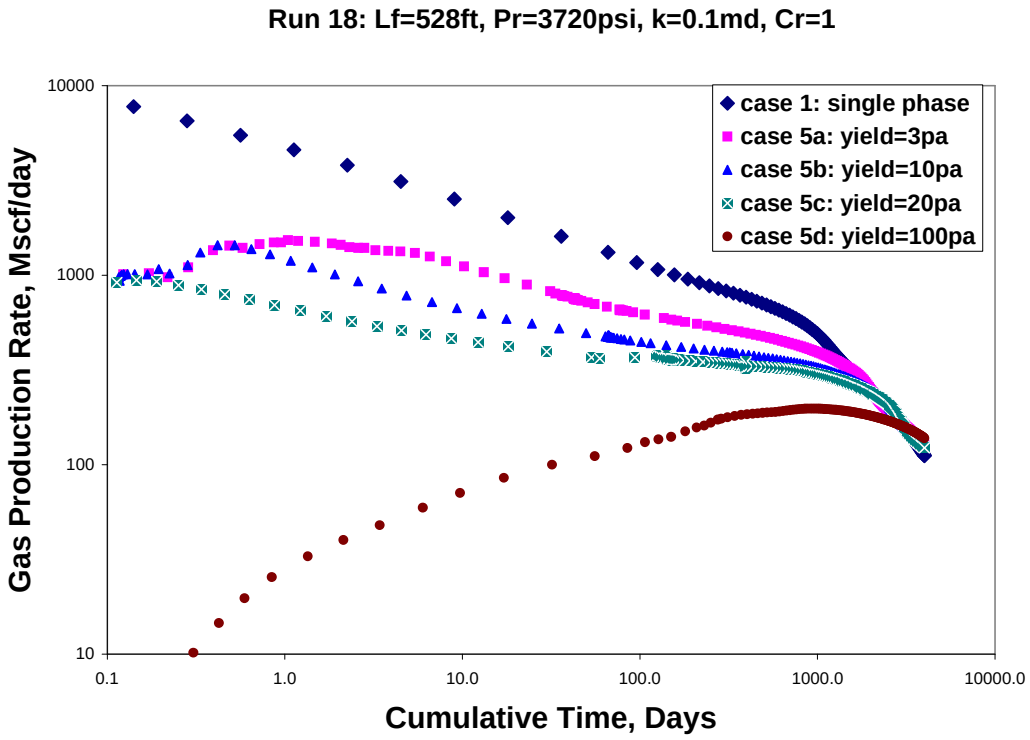

Figure 6.2.1—Gas production rate for different cases for run 18 (L_f = 528 ft, p_r = 3720 psi, k = 0.1 md, C_r =1, S_{wi} = 0.4 and h = 100 ft)

Figure 6.2.1 shows the gas production rate for different cases for run 18, modeling single phase and a gas/water/fracture fluid, three-phase system with different values of yield stress. We can see that the fracture cleans up faster, and the gas flow rate is higher for a lower value of yield stress. Even a small yield stress of 3 pa, however, reduces the gas production rate. When the yield stress increases to 100 pa, the well takes about 0.3 days for the well to produce at 10 Mscf/day.

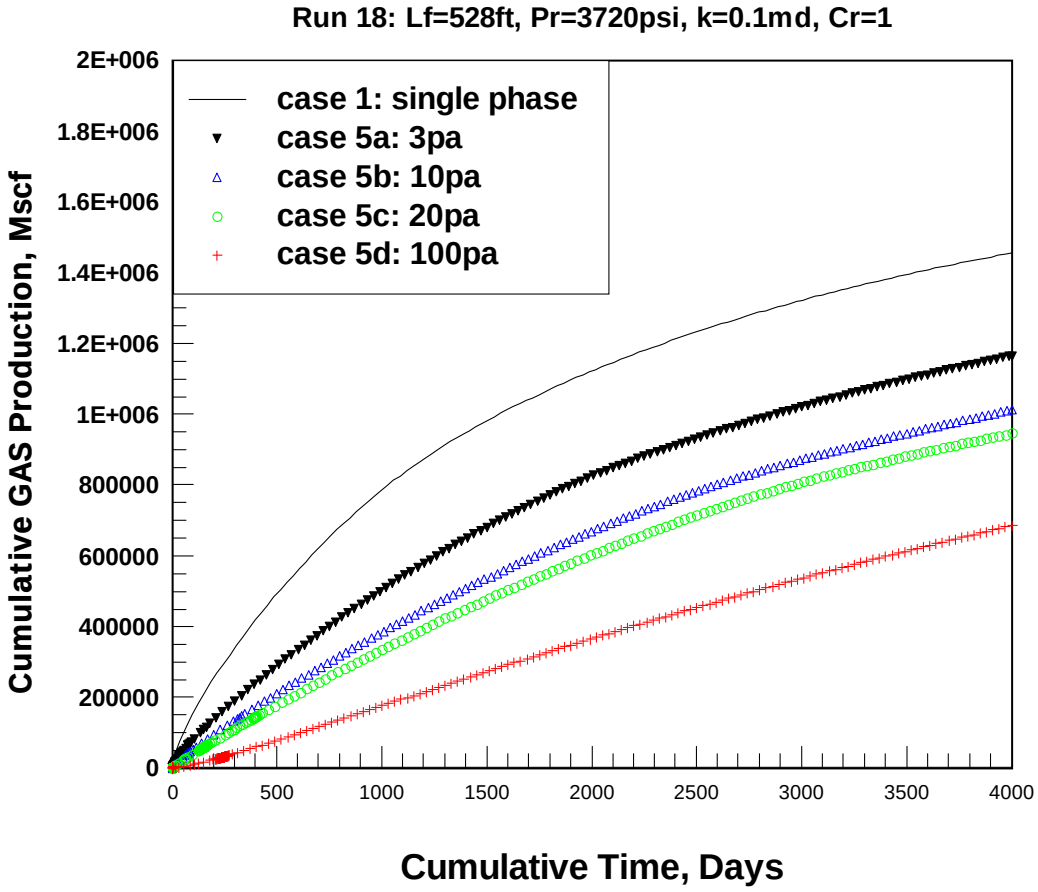

Figure 6.2.2—Cumulative gas production rate for different cases for run 18 (L_f = 528 ft, p_r = 3720 psi, k = 0.1 md, C_r =1, S_{wi} = 0.4 and h = 100 ft)

Figure 6.2.2 shows the cumulative gas production for different cases for run 18, modeling of a single phase and a gas/water/fracture fluid three-phase system with different values of yield stress. We can see that more gas will be produced as the value of yield stress decreases. If the yield stress is reduced from 100 pa to 3 pa, the cumulative gas production will increase about 2.0 bcf per well in ten years on 160 acre spacing.

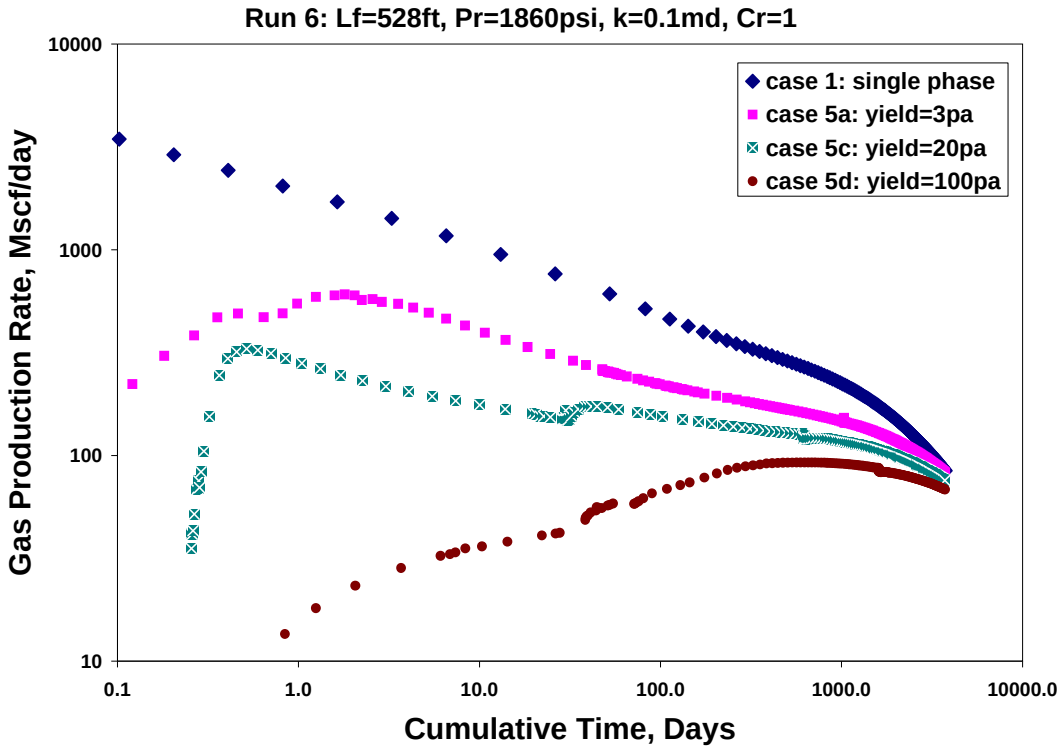

Figure 6.2.3—Gas production rate for different cases for run 6 (L_f = 528 ft, p_r = 1860 psi, k = 0.1 md, C_r =1, S_{wi} = 0.4 and h = 100 ft)

Figure 6.2.3 shows the gas production rate for different cases for run 6, modeling a single phase and a gas/water/fracture fluid three-phase system with different values of yield stress. We can see that the fracture cleans up faster, and gas flow rate is higher as the value of yield stress decreases. Even a small yield stress of 3 pa reduces the gas production rate substantially. It takes about 0.8 days for case 5d, and about 0.2 days for case 5a to produce at 10 Mscf/day.

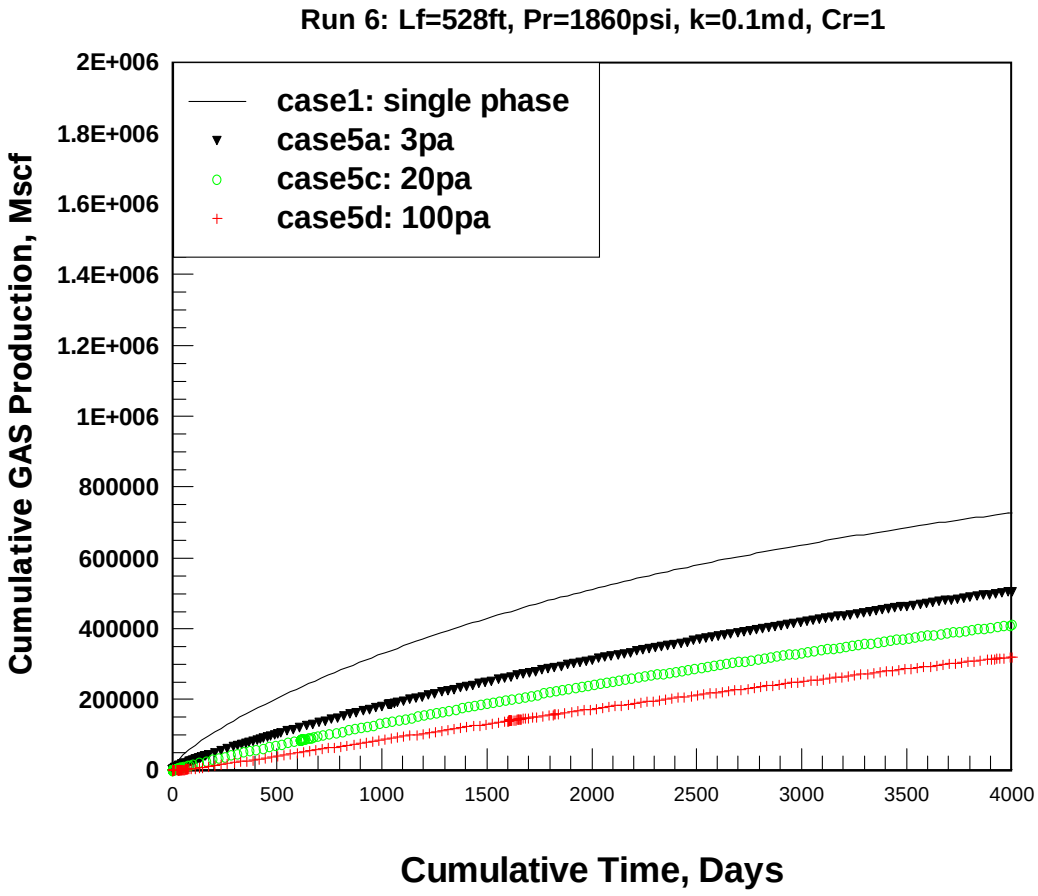

Figure 6.2.4—Cumulative gas production rate for different cases for run 6 (L_f = 528 ft, p_r = 1860 psi, k = 0.1 md, C_r =1, S_{wi} = 0.4 and h = 100 ft)

Figure 6.2.4 shows the cumulative gas production for different cases for run 6, modeling of a single phase and a gas/water/fracture fluid three-phase system. We can see that more gas will be produced as the value of yield stress decreases. If the yield stress is reduced from 100 pa to 3 pa, the cumulative gas production will be increased about 0.8 bcf per well in ten years. If the yield stress is decreased from 3 pa to 0 pa (ideal single-phase flow), there is another 0.8 bcf that will be produced.

Figure 6.2.2 and 6.2.4 show that a yield stress of 20 pa will reduce the cumulative gas production to 63% and 50% of the ideal single-phase case respectively. The fracture fluid with yield stress that remains in the fracture will require a lot of reservoir energy to clean it up. If the pressure gradient down the fracture is less than the static yield stress of the gel, the gel stays inside the fracture, reducing permeability to gas. Gel remaining in the fracture is probably the most important problem affecting fracture fluid cleanup. So it is recommended for the industry to design and use some fracturing fluids which can degrade effectively ideally to a Newtonian fluid so that the fracture can be cleaned up effectively and the productivity of the fractured well can be increased.

6.3 Fracture length

Based on the simulation results and by using 30% gas saturation cutoff, we determined a percentage of fracture that has cleaned up one year after the treatment for each simulation run with gel damage. As shown in Figure 6.3.1, the percentage of fracture that cleans up is the ratio of effective fracture length to propped fracture length that we defined in Chapter I. In the portion of the propped fracture, the gel has been recovered and gas has been flowing. However, the other portion of propped fracture length is still plugged up by gel. We presented some results in figures to quantify the effect of fracture length on the cleanup process as follows.

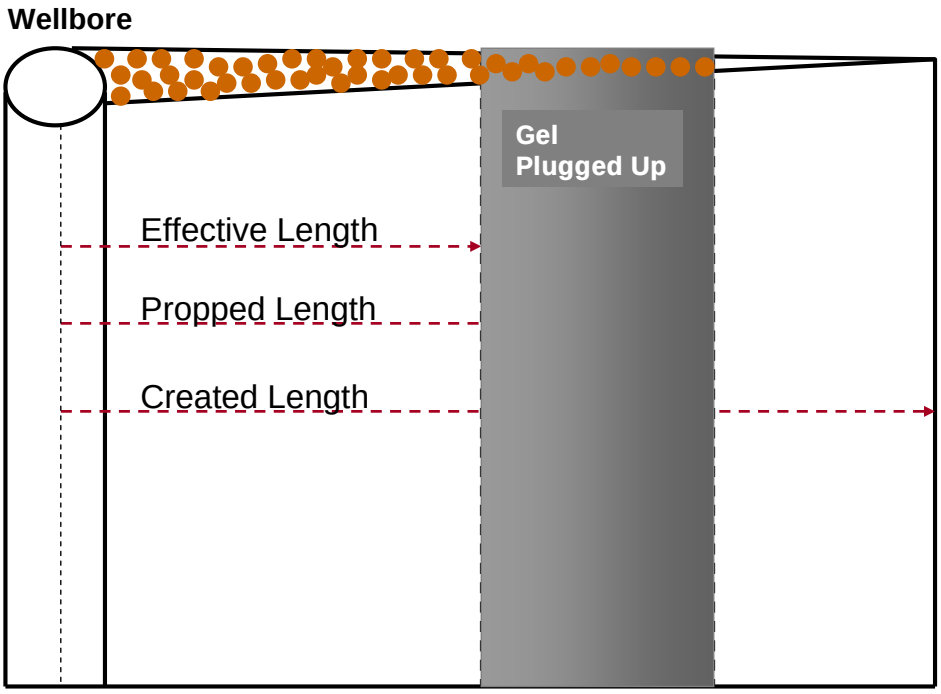

Figure 6.3.1—Illustration of percentage of fracture that cleans up (the ratio of effective fracture length to propped fracture length)

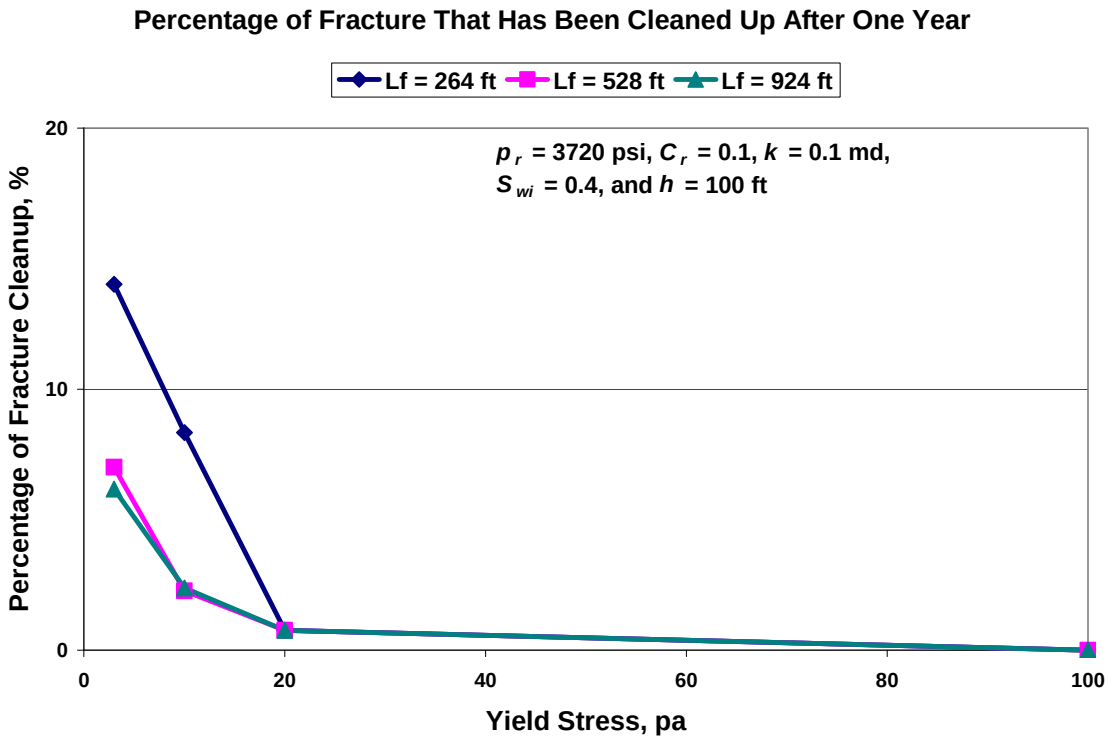

Figure 6.3.2—Percentage of fracture that cleans up one year after a fracture treatment vs. yield strength for different fracture lengths for the scenario where p_r = 3720 psi, k = 0.1 md, C_r =0.1, S_{wi} = 0.4 and h = 100 ft

Figure 6.3.2 show the percentage of fracture that cleans up vs. yield stress for different fracture lengths, where p_r = 3720 psi, k = 0.1 md, C_r =0.1, S_{wi} = 0.4 and h = 100 ft. It is obvious that the percentage of fracture cleanup decreases with longer fracture. However, if the gel has a yield stress of 20 pa or more, the percentage is the same for all three cases. This means that fracture fluid cleanup is very important, otherwise all the efforts spent on the fracture treatment design and field operation are worthless.

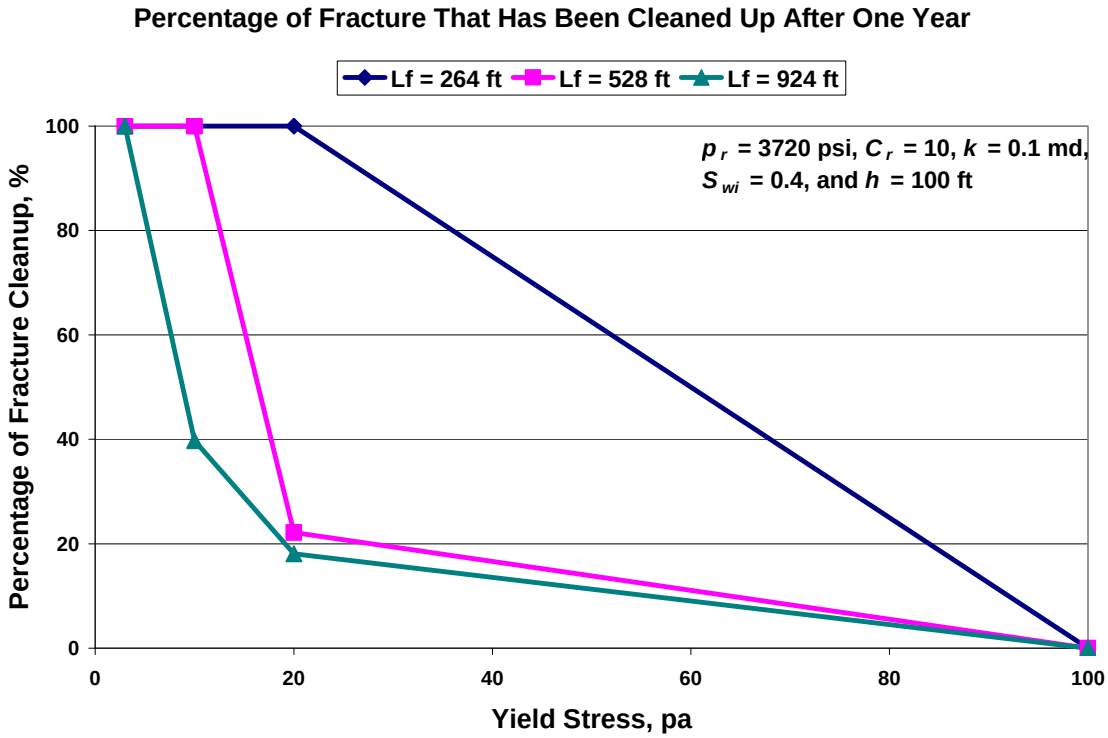

Figure 6.3.3—Percentage of fracture that cleans up one year after a fracture treatment for different yield strength for the scenario where p_r = 3720 psi, k = 0.1 md, C_r =10, S_{wi} = 0.4 and h = 100 ft

Figure 6.3.3 show the percentage of fracture that cleans up vs. yield stress for different fracture lengths, where p_r = 3720 psi, k = 0.1 md, C_r = 10, S_{wi} = 0.4 and h = 100 ft. Compared to previous Figure 6.3.2, this is a higher conductivity scenario. It is obvious that the percentage of fracture cleanup decreases with longer fracture. Interestingly, based on the percentage of fracture cleanup, the optimal fracture should be: L_f = 924 ft for yield stress of 3 pa; L_f = 528 for yield stress of 10 pa; and L_f = 264 ft for yield stress of 20 or more. This means that fracture fluid cleanup is very important, otherwise all the effort on the fracture treatment design and field operation is worthless.

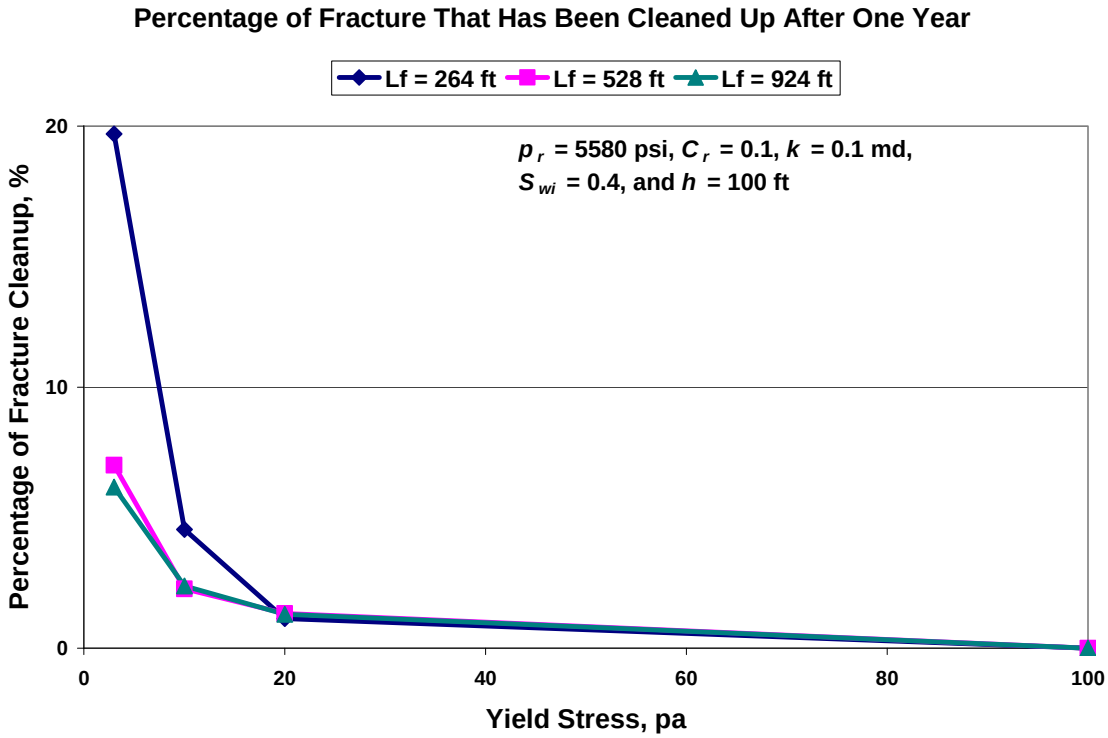

Figure 6.3.4—Percentage of fracture that cleans up one year after a fracture treatment for different yield strength for the scenario where p_r = 5580 psi, k = 0.1 md, C_r =0.1, S_{wi} = 0.4 and h = 100 ft

Figure 6.3.4 show the percentage of fracture that cleans up vs. yield stress for different fracture lengths, where p_r = 3720 psi, k = 0.1 md, C_r = 0.1, S_{wi} = 0.4 and h = 100 ft. This is a higher reservoir pressure scenario compared to Figure 6.3.2. It is obvious that the percentage of fracture cleanup decreases with longer fracture. However, if the gel has a yield stress of 20 pa or more, the percentage is the same for all three cases.

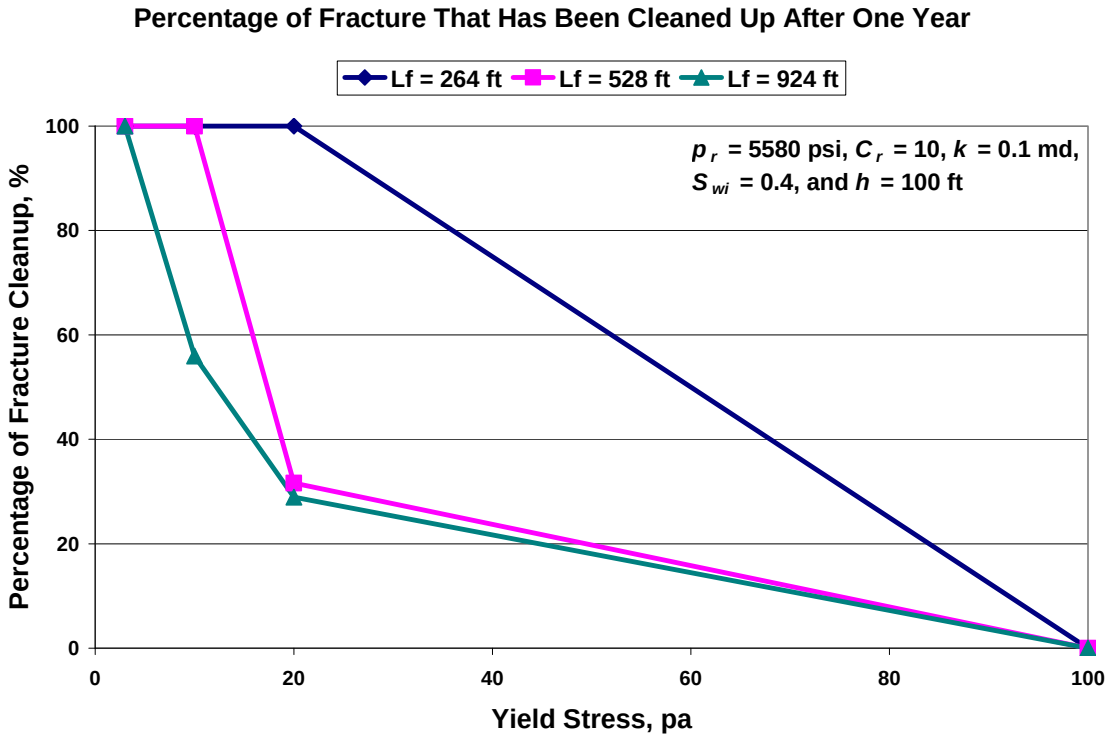

Figure 6.3.5—Percentage of fracture that cleans up one year after a fracture treatment for different yield strength for the scenario where p_r = 5580 psi, k = 0.1 md, C_r =10, S_{wi} = 0.4 and h = 100 ft

Figure 6.3.5 show the percentage of fracture that cleans up vs. yield stress for different fracture lengths, where p_r = 5580 psi, k = 0.1 md, C_r = 10, S_{wi} = 0.4 and h = 100 ft. Compared to previous Figure 6.3.4, this is a higher conductivity scenario. It is obvious that the percentage of fracture cleanup decreases with longer fracture. Interestingly, based on the percentage of fracture cleanup, the optimal fracture should be: L_f = 924 ft for yield stress of 3 pa; L_f = 528 for yield stress of 10 pa; and L_f = 264 ft for yield stress of 20 or more. This means that fracture fluid cleanup is very important, otherwise all the effort on the fracture treatment design and field operation is worthless.

6.4 Initial reservoir pressure

Similar to section 6.3, we determined a percentage of fracture that has cleaned up one year after the treatment for each simulation run with gel damage, based on the simulation results and by using 30% gas saturation cutoff. Each point in the figures is one simulation run that represents different fracture length, dimensionless fracture conductivity, formation permeability, or reservoir pressure. The bottomhole pressure is 10% of initial reservoir pressure, which is a reasonable assumption for gas wells without liquid loading problems. As the reservoir pressure increases, there is more energy to flow back the fracture filtrate, and gel inside the fracture. This should help clean up the fracture. We presented part of our results in figures to quantify the effect of initial reservoir pressure on the cleanup process.

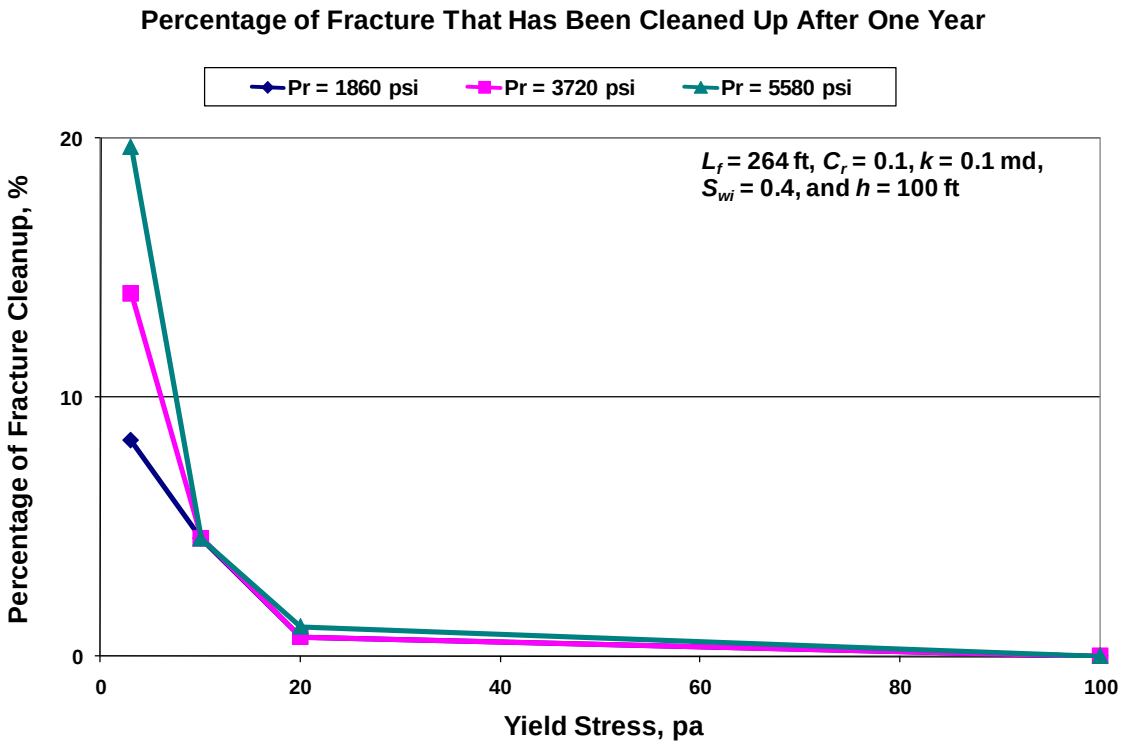

Figure 6.4.1—Percentage of fracture that cleans up one year after a fracture treatment vs. yield strength for different reservoir pressures for the scenario where L_f = 264 ft, k = 0.1 md, C_r =0.1, S_{wi} = 0.4 and h = 100 ft

Figure 6.4.1 show the percentage of fracture that cleans up vs. yield stress for different initial reservoir pressures, where L_f = 264 ft, k = 0.1 md, C_r = 0.1, S_{wi} = 0.4 and h = 100 ft. It is obvious that the percentage of fracture cleanup increases with higher reservoir pressure. However, if the gel has a yield stress of 20 pa or more, the percentage is almost the same for all three cases. This means that fracture fluid cleanup is very important, and at low fracture conductivity (C_r = 0.1), the fracture could not clean up effectively.

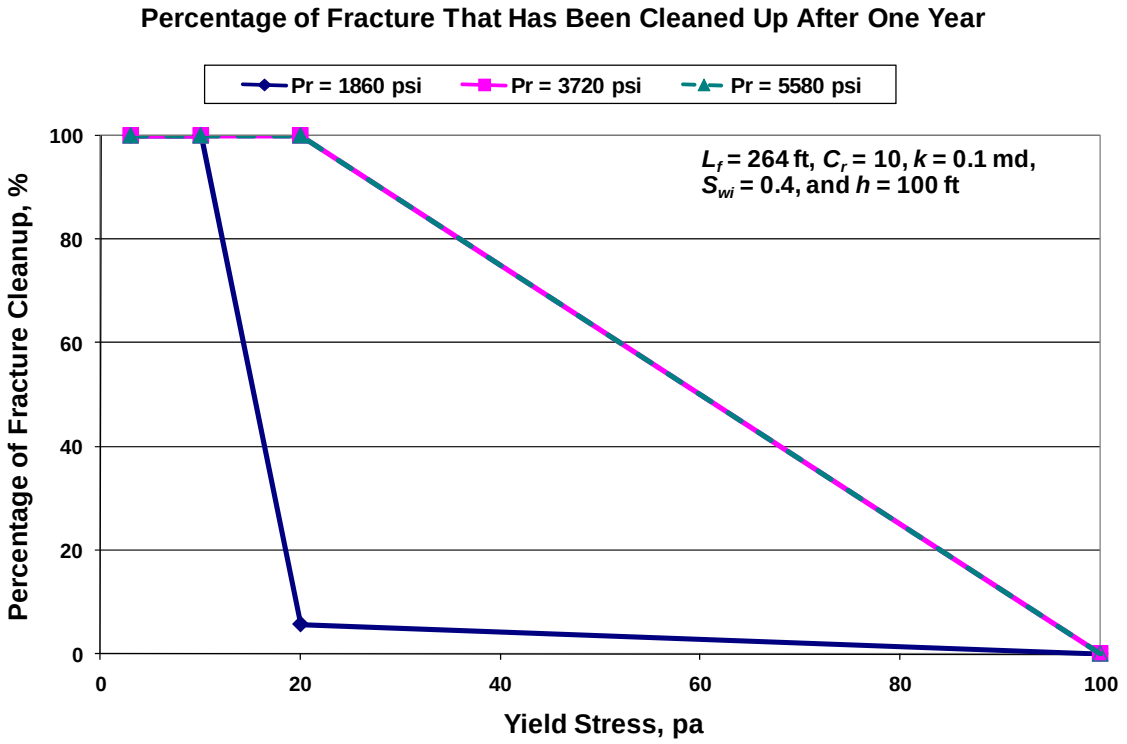

Figure 6.4.2—Percentage of fracture that cleans up one year after a fracture treatment vs. yield strength for different reservoir pressures for the scenario where L_f = 264 ft, k = 0.1 md, C_r = 10, S_{wi} = 0.4 and h = 100 ft

Figure 6.4.2 show the percentage of fracture that cleans up vs. yield stress for different initial reservoir pressures, where L_f = 264 ft, k = 0.1 md, C_r = 10, S_{wi} = 0.4 and h = 100 ft. Compared to previous Figure 6.4.1, this is a higher conductivity scenario. It is obvious that the percentage of fracture cleanup increases with higher reservoir pressures. If the reservoir pressure is 3720 psi or above, the fracture can clean up 100% after a year for yield stress less than 20 pa; while if the reservoir pressure is 1860 psi, the fracture can

clean up 100% after a year for yield stress less than 10 pa. This means that reservoir energy is a critical factor for fracture fluid cleanup. With higher reservoir energy, more gel damage can be overcome.

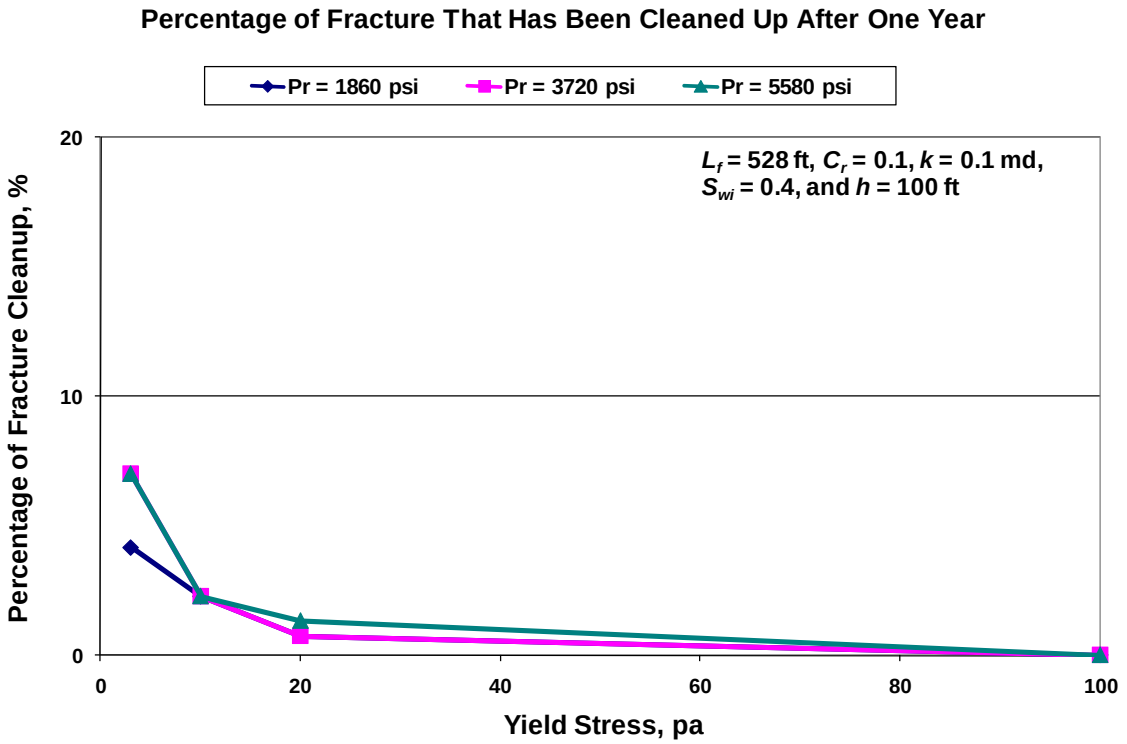

Figure 6.4.3—Percentage of fracture that cleans up one year after a fracture treatment vs. yield strength for different reservoir pressures for the scenario where L_f = 528 ft, k = 0.1 md, C_r =0.1, S_{wi} = 0.4 and h = 100 ft

Figure 6.4.3 show the percentage of fracture that cleans up vs. yield stress for different initial reservoir pressures, where L_f = 528 ft, k = 0.1 md, C_r = 0.1, S_{wi} = 0.4 and h = 100 ft. This is a longer fracture compared to Figure 6.4.1. It is obvious that the percentage of fracture cleanup increases with higher reservoir pressure. However, if the gel has a yield stress of 20 pa or more, the percentage is almost the same for all three cases. This means that fracture fluid cleanup is very important, and at low fracture conductivity (C_r = 0.1), the fracture could not clean up effectively.

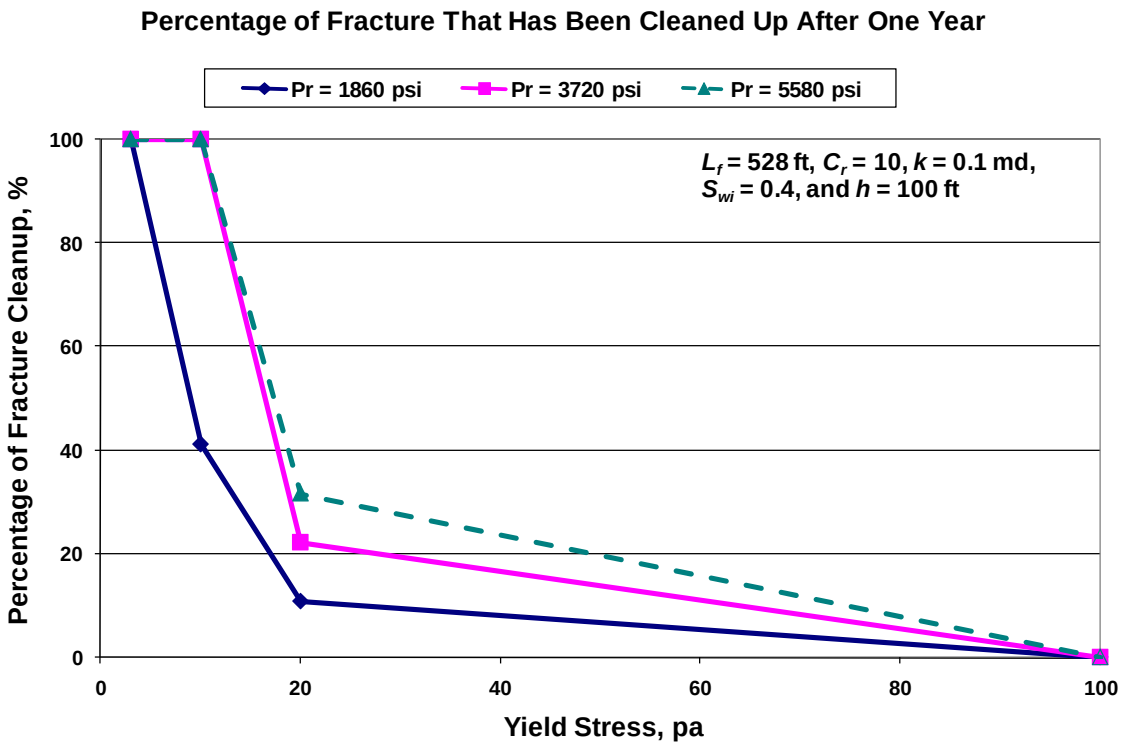

Figure 6.4.4—Percentage of fracture that cleans up one year after a fracture treatment vs. yield strength for different reservoir pressures for the scenario where L_f = 528 ft, k = 0.1 md, C_r = 10, S_{wi} = 0.4 and h = 100 ft

Figure 6.4.4 show the percentage of fracture that cleans up vs. yield stress for different initial reservoir pressures, where L_f = 528 ft, k = 0.1 md, C_r = 10, S_{wi} = 0.4 and h = 100 ft. Compared to previous Figure 6.4.3, this is a higher conductivity scenario. It is obvious that the percentage of fracture cleanup increases with higher reservoir pressures. If the reservoir pressure is 3720 psi or above, the fracture can clean up 100% after a year for yield stress less than 10 pa; while if the reservoir pressure is 1860 psi, the fracture can clean up 100% after a year for yield stress less than 3 pa. This means that reservoir energy is a critical factor for fracture fluid cleanup. With higher reservoir energy, more gel damage can be overcome.

CHAPTER VII

CONCLUSIONS AND RECOMMENDATIONS

The mechanisms of fracture fluid cleanup have been investigated in this research, mathematical expressions and computer code have been developed to model the cleanup process, and the code has been linked to a 3D, 3-phase reservoir simulator (SABRE). Systematic simulation study of fracture fluid cleanup has been carried out by varying formation permeability, reservoir pressure, fracture length, fracture conductivity, flowing bottomhole pressure (FBHP), and yield stress. The main conclusions are:

1. The factors affecting how a gas well will clean up after a fracture treatment are multi-phase flow, fracture proppant crushing, and the gel that remains in the fracture that does not break back to small molecules resulting in a low viscosity.
2. To properly analyze a well that has been fracture treated, one should not only measure everything that is pumped during the fracture treatment, but also what is produced back after the treatment including flowing pressures, gas flow rates, water flow rates, and polymer concentration in the produced water.
3. To analyze the post-fracture data correctly, one may need to use a multi-phase reservoir model that is capable of simulating non-Newtonian flow behavior of the gel in the fracture after fracture closure.
4. The two most important factors affecting fracture fluid cleanup are the value of fracture conductivity and the yield stress of the gelled fluid left in the fracture after fracture closure.
5. If the fracture fluid breaks down to a low viscosity and behaves as a Newtonian fluid, then a dimensionless fracture conductivity (C_r) of 10 or greater is all that is required to optimize gas production and fracture fluid cleanup.
6. If the fracture fluid does not break completely and retains gel strength of 3-100 pa, then the fracture fluid will either clean up slowly or never clean up when the dimensionless fracture conductivity (C_r) is 10 or less.

7. It is recommended for the industry to design and use some fracturing fluids which can degrade effectively ideally to a Newtonian fluid after the treatment so that the fracture can be cleaned up effectively and the productivity of the fractured well can be optimized.

NOMENCLATURE

P_c	=	capillary pressure, psi
p_i	=	initial reservoir pressure, psi
p_r	=	reservoir pressure, psi
p_{wf}	=	bottomhole flowing pressure, psi
q	=	gas flow rate, Mscf/D
S_g	=	gas saturation, fraction
S_w	=	water saturation, fraction
c_f	=	rock compressibility, 1/psi
c_w	=	water compressibility, 1/psi
$\Delta p/\Delta L$	=	pressure gradient, psi/ft
Δx	=	grid size in the x-direction, ft
Δy	=	grid size in the y-direction, ft
γ_g	=	specific gas gravity, dimensionless
h	=	reservoir net thickness, ft
k	=	formation permeability, md
k_d	=	formation permeability in damage zone, md
k_f	=	fracture permeability, md
k_g	=	effective gas permeability, md
k_w	=	effective water permeability, md
k_r	=	relative permeability, md
k_{rg}	=	relative permeability to gas, md
k_{rw}	=	relative permeability to water, md
L_f	=	fracture half-length, ft
ϕ	=	porosity, percent
t	=	time, day
t_p	=	production time, day
T	=	temperature, ^oF
μ	=	viscosity, cp
μ_w	=	water viscosity, cp

v = velocity, ft/sec

w = fracture width, in

w_d = damaged-zone width, in.

wk_f = fracture conductivity, md-ft

C_r = dimensionless fracture conductivity, $(wk_f)/(\pi L_f k)$

F_{CD} = dimensionless fracture conductivity, $(wk_f)/(L_f k)$

REFERENCES

Ayoub, J.A., Hutchins,R.D., van der Bas, F., Cobianco, S., Emiliani, C.N., and et al. 2006. New Findings in Fracture Cleanup Change Common Industry Perceptions. Paper SPE 98746 presented at the SPE International Symposium and Exhibition on Formation Damage Control, Lafayette, Louisiana, 15-17 Feburary.

Balhoff, M.T. and Miller, M.J. 2002. An Analytical Model for Cleanup of Yield-Stress Fluids in Hydraulic Fractures. Paper SPE 77596 presented at the SPE Annual Technical Conference and Exhibition, San Antonio, Texas, 29 September–2 October.

Barree, R.D., Cox, S.A., Gilbert, J.V., and Dobson, M. 2003. Closing the Gap: Fracture Half Length from Design, Buildup, and Production Analysis. Paper SPE 84491 presented at the SPE Annual Technical Conference and Exhibition, Denver, Colorado, 5-8 October.

Carr, M.A. and Yang, B.H. 1998. Evaluation for Polymer Damage Aids in Candidate Selection for Removal Treatment. Paper SPE 39785 presented at the SPE Gas Technology Symposium, Calgary, Canada, 23-26 March.

Cinco-Ley, H. and Samaniego-V., F. 1981. Transient Pressure Analysis: Finite Conductivity Fracture vs. Damaged Fracture Case. Paper SPE 10179 presented at the SPE Annual Technical Conference and Exhibition, San Anotonio,Texas, 4-7 October.

Cooke, C.E. 1975. Effect of Fracturing Fluids on Fracture Conductivity. *JPT* **27** (10) 1273-1282.

Coulter, G.R., Benton, E.G., and Thomson, C.L. 2004. Water Fracs and Sand Quantity: A Barnett Shale Example. Paper SPE 90891 presented at the SPE Annual Technical Conference and Exhibition, Houston,Texas, 26-29 September.

Elbel, J. and Ayoub, J. 1992. Evaluation of Apparent Fracture Lengths Indicated from Transient Tests. *JCPT* **01** (12) 41-46.

Gdanski, R., Weaver, J., Slabaugh, B., Walter, H. and Parker, M. 2005. Fracture Face Damage – It Matters. Paper SPE 94649 presented at SPE European Formation Damage Conference, Sheveningnen, Netherlands, 25-27 May.

Penny, G.S. and Jin, L. 1996. The Use of Inertial Force and Low Shear Viscosity to Predict Cleanup of Fracturing Fluids within Proppant Packs. Paper SPE 31096 presented at SPE Formation Damage Control Symposium, Lafayette, Louisiana, 14-15 February.

Grieser, B., Hobbs, J., Hunter, J., and Ables, J. 2003. The Rocket Science Behind Water Frac Design. Paper SPE 80933 presented at SPE Production and Operations Symposium, Oklahoma City, Oklahoma, March 23-25.

Holditch, S. A., and Ely, J. 1973. Successful Stimulation of Deep Wells Using High Proppant Concentrations. JPT **25** (08) 959-964.

Holditch, S.A. and Laufer, W.L. 1978. The Analysis of Fractured Gas Wells Using Simulation. Paper SPE 7473 presented at the SPE Annual Technical Conference and Exhibition, Houston,Texas 1-2 October.

Holditch, S.A. 1979. Factors Affecting Water Blocking and Gas Flow from Hydraulically Fractured Gas Wells. Paper SPEJ 7561, 1515-1524.

Hresko, J.C. 1985. A Qualitative Analysis of Non-Darcy Flow Effects in Hydraulically Fractured Gas Wells. MS thesis, Texas A&M University, College Station, Texas.

Iqbal, G.M., Zadco, PDR and Civan, F. 1993. Simulation of Skin Effects and Liquid Cleanup in Hydraulically Fractured Wells. Paper SPE 25482 presented at SPE Production Operation Symposium, Oklahoma City, Oklahoma 21-23 March.

Khouryieh, H. 2006. Rheological Characterization of Xanthan-Guar Mixtures in Dilute Solution. PhD dissertation, Kansas State University.

Lee, W.J. and Holditch, S.A. 1981. Fracture Evaluation with Pressure Transient Testing in Low-Permeability Gas Reservoirs. *JPT* **33** (09) 1776-1792.

Lolon, E.P., McVay, D, and Schubarth, S.K. 2003. Effect of Fracture Conductivity on Effective Fracture Length. Paper SPE 84311 presented at the SPE Annual Technical Conference and Exhibition, Denver, CO 5-8 October.

Lolon, E.P., Chipperfield, S.T., McVay, D, and Schubarth, S.K. 2004. The Significance of Non-Darcy and Multiphase Flow Effects in High-Rate, Frac-Pack Gas Completions. Paper SPE 90530 presented at the SPE Annual Technical Conference and Exhibition, Houston,Texas 26-29 September.

Mahadevan, J. and Sharma, M.M. 2003. Cleanup of Water Blocks in Low Permeability Formations. Paper SPE 84216 presented at the SPE Annual Technical Conference and Exhibition held in Denver, Colorado, 5-8 October.

May E.A., Britt, L.K. and Nolte, K.G. 1997. The Effect of Yield Stress on Fracture Fluid Cleanup. Paper SPE 38619 presented at the SPE Annual Technical Conference and Exhibition, San Antonio,Texas, 5-8 October.

Montgomery, K.T. and Holditch, S.A. 1990. Effects of Fracture Fluid Invasion on Cleanup Behavior and Pressure Buildup Analysis. Paper SPE 20643 presented at the SPE Annual Technical Conference and Exhibition, New Orleans, Louisiana, 23-26 September.

Parekh, B., and Sharma, M.M. 2004. Cleanup of Water Blocks in Depleted Low-Permeability Reservoirs. SPE paper 89837 presented at the SPE Annual Technical Conference and Exhibition, Houston, 26-29 September.

Rao, M. A. 1999. Rheology of Fluid and Semisolid Foods. (pp. 1-24). Gaithersburg: Aspen Publishers, Inc.

Romeo, D.J., Valko, P.P. and Economides, M.J. 2002. Optimization of the Productivity Index and the Fracture Geometry of a Stimulated Well with Fracture Face and Choke Skins. Paper SPE 73758 presented at the International Symposium and Exhibition on Formation Damage Control, Lafayette, Louisiana, 20-21 February.

Runshing, J.A., Newsham, K.E., and Van Fraassen, K.C. 2003. Measurement of the Two-phase Gas Slippage Phenomenon and Its Effect on Gas Relative Permeability in Tight Gas Sands. Paper SPE 84297 presented at the SPE Annual Technical Conference and Exhibition, Denver, Colorado, 5-8 October.

Samuelson, M.L. and Constien, V.G. 1996. Effects of High Temperature on Polymer Degradation and Cleanup. Paper SPE 36495 presented at the SPE Annual Technical Conference and Exhibition, Denver,Colorado, 6-9 October.

Card, R.J., Nelson, E.B., Brown, J.E., Vinod, P.S., Temple H.L. et al. 1997. Polymer-Free Fluid for Hydraulic Fracturing. Paper SPE 38622 presented at Annual Technical Conference and Exhibition, San Antonio, Texas, 5-8 October .

Sherman, J.B. and Holditch, S.A. 1991. Effect of Injected Fracture Fluids and Operating Procedures on Ultimate Gas Recovery. Paper SPE 21496 presented at the Gas Technology Symposium, Houston,Texas, 22-24 January.

Siddiqui, M.A., Nasr-El-Din, H.A., Al-Anazi, M.S., and Bartko, K.M. 2004. Formation Damage in Gas Sandstone Formations by High-Temperature Borate Gels Due to Long Term Shut-In Periods. Paper SPE 89476 presented at the SPE/DOE Fourteenth Symposium on Improved Oil Recovery, Tulsa, Oklahoma, 17-21 April.

Soliman, M.Y. and Hunt, J.L. 1985. Effect of Fracturing Fluid and its Cleanup on Well Performance. Paper SPE 14514 presented at the SPE Eastern Regional Meeting, Morgantown, West Virginia, 6-8 November.

Speyer, N., Li, K., and Horne, R. 2007. Experimental Measurement of Two-phase Relative Permeability in Vertical Fractures. SGP-TR-183, Thirty-second Workshop on Geothermal Reservoir Engineering, Stanford University, Stanford, California, 22-24 January.

Sullivan, R.B., Rushing, J.A., Bachman, R.C., Settari, A., Ji. L. et al. 2006. Evaluation of Nonlinear Fracture Relative Permeabilities and Their Impact on Waterfrac Performance

in Tight Gas Sands. Paper SPE 98329, presented at the SPE International Symposium and Exhibition on Formation Damage Control, Lafayette, Louisiana, 15-17 February.

Surdam, R.C. 1995. The Age of Natural Gas, from Proceedings of a Workshop on the Future of Natural Gas in Wyoming: Laramie, Wyoming, Institute for Energy Research.

Tannich, J.D. 1975. Liquid Removal from Hydraulically Fractured Gas Wells. Paper *SPEJ* **27** (11) 1309-1317.

Voneiff, G.W., Robinson, B.M., and Holditch, S.A. 1996. The Effects of Unbroken Fracture Fluid on Gas Well Performance. *SPEJ* **11** (04) 223-229.

Wong, S.W. and Hii, K.K. 2001. Hydraulic Fracture Stimulation in Changbei Tight Gas Reservoir – Challenges and Achievements. Paper SPE 72165 presented at SPE Asia Pacific Improved Oil Recovery Conference, Kuala Lumpur, Malaysia, 6-9 October.

Yi, X. 2004. Model for Displacement of Herschel-Bulkley Non-Newtonian Fluid by Newtonian Fluid in Porous Media and Its Application in Fracturing Fluid Cleanup. Paper SPE 86491 presented at International Symposium and Exhibition on Formation Damage Control, Lafayette, Louisiana, 18-20 February.

APPENDIX A

DATA FILE FOR THE SIMULATION STUDY

```
#....INITIALIZATION SECTION.....................................

DATADUMP OFF

  MAXPHASES      MAXCELLS   MAXDIMENSION
       3          672           2

TITLE1 'SABRE DOCUMENTATION EXAMPLE 1: FIRST SPE COMPARATIVE SOLUTION PROJECT'
TITLE2 '10X10X3 3-PHASE BLACK OIL SIMULATION'

PHASES OIL GAS WAT

FMTP  '(F9.2)'
FMTS  '(F9.5)'
FMTPV '(G9.2)'

    MAPDIR      COLWIDTH     ABTRMFREQ       NUMCOLS
      XY            9            0           10

    KRGHYS        ITMAX        ITFRZ
      YES          20           4

   SOLMETH       DPLEVEL      KRWEIGHT      PRODALLOC
    SS           OLD        1PTUPSTR       MOBILITY

PHASEGRAVPOT      WELLSMIN       GASEQN
    UPDATE            1          NORM

  PLOTFILE
   BINARY

MAPS ROCK PRESPROP SATPROP PRESSAT GRSNET

  MIGRATION     REWINDRST
  NONE           NO

# Note: DX, DY, and DZ must appear before any array properties such as
#  PORIG, PHI, PB, etc.

      GRID
 RECTANGULAR


DX        1      1      2      3      5      10      15      20     30      50
     73      100    100    150    150    100    85     60     30     15
     15    30    60   85   100   160   325   625

DY     0.188  0.25   0.25  0.25  0.5  0.75  1  1.5  2  3
     5   10      20   30  50  75.25  80  80  80  80
     80   80   80  80

DZ     40

    PDATUM        HDATUM       PSATORIG       DAYSMAX
     5830         -8000         0              0
```

```
     HGOC          HOWC          HGWC
    -9400          0             0

   GORMAX     WELLGORMAX        WORMAX     WELLWORMAX
     0            0             0            0

   FTPMIN         FTPMAX           BHPMAX
     0            0             9000

    QOMIN         QGMIN
     0            0

 KRGHYSMLT    KRGHYSMAXSG   KRGHYSMAXDSG      KRGHYSPV
      4          0.11          0.08             1

    KBASE       PCGOMLT       PCOWMLT       PCGWMLT
     0            0             0             0

   DSWMAX         DSGMAX         DPMAX
    0.1           0.1           1000

              PEPS          SEPS
              0.1          0.05

PHI           KX            KY            KZ
0.072          0.01          0.01          0.01

PVTTABLE 'PVT TABLE 1'

PVTUOTAB
       PO          BO          VO         DENO
    9014.7       0.9812         9.6         0.44
    14.7         0.97           9.5         0.43

PVTUGTAB
       PG          BG          VG         DENG
    7914.7       2.30296       0.0426       0.1725
    5014.7       1.54083       0.0309       0.1154
    4014.7       1.23304       0.0268       0.0923
    3014.7       0.92593       0.0228       0.0693
    2514.7       0.77279       0.0208       0.0579
    2000        0.728359      0.0155975       0.04092
     1900        0.690318      0.0153781       0.04092
     1800        0.652051      0.0151587       0.04092
     1700        0.613633      0.0149393       0.04092
     1600        0.575139      0.0147199       0.04092
     1500        0.536646      0.0145005       0.04092
     1400        0.498229      0.0142811       0.04092
     1300        0.459962       0.014067       0.04092
     1200        0.421913      0.0138606       0.04092
     1100        0.384149      0.0136634       0.04092
     1000        0.346728      0.0134925       0.04092
      900        0.309703      0.0133194       0.04092
      800        0.273121      0.0131287       0.04092
      700        0.237024       0.012898       0.04092
      600        0.201444      0.0127491       0.04092
      500         0.16641      0.0125435      0.004092
      400        0.131943      0.0124325      0.004092
      300        0.098059      0.0122853      0.004092
      200         0.06477      0.0121755      0.004092
      100       0.0320826      0.0120891      0.004092
```

PVTUWTAB

PW	BW	VW	DENW
7914.7	0.9838	0.31	0.44263
5014.7	0.9748	0.31	0.43861
4014.7	0.9718	0.31	0.43725
3014.7	0.969	0.31	0.43598
2514.7	0.9676	0.31	0.43535
2014.7	0.9662	0.31	0.43472
1014.7	0.9634	0.31	0.43346
514.7	0.962	0.31	0.43283
264.7	0.9613	0.31	0.43252
14.7	0.9606	0.31	0.43221

KRTABLE '1'

KROGTAB

SG	KROG	KRG
1	0	1
0.7	0	0.94
0.6	0.0001	0.87
0.5	0.001	0.72
0.45	0.01	0.6
0.4	0.021	0.41
0.3	0.09	0.19
0.25	0.2	0.125
0.2	0.35	0.075
0.12	0.7	0.025
0.05	0.98	0.005
0.02	1	0
0.001	1	0
0	1	0

KROWTAB

SW	KROW	KRW
1	0	1
0.2	1	0
0	1	0

KRTABLE '2'

KROGTAB

SG	KROG	KRG
1	0	1
0.9	0.1	0.9
0.8	0.2	0.8
0.7	0.3	0.7
0.6	0.4	0.6
0.5	0.5	0.5
0.4	0.6	0.4
0.3	0.7	0.3
0.2	0.8	0.2
0.1	0.9	0.1
0.05	0.95	0.05
0.02	0.98	0.02
0	1	0

KROWTAB

SW	KROW	KRW
1	0	1
0	1	0

```
ROCKTABLE 'R1'
CLOSURECALC NONE
CPORE 3.E-06

ROCKTABLE 'R2'
CLOSURECALC        KTURB        BTURB
     CONST            0            0

    FDEPTH      FRACGRAD
      8000           1

    KPHITAB
      PNET        PRMRAT
      10000        0.5
      5000         0.63
      1500         0.7
      1000         0.8
       500         0.9
        0          1.0


ROCK ARRAY
2 2 2 2 2 2 2 2 2 2 2 2 2 2 2 2 2 2 2 2 2 2 2 2 2 2 2 2
1 1 1 1 1 1 1 1 1 1 1 1 1 1 1 1 1 1 1 1 1 1 1 1 1 1 1 1
1 1 1 1 1 1 1 1 1 1 1 1 1 1 1 1 1 1 1 1 1 1 1 1 1 1 1 1
1 1 1 1 1 1 1 1 1 1 1 1 1 1 1 1 1 1 1 1 1 1 1 1 1 1 1 1
1 1 1 1 1 1 1 1 1 1 1 1 1 1 1 1 1 1 1 1 1 1 1 1 1 1 1 1
1 1 1 1 1 1 1 1 1 1 1 1 1 1 1 1 1 1 1 1 1 1 1 1 1 1 1 1
1 1 1 1 1 1 1 1 1 1 1 1 1 1 1 1 1 1 1 1 1 1 1 1 1 1 1 1
1 1 1 1 1 1 1 1 1 1 1 1 1 1 1 1 1 1 1 1 1 1 1 1 1 1 1 1
1 1 1 1 1 1 1 1 1 1 1 1 1 1 1 1 1 1 1 1 1 1 1 1 1 1 1 1
1 1 1 1 1 1 1 1 1 1 1 1 1 1 1 1 1 1 1 1 1 1 1 1 1 1 1 1
1 1 1 1 1 1 1 1 1 1 1 1 1 1 1 1 1 1 1 1 1 1 1 1 1 1 1 1
1 1 1 1 1 1 1 1 1 1 1 1 1 1 1 1 1 1 1 1 1 1 1 1 1 1 1 1
1 1 1 1 1 1 1 1 1 1 1 1 1 1 1 1 1 1 1 1 1 1 1 1 1 1 1 1
1 1 1 1 1 1 1 1 1 1 1 1 1 1 1 1 1 1 1 1 1 1 1 1 1 1 1 1
1 1 1 1 1 1 1 1 1 1 1 1 1 1 1 1 1 1 1 1 1 1 1 1 1 1 1 1
1 1 1 1 1 1 1 1 1 1 1 1 1 1 1 1 1 1 1 1 1 1 1 1 1 1 1 1
1 1 1 1 1 1 1 1 1 1 1 1 1 1 1 1 1 1 1 1 1 1 1 1 1 1 1 1
1 1 1 1 1 1 1 1 1 1 1 1 1 1 1 1 1 1 1 1 1 1 1 1 1 1 1 1
1 1 1 1 1 1 1 1 1 1 1 1 1 1 1 1 1 1 1 1 1 1 1 1 1 1 1 1
1 1 1 1 1 1 1 1 1 1 1 1 1 1 1 1 1 1 1 1 1 1 1 1 1 1 1 1
1 1 1 1 1 1 1 1 1 1 1 1 1 1 1 1 1 1 1 1 1 1 1 1 1 1 1 1
1 1 1 1 1 1 1 1 1 1 1 1 1 1 1 1 1 1 1 1 1 1 1 1 1 1 1 1
1 1 1 1 1 1 1 1 1 1 1 1 1 1 1 1 1 1 1 1 1 1 1 1 1 1 1 1
1 1 1 1 1 1 1 1 1 1 1 1 1 1 1 1 1 1 1 1 1 1 1 1 1 1 1 1

KR ARRAY
2 2 2 2 2 2 2 2 2 2 2 2 2 2 2 2 2 2 2 2 2 2 2 2 2 2 2 2
1 1 1 1 1 1 1 1 1 1 1 1 1 1 1 1 1 1 1 1 1 1 1 1 1 1 1 1
1 1 1 1 1 1 1 1 1 1 1 1 1 1 1 1 1 1 1 1 1 1 1 1 1 1 1 1
1 1 1 1 1 1 1 1 1 1 1 1 1 1 1 1 1 1 1 1 1 1 1 1 1 1 1 1
1 1 1 1 1 1 1 1 1 1 1 1 1 1 1 1 1 1 1 1 1 1 1 1 1 1 1 1
1 1 1 1 1 1 1 1 1 1 1 1 1 1 1 1 1 1 1 1 1 1 1 1 1 1 1 1
1 1 1 1 1 1 1 1 1 1 1 1 1 1 1 1 1 1 1 1 1 1 1 1 1 1 1 1
1 1 1 1 1 1 1 1 1 1 1 1 1 1 1 1 1 1 1 1 1 1 1 1 1 1 1 1
1 1 1 1 1 1 1 1 1 1 1 1 1 1 1 1 1 1 1 1 1 1 1 1 1 1 1 1
1 1 1 1 1 1 1 1 1 1 1 1 1 1 1 1 1 1 1 1 1 1 1 1 1 1 1 1
1 1 1 1 1 1 1 1 1 1 1 1 1 1 1 1 1 1 1 1 1 1 1 1 1 1 1 1
```

```
1 1 1 1 1 1 1 1 1 1 1 1 1 1 1 1 1 1 1 1 1 1 1 1 1 1 1 1
1 1 1 1 1 1 1 1 1 1 1 1 1 1 1 1 1 1 1 1 1 1 1 1 1 1 1 1
1 1 1 1 1 1 1 1 1 1 1 1 1 1 1 1 1 1 1 1 1 1 1 1 1 1 1 1
1 1 1 1 1 1 1 1 1 1 1 1 1 1 1 1 1 1 1 1 1 1 1 1 1 1 1 1
1 1 1 1 1 1 1 1 1 1 1 1 1 1 1 1 1 1 1 1 1 1 1 1 1 1 1 1
1 1 1 1 1 1 1 1 1 1 1 1 1 1 1 1 1 1 1 1 1 1 1 1 1 1 1 1
1 1 1 1 1 1 1 1 1 1 1 1 1 1 1 1 1 1 1 1 1 1 1 1 1 1 1 1
1 1 1 1 1 1 1 1 1 1 1 1 1 1 1 1 1 1 1 1 1 1 1 1 1 1 1 1
1 1 1 1 1 1 1 1 1 1 1 1 1 1 1 1 1 1 1 1 1 1 1 1 1 1 1 1
1 1 1 1 1 1 1 1 1 1 1 1 1 1 1 1 1 1 1 1 1 1 1 1 1 1 1 1
1 1 1 1 1 1 1 1 1 1 1 1 1 1 1 1 1 1 1 1 1 1 1 1 1 1 1 1
1 1 1 1 1 1 1 1 1 1 1 1 1 1 1 1 1 1 1 1 1 1 1 1 1 1 1 1
1 1 1 1 1 1 1 1 1 1 1 1 1 1 1 1 1 1 1 1 1 1 1 1 1 1 1 1
```

ELEVATION NOGRAVITY
#ELEV -8000

EXCEPT (1..N,1..N)
SG ARRAY

```
0.0010  0.0010  0.0010  0.0010  0.0010  0.0010  0.0010  0.0010  0.0010  0.0010  0.0010  0.0010
        0.0010  0.0010  0.0010  0.0010  0.0010  0.0010  0.0010  0.0010  0.0010  0.0010  0.0010
        0.0010  0.0010  0.0010  0.0010  0.8000
0.0192  0.0192  0.0192  0.0193  0.0419  0.0420  0.0422  0.0425  0.0428  0.0434  0.0442  0.0453
        0.0463  0.0479  0.0499  0.0510  0.0494  0.0467  0.0446  0.0429  0.4342  0.7970  0.8001
        0.8001  0.8000  0.8000  0.8000  0.8000
0.0192  0.0192  0.0192  0.0192  0.0445  0.0446  0.0448  0.0449  0.0452  0.0457  0.0464  0.0473
        0.0481  0.0496  0.0513  0.0523  0.0507  0.0483  0.0464  0.0448  0.4990  0.7974  0.8001
        0.8001  0.8000  0.8000  0.8000  0.8000
0.0193  0.0193  0.0193  0.0193  0.0464  0.0465  0.0466  0.0468  0.0470  0.0474  0.0480  0.0489
        0.0497  0.0510  0.0526  0.0535  0.0519  0.0497  0.0479  0.0463  0.5140  0.7975  0.8001
        0.8001  0.8000  0.8000  0.8000  0.8000
0.0195  0.0195  0.0195  0.0458  0.0494  0.0494  0.0495  0.0497  0.0499  0.0503  0.0509  0.0516
        0.0523  0.0536  0.0550  0.0557  0.0541  0.0521  0.0504  0.0488  0.5320  0.7977  0.8001
        0.8001  0.8000  0.8000  0.8000  0.8000
0.0197  0.0197  0.0489  0.0509  0.0528  0.0529  0.0530  0.0531  0.0534  0.0537  0.0543  0.0550
        0.0558  0.0570  0.0582  0.0587  0.0572  0.0553  0.0535  0.0517  0.5588  0.7981  0.8001
        0.8001  0.8000  0.8000  0.8000  0.8000
0.0200  0.0200  0.0546  0.0555  0.0566  0.0566  0.0568  0.0569  0.0572  0.0576  0.0582  0.0591
        0.0600  0.0613  0.0626  0.0627  0.0612  0.0591  0.0571  0.0551  0.5937  0.7985  0.8001
        0.8001  0.8000  0.8000  0.8000  0.8000
0.0585  0.0585  0.0611  0.0615  0.0620  0.0621  0.0623  0.0625  0.0629  0.0635  0.0644  0.0657
        0.0672  0.0693  0.0714  0.0710  0.0686  0.0654  0.0624  0.0599  0.6392  0.7990  0.8001
        0.8001  0.8000  0.8000  0.8000  0.8000
0.0691  0.0691  0.0700  0.0703  0.0706  0.0707  0.0711  0.0716  0.0724  0.0737  0.0759  0.0793
        0.0839  0.0925  0.1058  0.1008  0.0886  0.0779  0.0711  0.0670  0.6929  0.7995  0.8001
        0.8001  0.8000  0.8000  0.8000  0.8000
0.1141  0.1144  0.1156  0.1170  0.1192  0.1219  0.1261  0.1325  0.1443  0.1652  0.2039  0.2697
        0.3526  0.4661  0.5576  0.5345  0.4199  0.2392  0.1216  0.0918  0.7526  0.7999  0.8001
        0.8001  0.8000  0.8000  0.8000  0.8000
0.6170  0.6174  0.6188  0.6213  0.6258  0.6322  0.6422  0.6563  0.6754  0.7033  0.7364  0.7664
        0.7829  0.7922  0.7957  0.7949  0.7894  0.7561  0.6334  0.5198  0.7963  0.8001  0.8001
        0.8001  0.8000  0.8000  0.8000  0.8000
0.7981  0.7982  0.7982  0.7982  0.7983  0.7984  0.7986  0.7988  0.7991  0.7994  0.7998  0.8001
        0.8002  0.8003  0.8003  0.8003  0.8002  0.7999  0.7984  0.7966  0.8001  0.8001  0.8001
        0.8001  0.8000  0.8000  0.8000  0.8000
```

```
0.8003  0.8003  0.8003  0.8003  0.8003  0.8003  0.8003  0.8003  0.8003  0.8003  0.8003  0.8003
        0.8003  0.8003  0.8003  0.8003  0.8003  0.8002  0.8002  0.8002  0.8002  0.8001  0.8001
        0.8001  0.8000  0.8000  0.8000  0.8000
0.8003  0.8003  0.8003  0.8003  0.8003  0.8003  0.8003  0.8003  0.8003  0.8003  0.8003  0.8003
        0.8003  0.8003  0.8002  0.8002  0.8002  0.8002  0.8002  0.8001  0.8001  0.8001  0.8001
        0.8000  0.8000  0.8000  0.8000  0.8000
0.8002  0.8002  0.8002  0.8002  0.8002  0.8002  0.8002  0.8002  0.8002  0.8002  0.8002  0.8002
        0.8002  0.8002  0.8002  0.8002  0.8002  0.8002  0.8001  0.8001  0.8001  0.8001  0.8001
        0.8000  0.8000  0.8000  0.8000  0.8000
0.8002  0.8002  0.8002  0.8002  0.8002  0.8002  0.8002  0.8002  0.8002  0.8002  0.8002  0.8002
        0.8002  0.8002  0.8001  0.8001  0.8001  0.8001  0.8001  0.8001  0.8001  0.8001  0.8001
        0.8000  0.8000  0.8000  0.8000  0.8000
0.8001  0.8001  0.8001  0.8001  0.8001  0.8001  0.8001  0.8001  0.8001  0.8001  0.8001  0.8001
        0.8001  0.8001  0.8001  0.8001  0.8001  0.8001  0.8001  0.8000  0.8000  0.8000  0.8000
        0.8000  0.8000  0.8000  0.8000  0.8000
0.8000  0.8000  0.8000  0.8000  0.8000  0.8000  0.8000  0.8000  0.8000  0.8000  0.8000  0.8000
        0.8000  0.8000  0.8000  0.8000  0.8000  0.8000  0.8000  0.8000  0.8000  0.8000  0.8000
        0.8000  0.8000  0.8000  0.8000  0.8000
0.8000  0.8000  0.8000  0.8000  0.8000  0.8000  0.8000  0.8000  0.8000  0.8000  0.8000  0.8000
        0.8000  0.8000  0.8000  0.8000  0.8000  0.8000  0.8000  0.8000  0.8000  0.8000  0.8000
        0.8000  0.8000  0.8000  0.8000  0.8000
0.8000  0.8000  0.8000  0.8000  0.8000  0.8000  0.8000  0.8000  0.8000  0.8000  0.8000  0.8000
        0.8000  0.8000  0.8000  0.8000  0.8000  0.8000  0.8000  0.8000  0.8000  0.8000  0.8000
        0.8000  0.8000  0.8000  0.8000  0.8000
0.8000  0.8000  0.8000  0.8000  0.8000  0.8000  0.8000  0.8000  0.8000  0.8000  0.8000  0.8000
        0.8000  0.8000  0.8000  0.8000  0.8000  0.8000  0.8000  0.8000  0.8000  0.8000  0.8000
        0.8000  0.8000  0.8000  0.8000  0.8000
0.8000  0.8000  0.8000  0.8000  0.8000  0.8000  0.8000  0.8000  0.8000  0.8000  0.8000  0.8000
        0.8000  0.8000  0.8000  0.8000  0.8000  0.8000  0.8000  0.8000  0.8000  0.8000  0.8000
        0.8000  0.8000  0.8000  0.8000  0.8000
0.8000  0.8000  0.8000  0.8000  0.8000  0.8000  0.8000  0.8000  0.8000  0.8000  0.8000  0.8000
        0.8000  0.8000  0.8000  0.8000  0.8000  0.8000  0.8000  0.8000  0.8000  0.8000  0.8000
        0.8000  0.8000  0.8000  0.8000  0.8000
0.8000  0.8000  0.8000  0.8000  0.8000  0.8000  0.8000  0.8000  0.8000  0.8000  0.8000  0.8000
        0.8000  0.8000  0.8000  0.8000  0.8000  0.8000  0.8000  0.8000  0.8000  0.8000  0.8000
        0.8000  0.8000  0.8000  0.8000  0.8000
```

SW ARRAY

```
0.0000  0.0000  0.0000  0.0000  0.0000  0.0000  0.0000  0.0000  0.0000  0.0000  0.0000  0.0000
        0.0000  0.0000  0.0000  0.0000  0.0000  0.0000  0.0000  0.0000  0.0000  0.2058  0.1999
        0.1999  0.2000  0.2000  0.2000  0.2000
0.9917  0.9917  0.9915  0.9914  0.9742  0.9741  0.9738  0.9734  0.9728  0.9718  0.9703  0.9684
        0.9665  0.9632  0.9592  0.9570  0.9612  0.9668  0.9712  0.9757  0.5656  0.2030  0.1999
        0.1999  0.2000  0.2000  0.2000  0.2000
0.9846  0.9845  0.9844  0.9844  0.9604  0.9602  0.9599  0.9596  0.9590  0.9581  0.9569  0.9553
        0.9538  0.9514  0.9488  0.9478  0.9501  0.9540  0.9578  0.9621  0.5008  0.2026  0.1999
        0.1999  0.2000  0.2000  0.2000  0.2000
0.9815  0.9815  0.9814  0.9814  0.9535  0.9533  0.9532  0.9529  0.9525  0.9519  0.9511  0.9500
        0.9489  0.9474  0.9460  0.9453  0.9467  0.9490  0.9516  0.9546  0.4857  0.2025  0.1999
        0.1999  0.2000  0.2000  0.2000  0.2000
0.9802  0.9802  0.9802  0.9561  0.9486  0.9485  0.9484  0.9482  0.9479  0.9475  0.9469  0.9462
        0.9456  0.9447  0.9436  0.9431  0.9443  0.9458  0.9474  0.9494  0.4678  0.2023  0.1999
        0.1999  0.2000  0.2000  0.2000  0.2000
```

```
0.9799  0.9799  0.9511  0.9470  0.9450  0.9450  0.9449  0.9448  0.9446  0.9443  0.9439  0.9433
        0.9427  0.9418  0.9408  0.9404  0.9417  0.9431  0.9445  0.9460  0.4410  0.2019  0.1999
        0.1999  0.2000  0.2000  0.2000  0.2000
0.9796  0.9796  0.9435  0.9428  0.9421  0.9420  0.9419  0.9418  0.9415  0.9412  0.9407  0.9399
        0.9392  0.9380  0.9369  0.9368  0.9381  0.9399  0.9416  0.9433  0.4062  0.2015  0.1999
        0.1999  0.2000  0.2000  0.2000  0.2000
0.9399  0.9399  0.9380  0.9377  0.9373  0.9372  0.9371  0.9368  0.9365  0.9360  0.9351  0.9339
        0.9326  0.9306  0.9285  0.9290  0.9312  0.9342  0.9369  0.9392  0.3608  0.2010  0.1999
        0.1999  0.2000  0.2000  0.2000  0.2000
0.9306  0.9306  0.9298  0.9296  0.9293  0.9292  0.9288  0.9283  0.9275  0.9262  0.9241  0.9207
        0.9161  0.9075  0.8942  0.8992  0.9114  0.9221  0.9288  0.9328  0.3071  0.2005  0.1999
        0.1999  0.2000  0.2000  0.2000  0.2000
0.8859  0.8856  0.8844  0.8830  0.8808  0.8781  0.8739  0.8675  0.8557  0.8348  0.7961  0.7303
        0.6474  0.5339  0.4424  0.4655  0.5801  0.7608  0.8784  0.9082  0.2474  0.2001  0.1999
        0.1999  0.2000  0.2000  0.2000  0.2000
0.3830  0.3826  0.3812  0.3787  0.3742  0.3678  0.3578  0.3437  0.3246  0.2967  0.2636  0.2336
        0.2171  0.2078  0.2043  0.2051  0.2106  0.2439  0.3666  0.4802  0.2037  0.1999  0.1999
        0.1999  0.2000  0.2000  0.2000  0.2000
0.2019  0.2018  0.2018  0.2018  0.2017  0.2016  0.2014  0.2012  0.2009  0.2006  0.2002  0.2000
        0.1998  0.1998  0.1997  0.1997  0.1998  0.2001  0.2016  0.2034  0.1999  0.1999  0.1999
        0.1999  0.2000  0.2000  0.2000  0.2000
0.1997  0.1997  0.1997  0.1997  0.1997  0.1997  0.1997  0.1997  0.1997  0.1997  0.1997  0.1997
        0.1997  0.1997  0.1997  0.1997  0.1997  0.1998  0.1998  0.1998  0.1998  0.1999  0.1999
        0.2000  0.2000  0.2000  0.2000  0.2000
0.1997  0.1997  0.1997  0.1997  0.1997  0.1997  0.1997  0.1997  0.1997  0.1997  0.1997  0.1997
        0.1997  0.1997  0.1998  0.1998  0.1998  0.1998  0.1998  0.1999  0.1999  0.1999  0.1999
        0.2000  0.2000  0.2000  0.2000  0.2000
0.1998  0.1998  0.1998  0.1998  0.1998  0.1998  0.1998  0.1998  0.1998  0.1998  0.1998  0.1998
        0.1998  0.1998  0.1998  0.1998  0.1998  0.1998  0.1999  0.1999  0.1999  0.1999  0.1999
        0.2000  0.2000  0.2000  0.2000  0.2000
0.1998  0.1998  0.1998  0.1998  0.1998  0.1998  0.1998  0.1998  0.1998  0.1998  0.1998  0.1998
        0.1998  0.1998  0.1999  0.1999  0.1999  0.1999  0.1999  0.1999  0.1999  0.1999  0.1999
        0.2000  0.2000  0.2000  0.2000  0.2000
0.1999  0.1999  0.1999  0.1999  0.1999  0.1999  0.1999  0.1999  0.1999  0.1999  0.1999  0.1999
        0.1999  0.1999  0.1999  0.1999  0.1999  0.1999  0.1999  0.2000  0.2000  0.2000  0.2000
        0.2000  0.2000  0.2000  0.2000  0.2000
0.2000  0.2000  0.2000  0.2000  0.2000  0.2000  0.2000  0.2000  0.2000  0.2000  0.2000  0.2000
        0.2000  0.2000  0.2000  0.2000  0.2000  0.2000  0.2000  0.2000  0.2000  0.2000  0.2000
        0.2000  0.2000  0.2000  0.2000  0.2000
0.2000  0.2000  0.2000  0.2000  0.2000  0.2000  0.2000  0.2000  0.2000  0.2000  0.2000  0.2000
        0.2000  0.2000  0.2000  0.2000  0.2000  0.2000  0.2000  0.2000  0.2000  0.2000  0.2000
        0.2000  0.2000  0.2000  0.2000  0.2000
0.2000  0.2000  0.2000  0.2000  0.2000  0.2000  0.2000  0.2000  0.2000  0.2000  0.2000  0.2000
        0.2000  0.2000  0.2000  0.2000  0.2000  0.2000  0.2000  0.2000  0.2000  0.2000  0.2000
        0.2000  0.2000  0.2000  0.2000  0.2000
0.2000  0.2000  0.2000  0.2000  0.2000  0.2000  0.2000  0.2000  0.2000  0.2000  0.2000  0.2000
        0.2000  0.2000  0.2000  0.2000  0.2000  0.2000  0.2000  0.2000  0.2000  0.2000  0.2000
        0.2000  0.2000  0.2000  0.2000  0.2000
0.2000  0.2000  0.2000  0.2000  0.2000  0.2000  0.2000  0.2000  0.2000  0.2000  0.2000  0.2000
        0.2000  0.2000  0.2000  0.2000  0.2000  0.2000  0.2000  0.2000  0.2000  0.2000  0.2000
        0.2000  0.2000  0.2000  0.2000  0.2000
0.2000  0.2000  0.2000  0.2000  0.2000  0.2000  0.2000  0.2000  0.2000  0.2000  0.2000  0.2000
        0.2000  0.2000  0.2000  0.2000  0.2000  0.2000  0.2000  0.2000  0.2000  0.2000  0.2000
        0.2000  0.2000  0.2000  0.2000  0.2000
0.2000  0.2000  0.2000  0.2000  0.2000  0.2000  0.2000  0.2000  0.2000  0.2000  0.2000  0.2000
        0.2000  0.2000  0.2000  0.2000  0.2000  0.2000  0.2000  0.2000  0.2000  0.2000  0.2000
        0.2000  0.2000  0.2000  0.2000  0.2000


EXCEPT (1..20,1..1)
    PHI       KX        KY        KZ
    0.3       1E+03     1E+03     1E+03
```

```
EXCEPT (1..N,1..N)
PHI MULT          1
KX  MULT          1
KY  MULT          1
KZ  MULT          1

   RESTART       STEPMAX      RSTINTRP       RSTFREQ
       0         300000           NO             0



#.....TIME DEPENDENT SECTION.....


START     DATE   6/1/1987 TIME 00:00:00
 PLTMAPFREQ    PLTRGNFREQ    PLTWELFREQ       PSDFREQ
       1             1             1             0

   DTSTART         DTMAX         DTMLT       OUTFREQ      OUTINTRPT
    0.0000001        0.01          2             3        BEFORE
     OUTPUTON  MIGRAT  PWMAP  SWMAP  PGMAP SGMAP  SOMAP TIMEDEP
WELL 'WEL2'  LOC ( 1, 1     ) WKR '2' TYPE CFBP WC        10.59  BHP       4500
INTERRUPT CUMDAYS 0.1
WELL 'WEL2'  LOC ( 1, 1     ) WKR '2' TYPE CFBP WC        10.59  BHP       4200
INTERRUPT CUMDAYS 5
WELL 'WEL2'  LOC ( 1, 1     ) WKR '2' TYPE CFBP WC        10.59  BHP       3820
   DTSTART         DTMAX         DTMLT       OUTFREQ      OUTINTRPT
    0.01            50          2             3        BEFORE
     OUTPUTON  MIGRAT  PWMAP  SWMAP  PGMAP SGMAP  SOMAP TIMEDEP
INTERRUPT CUMDAYS 12
WELL 'WEL2'  LOC ( 1, 1     ) WKR '2' TYPE CFBP WC        10.59  BHP       3300
INTERRUPT CUMDAYS 21
WELL 'WEL2'  LOC ( 1, 1     ) WKR '2' TYPE CFBP WC        10.59  BHP       3000
INTERRUPT CUMDAYS 28
WELL 'WEL2'  LOC ( 1, 1     ) WKR '2' TYPE CFBP WC        10.59  BHP       2600
INTERRUPT CUMDAYS 45
WELL 'WEL2'  LOC ( 1, 1     ) WKR '2' TYPE CFBP WC        10.59  BHP       2160
INTERRUPT CUMDAYS  60
WELL 'WEL2'  LOC ( 1, 1     ) WKR '2' TYPE CFBP WC        10.59  BHP       1950
INTERRUPT CUMDAYS   85
WELL 'WEL2'  LOC ( 1, 1     ) WKR '2' TYPE CFBP WC        10.59  BHP       1675
INTERRUPT CUMDAYS   105
WELL 'WEL2'  LOC ( 1, 1     ) WKR '2' TYPE CFBP WC        10.59  BHP       1450
INTERRUPT CUMDAYS   120
WELL 'WEL2'  LOC ( 1, 1     ) WKR '2' TYPE CFBP WC        10.59  BHP       1200

INTERRUPT  DATE 12/31/1997 TIME 00:00:00
STOP
```

APPENDIX B

CARBO PROPPANT DATA USED IN THIS RESEARCH

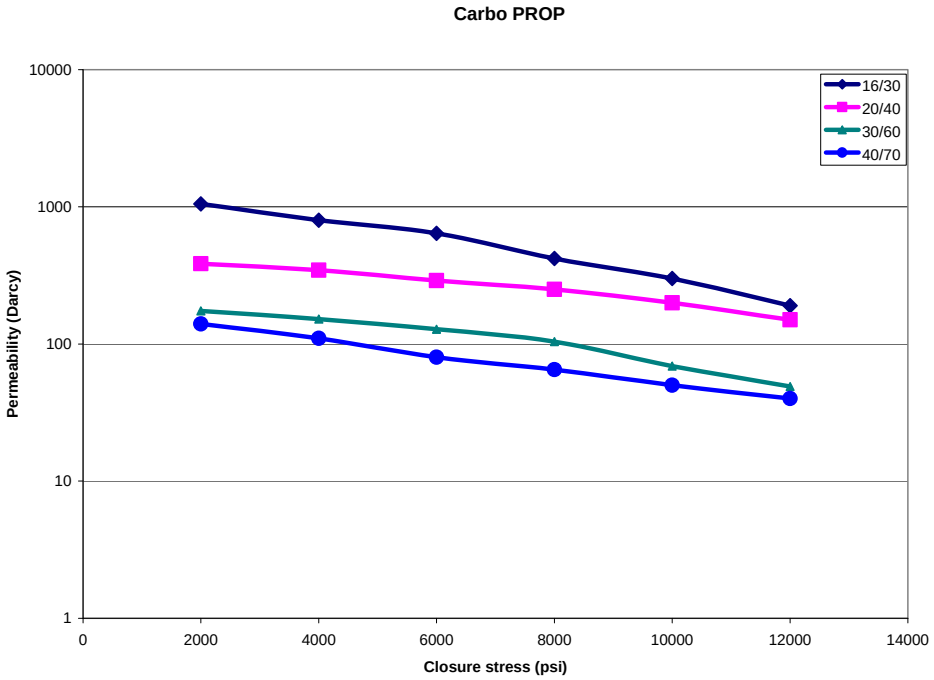

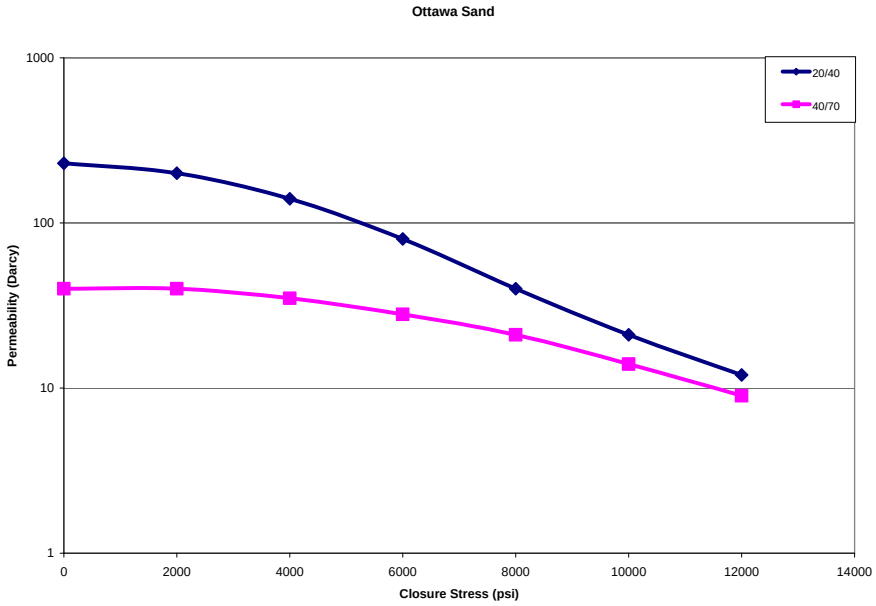

APPENDIX C

COMMONLY USED POLYMERS IN PETROLEUM INDUSTRY

Table C.1 Water-based polymers available in the industry (from World Oil 2007)

Product	Company				
	Baker Oil Tools	BJ Services	Schlumberger (Dowell)	Halliburton	Nowsco / Fracmaster
Powdered guar gum polymer. Delayed hydration for batch mix:	Available	GW-27	J424, J877	WG-19	WG-15
Powdered guar gum polymer, rapid hydration for continuous mix. Contains internal breaker:			J133		
Powdered hydroxypropylguar gum, delayed hydration polymer, for batch mix. No internal breaker:		GW-32	J347, J362	WG-11	Available
Powdered hydroxypropylguar viscosifier with internal breaker. Rapid hydration for continuous mix:					
Powdered hydroxethylcellulose viscosifier. Delayed hydration polymer for use as a secondary gel or batch mix:	WG 2	AG-21R	J164	WG-17	AG-21R
Chemically modified HEC for cross- linked fluid. No internal breaker:				WG-33	
Powdered HPG. Delayed hydration polymer, designed for batch mix applications for borate crosslink:				WG-11	
CMHPG gum in oil base slurry:	Available	XLFC-3	J916	LGC-VI	Available
Powdered CMHPG for oil base slurry:		GW-38	J486	WG-18	GW-38
Powdered guar gum polymer. Rapid hydration for use in oil base slurrys:		GW-4	J457	WG-31, WG-22	WG-15
Guar gum in oil base slurry:	WG 1(L)	XLFC-1	J877	LGC-IV, LGC-8	Available
Powdered HPG for oil base		GW-32	J456	WG-11	WG-16

slurry:					
HPG gum in oil base slurry:		XLFC-2	J876	LGC-V	Available
High yield CMHPG (slurrible):		GW-38	J486	WG-18	GW-38
Powdered hydroxyethylcellulose		GW-21	(Internal breaker)	WG-17	GW-21
viscosifier:			J164		
Powdered carboxymethylhydrox-ethylcellulose viscosifier. Rapid hydration for batch and continuous mix:		GW-28			GW-28
Chemically modified natural polymer CMHPG:		GW-38	J486	WG-18	GW-38
Powdered xanthan gum gelling agent as carrier fluid for gravel packs:	WG 299	GW-22		WG-24	Available

Table C.2 Crosslinked gel system available in the industry (from World Oil 2007)

Product	**Company**				
	Baker Oil Tools	**BJ Services**	**Schlumberger (Dowell)**	**Halliburton**	**Nowsco / Fracmaster**
Crosslinked guar system:	Bora Fraq	Viking, Viking D	YF100.1 HTD	MY-T-GEL III,	Aquamaster-12
			YF100ST	MY-T-GEL LT,	Spectra Frac G
			YF300 Titanate,	MY-T-GEL HT,	
			YF500 Zirconate	Hybor Gel,	
			YF100LGD YF100LG	DeltaFrac,	
			YF400 Titanate	Boragel, Fracgel	
			(delayed available),		
Crosslinked HPG:			YF200, YF200D,	Versagel,	
			YF600 (zirconium)	Versagel LT, HT	
			InvertaFrac	Hybor, Boragel,	
			DivertaFrac	DeltaFrac H200	
Prepad with buoyant diverting agent to control upward growth:					

Oil prepad with polymer coated sand diverting agent to control downward and water encroachment:		Available	StrataFrac II service (available with most systems)		Available
Crosslinked HPG with 3-5% hydrocarbon for fluid loss:			YF600	VersaGel, Hybor Gel plus diesel	Available
Crosslinked HPG with high temperature stabilizers:		KrystalFrac	Available	VersaGel HT	
				Hybor Gel	
Crosslinked CMHEC:		KrystalFrac			
Crosslinked CMHEC for high temperature:		SpectraFrac G,	YF100 (guar),		Aquamaster 12
Crosslinked guar or HPG with borate:		Viking, Viking D	YF200 (HPG)	Boragel,	
		Medallion Frac	YF400, YF300	Hybor Gel	Medallion Frac
CO2 compatible fracturing fluid:		Viking	YF800LPH	Pur-Gel III,	Vistar II
			YF100, YF100 LG	VersaGel LT,	
				WaterFrac, MY-T-GEL LT	Aquamaster 12
Economical, low residue crosslinked system:	Bora Fraq LP	Viking D	YF100 LGD, YF100ST	FracGel HT	
			YF600		
Controllable delayed crosslinked HPG system:		SpectraFrac G,	YF400	VersaGel HT	SpectraFrac G,
			YF600 (HPG),		
Controllable delayed crosslinked high temperature system:		Medallion Frac,	YF500 (guar)	Thermagel,	Medallion Frac
		Medallion Frac HT,	YF100,1 HTD,	Pur Gel III,	Medallion Frac HT
		Medallion HT	YF100 HTD	VersaGel HT	Medallion HT
			YF800HT	Hybor Gel,	
			YF800HT	FracGel HT	
Crosslinked CMHPG high temperature fluids:		Medallion	YF800-LpH	Thermagel	Medallion
		Medallion			Medallion
Crosslinked CMHPG low pH CO2 compatible fluid:			Available	Pur-Gel III,	

APPENDIX D

DISCUSSION FOR MODELING OF FLOWING YIELD STRESS AND POLYMER RESIDUE

Simulation of the flowing yield stress on the cleanup process

The simulation results about yield stress in Chapter VI are essentially static yield stress. Previous researchers assumed that fracture fluid behaves like power law fluid after it yields, as we did. However, Figure D.1 shows an obvious difference between static and flowing yield stress. After the non-Newtonian fluid yields, the fluid will move, and the viscosity will decrease based on the fluid velocity and pressure gradient inside the fracture. However, if the pressure gradient drops below the flowing yield stress, the fluid will slow down and stop moving. Just like moving a heavy box across the floor (Figure D.2), it may be difficult to move, but once it starts sliding, it is easier to move. So far from the published literature, no one has studied the effect of flowing yield stress on the cleanup process and long-term gas production. Here we provide some new ideas how to model the effect flowing yield stress on the cleanup process.

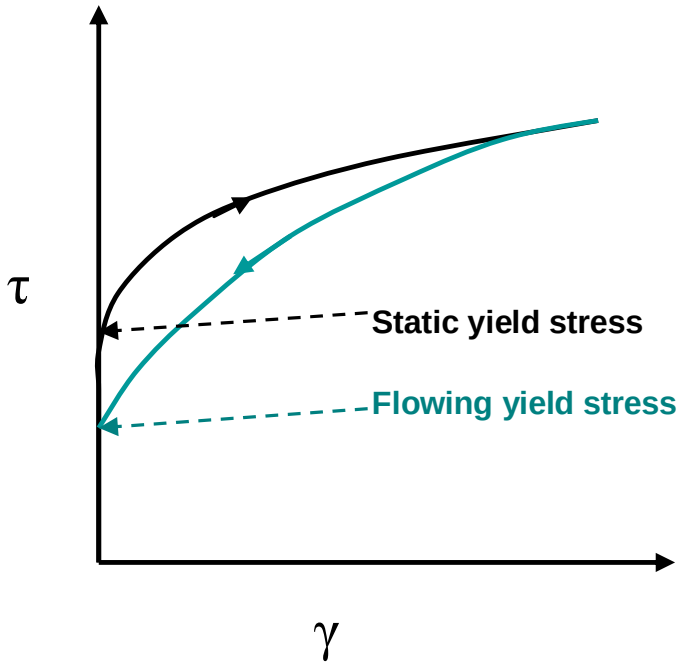

Figure D.1—Schematic drawing of static vs. flowing yield stress

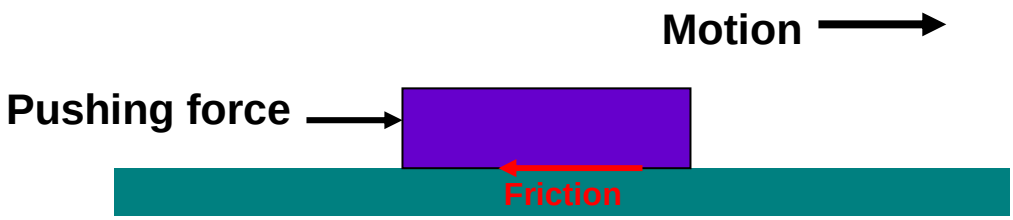

Figure D.2—Analogy between flowing yield stress and dynamic friction force

Figure D.2 shows an analogy between flowing yield stress of fracture and dynamic friction force. If the pushing force is less than static friction force, there is no motion and the objects remain static with respect to each other. However, once the box moves, the friction decreases from the static friction holding the object in place. You have seen this in trying to slide a heavy box across the floor. It may be very difficult to move, but once it starts sliding, it is easier to push. If the pushing force drops below the kinetic friction, the box slows down and stops after a certain period of time.

This is the basic theory for modeling of the effect of the flowing yield stress of fracture fluid during the cleanup process. Since there are no complete measured data on the flowing yield stress, it is assumed to be ¼ of the static yield stress for simulation study. Then we modified the programming to incorporate the flowing yield stress effect.

Simulation of the effect of polymer residue on the cleanup process

Samuelson and Constien (1996) presented laboratory fracture conductivity and residual polymer analysis for a degraded fracture fluid at temperature above 180^0F and provided a correlation of fracture permeability with volume of polymer recovered. This method could be used to evaluate the cleanup process after a fracture treatment in either a laboratory or a field.

Results from a field flowback analysis in Table D.1 (Samuelson et al., 1996) show that about 26% the polymer can be recovered if only breaker is used with a fracture fluid and

about 44% of the polymer can be recovered if a breaker plus additive are used together with a fracture fluid.

Table D.1—Polymer residue inside fracture

Well No.	Temp (^{0}F)	Sand (lb)	Ceramic (lb)	**Polymer Returned**
Wells with breaker only				**Average = 26%**
F-1	220	394500	50040	**27%**
F-2	220	301060	50780	**24%**
F-3	220	545900	0	**23%**
CV-1	270	0	328200	**10%**
CV-2	250	0	425000	**30%**
CV-3	230	0	265000	**35%**
Wells w/breaker &additive				**Average = 44%**
GW-1	195	0	225000	**58%**
GW-2	205	0	603327	**26%**
AW	205	0	196480	**62%**
F-1	210	590000	0	**33%**
F-2	220	507420	0	**62%**
CV	250		448000	**25%**

a

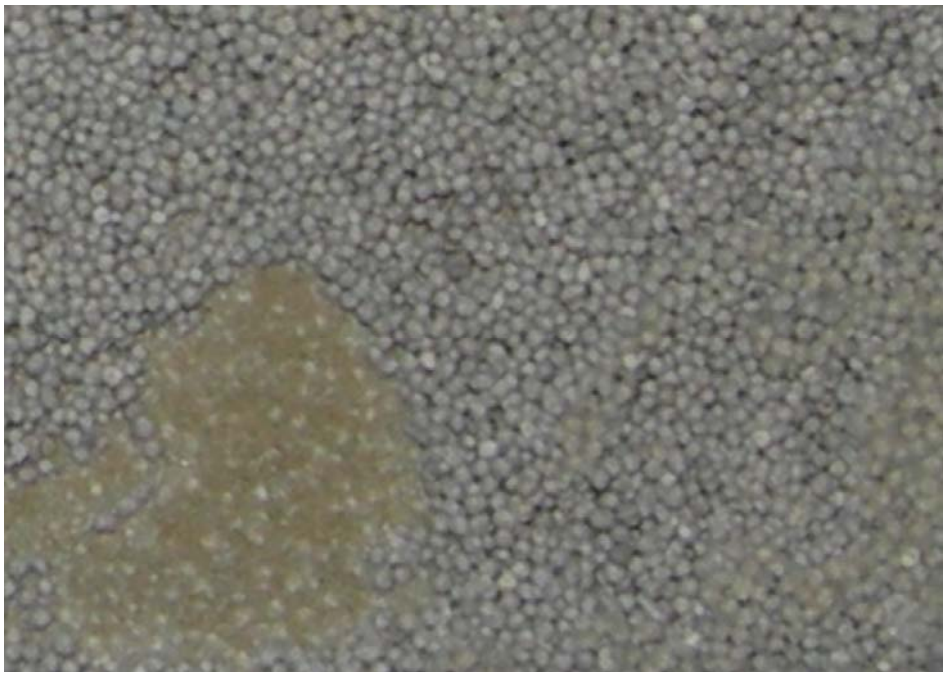

b

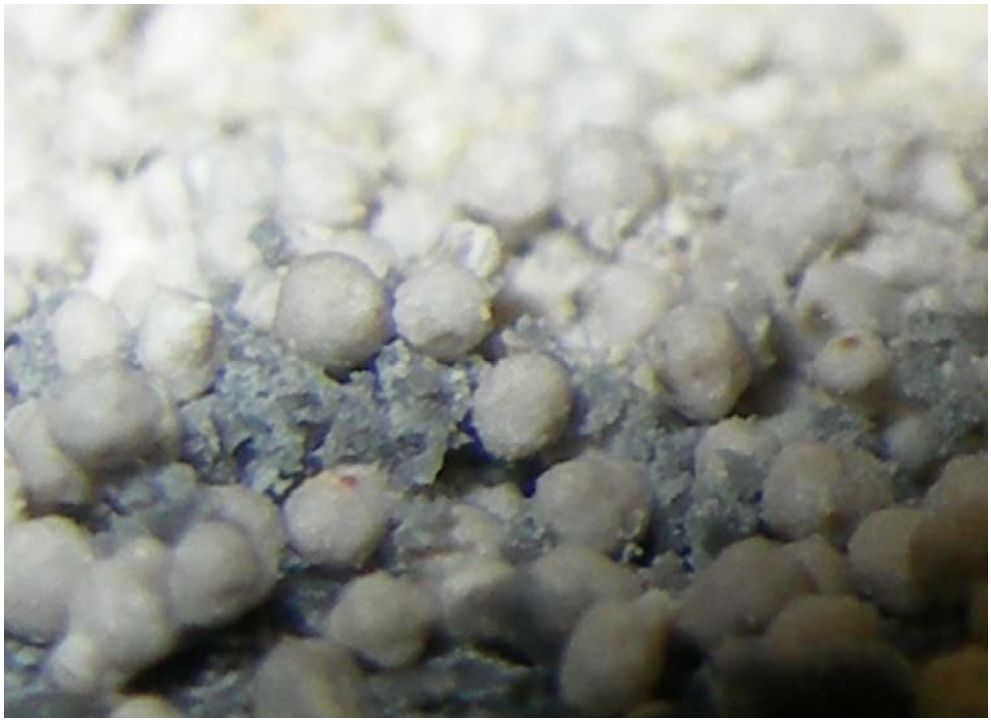

c

Figure D.3—Proppant with polymer residue from one laboratory test (from Chen *et al* at Texas A&M University 2007)

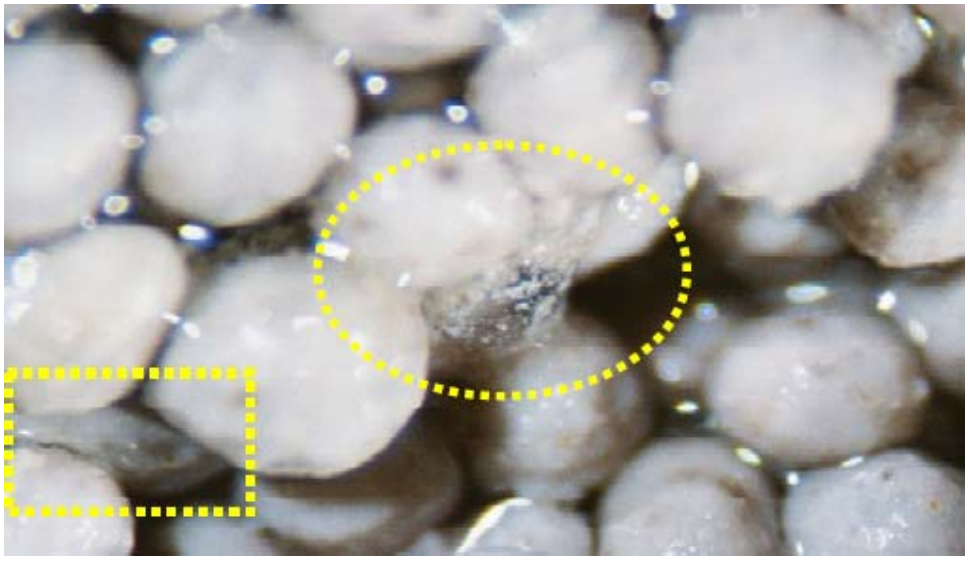

Figure D.4—Residual gel from 35 ppt CMHPG fluid with breaker by Stimlab

Figure D.3 and D.4 show that the polymer residues exist inside the fracture proppant after a treatment in the lab, which agrees with the results in Table D.1. Since the polymer

residue behaves like a solid if the pressure gradient is below the yield stress point, the polymer will stay inside the fracture and reduce the permeability and porosity of the fracture pack.

The amount of polymer in the proppant pack, W_p, is found to vary systematically with the measured retained permeability, K′ /K.

$$\frac{K'}{K} = A * e^{-B \bullet W_p} = (\frac{\varepsilon'}{\varepsilon})^3 \frac{(1-\varepsilon)^2}{(1-\varepsilon)^2} \quad \text{.....D.1}$$

$$\frac{V'}{V} = 1 - \frac{\varepsilon'}{\varepsilon} \quad \text{.....D.2}$$

$$\varepsilon = \frac{V}{A_A * l_w} \quad \text{.....D.3}$$

$$V = A_A * l_w - V_p \quad \text{.....D.4}$$

Table D.2—SUMMARY OF EXPONENTIAL FUNCTION COEFFICIENTS FROM EQUATION 1.		
Temperature (0F)	Constant A	Exponent B
200	91.1	-8.7
250	83.3	-12.9
275	107.3	-19.4

Where,

W_p = amount of polymer retained in the proppant pack, g

K = proppant pack permeability before polymer blockage, md

K′ = proppant pack permeability before polymer blockage, md

ε = initial porosity

ε' = porosity after polymer blockage

V = original undamaged pore volume of the pack, cm^3

V' = pore volume blocked by polymer residue, cm^3

V_p = volume of proppant placed in the cell, cm^3

ρ_{eff} = effective density, g/cm3

l_w = proppant pack width after closure, cm

A_A = fracture face area, cm^2

p = proppant

w = width

A = area

eff = effective

Insoluble polymer residue will lower gas production and reduce fracture fluid recovery for both low and high conductive fractures. Polymer or cross-linked polymer may not be broken fully and remain as insoluble, high-molecular-weight solids after a treatment. Even some degraded guar based fluids at high temperature tend to form insoluble fragments. (Samuelson 1996). The correlation between the retained permeability with polymer residue from Samuelson and Constien has been built into our 3D, 3-phase simulator to investigate the effect of polymer residue on the fracture fluid cleanup process and long-term gas production in tight gas wells. Incorporating this effect into our simulation will enable us to model the cleanup process more accurately. This is a better method than adjusting the conductivity by a factor, like 0.1 or 0.01, as some engineers did.

APPENDIX E

SIMULATION RESULTS FROM CASE 1 TO 6, RUN 1 TO 72.

More simulation results are presented in this Appendix E to help all understand the dissertation. The figures are in the following orders:

- case 1 – the single phase flow,
- case 2 – multi-phase flow,
- case 3 – adding proppant crushing,
- case 5c – adding gel damage with yield stress of 20 pa, and

We also presented table of gas recovery (Table E.1) and table of fracture cleanup in percentage (Table E.2).

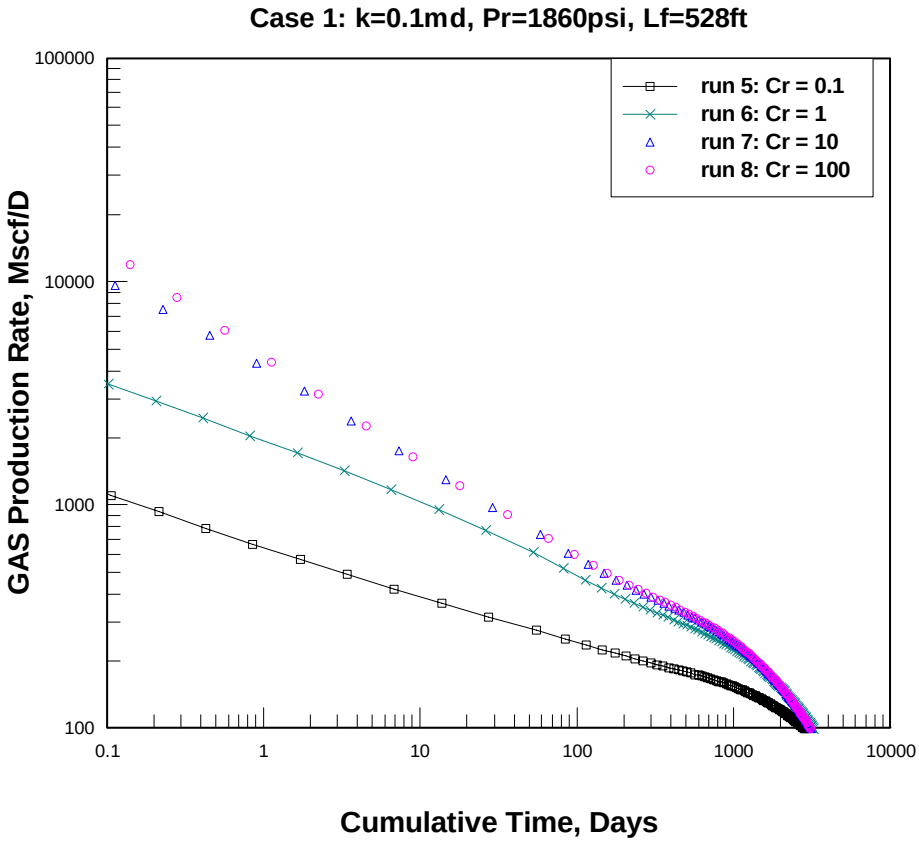

Figure E.1—Effect of fracture conductivity (run 5-8) on gas production rates for case 1: L_f = 528 ft, p_r = 1860 psi, k = 0.1 md, S_{wi} = 0.4 and h = 100 ft.

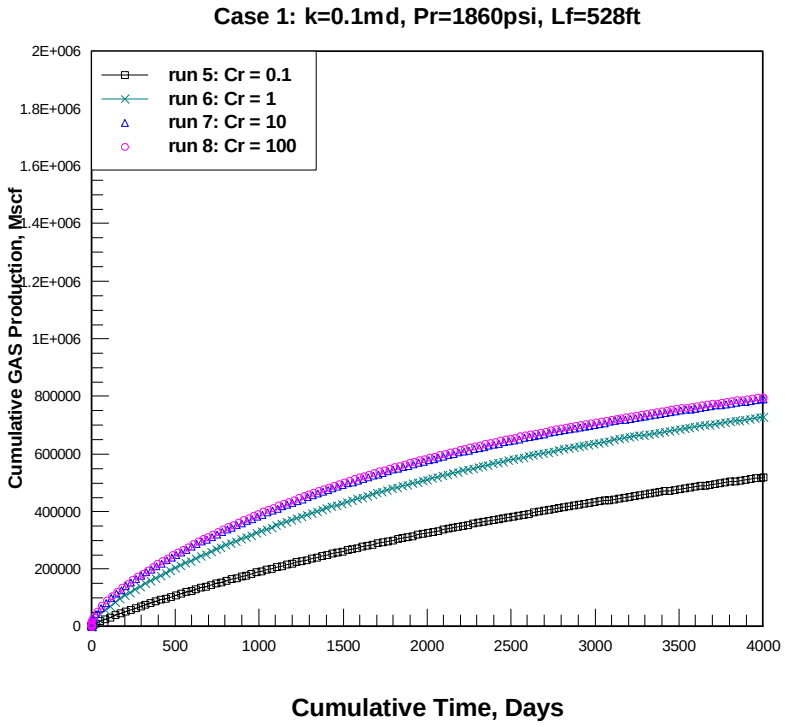

Figure E.2—Effect of fracture conductivity (run 5-8) on cumulative gas production for case 1: L_f = 528 ft, p_r = 1860 psi, k = 0.1 md, S_{wi} = 0.4 and h = 100 ft.

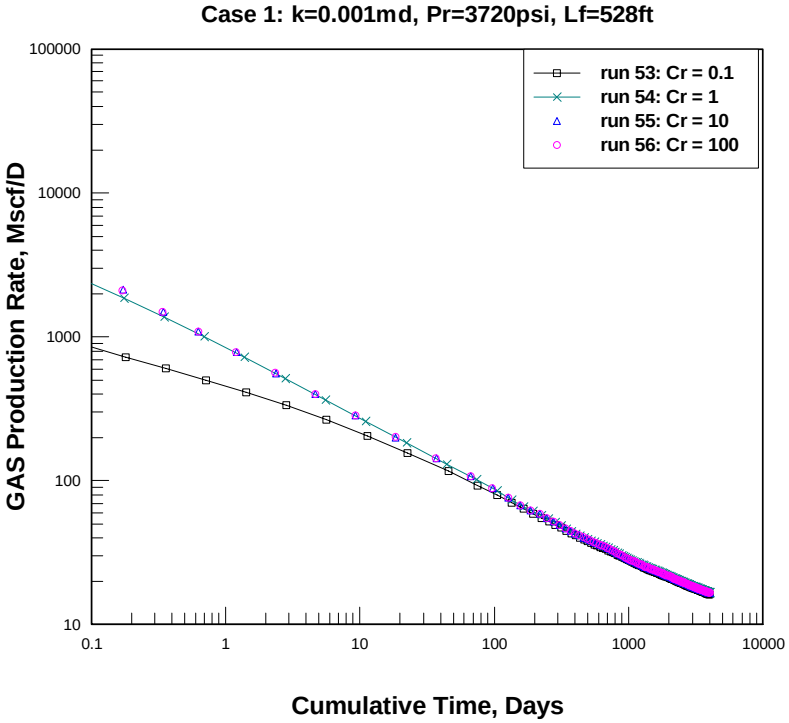

Figure E.3—Effect of fracture conductivity (run 53-56) on gas production rates for case 1: L_f = 528 ft, p_r = 3720 psi, k = 0.001 md, S_{wi} = 0.4 and h = 100 ft.

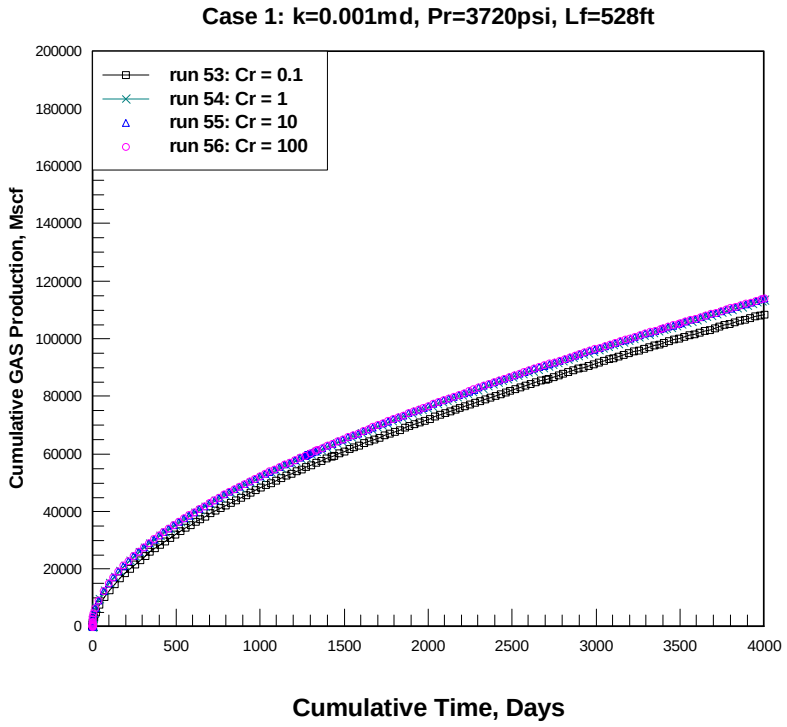

Figure E.4—Effect of fracture conductivity (run 53-56) on cumulative gas production for case 1: L_f = 528 ft, p_r = 3720 psi, k = 0.001 md, S_{wi} = 0.4 and h = 100 ft.

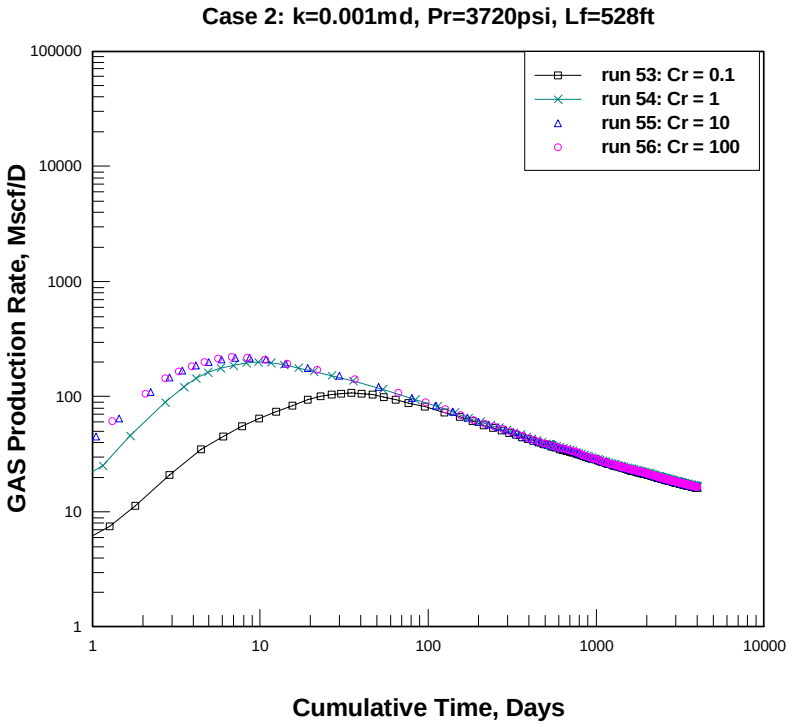

Figure E.5—Effect of fracture conductivity (run 53-56) on gas production rates for case 2: L_f = 528 ft, p_r = 3720 psi, k = 0.001 md, S_{wi} = 0.4 and h = 100 ft.

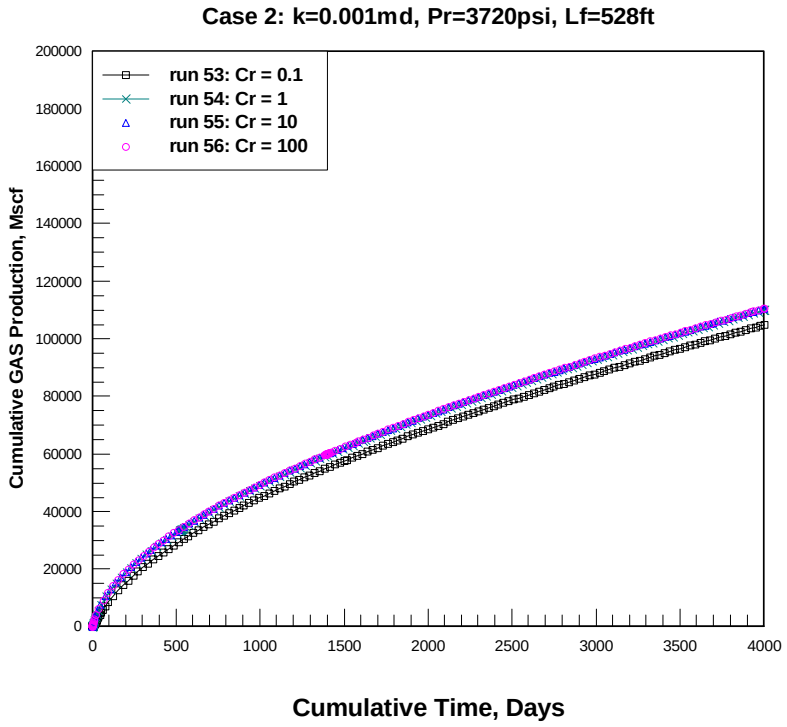

Figure E.6—Effect of fracture conductivity (run 53-56) on cumulative gas production for case 2: L_f = 528 ft, p_r = 3720 psi, k = 0.001 md, S_{wi} = 0.4 and h = 100 ft.

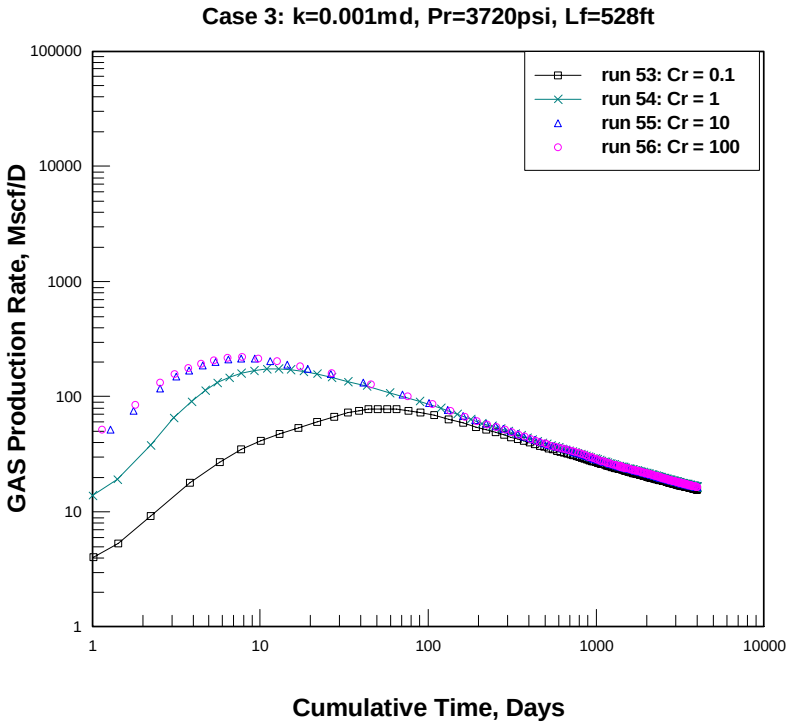

Figure E.7—Effect of fracture conductivity (run 53-56) on gas production rates for case3: L_f = 528 ft, p_r = 3720 psi, k = 0.001 md, S_{wi} = 0.4 and h = 100 ft.

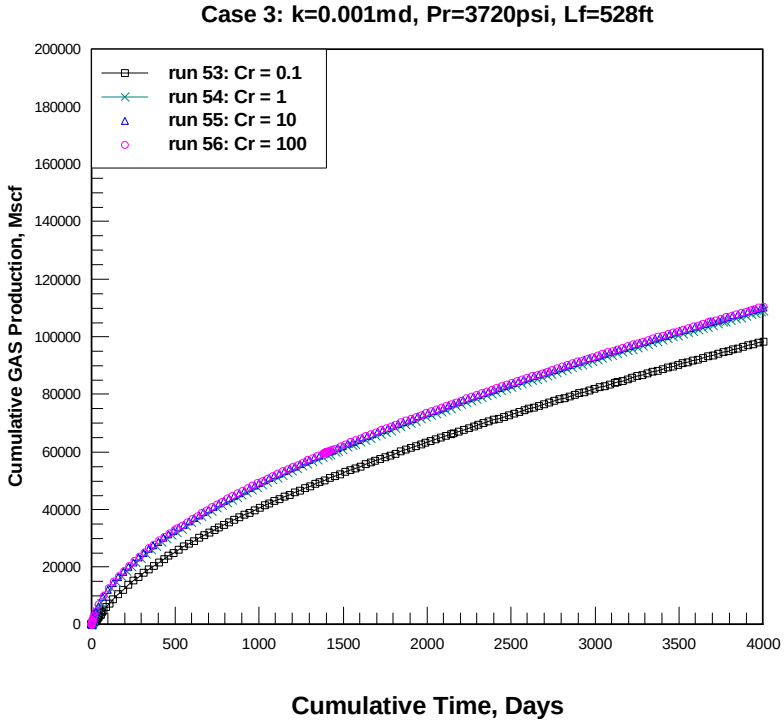

Figure E.8—Effect of fracture conductivity (run 53-56) on cumulative gas production for case 3: L_f = 528 ft, p_r = 3720 psi, k = 0.001 md, S_{wi} = 0.4 and h = 100 ft.

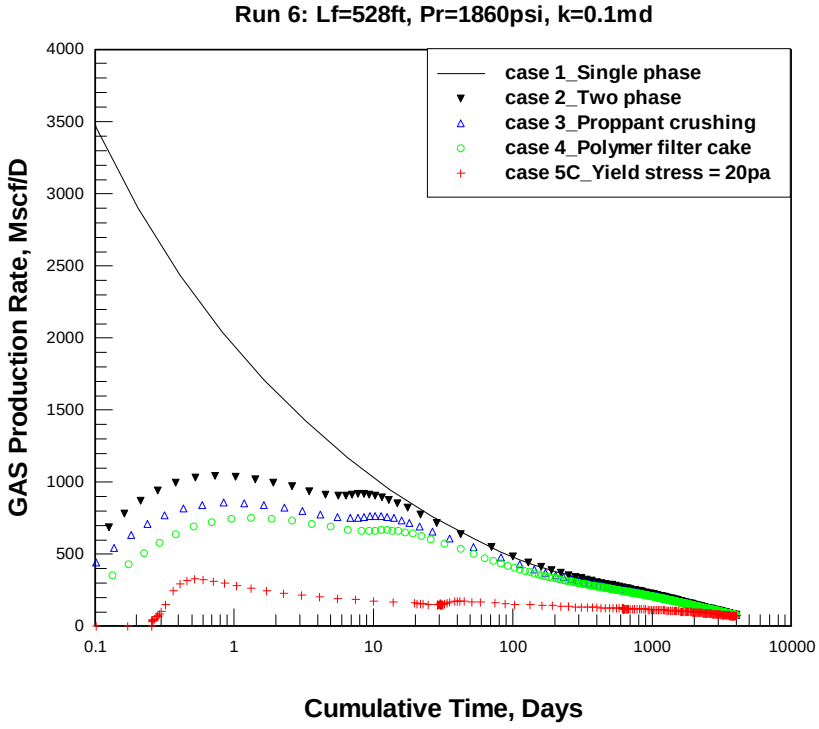

Figure E.9—Gas production rates for different cases at run 6: L_f = 528 ft, p_r = 1860 psi, k = 0.1 md, C_r =1, S_{wi} = 0.4 and h = 100 ft.

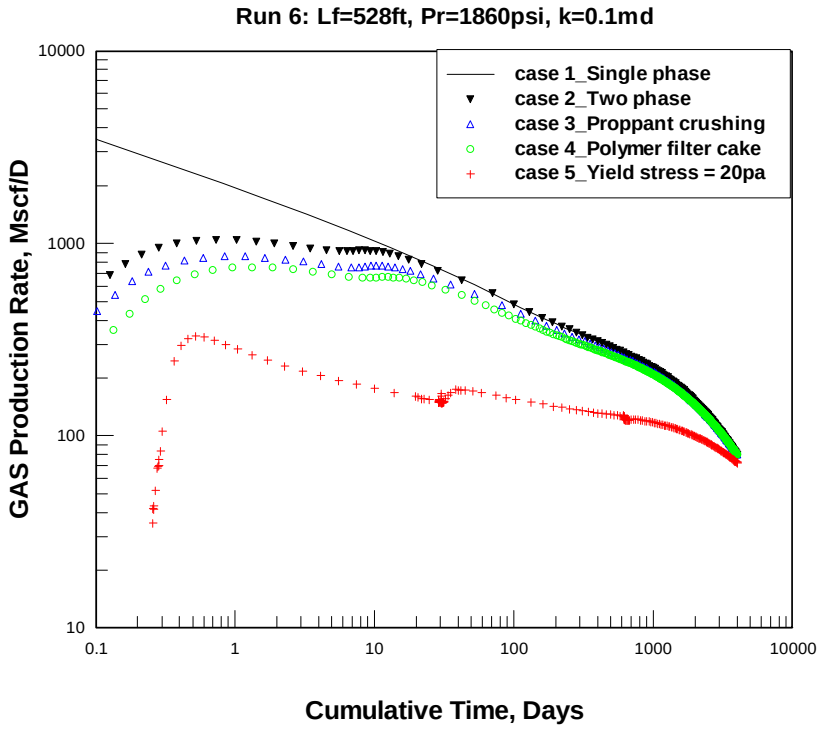

Figure E.10— Gas production rates for different cases at run 6: L_f = 528 ft, p_r = 1860 psi, k = 0.1 md, C_r =1, S_{wi} = 0.4 and h = 100 ft.

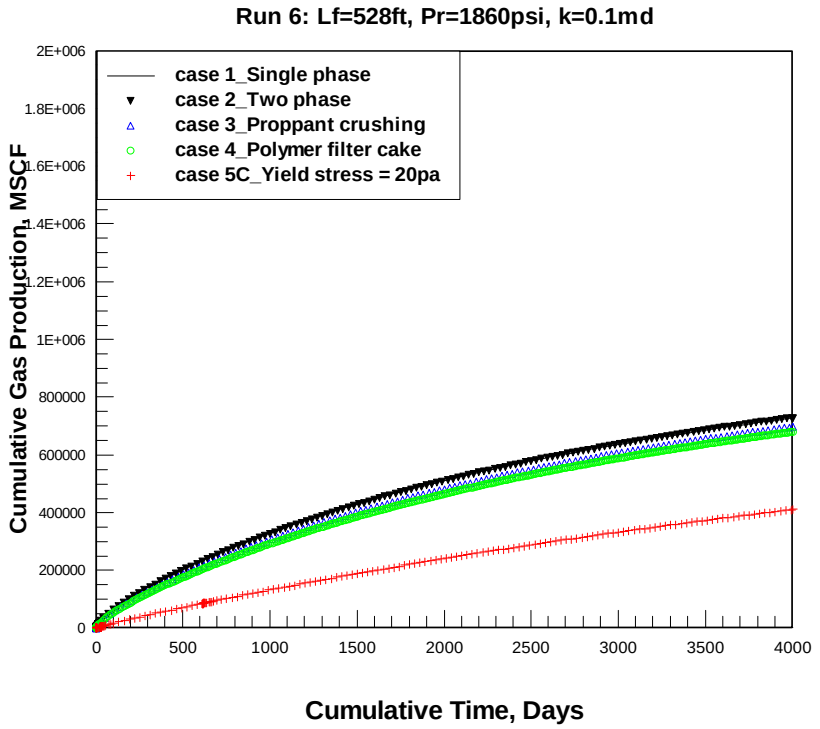

Figure E.11—Cumulative gas production for different cases at run 6: L_f = 528 ft, p_r = 1860 psi, k = 0.1 md, C_r =1, S_{wi} = 0.4 and h = 100 ft.

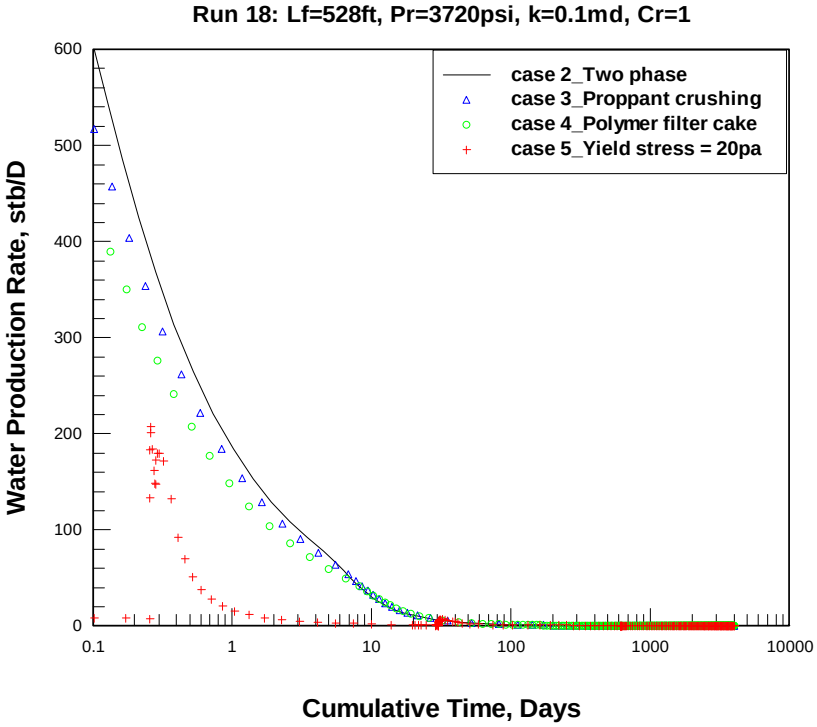

Figure E.12— Water production rates for different cases at run 18: L_f = 528 ft, p_r = 3720 psi, k = 0.1 md, C_r =1, S_{wi} = 0.4 and h = 100 ft.

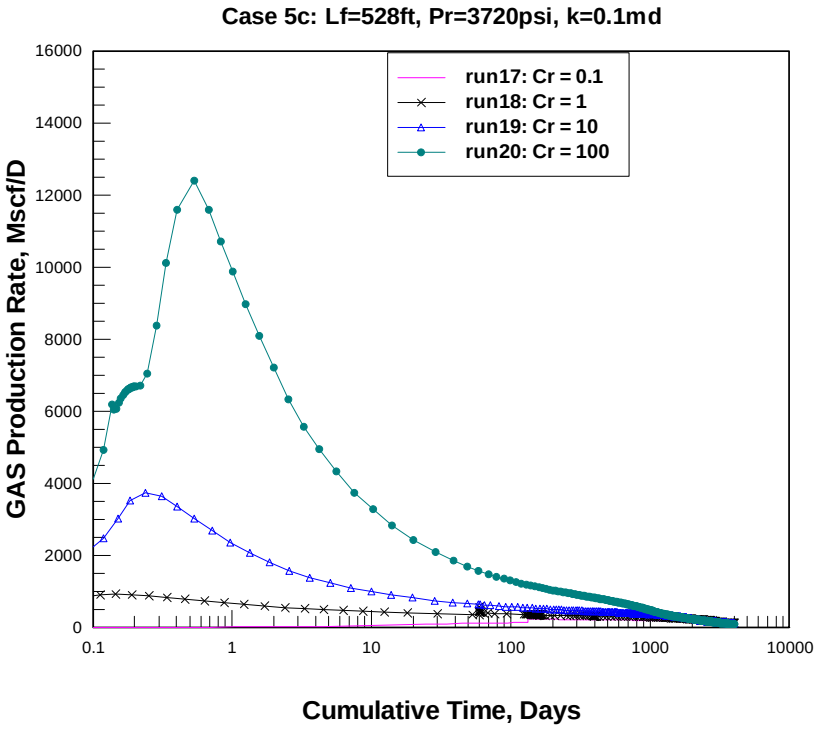

Figure E.13—Effect of fracture conductivity (run 17-20) on gas production rates for case 5c: L_f = 528 ft, p_r = 3720 psi, k = 0.1 md, S_{wi} = 0.4 and h = 100 ft.

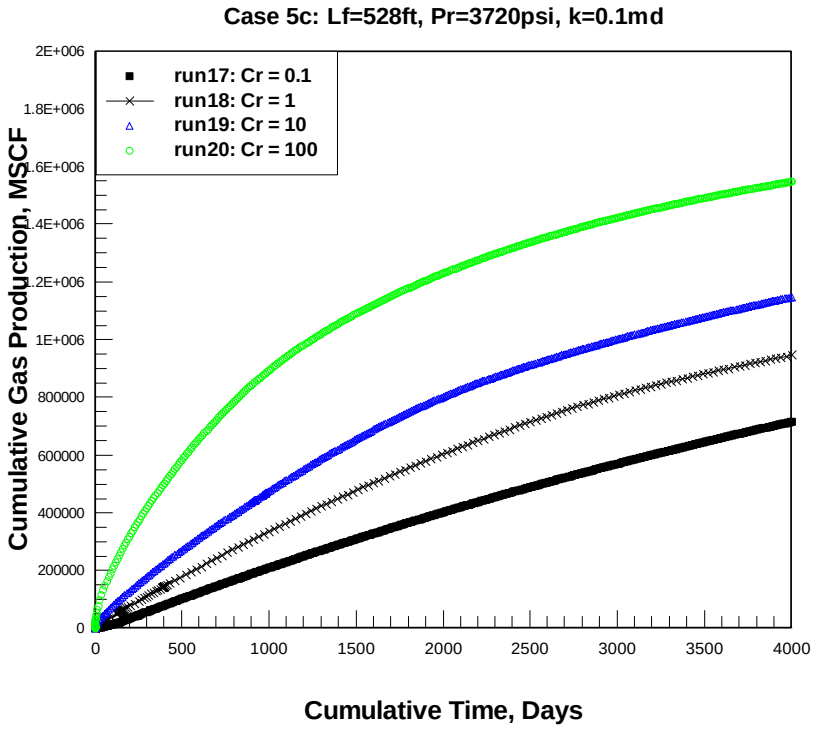

Figure E.14—Effect of fracture conductivity (run 17-20) on cumulative gas production for case 5c: L_f = 528 ft, p_r = 3720 psi, k = 0.1 md, S_{wi} = 0.4 and h = 100 ft.

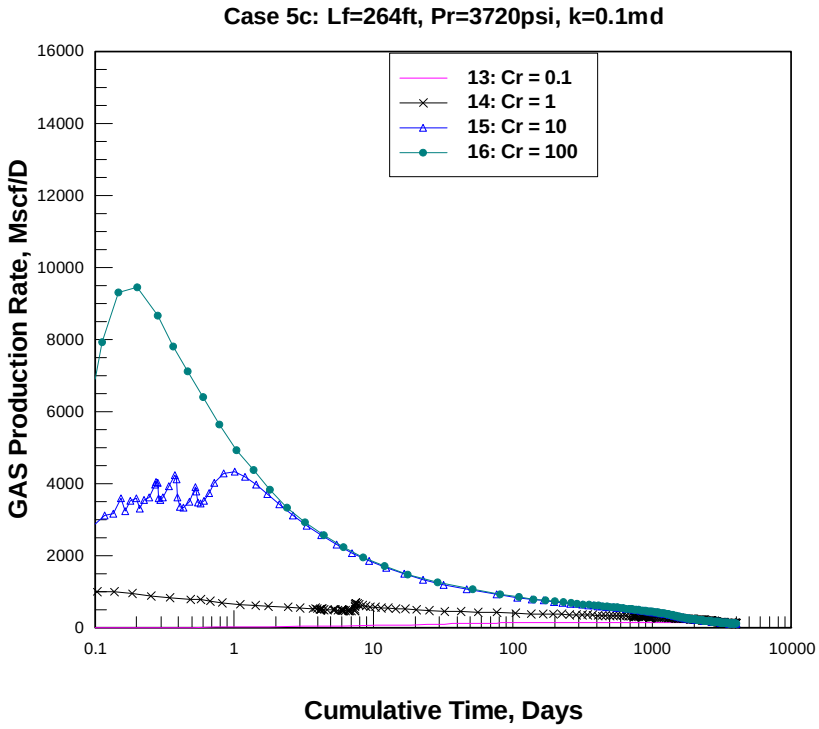

Figure E.18—Effect of fracture conductivity (run 13-16) on gas production rates for case 5c: L_f = 264 ft, p_r = 3720 psi, k = 0.1 md, S_{wi} = 0.4 and h = 100 ft.

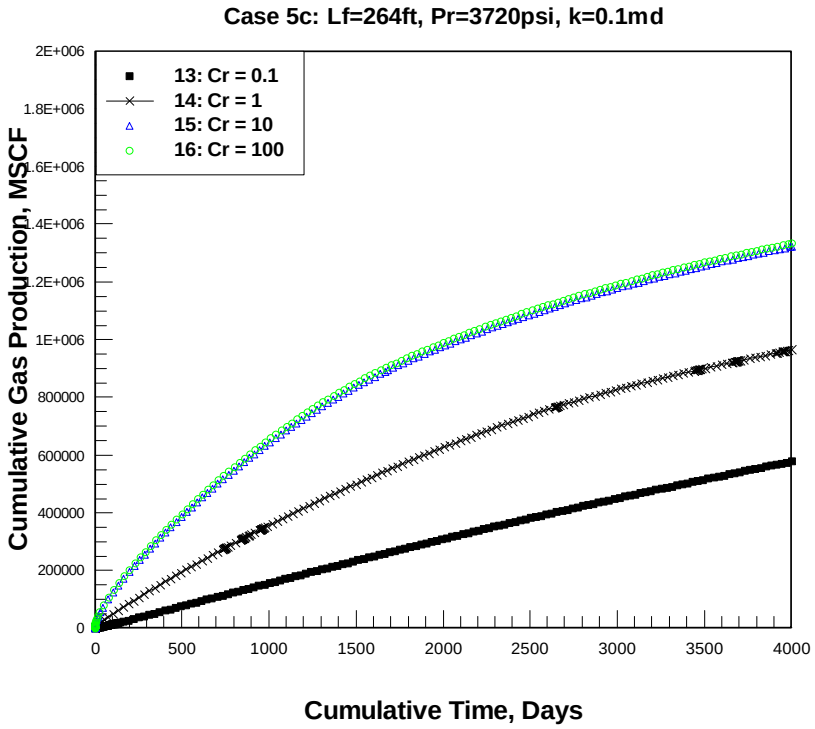

Figure E.19—Effect of fracture conductivity (run 13-16) on cumulative gas production for case 5c: L_f = 264 ft, p_r = 3720 psi, k = 0.1 md, S_{wi} = 0.4 and h = 100 ft.

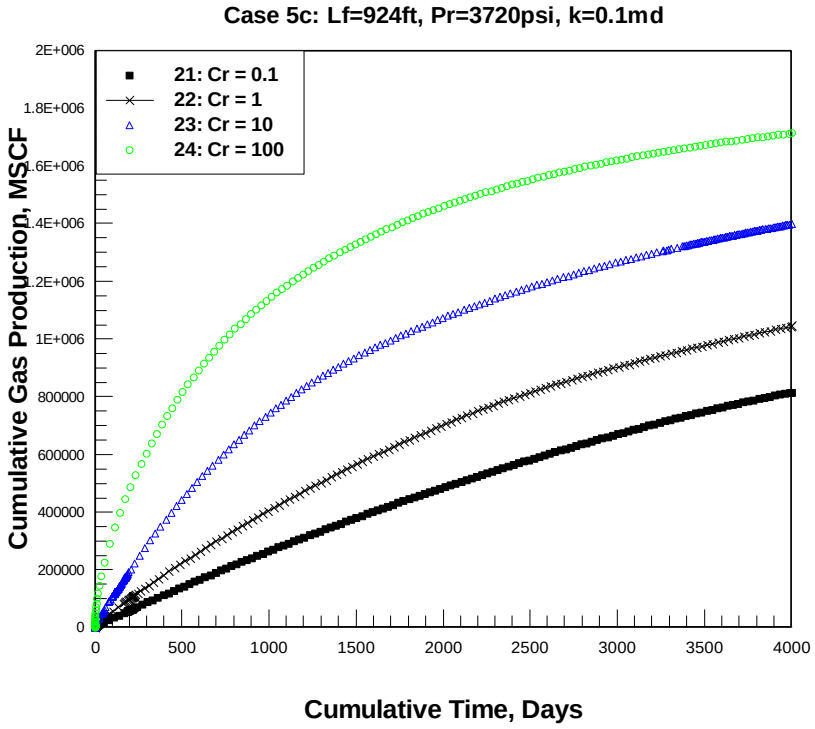

Figure E.21—Effect of fracture conductivity (run 21-24) on cumulative gas production for case 5c: L_f = 924 ft, p_r = 3720 psi, k = 0.1 md, S_{wi} = 0.4 and h = 100 ft.

Table E.1—Gas recovery with gel damage after ten years

Different Reservoir and Fracture Scenarios					Gas Recovery with Gel Damage*			
Run	k (md)	p_r (psi)	L_f (ft)	C_r	case5a	case5b	case5c	case5d
1	0.1	1860	264	0.1	72	68	59	53
2				1	93	81	77	47
3				10	100	100	79	56
4				100	100	100	100	82
5			528	0.1	68	63	42	42
6				1	69	65	56	44
7				10	99	89	63	63
8				100	100	100	100	66
9			924	0.1	74	71	56	48
10				1	74	60	49	40
11				10	100	88	67	39
12				100	100	100	98	71
13		3720	264	0.1	81	77	52	52
14				1	96	83	74	64
15				10	99	99	99	65
16				100	100	100	100	80
17			528	0.1	78	71	63	52
18				1	80	69	65	47
19				10	99	99	75	54
20				100	100	100	100	31
21			924	0.1	82	75	71	50
22				1	79	69	64	59
23				10	99	84	82	61
24				100	100	100	100	36
25		5580	264	0.1	81	70	65	51
26				1	95	90	82	68
27				10	99	99	99	71
28				100	99	99	99	77
29			528	0.1	76	68	65	50
30				1	86	73	74	59
31				10	98	98	86	78
32				100	100	100	100	69
33			924	0.1	82	74	68	56
34				1	85	77	69	58
35				10	99	91	83	65
36				100	100	100	100	87
37	0.001	1860	264	0.1	54	25	15	27
38				1	97	59	15	15
39				10	98	98	90	13
40				100	98	98	98	62
41			528	0.1	20	11	8	7
42				1	96	19	8	8
43				10	97	97	30	6
44				100	97	97	97	24

Table E.1 continued

Run	k (md)	p_r (psi)	L_f(ft)	C_r	case5a	case5b	case5c	case5d
45			924	0.1	13	7	6	5
46				1	22	12	5	5
47				10	97	22	18	4
48				100	97	97	44	17
49		3720	264	0.1	83	39	29	12
50				1	97	97	50	14
51				10	97	97	97	15
52				100	97	97	97	59
53			528	0.1	28	18	13	7
54				1	96	31	18	17
55				10	97	97	62	9
56				100	97	97	97	15
57			924	0.1	18	10	8	5
58				1	32	19	16	5
59				10	97	41	23	5
60				100	97	97	97	10
61		5580	264	0.1	92	40	35	12
62				1	96	96	55	14
63				10	97	97	97	15
64				100	97	97	97	57
65			528	0.1	32	15	13	13
66				1	95	32	22	8
67				10	96	96	96	8
68				100	97	97	97	17
69			924	0.1	21	12	8	5
70				1	42	19	13	5
71				10	96	55	24	5
72				100	97	97	97	10

*Percentage of gas recovery referred to ideal single-phase gas flow after 10 years

Table E.2—Percentage of propped fracture length that is cleaned up after one year

Run	k (md)	p_r (psi)	L_f (ft)	C_r	case5a cleanup*,%	case5b cleanup*,%	case5c cleanup*,%	case5d cleanup*,%
1	0.1	1860	264	0.1	8.33	4.55	0.76	0.00
2			264	1	82.20	25.38	5.68	0.00
3			264	10	100.00	100.00	5.68	0.00
4			264	100	100.00	100.00	100.00	0.00
5			528	0.1	4.17	2.27	0.76	0.00
6			528	1	22.16	10.80	4.17	0.00
7			528	10	100.00	41.10	10.80	0.00
8			528	100	100.00	100.00	100.00	0.00
9			924	0.1	4.00	2.38	0.43	0.00
10			924	1	18.07	6.17	2.38	0.00
11			924	10	100.00	28.90	18.07	0.00
12			924	100	100.00	100.00	55.95	0.00
13		3720	264	0.1	14.02	8.33	0.76	0.00
14			264	1	100.00	36.74	5.68	0.00
15			264	10	100.00	100.00	100.00	0.00
16			264	100	100.00	100.00	100.00	0.00
17			528	0.1	7.01	2.27	0.76	0.00
18			528	1	100.00	10.80	4.17	0.00
19			528	10	100.00	100.00	22.16	0.00
20			528	100	100.00	100.00	100.00	0.00
21			924	0.1	6.17	2.38	1.30	0.00
22			924	1	28.90	12.66	6.17	0.00
23			924	10	100.00	39.72	18.07	0.00
24			924	100	100.00	100.00	67.53	0.00
25		5580	264	0.1	19.70	4.55	1.14	0.00
26			264	1	100.00	19.70	5.68	0.00
27			264	10	100.00	100.00	100.00	0.00
28			264	100	100.00	100.00	100.00	0.00
29			528	0.1	7.01	2.27	1.33	0.00
30			528	1	41.10	10.80	7.01	0.00
31			528	10	100.00	100.00	31.63	0.00
32			528	100	100.00	100.00	100.00	0.00
33			924	0.1	6.17	2.38	1.30	0.00
34			924	1	28.90	12.66	6.17	0.76
35			924	10	100.00	55.95	28.90	2.38
36			924	100	100.00	100.00	100.00	18.07
37	0.001	1860	264	0.1	36.74	4.55	1.52	0.00
38			264	1	100.00	36.74	4.55	0.00
39			264	10	100.00	100.00	67.05	0.00
40			264	100	100.00	100.00	100.00	0.00
41			528	0.1	10.80	2.27	0.76	0.00
42			528	1	41.10	10.80	2.27	0.00
43			528	10	100.00	100.00	22.16	0.00
44			528	100	100.00	100.00	100.00	0.00

Table E.2 continued

Run	k (md)	p_r (psi)	L_f (ft)	C_r	case5a cleanup*,%	case5b cleanup*,%	case5c cleanup*,%	case5d cleanup*,%
45			924	0.1	6.17	1.30	0.43	0.00
46			924	1	18.07	6.17	1.30	0.00
47			924	10	100.00	18.07	12.66	0.00
48			924	100	100.00	100.00	28.90	0.00
49		3720	264	0.1	74.62	0.76	4.55	0.00
50			264	1	100.00	100.00	36.74	0.00
51			264	10	100.00	100.00	100.00	0.00
52			264	100	100.00	100.00	100.00	0.00
53			528	0.1	16.48	4.17	2.27	0.00
54			528	1	100.00	22.16	7.01	0.00
55			528	10	100.00	100.00	16.48	0.00
56			528	100	100.00	100.00	100.00	0.00
57			924	0.1	9.42	2.38	1.30	0.00
58			924	1	28.90	12.66	4.00	0.00
59			924	10	100.00	39.72	18.07	0.00
60			924	100	100.00	100.00	100.00	0.00
61		5580	264	0.1	100.00	8.33	8.33	0.00
62			264	1	100.00	100.00	44.32	0.00
63			264	10	100.00	100.00	100.00	0.00
64			264	100	100.00	100.00	100.00	0.00
65			528	0.1	22.16	4.17	2.27	0.00
66			528	1	100.00	22.16	10.98	0.00
67			528	10	100.00	100.00	100.00	0.00
68			528	100	100.00	100.00	100.00	0.00
69			924	0.1	12.66	2.38	1.30	0.00
70			924	1	39.72	12.66	6.17	0.00
71			924	10	100.00	55.95	18.07	0.00
72			924	100	100.00	100.00	100.00	0.00

* Refer to $S_g > 30\%$

VITA

Name:	YILIN WANG
Permanent Address:	Department of Petroleum Engineering Texas A&M University MS 3116 College Station, TX 77843-3116
Email:	Yilintx at tamu dot edu
Education:	Ph.D. at Texas A&M University, 2008; M.S. at University of Houston, 2004; B.S. at University of Petroleum of China, 2003; all in Petroleum Engineering.
Professional Membership:	Society of Petroleum Engineers